

# **DEVELOPMENT AND CHARACTERIZATION OF SUSTAINABLE GEOMATERIAL USING MINING AND INDUSTRIAL WASTES**

**Mahasakti Mahamaya**



Department of Civil Engineering

**National Institute of Technology Rourkela**



# **Development and Characterization of Sustainable Geomaterial Using Mining and Industrial Wastes**

*Dissertation submitted to the in partial fulfillment*

*of the requirements of the degree of*

**Doctor of Philosophy**

in

***Civil Engineering***

by

***Mahasakti Mahamaya***

Roll Number: 513CE1081

*based on research carried out  
under the supervision of*

***Dr. Sarat Kumar Das***



December, 2018

Department Civil Engineering

**National Institute of Technology Rourkela**





December 25, 2018

## Certificate of Examination

Roll Number: 513CE1081

Name: Mahasakti Mahamaya

Title of Dissertation: Development and Characterization of Sustainable Geomaterial Using Mining and Industrial Wastes

We the below signed, after checking the dissertation mentioned above and the official record book (s) of the student, hereby state our approval of the dissertation submitted in partial fulfilment of the requirement of the degree of Doctor of Philosophy in Civil Engineering at National Institute of Technology, Rourkela. We are satisfied with the volume, quality, correctness, and originality of the work.

-----  
Prof. Sarat Kumar Das  
Principal Supervisor

-----  
Prof. Manoj Kumar Mishra (MN)  
Member (DSC)

-----  
Prof. Prasant Kumar Bhuyan(CE)  
Member (DSC)

-----  
Prof. Kanhu Charan Patra (CE)  
Member (DSC)

-----  
Prof. G. L. Sivakumar Babu  
IISC, Bangalore  
Examiner

-----  
Prof. Suresh Prasad Singh (CE)  
Chairman (DSC)

-----  
Prof. Mahabir Panda (CE)  
Head of the Department



Department of Civil Engineering  
**National Institute of Technology Rourkela**

---

**Prof. Sarat Kumar Das**

December 25, 2018

## **Supervisor Certificate**

This is to certify that the work presented in this dissertation entitled “*Development and Characterization of Sustainable Geomaterial Using Mining and Industrial Wastes*” by “*Mahasakti Mahamaya*”, Roll Number: 513CE1081, is a record of original research carried out by her under my supervision and guidance in partial fulfillment of the requirements of the degree of *Doctor of Philosophy in Civil Engineering*. Neither this dissertation nor any part of it has been submitted for any degree or diploma to any institute or university in India or abroad.

-----  
Sarat Kumar Das

Principal Supervisor

**Dedicated**  
**To**  
**My Parents and Family**

# Declaration of Originality

I, Mahasakti Mahamaya, Roll Number: 513CE1081 hereby declare that this dissertation entitled "*Development and Characterization of Sustainable Geomaterial Using Mining and Industrial Wastes*" represents my original work carried out as a doctoral student of NIT Rourkela and, to the best of my knowledge, it contains no material previously published or written by another person, nor any material presented for the award of any degree or diploma of NIT Rourkela or any other institution. Any contribution made to this research by others, with whom I have worked at NIT Rourkela or elsewhere, is explicitly acknowledged in the dissertation. Works of other authors cited in this dissertation have been duly acknowledged under the section "References". I have also submitted my original research records to the scrutiny committee for evaluation of my dissertation.

I am fully aware that in case of my non-compliance detected in the future, the Senate of NIT Rourkela may withdraw the degree awarded to me on the basis of the present dissertation.

December 25, 2018

NIT Rourkela

*Mahasakti Mahamaya*

*Signature*



# Acknowledgement

First and foremost, appreciation to the God for imperceptible support and blessing to step forward in the long journey of Ph. D without losing the faith under difficult circumstances. I deeply obliged to my supervisor Dr. Sarat Kumar Das, Department of Civil Engineering, National Institute of Technology, Rourkela, India for his inspiring guidance, continual encouragement, and immense help towards my research. Sharing of his invaluable expertise and research enlightened me to stepping forward on the challenging path of research work with strong enthusiasm and hard work.

I am extremely grateful to Prof. S. K. Sarangi (former Director) and Prof. A. Biswas (Director) for their direct and indirect support towards academic requirement during the research work. I would like to appreciate all the DSC members, Robin Davis P, Prof. Prasant Kumar Bhuyan, Prof. Manoj Kumar Mishra, Prof. Suresh Prasad Singh for their valuable suggestion to rectify my mistakes and continual encouragement for the smooth progress of my research work and also, I would like to express my thanks to M. Panda (Head of the Department) and all other faculty members of Civil Engineering Department for their encouragement throughout my research journey.

I am thankful to Jindal Steel and Power, Raigarh, Chhatishgarh, FACOR, Bhadrakh, Odisha, Essar Power, Paradeep Odisha, NALCO, Angul, Odisha for supporting in supplying necessary industrial and mining wastes used for the present study. I am thankful to all laboratory staffs of Civil Engineering, , Chemistry, Mining, Ceramic, and Metallurgy for their helping hand in laboratory works.

I am very much thankful for my research colleagues Lasyamayee Garanayak, Shamshad Alam, Harishankar Jeevan Das along with M. Tech. students Shakti Suman, Anshumali, Akhila and Vinay for their strong moral support and help in the laboratory as well as in analytical work. Beyond that, the blessing of my parents, moral support from my family helped me a lot in completing my journey with patience.

December 25, 2018  
NIT Rourkela

Mahasakti Mahamaya  
Roll Number: 513CE1081

# Abstract

The rapid growth of infrastructure needs a vast amount of natural resources to be used as an engineering material; on the other, industries and mining sectors are facing difficulty in managing their by-products. Hence, research needs in the alteration of the industrial wastes that can overcome the above challenges with minimum or no adverse effect on the geoenvironment, which especially can be termed as a sustainable material. In the present study attempts have been made to develop sustainable materials, (i) controlled low strength material (CLSM), (ii) biopolymer based cementitious material and (iii) alkali activated material (AAM) from industrial and mining wastes. The controlled low strength materials are developed using (i) less explored industrial waste ferrochrome slag (FS) and (ii) coal mine overburden with fly ash and cement as the binder for both the cases. Experimental investigations like flowability, bleeding, compressive strength, California bearing ratio (CBR), settlement, ultrasonic pulse velocity and slake durability index are made on developed CLSM. Use of optical microscope to characterise the granular material FS in terms of sphericity and workability of the material is another aspect of the present work. The developed CLSM material can be used for different structural fill works with “Low flowability, to “High flowability” with the bleeding value less than 3.5%, with water content varying from 25 to 32%. The 28 days’ density varies from 15.7 kN/m<sup>3</sup> to 16.5 kN/m<sup>3</sup> with ultrasonic pulse velocity values close to 2000, and the water absorption values less than 3%. The unconfined compressive strength (UCS) value upto 2.75 MPa and CBR value more than 100% was obtained.

Biopolymer-based cementitious materials are made using (i) fly ash and (ii) fine fraction of coal mine overburden for wind and water erosion control using three types of biopolymers; xanthan gum (XG), guar gum (GG) and carboxyl methyl cellulose sodium (CMC) salt. The wind erodibility of the materials are studied using water retention, surface resistance and wind tunnel test, similarly pinhole test, cylindrical dispersion tests are conducted to know the water erosion resistance. For water erosion, the CMC is more effective followed by GG and XG for both shale and fly ash. The surface strength of CMC and XG treated shale and fly ash increased with increase in concentration of solution upto 2%, but optimum percentage of GG treated samples observed at 1%. Higher surface strength of CMC and GG showed better wind erosion resistance. The surface strength of

biopolymer treated cohesive material shale is more than that of non-cohesive material fly ash, with the denser microstructure of treated samples due to the bonding of particles.

The other sustainable material, alkali activated material using mine overburden and mine tailing is discussed in terms of compressive strength after 7 and 28 days of curing under ambient, alkali and sulphate solution to simulate different environmental conditions. Development of CLSM using AAM and use of slake durability index to assess the durability of developed sustainable material are some of the novelty of the present work. The AAM using mine overburdens are found to have 28 days compressive strength varying from 25.58MPa to 59.00 MPa depending upon the curing conditions and the base materials. The slake durability test indicates the developed AAM is “medium-high durable” to “high durable material”, similar to that of sandstone. The leachate analyses on the developed sustainable materials show no adverse effect on the geoenvironment.

The scanning electron microscope (SEM), x-ray diffraction (XRD), Fourier transform infrared spectroscopy (FTIR), electrical conductivity, zeta potential, etc. are also used for the characterization of basic material and the developed sustainable material to correlate with their macro properties.

The present work will help in the possible utilisation of the developed sustainable material in infrastructure. But, the future challenges are (i) development of suitable machinery and equipment for implementation of CLSM process, (ii) pilot project study on the implementation of biopolymers for erosion control at the site and (iii) identification of cost-effective activators, possibly from industrial wastes.

***Keywords:* Sustainable material; CLSM; Biopolymer; alkali activated material; coal mine overburden; fly ash; GGBS**



# Contents

<b>CERTIFICATE OF EXAMINATION .....</b>	<b>I</b>
<b>SUPERVISOR CERTIFICATE.....</b>	<b>II</b>
<b>DECLARATION OF ORIGINALITY .....</b>	<b>IV</b>
<b>ACKNOWLEDGEMENT .....</b>	<b>V</b>
<b>ABSTRACT .....</b>	<b>VI</b>
<b>CONTENTS .....</b>	<b>IX</b>
<b>LIST OF FIGURE .....</b>	<b>XIII</b>
<b>LIST OF TABLES.....</b>	<b>XXI</b>
<b>LIST OF SYMBOLS AND ABBREVIATIONS.....</b>	<b>XXIII</b>
<b>CHAPTER 1.....</b>	<b>1</b>
<b>INTRODUCTION .....</b>	<b>1</b>
1.1 General .....	1
1.2 An Overview and Problem Identification .....	1
1.3 Aim and Objective of the Research.....	5
1.4 Scope and Organization of the Thesis.....	6
<b>CHAPTER 2.....</b>	<b>9</b>
<b>LITERATURE REVIEW .....</b>	<b>9</b>
2.1 Introduction .....	9
2.2 Controlled low strength material (CLSM) .....	9
2.2.1 Base Materials used for CLSM .....	9
2.2.2 Mix Design of CLSM.....	11
2.2.3 Flowability of CLSM.....	11
2.2.4 Re-excavatability of CLSM.....	12
2.2.5 Other Properties of CLSM.....	12
2.3 Alkali Activated Material .....	13
2.3.1 Geopolymerization .....	14
2.3.2 Reaction Mechanism by AAFA .....	17
2.3.3 Base Materials in Geopolymer .....	18
2.3.4 Calcined Materials .....	19
2.3.5 Non-calcined Material .....	22
2.3.6 Role of Alkali Metals .....	22

2.3.7 Effect of Particle Size Distribution of Binder Phase .....	24
2.3.8 Role of Curing Temperature/ Condition/ Relative Humidity.....	25
2.4 Biopolymer Stabilized Material .....	26
2.5 Summary and Critical Review .....	32
2.5.1 Summary and Critical Review for CLSM.....	32
2.5.2 Summary and Critical Review for biopolymer modified material.....	32
2.5.3 Summary and Critical Review for Geopolymer.....	33
<b>CHAPTER 3.....</b>	<b>35</b>
<b>BASIC MATERIAL CHARACTERIZATION.....</b>	<b>35</b>
3.1 Introduction.....	35
3.2 Material Collection and Material Characterization.....	35
3.2.1 Basic Materials Collection .....	35
3.2.2 Alkali Activators .....	36
3.2.3 Biopolymers .....	36
3.2.4 Standard Sand.....	37
3.2.5 Material characterizations .....	38
3.3 Results and Discussion.....	38
3.3.1 X-Ray Fluorescence Analysis .....	38
3.3.2 Fourier Transform Infrared Analysis .....	41
3.3.3 X-Ray Diffraction Analysis.....	42
3.3.4 Scanning Electron Microscope Analysis.....	47
3.3.5 Energy Dispersive X-Ray Analysis.....	49
3.4 Summary .....	56
<b>CHAPTER 4.....</b>	<b>59</b>
<b>CHARACTERIZATION OF FERROCHROME SLAG AS A CONTROLLED LOW</b>	
<b>STRENGTH MATERIAL.....</b>	<b>59</b>
4.1 Introduction.....	59
4.2 Materials and Methods.....	60
4.3 Result and Discussion .....	66
4.4 Conclusions.....	83
<b>CHAPTER 5.....</b>	<b>85</b>
<b>COAL MINE OVERBURDEN AS A CONTROLLED LOW STRENGTH</b>	
<b>MATERIAL .....</b>	<b>85</b>
5.1 Introduction.....	85

5.2 Materials and Methods .....	86
5.2.1 Materials .....	86
5.2.2 Preparation of CLSM.....	87
5.2.3 Preparation of Test Cylinders .....	91
5.2.4 Slake Durability Index (SDI).....	92
5.3 Results and Discussion .....	94
5.4 Summary .....	106
<b>CHAPTER 6.....</b>	<b>109</b>
<b>BIOPOLYMER BASED CEMENTITIOUS MATERIAL FOR ENVIRONMENTAL CONTROL .....</b>	<b>109</b>
6.1 Introduction .....	109
6.2 Materials.....	112
6.3 Methods.....	113
6.3.1. Dispersion Test .....	113
6.3.2. Water Retention and Wind Tunnel Test .....	113
6.3.3 Surface Resistance Test .....	115
6.4 Results and Discussion.....	115
6.5 Summary .....	146
<b>CHAPTER 7.....</b>	<b>149</b>
<b>ALKALI ACTIVATED MATERIAL USING MINING WASTES .....</b>	<b>149</b>
7.1 Introduction .....	149
7.2 Materials and Methods .....	149
7.3 Results and Discussion.....	151
7.3.1 Development of AAM using Shale - GGBS .....	151
7.3.2 Alkali Activated Fly Ash as a CLSM.....	167
7.3.3 Cement Less Alkali Activated CLSM using Ferrochrome Slag.....	171
7.3.4 Alkali Activated Material for the CLSM using Mine Overburden .....	179
7.4 Summary .....	186
<b>CHAPTER 8.....</b>	<b>191</b>
<b>GENERAL OBSERVATIONS, CONCLUSIONS AND SCOPE OF FUTURE STUDIES .....</b>	<b>191</b>
8.1 Summary .....	191
8.2 General Observation and Concluding Remarks for Material Characterization. .	192

8.3 General Observations and Concluding Remarks for Characterization of Ferrochrome Slag as a Controlled Low Strength Material .....	193
8.4 General Observations and Concluding Remarks for Characterization of Coal Mine Overburden as a Controlled Low Strength Material .....	195
8.5 General Observations and Concluding Remarks for Dispersive Soil and its Stabilization using Biopolymer for Environmental Control .....	196
8.6 General Observations and Concluding Remarks for Alkali Activated Material (Geopolymer) .....	197
8.6 Scope of Future Studies .....	200
<b>REFERENCES .....</b>	<b>203</b>
<b>DISSEMINATION .....</b>	<b>221</b>



# List of Figure

<b>Figure 1.1:</b> The cyclic process of development of sustainable geoenvironment (modified from Jayanthi and Singh 2016).....	2
<b>Figure 1.2:</b> Percentage use of cement over last decade (Modified from Schneider et al. 2011).....	3
<b>Figure 1.3:</b> Proportion of the electrical energy required for the cement industry, Modified from Schneider et al. (2011).....	4
<b>Figure 1.4:</b> Flow diagram showing the organization of the main chapters .....	7
<b>Figure 2.1:</b> Classification of types of cement (Provis and van Deventer, 2014).....	14
<b>Figure 2.2:</b> Development of alkali-activated cementitious material .....	16
<b>Figure 2.3:</b> Descriptive model of alkali activated fly ash (Fernández-Jiménez <i>et al.</i> 2005).....	18
<b>Figure 3.1:</b> Particle size distribution of standard sand used in the present study.....	37
<b>Figure 3.2:</b> Different parameters of the slag used for the alkali activation along with the present slag .....	40
<b>Figure 3.3:</b> FTIR spectra of red mud, fly ash, granulated slag, and ferrochrome slag .....	42
<b>Figure 3.4:</b> XRD analysis of (a) NALCO fly ash (b) JSPL fly ash and (c) Paradeep fly ash. ....	44
<b>Figure 3.5:</b> XRD analysis of RSP GGBS .....	44
<b>Figure 3.6:</b> XRD plot of (a) FA and (b) GGBS .....	45
<b>Figure 3.7:</b> XRD plot of whole ferrochrome slag and magnetically separated particles. .	46
<b>Figure 3.8:</b> XRD plot of Indian standard sand. ....	46
<b>Figure 3.9:</b> XRD plot of coal mine overburden shale. ....	47
<b>Figure 3.10:</b> SEM micrograph of (a) JSPL fly ash (b) NALCO fly ash, (c ) Paradeep fly ash (d) ground granulated blast furnace slag (GGBS).....	48
<b>Figure 3.11:</b> SEM microphotograph of (a) Ferrochrome slag and (b) magnetic part.....	49
<b>Figure 3.12:</b> EDX analysis of (a) NALCO fly ash and (b) GGBS particles .....	51
<b>Figure 3.13:</b> EDX analysis of (a) typical ferrochrome slag sample (b) magnetic separated particles.....	51
<b>Figure 3. 14:</b> Optical microscope analysis of magnetically separated part. ....	52
<b>Figure 3.15:</b> Variation of EC of GGBS, HCFA, JSPL fly ash and NALCO fly ash with liquid to solid (L/S) ratio. ....	53

<b>Figure 3.16:</b> Variation of TDS of GGBS, Paradeep fly ash (HCFA), JSPL fly ash and NALCO fly ash with liquid to solid (L/S) ratio. ....	53
<b>Figure 3.17:</b> Variation of pH of GGBS, Paradeep fly ash (HCFA), JSPL fly ash and NALCO fly ash with liquid to solid (L/S) ratio. ....	54
<b>Figure 3.18:</b> Variation of EC of red shale, white shale and black with liquid to solid (L/S) ratio.....	54
<b>Figure 3.19:</b> Variation of TDS of red shale, white shale and black with liquid to solid (L/S) ratio. ....	55
<b>Figure 3.20:</b> Variation of pH of red shale, white shale and black with liquid to solid (L/S) ratio.....	55
<b>Figure 4.1:</b> Particle shape analysis (a) longest dimension, shortest dimension (b) largest radius and corner radius of the circle. ....	64
<b>Figure 4.2:</b> Flow diagram showing the details of the experimental investigation on CLSM using ferrochrome slag. ....	65
<b>Figure 4.3:</b> Grain size analysis of ferrochrome slag, fly ash and Indian natural sand. ....	67
<b>Figure 4.4:</b> Particle shape classification using Zingg diagram.....	69
<b>Figure 4.5:</b> Relationship between Shape factor and Sphericity. ....	69
<b>Figure 4.6:</b> Flowability of FS with different water cement ratio .....	70
<b>Figure 4.7:</b> Relationship between Shape factor, Sphericity and flakiness. ....	71
<b>Figure 4.8:</b> Relationship between roundness index and void ratio. ....	71
<b>Figure 4.9:</b> Variation of pH of FS, SS1 and SS2 with liquid to solid ratio (L/S). ....	72
<b>Figure 4.10:</b> Variation of EC of FS, SS1 and SS2 with liquid to solid ratio (L/S). ....	72
<b>Figure 4.11:</b> Variation of zeta potential with pH of ferrochrome slag and Indian standard sand. ....	74
<b>Figure 4.12:</b> Relationship between density and thermal resistivity .....	74
<b>Figure 4.13:</b> Stress- strain curves for M5S4 after 7, 28 and 56 days of curing period. ....	79
<b>Figure 4.14:</b> Stress- strain curves for M4S1 after 7, 28 and 56 days of curing period. ....	79
<b>Figure 4.15:</b> Unconfined compressive strength of CLSM mixtures (a) 7 days (b) 28 days (c) 56 days. ....	81
<b>Figure 4.16:</b> SEM morphology of the FS CLSM .....	82
<b>Figure 5.1:</b> Power plant present vicinity of mines area. ....	86
<b>Figure 5.2:</b> Overburden at coal mine area. ....	87
<b>Figure 5.3:</b> Process of development of CLSM using mine overburden. ....	89

<b>Figure 5.4:</b> Fabricated soil based mixture machine (a) pictorial diagram. (b) developed mixture machine. ....	90
<b>Figure 5.5:</b> (a) Measuring flow diameter of CLSM. (b) The test set of for measuring bleeding of CLSM. ....	91
<b>Figure 5.6:</b> Slake durability set up.....	92
<b>Figure 5.7:</b> Scanning electron micrograph of (a) fly ash (b) shale.....	94
<b>Figure 5.8:</b> XRD analysis of Shale. ....	95
<b>Figure 5.9:</b> FTIR spectroscopy of shale .....	95
<b>Figure 5.10:</b> Grain size distribution curves for the crushed shale and fly ash.....	96
<b>Figure 5.11:</b> Compaction characteristics of fly ash and shale. ....	96
<b>Figure 5.12:</b> Flow and bleeding characteristics of CLSM.....	98
<b>Figure 5.13:</b> Fresh and harden density of CLSM. ....	98
<b>Figure 5.14:</b> Ultrasonic pulse velocity measurement of CLSM sample.....	99
<b>Figure 5.15:</b> Ultrasonic pulse velocity and water absorption of different CLSM samples. ....	99
<b>Figure 5.16:</b> Stress-strain characteristics of sample ScM5S4. ....	100
<b>Figure 5.17:</b> Stress-strain characteristics of sample ScM1S1. ....	101
<b>Figure 5.18:</b> The unconfined compressive strength of shale CLSM at 7days and 28days of curing.....	101
<b>Figure 5.19:</b> CBR values of different CLSM samples. ....	102
<b>Figure 5.20:</b> Relationship between ultra-sonic pulse velocity and unconfined compressive strength of CLSM samples. ....	102
<b>Figure 5.21:</b> Cylindrical specimen samples (a) before the test and (b) after the test. ....	103
<b>Figure 5.22:</b> Failure patterns (a) showing internal aggregates (b) sample ScM3S2 (maximum UCS) (c) sample ScM6S3 (minimum UCS) at 28 days of curing. ....	104
<b>Figure 5.23:</b> Settlement test set up for CLSM samples. ....	104
<b>Figure 5.24:</b> Slake durability index corresponding to the different cycle of some selected CLSM samples. ....	105
<b>Figure 6.1:</b> (a) Surface crack of a typical mine overburden,(b) Temporary stabilization of dispersive soil by a sprinkling of water. ....	110
<b>Figure 6.2:</b> Flowchart of experimental investigations of the present chapter. ....	112
<b>Figure 6.3:</b> (a) Sample prepared for wind tunnel test (b) Wind tunnel set up. ....	115
<b>Figure 6.4:</b> Grain size distribution of fly ash and shale.....	116

<b>Figure 6.5:</b> Pinhole test of (a) fly ash, (b) fly ash treated with 0.5% of GG, (c) fly ash treated with 2.0% of XG, and (d) fly ash treated with 0.5% of CMC.....	118
<b>Figure 6.6:</b> Cylinder dispersion test of (a) fly ash (b) fly ash treated with 1.0% of GG and (c) fly ash treated with 1.0% of XG and (d) fly ash treated with 1.0% of CMC.....	118
<b>Figure 6.7:</b> Pin hole test of (a) shale, (b) shale treated with 0.5% of GG, (c) Shale treated with 2.0% of XG, and (d) Shale treated with 0.5% of CMC.....	119
<b>Figure 6.8:</b> Cylinder dispersion test of (a) shale (b) shale treated with 1.0% of guar gum (c) shale treated with 1.0% xanthan gum and (d) Shale treated with 1.0% of CMC .....	120
<b>Figure 6.9:</b> Log-log plot of penetration depth versus water content at different biopolymer concentrations for fly ash with GG .....	121
<b>Figure 6.10:</b> Log-log plot of penetration depth versus water content at different biopolymer concentrations for fly ash with XG .....	121
<b>Figure 6.11:</b> Log-log plot of penetration depth versus water content at different biopolymer concentration.....	122
<b>Figure 6.12:</b> Log-log plot of penetration depth versus water content at different biopolymer concentrations for shale with GG .....	122
<b>Figure 6.13:</b> Log-log plot of penetration depth versus water content at different biopolymer concentrations for shale with XG .....	123
<b>Figure 6.14:</b> Log-log plot of penetration depth versus water content at different biopolymer concentrations for shale with CMC .....	123
<b>Figure 6.15:</b> Biopolymer concentration versus the liquid limit of fly ash. ....	124
<b>Figure 6.16:</b> Biopolymer concentration versus the liquid limit of shale.....	124
<b>Figure 6.17:</b> Water retention test of fly ash using 0.5%, 1.0%, 1.5% and 2.0% of (a) guar gum (b) xanthan gum and (c) CMC. ....	126
<b>Figure 6.18:</b> Water retention test of shale using 0.5%, 1.0%, 1.5% and 2.0% of (a) guar gum (b) xanthan gum and (c) CMC. ....	128
<b>Figure 6.19:</b> Wind tunnel test of fly ash sample and fly ash sample treated with different concentration of guar gum and xanthan gum. ....	128
<b>Figure 6.20:</b> Wind tunnel test of shale sample treated with different concentration of guar gum and xanthan gum. ....	129
<b>Figure 6.21:</b> Typical penetration force versus penetration depth curve for fly ash treated with different concentration of (a) guar gum (b) xanthan gum and (c) CMC.....	131
<b>Figure 6.22:</b> Typical penetration force versus penetration depth curve for shale treated with different concentration of (a) guar gum (b) xanthan gum and (c) CMC.....	132

<b>Figure 6.23:</b> Average maximum penetration force for samples treated with guar gum, xanthan gum and CMC gum solutions at concentrations of 0.5, 1, 1.5, and 2%, respectively (a) fly ash (b) shale.....	133
<b>Figure 6.24:</b> Penetration surface of fly ash sample treated with (a) water (b) 1.0% of guar gum solution(c) 1.0% of xanthan gum solution and (d) 1.0% of CMC gum solution. ....	135
<b>Figure 6.25:</b> Penetration surface of shale sample treated with (a) water (b) 1.0% of guar gum solution (c). 1.0% of xanthan gum solution (d) 1.0% of CMC gum solution .....	137
<b>Figure 6.26:</b> Weight loss of fly ash and shale after wind tunnel test versus maximum penetration force. ....	138
<b>Figure 6.27:</b> Fly ash treated with 1.0% of guar gum. ....	138
<b>Figure 6.28:</b> Fly ash samples treated with 1.0% of xanthan gum.....	139
<b>Figure 6.29:</b> Fly ash treated with 1.0% OF CMC.....	139
<b>Figure 6.30:</b> Shale treated with 1.0% of XG. ....	139
<b>Figure 6.31:</b> Shale sample treated with 1.0% of guar gum. ....	140
<b>Figure 6.32:</b> Shale sample treated with 1.0% of CMC.....	140
<b>Figure 6.33:</b> Compaction curve of fly ash and biopolymer treated fly ash. ....	141
<b>Figure 6.34:</b> Compaction curve of shale and biopolymer treated shale. ....	141
<b>Figure 6.35:</b> Relationship between water content and flow diameter of fly ash and biopolymer treated fly ash samples. ....	142
<b>Figure 6.36:</b> Relationship between maximum dry density (MDD) and optimum moisture content (OMC) different biopolymer treated fly ash and shale samples. ....	142
<b>Figure 6.37:</b> UCS curve of fly ash and fly ash treated with different concentration of GG. ....	143
<b>Figure 6.38:</b> UCS curve of fly ash and fly ash treated with different concentration of XG. ....	143
<b>Figure 6.39:</b> UCS curve of fly ash and fly ash treated with different concentration of CMC. ....	144
<b>Figure 6.40:</b> UCS curve of shale and shale treated with different concentration of GG. ....	144
<b>Figure 6.41:</b> UCS curve of shale and Shale treated with different concentration of XG. ....	145
<b>Figure 6.42:</b> UCS curve of shale and shale treated with different concentration of CMC. ....	145
<b>Figure 7.1:</b> Alkali activated shale: GGBS- 30:70 (paste) with 3 mole of Na <sub>2</sub> SiO <sub>3</sub> .....	152
<b>Figure 7.2:</b> Alkali-activated shale: GGBS- 50:50 (paste) with 3 mole of Na <sub>2</sub> SiO <sub>3</sub> .....	152

<b>Figure 7.3:</b> Alkali-activated shale paste (Shale: FA: GGBS-30:20:50) with 3 moles of $\text{Na}_2\text{SiO}_3$ .....	153
<b>Figure 7.4:</b> Alkali activated shale paste (Shale: FA: GGBS-50:10:40) with 3 moles of $\text{Na}_2\text{SiO}_3$ .....	154
<b>Figure 7.5:</b> Alkali-activated shale mortar (shale: sand: GGBS-30:30:40) with 3 moles of $\text{Na}_2\text{SiO}_3$ .....	155
<b>Figure 7.6:</b> Alkali activated shale: GGBS- 30:70 (paste) with 0.5 mole of $\text{Na}_2\text{SiO}_3$ .....	156
<b>Figure 7.7:</b> Alkali activated shale: GGBS- 50:50 (paste) with 0.5 mole of $\text{Na}_2\text{SiO}_3$ .....	156
<b>Figure 7.8:</b> Alkali-activated shale paste (shale: GGBS- 30:70) with 6 moles of KOH. ..	157
<b>Figure 7.9:</b> Alkali-activated shale paste (shale: GGBS- 50:50) with 6 moles of KOH. ..	158
<b>Figure 7.10:</b> Slake durability test for AAM (shale: GGBS-30:70) with 3 moles of $\text{Na}_2\text{SiO}_3$ under ambient curing after 28 days. ....	159
<b>Figure 7.11:</b> Slake durability test for AAM (shale: GGBS-30:70) with 3 moles of $\text{Na}_2\text{SiO}_3$ under alkali cured after 28 days. ....	159
<b>Figure 7.12:</b> Slake durability test for AAM (shale: GGBS-30:70) with 3 moles of $\text{Na}_2\text{SiO}_3$ under sulphate solution curing for 28 days. ....	160
<b>Figure 7.13:</b> Slake durability test for AAM (shale: GGBS-30:70) with 0.5moles of $\text{Na}_2\text{SiO}_3$ under ambient curing condition .....	161
<b>Figure 7.14:</b> Slake durability test for AAM (shale: GGBS-30:70) with 0.5moles of $\text{Na}_2\text{SiO}_3$ under alkali curing condition. ....	161
<b>Figure 7.15:</b> Slake durability test for AAM, shale: FA: GGBS-30:20:50 with 3 moles of $\text{Na}_2\text{SiO}_3$ .....	161
<b>Figure 7.16:</b> Slake durability test for AAM, shale: FA: GGBS-50:10:40 with 3 moles of $\text{Na}_2\text{SiO}_3$ .....	162
<b>Figure 7.17:</b> Slake durability index test for alkali -activated shale mortar (shale: sand: GGBS-30:30:40) with 3 moles of $\text{Na}_2\text{SiO}_3$ under ambient curing .....	162
<b>Figure 7.18:</b> Slake durability index test for alkali -activated shale mortar (shale: sand: GGBS-30:30:40) with 3 moles of $\text{Na}_2\text{SiO}_3$ under alkali curing condition. ....	162
<b>Figure 7.19:</b> Slake durability index test for alkali -activated shale mortar (shale: sand: GGBS-30:30:40) with 3 moles of $\text{Na}_2\text{SiO}_3$ under sulphate solution curing.....	163
<b>Figure 7.20:</b> Slake durability index test for AAM (shale: GGBS-30:70) with 6 moles of KOH under ambient curing .....	163
<b>Figure 7.21:</b> Water erosion of (a) white shale (b) red shale.....	164

<b>Figure 7.22:</b> (a) Pin hole test of (a) red shale (b) white shale and (b) black shale treated with 30% GGBS and 0.5% of sodium silicate solution.....	164
<b>Figure 7.23:</b> Cylinder dispersion test on alkali activated (a) red shale (b) white shale (c) black shale treated with 30% GGBS and 0.5% of sodium silicate solution.....	165
<b>Figure 7.24:</b> XRD analysis of Alkali activated black shale paste (shale: GGBS- 30:70) with 3 moles of $\text{Na}_2\text{SiO}_3$ under ambient after 28 days .....	166
<b>Figure 7.25:</b> XRD analysis of Alkali activated black shale paste (shale: GGBS- 30:70) with 3 moles of $\text{Na}_2\text{SiO}_3$ under alkali curing condition after 28 days.....	166
<b>Figure 7.26:</b> XRD analysis of Alkali activated black shale paste (shale: GGBS- 30:70) with 3 moles of $\text{Na}_2\text{SiO}_3$ under sulphate solution curing condition after 28 days. ....	167
<b>Figure 7.27:</b> Compressive strength of Alkali activated Nalco fly ash.....	168
<b>Figure 7.28:</b> Compressive strength of Alkali activated JSPL fly ash.....	168
<b>Figure 7.29:</b> Alkali activated Paradeep (HCFA) fly ash. ....	169
<b>Figure 7.30:</b> Failure pattern of alkali activated Paradeep fly ash.....	169
<b>Figure 7.31:</b> slake durability index test for alkali-activated Paradeep fly ash after 28 days of ambient curing.....	170
<b>Figure 7.32:</b> SEM analysis of alkali activated HCFA+4 moles of NaOH.....	170
<b>Figure 7.33:</b> Flow and bleeding of the FS based cement less alkali activated CLSM material .....	172
<b>Figure 7.34:</b> Fresh and harden density of alkali activated CLSM.....	173
<b>Figure 7.35:</b> Stress-strain curve of CLSM (a) FSAM1S2 (b) FSAM3S1 .....	174
<b>Figure 7.36:</b> UCS of alkali activated FS based CLSM.....	175
<b>Figure 7.37:</b> Slake durably index of alkali activated CLSM corresponding to a different cycle.....	175
<b>Figure 7.38:</b> SEM image of alkali activated FS CLSM samples.....	178
<b>Figure 7.39:</b> Flow and bleeding of alkali activated CLSM. ....	180
<b>Figure 7.40:</b> Fresh and harden density of CLSM. ....	181
<b>Figure 7.41:</b> Ultrasonic pulse velocity and water absorption of CLSM at 7 days curing.....	181
<b>Figure 7.42:</b> Ultrasonic pulse velocity and water absorption of CLSM at 28 days curing.....	182
<b>Figure 7.43:</b> Relationship between ultra-sonic pulse velocity and UCS of alkali activated CLSM at 7 days of curing.....	182

<b>Figure 7.44:</b> Relationship between ultra-sonic pulse velocity and UCS of alkali activated CLSM at 28 days of curing. ....	183
<b>Figure 7.45:</b> UCS of alkali activated shale based CLSM at 7days and 28 days. ....	183
<b>Figure 7.46:</b> shows the SEM and EDX analysis of CLSM. ....	184
<b>Figure 7.47:</b> slake durability index test for alkali-activated CLSM at its 28 days of ambient curing. ....	185
<b>Figure 7.48:</b> Variation of unconfined compressive strength and slake durability index of AAM and CLSM developed in the present study and its comparison with natural rocks. ....	185



# List of Tables

<b>Table 1.1:</b> Exhaust gases produced from cement process (Ali <i>et al.</i> 2011).....	3
<b>Table 2.1:</b> Literature review in bioremediation of various soils.....	30
<b>Table 3.1:</b> Chemical composition of fly ashes.....	39
<b>Table 3.2:</b> Chemical composition of RSP slag .....	39
<b>Table 3.3:</b> Chemical Composition of Ferrochrome Slag.....	41
<b>Table 4.1:</b> Mechanical properties of coarse-grained ferrochrome slag .....	62
<b>Table 4.2:</b> Particle shape parameters of FS and Indian standard sand.....	67
<b>Table 4.3:</b> Classification of particles based on Powers' roundness criteria (Yudhbir and Abedinzadeh 1991).....	68
<b>Table 4.4:</b> Mix design of CLSM using FS+fly ash +cement. ....	78
<b>Table 4.5:</b> CBR of Different CLSM Mixtures (7 days of curing + 4 days of soaking).....	81
<b>Table 4.6:</b> Settlement Analysis of Different CLSM Mixtures.....	81
<b>Table 4.7:</b> pH Value of CLSM Mixtures .....	82
<b>Table 4.8:</b> Thermal Resistivity of Ferrochrome Slag and Different CLSM Mixtures.....	82
<b>Table 4.9:</b> Leachate analysis of base material and FS CLSM .....	83
<b>Table 5.1:</b> Aggregate test reports of the coal mine overburden.....	88
<b>Table 5.2:</b> Mix design of CLSM using shale (coal mine overburden, all in aggregate), fly ash, cement and water.....	93
<b>Table 5.3:</b> Settlement test of CLSM (Cylinder size 10cm dia, 20cm height) (in mm from top).....	104
<b>Table 5.5:</b> Leachate analysis of shale CLSM. ....	106
<b>Table 6.1:</b> Leachate analysis of fly ash and biotreated fly ash. ....	146
<b>Table 6.2:</b> Leachate analysis of shale and biotreated shale. ....	146
<b>Table 7.1:</b> Leachate analysis of HCFA and alkali activated HCFA. ....	171
<b>Table 7.2:</b> Design mix of alkali activated cement less CLSM using FS .....	171
<b>Table 7.3:</b> Slake durability index of CLSM.....	177
<b>Table 7.4:</b> Settlement of FS CLSM .....	178
<b>Table 7.5:</b> Leachate analysis of FS CLSM. ....	178
<b>Table 7.6:</b> Proportion and properties of Shale, GGBS, Fly ash and NaOH solution- CLSM .....	179

<b>Table 7.7:</b> Settlement test of CLSM (Cylinder size 10cm dia, 20cm height) (in mm from top).....	184
<b>Table 7.8:</b> Leachate analysis of shale CLSM. ....	186

# List of Symbols and abbreviations

AAFA	Alkali Activated Fly Ash
AAM	Alkali Activated Material
AAS	Alkali Activated Slag
AAS	Atomic Absorption Spectroscopy
Al	Aluminium
Al(OH) <sub>3</sub>	Gibbsite
Al <sub>2</sub> O <sub>3</sub>	Aluminium Oxide
Al <sub>2</sub> SiO <sub>5</sub>	Sillimanite
BET	Brunauer Emmett Teller
BOFS	Basic Oxygen Furnace Slag
Ca	Calcium
Ca(OH) <sub>2</sub>	Calcium Hydroxide
CaCO <sub>3</sub>	Calcite
CBR	California bearing ratio
CKD	Cement Kiln Dust
CLSM	Controlled Low Strength Material
CMC	Carboxyl Methyl Cellulose Sodium Salt
CO <sub>2</sub>	Carbon Dioxide
Cr <sub>2</sub> O <sub>3</sub>	Chromium Oxide
Cu	Copper
DS	Dewatered Sludge
DS	Dispersive Soil
EC	Electrical conductivity
EDS	Energy Dispersive X-ray Spectroscopy
EDX	Electron Dispersive X-ray
FA	Fly Ash
FACOR	Ferro Alloys Corporation
Fe	Iron
Fe <sub>2</sub> O <sub>3</sub>	Hematite
Fe <sub>3</sub> O <sub>4</sub>	Magnetite

FESEM	Field Emission Scanning Electron Microscope
FGD	Flue Gas Desulfurization
FS	Ferrochrome Slag
FTIR	Fourier Transform Infra-Red
GBFS	Granulated Blast Furnace Slag
GG	Guar Gum
GGBS	Ground Granulated Blast Furnace Slag
H <sub>2</sub> O	Water
HCFA	High Calcium Fly Ash
HCl	Hydrochloric Acid
HRS	Hindalco Red Sand
IS	Indian Standard
JSPL	Jindal Steel Plant Limited
K	Potassium
KOH	Potassium Hydroxide
LDA	Laser Diffraction Size Analyser
Li	Lithium
MDD	Maximum Dry Density
Mg	Magnesium
MgAl <sub>2</sub> O <sub>4</sub>	Spinel
MgO	Magnesium Oxide
MICP	Microbially Induced Calcite Precipitation
Mn	Manganese
MSWI	Municipal Solid Waste Incineration
MT	Mine Tailing
N/mm <sup>2</sup>	Newton/millimeter <sup>2</sup>
Na	Sodium
Na <sub>2</sub> CO <sub>3</sub>	Sodium Carbonate
Na <sub>2</sub> O	Sodium Oxide
Na <sub>2</sub> SiO <sub>3</sub>	Sodium Silicate
Na <sub>2</sub> SO <sub>4</sub>	Sodium Sulfate
NaCl	Sodium Chloride
NALCO	National Aluminium Company Limited

NaOH	Sodium Hydroxide
NO <sub>x</sub>	Nitrogen oxide
NRS	Nalco Red Sand
OB	Overburden
OMC	Optimum Moisture Content
OPC	Ordinary Portland Cement
PSC	Portland Slag Cement
RCC	Reinforced Cement Concrete
RM	Red Mud
RSP	Rourkela Steel Plant
S	Sulfur
S/L	Solid/Liquid
SDI	Slake Durability Index
SEM	Scanning Electron Microscopy
Si	Silicon
SiO <sub>2</sub>	Quartz
SO <sub>2</sub>	Sulfur Dioxide
SO <sub>3</sub>	Sulfur Trioxide
SSA	Specific Surface Area
SSRS	Stainless Steel Reducing Slag
TDS	Total dissolved solids
Ti	Titanium
UCS	Unconfined Compressive Strength
UPV	Ultrasonic Pulse Velocity
W	Water
WHO	World Health Organization
XG	Xanthan Gum
XRD	X-ray Diffraction
XRF	X-Ray Fluorescence



# CHAPTER 1

## INTRODUCTION

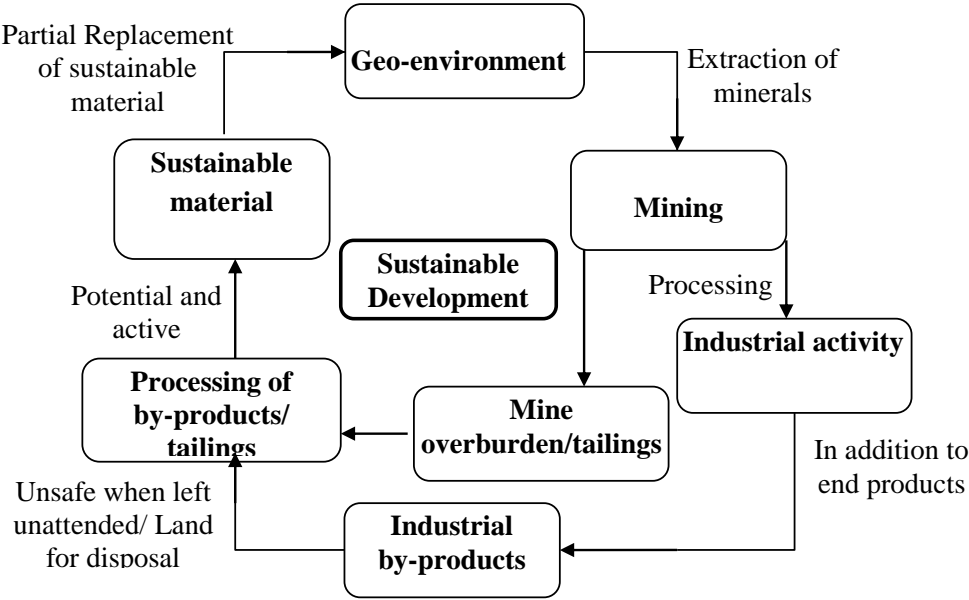
### 1.1 General

The rapid growth of infrastructure needs a vast amount of engineering material in general with emphasis on cementitious material, which uses natural resources. Industries have to focus on the appropriate management and utilization of its waste materials and by-products economically, and attempts have been made to use industrial waste and by-products in construction as a substitute for natural resources. Hence, research has advanced in the modification of municipal, agricultural, industrial wastes and less explored mining wastes for development of sustainable material that can overcome all the challenges and has a minimum or no adverse effect on the geo-environment. In a way, the sustainable material can be considered as a human-made resource, originated from the industrial waste, which remains toxic and hazardous to the environment when left unattended (Jayanthi and Singh 2016). In the following section, an effort has been made briefly to trace the need and development of sustainable material to decide upon the course of studies to be taken up in the present thesis.

### 1.2 An Overview and Problem Identification

The sustainable material originated and refined from the so-called industrial waste that can otherwise be considered as a human-made resource, which remains toxic and hazardous to the environment when left unattended (Albusoda and Salem 2012; Jayanthi and Singh 2016). The concept of sustainability can be explained as a cyclic process (Figure 1.1) of extraction of minerals from nature by human intervention for technological development and giving back the same in the form of processed industrial by-products through sustainable geomaterial to enrich the lost properties of the geomaterial by anthropogenic activities. As an alternative, research has been advanced in the alteration of the industrial wastes like fly ash, slag, etc. as an alternate construction material to replace the natural resources. The development of sustainable material from mine tailing/mine overburden and industrial waste or in combination is a challenge to the research community in

identifying the suitable technology/process to achieve the same. For example, out of various activation processes, chemical activation, mechanical activation, thermal activation, from the research point of view, chemically activated fly ash has better strength and corrosion resistance properties, than thermal and physical activated fly ash (Saraswathi *et al.* 2003).



**Figure 1.1:** The cyclic process of development of sustainable geoenvironment (modified from Jayanthi and Singh 2016).

The cement and lime are the most common cementitious material used in different infrastructure development works. However, considering the existing environment norms and practices followings are the limitations of the lime as a cementitious material. Carbonation of lime in the presence of CO<sub>2</sub> resulting in the formation of CaCO<sub>3</sub>, which results in low strength on continuous exposure to environmental conditions. Formation of ettringite with the sulphate bearing sediments, which exhibits swelling under high moisture condition results in volumetric heaving, improper hydration of lime in organic soil, especially humic soils; and release of greenhouse gases, the most critical issue for environmental degradation, due to the presence of calcined products.

Cement, which uses lime as a major raw material, is an important component of the present day infrastructure development. The improper percentage of cement corresponding to soil type may result in excess shrinkage stress (Jayanthi and Singh 2016). In situ cement stabilization may result in intensive cracking of the pavement with an increase in cement content (Adaska and Luhr 2004). Formation of ettringite, resulting formation of cracks in sulphate rich soils is an inherent issue in cement stabilization (Rajasekaran 2005). In case

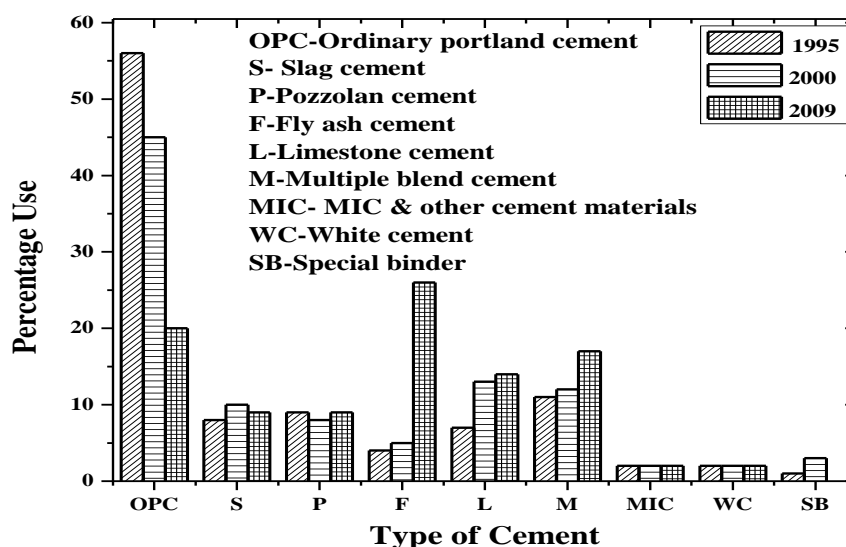


of the organic soil, suitable admixture(s) are required for cement stabilization to manage the pH and humus content (Chen and Wang 2006). In the long run, the cement industries are becoming unsustainable due to following reason.

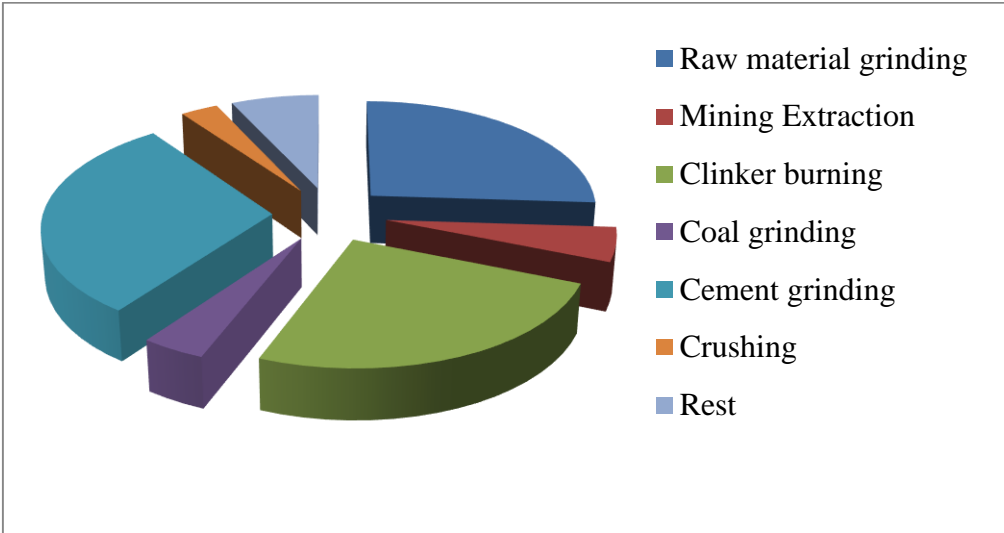
In addition to consumption of raw materials like limestone and sand, cement industry also consumes energy as - 1700 to 1800MJ/ton clinker. Every ton of cement production requires 1.5 tons of raw materials,i.e., limestone and sand (Rashad, 2014). One ton of ordinary Portland cement (OPC) is responsible for the generation of 0.94 tons of carbon dioxide (Pacheco-Torgal *et al.* 2012), through fuel emission and crushing of clinkers, etc. Other than carbon dioxide, sulfur trioxide (SO<sub>3</sub>) and nitrogen oxide (NO<sub>x</sub>), discharge from cement industries are responsible for climatic changes, which cause an increase in sea level, the occurrence of natural disasters and can be responsible for the falling of world economy in future (Rashad, 2014). Table 1.1 presents the types of gas discharged and their concentration during the production process of cement. Hence, there is a reduction in the use of OPC over the years as shown in Figure 1.2. Figure 1.3 represents the percentages of electrical energy consumed during the process of cement production.

**Table 1.1:** Exhaust gases produced from cement process (Ali *et al.* 2011)

Component	Concentration
CO <sub>2</sub>	14-33% (w/w)
NO <sub>2</sub>	5-10 of NO <sub>x</sub>
NO <sub>x</sub>	<200-3000 mg/Nm <sup>3</sup>
SO <sub>2</sub>	<10-3500 mg/Nm <sup>3</sup>
O <sub>2</sub>	8-14% (v/v)



**Figure 1.2:** Percentage use of cement over last decade (Modified from Schneider *et al.* 2011)



**Figure 1.3:** Proportion of the electrical energy required for the cement industry, Modified from Schneider et al. (2011)

Use of synthesized chemicals as an alternate cementitious material also uses natural resources. It is not economical and may contaminate the soil and groundwater. Hence, there is an increase in demand for sustainable construction practices by using the by products as an alternate resource of binder material for developing better infrastructure and producing a green environment without excessive consumption of natural resources. The most commonly used sustainable materials include fly ash from thermal power plant, ground granulated blast furnace slag from the steel industry, cement kiln dust from the cement manufacturing industry, silica fume from silicon and ferrosilicon industry, mine tailings, bagasse ash, carpet waste, red mud that is a by-product from aluminium processing plants, and rice husk ash from the agro-based industry (Jayanthi and Singh 2016). One of the biggest advantages of a sustainable material is that it does not need any separate manufacturing process, as it is a by-product. Hence, utilization of these materials for infrastructure development is a boon than a bane (Jayanthi and Singh 2016). Some of the product based sustainable material can be named as controlled low-strength material (CLSM), biopolymer treated geomaterial and alkali activated material (AAM).

Development of controlled low-strength material (CLSM) using industrial wastes is an effective way of obtaining a flowable and self-compacting material to be used as a compacted fill in infrastructure development and construction. The CLSM is similar to self-compacting concrete but with a small amount of cement and low strength and is considered as a sustainable material. It is being used in a wide range of civil engineering

applications like structural fill, conduit bedding and sides of the embankment (Siddique 2009). Due to self-levelling and early setting nature of CLSM, it is energy efficient.

Biopolymers are produced by biological systems such as microorganisms, plants, and animals are synthesized chemically. But they originated from biological starting materials such as amino acids, sugars, natural fats, or oils. Because of their unique properties and the growing awareness of environmental sustainability and stability, biopolymers have been increasingly investigated for their potential use in soil stabilization (Martin et al. 1996; Karimi 1998; Ivanov and Chu 2008; Dejong et al. 2010), dust control (Chen et al. 2013,2015) and sustainable mine filling. But efforts are still very limited.

The technology of alkali-activation is more than hundred years old, with a patent awarded to Kuhl in 1908, but the name ‘geopolymer’ was introduced by Davidovits in the 1970s after continuous research and commercial work by Purdon and Glukhovsky (Provis 2014). In the recent years, it is gaining increasing recognition and interest in its relation to the potential reduction of CO<sub>2</sub> emission in comparison to Portland cement-based materials. From AAM or geopolymer cement, emission of carbon dioxide is 80% less, with a consumption of 30 to 40% lower embodied energy compared to Portland cement (Nath *et al.* 2016). Other important properties of geopolymers are (i) excellent mechanical properties due to a high degree of Polycondensation (ii) rapid strength (iii) better resistance to acid, long-term durability (iv) high-temperature endurance (v) better fire resistance, that can sustain up to 1000°C to 1200°C, (vi) can be developed as hazardous waste disposal binder for heavy metal fixation particularly for nuclear waste solidification.

### **1.3 Aim and Objective of the Research**

The aim of the present study is to develop a sustainable geoenvironment in mining and industrial areas with suitable management and utilization of industrial and mine wastes, which can withstand aggressive conditions and is environmentally sustainable. The objective of the present study is to develop and characterize and evaluate sustainable geomaterials like (i) biopolymer modified shale and fly ash to control the air and water erosion using biopolymers xanthan gum, Guar gum and carboxyl methyl cellulose (CMC) (ii) controlled low strength material (CLSM) using coal mine overburden and industrial waste ferrochrome slag as base material and (iii) alkali activated material using ground granulated blast furnace slag (GGBS) with NaOH and Na<sub>2</sub>SiO<sub>3</sub> as the activators with mine overburden and mine tailings.

The scope of the research includes: (i) basic material characterization and evaluation using physical, chemical, geotechnical and microstructural analysis (ii) development, characterization and evaluation of sustainable geomaterials through biopolymer modification, alkali activation and blending using cementitious material (iii) identifications of possible applications of developed geomaterials.

## 1.4 Scope and Organization of the Thesis

After the brief introduction (Chapter 1), the basic concepts of sustainable geomaterials, CLSM, biopolymer treatment/ bioremediation and AAM (geopolymer) are described in Chapter 2. The literature pertaining to development and characterization of CLSM, bioremediation and AAM are critically evaluated in this chapter.

Chapter 3 describes the basic material properties of the industrial wastes used as the base materials for the development of sustainable material. The basic material properties regarding chemistry, morphology, mineralogy and other physical properties are presented and discussed vis-à-vis in comparison with the material properties available in the literature.

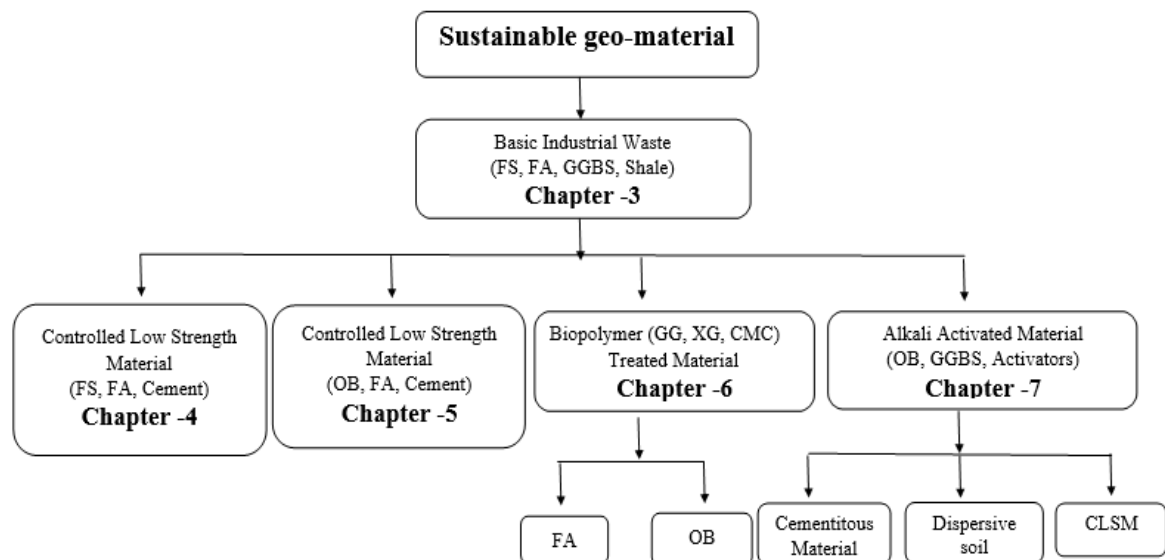
In Chapter 4 and 5 are devoted to the development of a sustainable material, CLSM using less explored industrial waste (ferrochrome slag) and mining waste (coal mine overburden), respectively. The CLSM is developed using ferrochrome slag (FS) as the base material with fly ash and cement as the cementitious material and presented in Chapter 4. In the 1<sup>st</sup> stage, the FS is characterized in terms of morphology, mineralogy, chemical properties, zeta potential, electrical conductivity (EC) and total dissolved solids (TDS). The detailed investigation of particle shape analysis of the FS using particle size analyzer through an optical microscope is another novelty of the work. Then flowability, fresh density, bleeding, segregation, unconfined compressive strength (UCS), settlement analysis, slake durability index, and California bearing ratio (CBR) values are discussed for its use as a CLSM. Similar studies are made for CLSM, developed using coal mine overburden and presented in Chapter 5.

In Chapter 6, development of biopolymer treatment for control of dispersiveness of two geomaterials pertaining to mining (shale) and industrial sector (fly ash) is discussed. The chapter focuses on stabilization of fly ash and mine overburden using biopolymer for wind and water erosion by incorporation of two natural biopolymers; guar gum (GG), xanthan gum (XG) and carboxyl methyl cellulose sodium salt (CMC). Different measures like

dispersiveness, surface resistance, water retention capacity and wind tunnel test are used to assess the effectiveness of biopolymer stabilization.

Chapter 7 pertains to the development of alkali activated material (AAM) using mining waste with another industrial waste ground granulated blast furnace as the source of cementitious material. The characterization of the developed AAM is discussed in terms of macro properties unconfined compressive strength. The sustainability of the developed AAM in terms of its serviceability is studied using slake durability index (SDI). The micro properties of the developed AAM are presented in terms of scanning electron microscope (SEM) and x-ray diffraction (XRD) to discuss the strength and durability. The development of CLSM using AAM is discussed to show the application of developed AAM. Suitability of the AAM in control of dispersiveness of soil is also discussed in this chapter.

In Chapter 8, generalized conclusions made from various studies made in this thesis are presented and the scope for the future work is indicated. The different methodology adopted for the development of sustainable geomaterial using industrial and mining wastes and their characterization is shown in a flow diagram for ready reference.



**Figure 1.4:** Flow diagram showing the organization of the main chapters



## **CHAPTER 2**

# **LITERATURE REVIEW**

### **2.1 Introduction**

As discussed in Chapter 1, the sustainable materials discussed in the present work are controlled low strength material (CLSM), biopolymer modified material and alkali activated material. The above materials are not very common in the purview of the geotechnical engineering; hence, the basic concepts of these materials are presented. The literature pertaining to development and characterization of above materials are also discussed separately as follows and finally, the critical review of above sustainable material are presented.

### **2.2 Controlled low strength material (CLSM)**

Controlled low-strength material (CLSM), a flowable self- compacting material using industrial wastes is an effective way of incorporating sustainability in infrastructure development (Folliard et al. 2008).CLSM was first introduced in the US in 1964 and is now widely used as a backfill material for utility trenches by many other countries. ACI Committee 229 Report is the main design manual and guideline used in the USA and referenced by most of the countries in which a few testing methods of ASTM are also used. The advantages of CLSM over traditional soil-compacted method are less on-site labour and equipment requirements, fast construction speed as well as feasible to use in tight or restricted-access areas. Various aspects of CLSM are discussed as follows.

#### **2.2.1 Base Materials used for CLSM**

One of the important features of CLSM is the versatility of the base material. Various efforts have been made to use the locally available materials as the same. Naik and Singh (1997) investigated the environmental impact of CLSM, consisting of fly ash and clean foundry sand, and observed that addition of foundry sand caused substantial reduction in concentration of the hazardous and compressive strength of 0.3 to 0.7 MPa. Abelleira et al. (1998) studied the corrosion resistance of CLSM developed using sand as the base

material and found to be more corrosion resistant than sand. They also suggested that resistivity measurement does not provide good indications for CLSM performance and improvement of corrosion performance in the underground applications. Efforts have been made to develop CLSM using pond ash and finely crushed sand with cement (Naik et al. 2002), spray dryer and wet fixated flue gas desulfurization (FGD) material (Butalia et al. 2004), foundry sands with bentonite content  $> 6\%$  as the fine aggregate (Dingrando et al. 2004), incineration bottom ash and cement (Razaka et al. 2009). Naik et al. (2004) observed that CLSM using high carbon fly ash showed 5 to 10 times lower electrical resistance than concrete, hence can be used for conducting electrical charge from lightening to the ground safely. Lachemi et al. (2008) developed CLSM using cement kiln dust (CKD) as the binder and observed that larger quantities of CKD showed higher drying shrinkage and lower freeze-thaw and wetting-drying resistance. Siddique (2009) studied the feasibility of CLSM using different industrial waste (fly ash, bottom ash), wood ash, spent foundry sand, cement kiln dust and scrap tire rubber. Similarly, other materials like the investigated performance of industrial waste as CLSM and mixture composed of bottom ash and cement. Sheen et al. (2014) used stainless steel reducing slag (SSRS) as a cement substitute in the production of soil-based controlled low-strength material (CLSM).

Zhen et al. (2013) studied the potential use of dewatered sludge (DS) and municipal solid waste incineration (MSWI) bottom ash as components for the production of CLSM. Bouzalakos et al. (2013) studied mixture design methodology to develop formulations of cement-based materials consisting of several components, as their properties are a function of the proportions of the components, instead of executing trial-and-error runs. Miren et al. (2013) studied the use of recycled fine aggregated in the production of CLSM and found to satisfy the required physical properties as per the requirement of structural fill. Fay et al. (2014) use CLSM for interlocking soil-cement blocks for masonry construction. Bassani et al. (2015) conducted a test on the resilient characterization of alternative CLSM formulations for application in the pavement as a substitute of granular fill materials in which fly ash is absent. The CLSM from municipal solid waste bottom ash and sediments have better compressive strength than sediment and inhibit heavy metal mobilization (Yan et al. 2014). Alizadeh et al. (2014) investigated several experiments for the assessment of a suitable CLSM to be used as a structural fill in case of an abutment construction and observed that there is a direct relationship between the compressive strength and bond



strength. Udayashankar and Raghavendra (2014) studied industrial by-product, namely, ground-granulated blast furnace slag, as a constituent material in CLSM.

### **2.2.2 Mix Design of CLSM**

There is no standard mix design method for CLSM due to flexibility in base materials used. Mostly based on past experience or trial and error, it is usually a mixture of fly ash, fine aggregate (or other waste materials), water, and a small amount of Portland cement (25–59 kg/m<sup>3</sup>) and chemical admixtures. According to American Concrete Institute (ACI 229), the upper and lower limits of 28 days unconfined compressive strength of CLSM are limited to 8.3 MPa and 0.3 MPa respectively (ACI 2013; Trejo et al. 2004). Most of the efforts have been made for high flowability (>200 mm spread) and a low compressive strength of 2.1 MPa that allows re-excavation in future, at the same time strong enough for backfilling needs (ACI 2013; Trejo et al. 2004; Naik and Singh 1997; NRMCA 2006; Pierce et al. 2003).

### **2.2.3 Flowability of CLSM**

High flowability with a slump flow value more than 200 mm is usually required for CLSM to achieve self-flowable characteristic for placement and backfilling. Due to its self-levelling and high flowability, no compaction is required at the bottom of the trench, making it easier to maintain the pipe alignment as well as less chance for settlement (Dockter 1998; Kaneshiro et al. 2001; Abelleira et al. 1998). In addition, it minimizes the working area required within the trench and perhaps, more importantly, improves labour safety (Kaneshiro et al. 2001). Depending on the type and location of the trench to be filled, it can be placed by a chute, a conveyor, a pump or buckets, and thereby can speed up the construction time and reduce the labour requirements (ACI 2013; Kaneshiro et al. 2001; NRMCA 2006). The water content and properties of the materials used are the critical factors affecting the flowability of CLSM. The flowability of CLSM increases with an increase of water content; however, more water content can lead to segregation and bleeding. The presence of a high volume of fine particles and porous materials could increase the demand for water and reduce the flowability of CLSM. Therefore, the selection of suitable materials and design a proper mix design is important to achieve the desired flowability (>200 mm) without segregation.

### **2.2.4 Re-excavatability of CLSM**

Re-excavatability is one of the critical properties for backfilling utility trenches. Generally, CLSM with an unconfined compressive strength of 0.3 MPa or less can be excavated manually (ACI 2013; NRMCA 2006). However, the strength limits for future excavation are somewhat arbitrary. For instance, mixtures with high quantities of coarse aggregate can be difficult to be removed by hand even at low strength, while CLSM prepared with fine sand or only fly ash as an aggregate can be excavated with a backhoe up to the strength of 2.1 MPa (ACI 2013; NRMCA 2006).

Based on 10 years of field performances non-shrink slurry backfills for utility trench installation used in the City of Prescott, Arizona, Brinkley and Mueller (1998) reported that slurry had been proven to be a fast and effective tool for backfilling underground utility. The hardened CLSM was also re-excavated around the pipe systems of buried trenches using standard equipment. The performance of the slurry material used in the City of Prescott had been positive over the past 10-year, with a failure rate of less than 1%. Brinkley and Mueller (1998) found that the amount of cement and water were far more critical in influencing the flow and strength characteristics than the type and size of aggregate used. Based on different excavatable flowable fill site conditions Crouch et al. (2004) all the trenches were excavated to years after placing using a Case 580E backhoe, to assess the excavation difficulty by rating from 1 to 10 (the easiest to the most difficult for excavation). However, the air-entrained EFF mixtures were easier to excavate than non-air-entrained mixtures of the same compressive strength. The excavation difficulty rating was found to be closely correlated with the two years compressive strength results (Crouch et al. 2004).

### **2.2.5 Other Properties of CLSM**

Risk of corrosion would be a major concern in buried metal materials (e.g. water pipes, drainage pipes, etc.) (Abelleira et al. 1998). A few studies (Abelleira et al. 1998; Schwerdtfeger and Romanoff 1972; Trejo et al. 2005; Halmen et al. 2005; Naik et al. 2006; Halmen et al. 2006) were conducted on the corrosion activity of steel coupons placed in simulated soil with steel coupons covered with a cement-based CLSM placed in simulated soil and it was observed that the CLSM had a better corrosion resistance compacted backfill (Abelleira et al. 1998).

Another important property for utility trench backfilling is the thermal resistivity. Installation of underground electric transmission and distribution systems involves digging a trench, laying cable, pipe or conduit, and then backfilling the trench. Totally dried CLSM has higher thermal stability and therefore might be a better option as backfilling materials comparing with sand. The self-levelling nature also eliminates the formation of large voids, which decrease the possibility of thermal runaway in CLSM (Parmar and Steinmanis 2017; Scola and Alto 2009; Williams at al. 1994).

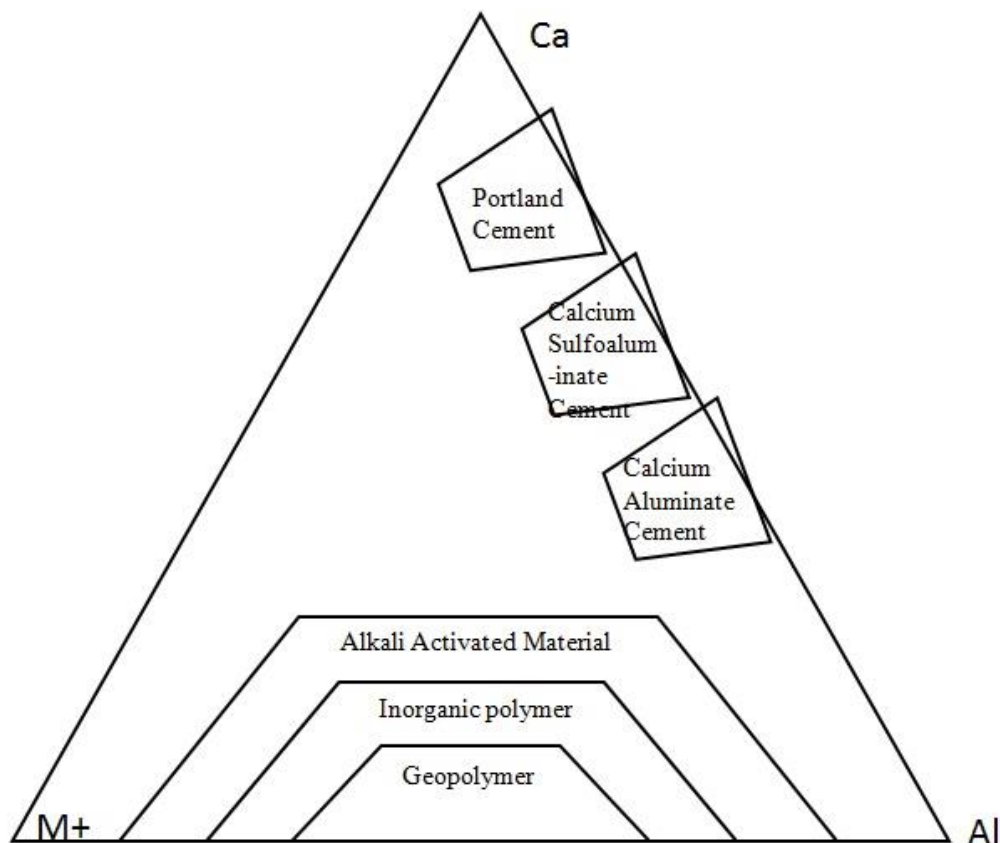
Although the material cost of fluidized thermal backfills may be higher than traditional thermal backfills (native soils), it is recommended for general usage because of its assured quality and quick installation that could speed up the construction process and reduce the overall costs of construction (Parmar and Steinmanis 2017).

### **2.3 Alkali Activated Material**

The alkali-activated material ‘geopolymer,’ is considered as the third generation cement after lime and ordinary cement for sustainable development considering global changes. The alkali-activated systems were utilized in the construction of tall buildings in Russia (Komnitsas and Zaharaki, 2007), the technology of alkali-activation is patented by Kühl in 1908. The process is similar to the geological transformation of volcanic rocks into zeolites at low temperatures and pressure, during formation of sedimentary rocks (Komnitsas and Zaharaki, 2007). Later in the 1970s, Prof. Joseph Davidovits use the word “geopolymers”, which consists of tri-dimensional aluminosilicate phase produced at low temperature from alumino-silicates source materials activated with the alkaline solution (Komnitsas and Zaharaki, 2007; Provis and Deventer, 2009) is considered as an inorganic polymer that can transform the elemental structure, polymerize and get hardened at low temperature. It also performed as a stable, non-inflammable and hard structure under high temperature (Pacheco-Torgal *et al.* 2008). After 1970, the theory of Davidovits shows the example of pyramid structures in Egypt, which was built through casting in place and endorsed to set developing as an artificial zeolitic rock (Komnitsas and Zaharaki, 2007). In between 1979 and 1995, many papers and patents were published on geopolymerisation, by Davidovits and his research group. These works of Davidovits are based on – development of solid solution related to the silico-aluminate mineral polymer formed at the temperature up to 120°C, the method of developing geopolymeric binder, development of fully hydrated aluminosilicate geopolymer etc. (Komnitsas and Zaharaki, 2007). Theory

of geopolymeric material structure assumed that – during polymerization, agglomeration of zeolitic nanocrystallites is bound together by alumino-silicate gel and develops as binder phase in geopolymer. This concept is acceptable from chemical, thermodynamic and mechanistic viewpoints, which enables the explanation of several features of existing experimental data with inclusive analysis (Komnitsas and Zaharaki, 2007). A typical difference between difference cementitious materials is shown in Figure 2.1, where  $M^+$  indicates  $Na^+$  or  $K^+$ .

The literature on alkali-activated material/geopolymer has wide spectrum concern with different aspects. Some of the aspects related to the present study like, (i) geopolymerization, (ii) base materials (iii) activators and (iv) strength are discussed here. A different milestone in the development of alkali activated material (geopolymer) is presented in Figure 2.2.



**Figure 2.1:** Classification of types of cement (Provis and van Deventer, 2014)

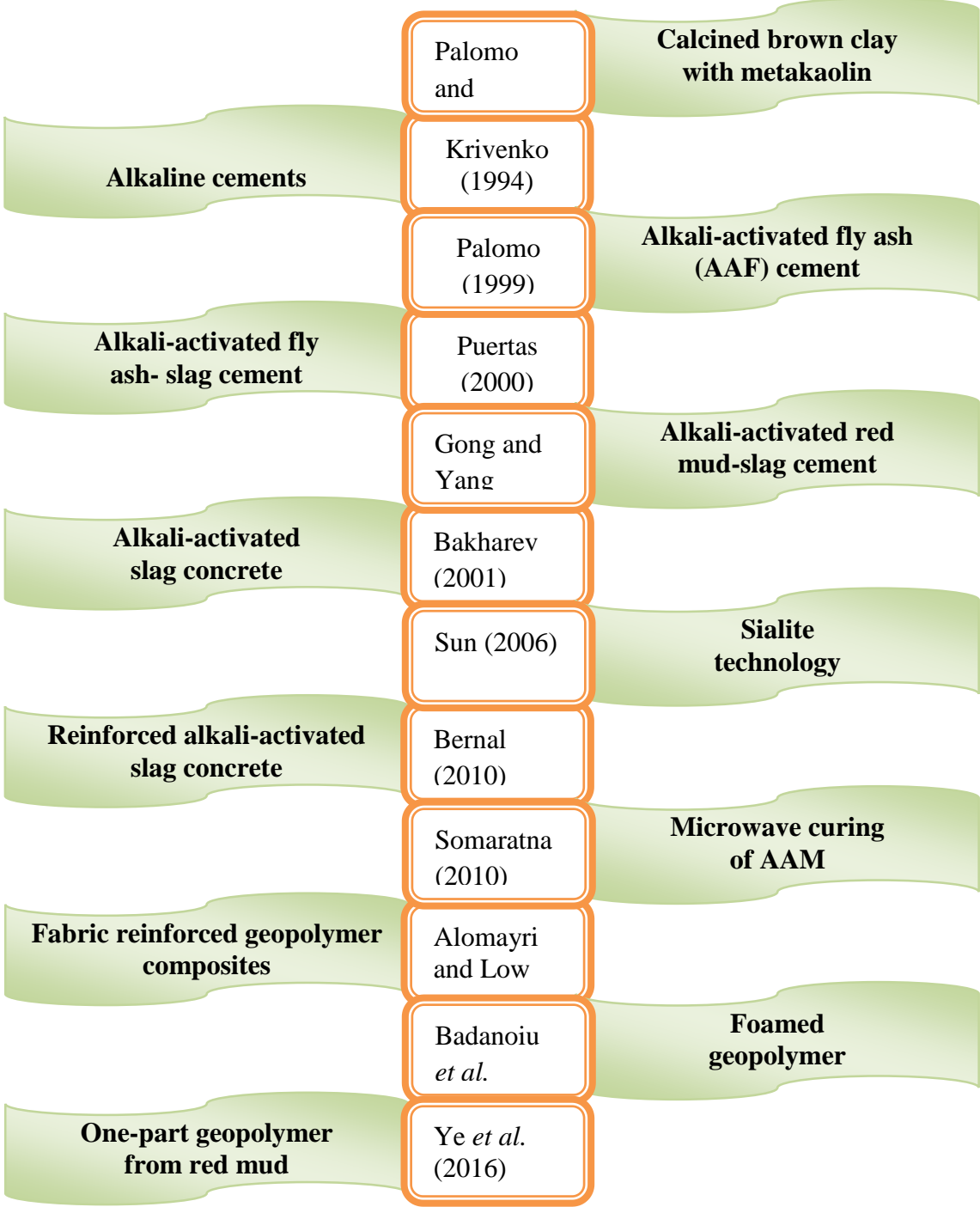
### 2.3.1 Geopolymerization

The geo-polymerization process can be described with three major steps – dissolution, polycondensation, and polymerization. The 1<sup>st</sup> step is the dissolution of reactive silicate

and aluminate tetrahedra of aluminosilicate raw materials in alkali hydroxide solution or alkali silicate solution. The 2<sup>nd</sup> phase is polycondensation of released Si- and Al-tetrahedral into amorphous or semi-crystalline oligomers and 3<sup>rd</sup> phase is further polymerization of different type oligomers and their hardening into synthetic aluminosilicates, named as geopolymer gel (Zhang *et al.* 2014).

	Author (Year)	
	Kuhl (1908) (1992)	Alkali activation system
Alkali-slag cement	Purdon (1940)	
	Glukhovsky (1965)	Alkaline cement
Geopolymer Cement	Davidovits (1979)	
	Forss (1983)	F-cement by slag-alkali-superplasticizer
Pyrament cement	Davidovits and Sawyer (1985)	
	Krivenko (1986)	R <sub>2</sub> O-RO-SiO <sub>2</sub> -H <sub>2</sub> O system
Ancient concretes analogs	Roy and Langton (1989)	
	Majundar, <i>et al.</i> 1989	C <sub>12</sub> A <sub>7</sub> –slag activation
Alkali activated slag (AAS) cement	Talling and Brandstetr (1989)	
	Wu et al. (1990)	Activation of slag cement
Rapid setting alkali-activated cements	Roy et al. (1991)	

(a)



(b)

**Figure 2.2:** Development of alkali-activated cementitious material

The dissolution of base materials particles depends on four main factors, i.e. (1) mineralogy of source material; (2) Silica and alumina content; (3) fineness or reactive surface area; and (4) morphology of source material (van Jaarsveld *et al.* 1997). In the activation solution, the degree of polymerization of predominant silica species plays an important role in the kinetics, structure, and composition of the initial gel formed. But, it

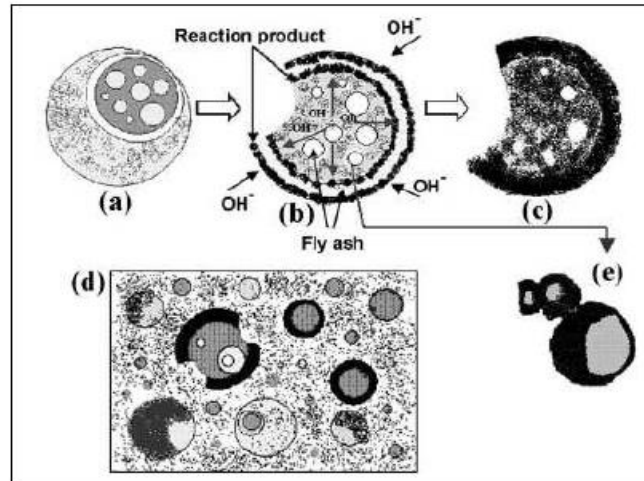
affects only the intermediate stage of the activation reaction. It reduces gel formation time by monomers and dimers, but, higher percentages of dimers leads to quick gel formation. The cyclic silicate trimer is responsible for the formation of stable gels which retards the subsequent reaction of ash. (Criado *et al.* 2008): It has three-dimensional silico-aluminate structures and varies from amorphous to semi-crystalline in nature (Davidovits, 2005). During the synthesis reaction, glassy structures (partially or totally amorphous and/or metastable) of waste materials changes into compact well-cemented composites (Palomo *et al.* 1999).

### 2.3.2 Reaction Mechanism by AAFA

A typical reaction mechanism of the AAM is presented in terms of alkali activated fly ash (AAFA). The reactive silica and reactive alumina are the major factors in developing reaction between fly ash and alkalis in alkali activated fly ash. The reaction has three stages i.e. (1) destruction-coagulation (2) coagulation-condensation (3) condensation-crystallization (Duxson *et al.* 2007). Conversion of aluminosilicate particles to synthetic alkali aluminosilicate has classified into five stages, i.e. (a) dissolution, (b) speciation equilibrium (c) gelation (d) reorganization and (e) polymerization and hardening (Duxson *et al.* 2007).

According to Fernández-Jiménez *et al.* (2005) and Rees *et al.* (2007), in NaOH-activated fly ash, Al and Si of precursor material get dissolution in an alkaline solution, followed by polymerization including nucleation. It produces “Al-rich” as an initial phase which progresses to a later phase, producing more Si-rich as final geopolymer gel (Zhang *et al.* 2014). This reaction mechanism is also similar for metakaolin, but dissolution process of fly ash is much slower than the dissolution of metakaolin (Zhang *et al.* 2014). The dissolution rate of metakaolin at 40°C is faster than fly ash at 50°C. In NaOH-activated fly ash, the dissolution rate is 70 times larger at 60°C than 20°C. Slower activation rate of fly ash is the main reason for the extension of reaction time, reflected by heat evolution peak (Zhang *et al.* 2014).

Fly ash particles are spherical in texture, which changes into different shapes depending upon nature and concentration of chemicals used, curing condition related to temperature and age, percentages of humidity, and types of additives used. Fernández-Jiménez *et al.* (2005) described the internal model of alkali-activated fly ash as shown in Fig. 2.3.



**Figure 2.3:** Descriptive model of alkali activated fly ash (Fernández-Jiménez *et al.* 2005)

At the initial stage, chemical, i.e., alkaline solution attacks one end of the spherical surface of the fly ash particle and enlarges into a large hole so that it exposes the smaller particles (Figure 2.3a). As the attack of the alkaline solution is of bidirectional type, smaller particles (uncovered) of that hole are filled by other smaller ashes either wholly or partially, i.e., from outside in and from inside out (Figure 2.3b). It causes the development of reaction products inside and outside the shell of the sphere until complete consumption of ash particles which signifies the dissolution stage (Figure 2.3 c). At the same time, a dense matrix is developed by blocking interior spaces of smaller particles (retained in the large sphere) owing to the entry and interaction of alkaline solution. But some reaction products form crusts, covering certain portions of small spheres, preventing its contact with an alkaline medium, resulting in unreacted fly ash particles (Figure 2.3 e). So in a single paste, various numbers of morphologies are observed like – unreacted particles, particles attacked by alkaline solution upholding spherical shape, reaction products and so on (Figure 2.3d). This activation process is not uniform but closely related to particle size distribution and local chemistry of fly ash (Fernández-Jiménez *et al.* 2005).

### 2.3.3 Base Materials in Geopolymer

Compositions of raw material play a major role in the formation of geopolymer. Si-rich materials (i.e., fly ash, slag, and rice husk), and Al-rich (clay like kaolin, bentonites) are the primary raw materials. A wide range of materials is used for geopolymerization which includes – pozzolanic, supplementary cementitious materials, chemicals, and mineral additives. Some other materials can be utilized as reactive fillers or additives like Portland cement, kiln dust, etc. to improve the mechanical properties (Khale and Chaudhary, 2007).



In geo-polymerization, two types of source materials are used: (a) calcined materials – fly ash, bottom ash, granulated blast furnace slag, burnt clay, meta-kaolinite, sintered red mud, construction residues, pozzolanic wastes etc. and (b) non-calcined materials – natural pozzolana, kaolinite, feldspars, rock type alumino-silicate minerals, mine tailings, etc. (Xu and van Deventer 2003). In geopolymerisation, higher reactivity is observed from the calcined source material than non-calcined material. Improved activities are observed in alkali activated calcined material due to the storage of extra energy during conversion of crystalline structure to an amorphous structure which results in the increase in compressive strength (Khale and Chaudhary 2007). Some of the materials used for alkali activation are discussed here. In other classification, aluminosilicate-based solid raw materials are under two categories, i.e., (a) from natural sources and (b) from industrial waste sources (Singh *et al.* 2015).

### **2.3.4 Calcined Materials**

Literature review on some of the calcined material used in the present study is discussed as follows.

#### **i. Fly ash**

The coal-based thermal power plants are generating a huge amount of by-products called coal ash in general consisting of fly ash and bottom ash. The storage of unutilized coal ash is a threat to the environment with occasional failure of the containment, polluting, water land and air, endangering plant and aquatic life (Kumar *et al.* 2016). The fly ash can be classified as Class F and Class C depending upon the lime percentages. If CaO content varies in between 10 to 20%, then fly ash is designated as both cementitious material and pozzolanic material and is considered as Class F fly ash. The CaO present in Class C fly ash exhibit as self-cementitious material (hydraulic activity) (Papadakis, 2000), but is not sufficient to react with all the quantity of pozzolanic material.

Different activation techniques applied to maximize the reactivity of fly ash in the absence of cement are (a) chemical activation – alkali solution, (b) mechanical activation – grinding, sieving, air separation (c) thermal activation – heating and cooling at the slow or rapid procedure. From the research point of view, it is observed that chemically activated fly ash has better strength and corrosion resistance properties, than thermal and physical activated fly ash (Saraswathy *et al.* 2003).

Reactivity of fly ash depends on – (i) fineness of particle, (ii) percentages of reactive silica present (iii) quality of coal used as fuel (Joshi and Kadu 2012). The optimal parameters for alkali-activated fly ash are (a) 40 to 50% of reactive silica, (b) high content of glassy phase, (c) lower (5%) unburnt material, (d) low content of CaO, (e) low (10%)  $\text{Fe}_2\text{O}_3$  content and (f) finer particles with 80 to 90% less than  $45\mu\text{m}$  (Fernandez-Jimenez and Palomo, 2003). The cenospheres and plerospheres are primary sources of amorphous phase/zeolite in fly ash (Kolay and Singh, 2001). The other factors which affect the initial and final products of alkali-activated fly ash (AAF) are alkali metal content, water content, thermal curing, the degree of crystallinity or amorphous, morphology and origin of fly ash, particle size, and calcium content. The workability and setting time depends upon calcium-containing compounds such as calcium silicates, calcium aluminate hydrates, and calcium–silica–aluminates (C-S-A) which are developed during geo-polymerization of fly ash. Consequently, compressive strength is affected by CaO content of fly ash and water/fly ash ratios (Jaarsveld *et al.* 2003).

It is observed that fly ash is an alumino-silicate-type mineral containing silica and alumina approximately 75 to 95% whose oxide form changes to the hydrous silico-aluminate structure under chemical activation by an alkaline solution with lime (Sunku, 2006). Its activation is accomplished by some alkali like NaOH,  $\text{Na}_2\text{CO}_3$  or  $\text{Na}_2\text{SiO}_3$  which undergoes curing process at elevated temperatures started from  $40^\circ\text{C}$  up to  $80^\circ\text{C}$  with different percentages of relative humidity (Ma, 2013). Koshy and Singh (2016) observed that calcium-based alkali activation of fly ash results in an increase in surface area, average pore sizes due to the deposition of zeolites and precipitates on the surface of unreacted fly ash spherules and can be used for heavy metal removal.

## **ii. Ground Granulated Blast Furnace Slag (GGBS)**

The GGBS is being used as the supplementary cementitious material or as a partial replacement of Ordinary Portland cement (OPC) (Collins and Sanjayan, 1999) as the blended cement has a low heat of hydration, high sulfate, better resistance to salt water, earlier and higher mechanical strength, and superior durability. Some disadvantageous qualities like quick setting, high shrinkage, along with the micro-crack formation are also observed (Collins and Sanjayan, 1999; Puertas *et al.* 2000). As the GGBS contains CaO, along with  $\text{SiO}_2$  and  $\text{Al}_2\text{O}_3$ , it can be used as both pozzolanic materials and as a calcium-based binding material. Calcium silicate hydrated (CSH) gel is the main reaction product

obtained from alkali activated slag which depends on – type and quantity of activator used, structure and composition of slag and curing condition for hardening of the reaction product exhibiting a low Ca/Si ratio. Glassy structure with the granular material is observed in granulated blast furnace slag consisting of SiO<sub>2</sub>, CaO, Al<sub>2</sub>O<sub>3</sub>, and MgO as the major components (Puertas *et al.* 2000). Alkali activation and hydration of slag strongly depend on – its particle size, chemistry, mineralogy, the quantity of amorphous phase, nature and concentration of alkaline activator, and curing condition (Xu *et al.* 2014). The appreciable silicon and aluminium content in the slag is responsible for its use as an ideal base material for geopolymer.

High early strength with greater acid resistance is observed in slag based geopolymer compared to metakaolin and fly ash based geopolymers (Singh *et al.* 2015). At an early age (3 days), slag activated by NaOH has better strength than that activated with Na<sub>2</sub>CO<sub>3</sub> (Fernández-jiménez *et al.* 1999).

### iii. Ferrochrome slag

Ferrochrome slag (FS) is a residue of combustion of chromite from a Ferro alloys company. Due to its high MgO and Cr<sub>2</sub>O<sub>3</sub> content, its disposal, removal, and storage are a big problem. One of these by-products is FS. Karakoç *et al.* (2014) activated FS from Turkey, with MgO content of 35.88% and chromium oxide of 2.12% with 33.80+25.48% of SiO<sub>2</sub>+ Al<sub>2</sub>O<sub>3</sub> with a combination of NaOH and Na<sub>2</sub>SiO<sub>3</sub> with silica modulus varying from 0.5 to 0.7 with Na<sub>2</sub>O concentration 4, 7, 10 and 12%. They observed that maximum compressive strength of paste was obtained at 7 days with 0.7 silica modulus and 7% Na<sub>2</sub>O as 17.96MPa, which decreased to 13.82 MPa at 28 days due to high alkali concentration, which makes sample vulnerable to weathering. The mortar strength with FS and sand mixture has the maximum compressive strength of 17.52 MPa after 7 days which can increase up to 22.04 MPa in 28 days under ambient condition. Its value decreased with curing at a higher temperature (60 and 80°C). Karakoç *et al.* (2016) discussed the sulfate resistance of concrete with FS, activated with NaOH and Na<sub>2</sub>SiO<sub>3</sub>, river sand and crushed aggregate. After being exposed to 7% MgSO<sub>4</sub> solution up to 180 days, geopolymer concrete was observed to show a lesser reduction in compressive strength (25%) compared OPC. Eliobol and Sengul (2016) used FS as a fine aggregate in the alkali-activated blast furnace slag mortar. In comparison to OPC and natural aggregate, the alkali-activated slag

mortar has higher strength under hot water curing and lower strength under normal water curing at 20 ° C.

### 2.3.5 Non-calcined Material

Out of various non-calcined material used as base material for AAM, studies related to natural pozzolana is discussed here.

#### Natural Pozzolana

Raw or Calcined naturally occurring materials with pozzolanic properties like volcanic ash or pumice, opaline chert and shale, tuffs, and diatomaceous earth are considered as Natural pozzolana. These are being used with lime as a construction material since early days and later on, used as blended cement for developing Portland-pozzolan cement (Turanli *et al.* 2004). Tchakoute *et al.* (2013) activated volcanic ash using NaOH and Na<sub>2</sub>SiO<sub>3</sub> solution and obtained the compressive strength of about 23- 50Mpa after 28 days. Lemouagna *et al.* (2014) discussed the alkali activation of four volcanic ashes from Cameroon which are activated with a different molar concentration of NaOH. They observed that the variation of compressive strength depends upon the Na<sub>2</sub>O/Al<sub>2</sub>O<sub>3</sub> ratio and chemical composition of the volcanic ash. There was a reduction in strength when the samples are immersed in water overnight before testing after 5 days in the oven at 90 ° C in comparison to those which were not immersed in water.

### 2.3.6 Role of Alkali Metals

Most common alkali activators used in geopolymer are hydroxide and silicate-based ones. In some studies combination of hydroxide and silicate solutions are selected as alkali activator i.e., the mixture of sodium or potassium hydroxide (NaOH, KOH) with sodium water glass (nSiO<sub>2</sub>Na<sub>2</sub>O) or potassium water glass (nSiO<sub>2</sub>K<sub>2</sub>O) (Pacheco-Torgal *et al.* 2008). Alkali element referred as M is related to alkali and alkali earth material. But in geopolymer, most of the research is based on sodium (Na<sup>+</sup>) or potassium (K<sup>+</sup>) based alkali element. In a regular hydrothermal synthesis, sodium hydroxide has a greater tendency for utilization than hydroxides of other than hydroxides of other cations like K<sup>+</sup>, Rb<sup>+</sup> or Cs<sup>+</sup> which are larger than Na<sup>+</sup> or Li<sup>+</sup> which is of smaller size (strongly hydrated) (Duxson *et al.* 2007). In higher-silicate activating solution, the role of K<sup>+</sup> is significantly increased which affect the kinetics of the reaction due to larger ion size and response to the formation of larger silicate oligomers (Duxson *et al.* 2007). Cations of original materials

or added alkali metal hydroxide have a major effect on the synthesis of polymerization (Komnitsas and Zaharaki 2007). Optimum curing and polymer properties are based on Na concentration which is responsible for sufficient charge balancing mechanism for the substitution of tetrahedral Si by Al but not in sufficient excess to form sodium carbonates by atmospheric carbonation (Barbosa *et al.* 2000). In geo-polymerization, the weight ratio of aluminosilicate powder to the alkaline solution is very high which varies as 3 to 5.5. With shorter setting time and hardening time, geopolymers are formed as tightly packed polycrystalline structure which resembles a cage-like structure (Xu and van Deventer 2000). In some cases, undissolved aluminosilicate solids behave as reinforcement of matrix (Xu and van Deventer 2000). The dissolution rate of Al and Si of fly ash is greatest in NaOH solutions and dissolution rate of Ca and Mg is greater in KOH solutions. Since  $K^+$  is more basic and larger in size compared to  $Na^+$ , it has a greater effect towards the higher rate of solubilized polymeric silicate ionization as well as dissolution and formation of larger silicate oligomers such as monomers with which  $Al(OH)_4^-$  chooses to bind. A denser and intimate polycondensation reaction of higher degree is caused by  $K^+$  due to the availability of smaller hydration sphere than  $Na^+$  and it results in stronger compressive strength with a better setting, higher specific surface area, low degree of crystallinity and a better resistance to HCl acid attack (Phair and van Deventer 2001; Komnitsas and Zaharaki 2007). Soluble silicates (sodium or potassium silicate) has higher activation rate than hydroxide solution (Palomo *et al.* 1999). The addition of water glass to the activating solution leads to the formation of ionic species during polymerization and consequently produces Si-enriched product with high mechanical strength (Criado *et al.* 2005). Geopolymers with a stable structure is developed by increasing the amount of addition of soluble silicon to the activating solution. As per the observations, the formation of aluminosilicate gel depends on – concentration of added soluble silica, and polymerization degree which depends on the type of alkaline solution (Dixson *et al.* 2007b). It is observed that the mixture of sodium or potassium hydroxide (NaOH /KOH) with sodium or potassium water glass ( $nSiO_2Na_2O/ nSiO_2K_2O$ ) is more effective than any other alkaline solution, as alkaline activators (Pacheco-Torgal *et al.* 2008). But due to ease of availability of chemicals, maximum researchers are based on the combined solution of sodium based hydroxide and silicate solution. Strength function varies with nature of alkaline activator which can be observed as  $Na_2SiO_3 \cdot nH_2O + NaOH \gg Na_2CO_3 > NaOH$  (Fernández-jiménez *et al.* 1999). It is observed that  $Na_2CO_3$  with

lower pH has lower activation rate with lower strength at earliest ages and gains higher strength than NaOH at later ages due to the effect of its anion:  $(\text{CO}_3)^{-2}$  (Wang *et al.* 1994; Fernández-jiménez *et al.* 1999).

During geopolymerization process, sodium silicate or water glass ( $\text{Na}_2\text{SiO}_3$ ) act as a binder, alkali activator, and dispersant or plasticizer which provide the additional soluble silicate (i.e.  $\text{SiO}_2$  content) and alkali content (i.e.  $\text{Na}_2\text{O}$  content) (Hafid *et al.* 2017). Sodium hydroxide accelerates the dissolution process of aluminosilicates present in the pozzolanic material (Yahya *et al.* 2015). The NaOH based geopolymer is more preferred over  $\text{Na}_2\text{SiO}_3$  based geopolymer as it easily available in the market, cost-effective and gives lesser carbon footprint (Turner and collins 2013). In geopolymerisation,  $\text{SiO}_2$  content provides silicate species to endorse the rapid exchange and oligomerization reaction between aluminate and silicate species of aluminosilicate-based material, and silicate species of water glass. However,  $\text{Na}_2\text{O}$  content helps in the dissolution of aluminosilicate-based material which affects significantly, the rate and extent of polymerization and stabilization of final products (Hafid *et al.* 2017).

In the absence of NaOH, high modulus of water glass ( $\text{Na}_2\text{SiO}_3$ ) ( $M_s = \text{SiO}_2/\text{Na}_2\text{O} = 3.22$ ) reduces the workability of Ca- rich paste, which results in low strength development. The addition of water glass ( $\text{Na}_2\text{SiO}_3$ ) to the NaOH enhances the compressive strength and rate of strength development (Oh *et al.* 2010). Use of ONLY sodium hydroxide or sodium silicate solution produced lower strength compared to the combined use of the two solutions under ambient curing temperature (Phoo-Ngernkham *et al.* 2015).

### 2.3.7 Effect of Particle Size Distribution of Binder Phase

Nature and fineness of the source materials have a major effect on strength development, durability and microstructure formation of the consequential geopolymer matrices (Ken *et al.* 2015). According to many researches, it is observed that – compressive strength, physical properties, and microstructure of the produced geopolymer paste are directly affected by particle size distribution of binder phase (Ken *et al.* 2015). Binder phase with a particles size of fibre has higher reactivity which produces geopolymer paste of denser microstructure, with higher compressive strength and refined physical properties Ken *et al.* 2015). According to a specific surface, the reaction rate is inversely affected by the particle size of the source material. But this effect is lowered when the specific surface is more than  $14\text{m}^2/\text{g}$  (Rahier *et al.* 2003). It is assumed that presence of soluble material in

finer particles results in its dissolution by alkaline activator at a higher rate producing high strength depending upon the grinding time (Antoni *et al.* 2015).

### 2.3.8 Role of Curing Temperature/ Condition/ Relative Humidity

In the case of alkali activated material, curing condition (i.e. temperature, time, relative humidity etc.) plays a crucial role in the development of micro and nanostructure, the composition of reaction products as well as the degree of reaction and also affects the mechanical properties of the material (Criado *et al.* 2012). Curing temperature is the most important factor affecting the setting of geopolymer. Increase of curing temperature affects the strength of slag mortar i.e., (a) for activated solution with NaOH, it leads to decrease in strength for all the testing ages, (b) for activated solution with Na<sub>2</sub>CO<sub>3</sub>, it leads to strength development at earlier ages and (c) for activated solution with combination of Na<sub>2</sub>SiO<sub>3</sub>.nH<sub>2</sub>O and NaOH, it leads to decrease in strength (Fernández-jiménez *et al.* 1999). Curing temperature affected the strength development at early ages and accelerated the activation process of the slag. Curing at relative humidity > 90%, geopolymer pastes (kept in an airtight container) which are dense. The compact material which is initially high-aluminium-content and silicon reacted with each other and developed improved mechanical properties over time (Criado *et al.* 2010). But curing at low relative humidity produces geopolymer pastes (kept in the direct atmosphere) which is granular, and porous termed as the weaker material whose aluminium-rich reaction products with unchanged chemical composition is maintained throughout the curing process (Criado *et al.* 2010). Compared to raw fly ash geopolymer paste, 80% increased compressive strength is observed from mechanically activated fly ash geopolymer paste at the ambient curing temperature (Temuujin *et al.* 2009b). But no X-ray crystalline phases are obtained from activating solution consists of the high concentration of silicon curing at the mild temperature (40°C) and even after longer curing period (Dixson *et al.* 2007b). It is observed that compressive strength is more homogeneous than flexural strength at different curing temperatures. The increase in curing temperature accelerates the activation process of slag which improves strength at early ages but decreases the final strength with progress in reaction, in later stages (Fernández-jiménez *et al.* 1999). For water glass activated slag cement, increase in strength is observed to be maximum for a curing of 7h at 50°C and for 16h curing at 80°C. In Na<sub>2</sub>CO<sub>3</sub> activated slag cement, the increase of curing time from 6 to 16h at 80°C has no positive impact on the strength (Wang *et al.* 1994).

Hydrate products of alkali-activated slag (AAS) cement are of the amorphous type which can transform to crystalline hydrate products at the higher temperature (Wang *et al.* 1994). The combination of steam and air curing also helps in hardening of geopolymer improving the compressive strength (Yunshenget *al.* 2009).

Dry curing is suggested for NaOH based system, with the low  $\text{SiO}_2/\text{Al}_2\text{O}_3$  ratio (Kovalchuk *et al.* 2007). Alkali-activated fly ash gets slowly hardened at ambient temperature which is subjected to mild temperature. In NaOH-activated slag cement, steam curing has the negative impact on both compressive and flexural strengths compared to water and air curing. But in NaOH-activated phosphorus slag, higher strength is observed at 8h steam curing at  $95^\circ\text{C}$  (Wang *et al.* 1994).

## 2.4 Biopolymer Stabilized Material

In various researches it has been found that microorganisms produce exopolysaccharides which have cementitious properties that help in soil aggregation, bio-clogging and bio-cementation and can be helpful in stabilization, mitigation of liquefaction potential, strengthening tailing dams, binding etc. (Ivanov and Chu, 2008). Similarly, industrially produced water-insoluble gel-forming biopolymers of microbial origin such as xanthan, chitosan, polyglutamic acid, sodium alginate, and polyhydroxybutyrate can also be used as a cementitious material for soil erosion control, enclosing of bioremediation zone, and mitigating soil liquefaction. Some of the major work in the bio-modified cementitious material is presented as follows.

**Lovley et al. (1995)** studied that microbial metal reduction has the potential to be a useful technique for the bioremediation of environments contaminated with organic sand. As recently reviewed microorganisms may enzymatically reduce other metals such as vanadium, molybdenum, copper, gold, and silver.

**Dejong et al. (2006)** studied the results of a study in which natural microbial biological processes were used to engineer a cemented soil matrix within initially loose, collapsible sand. Microbially induced calcite precipitation (MICP) was achieved using the microorganism *Bacillus pasteurii*, anaerobic bacterium pervasive in natural soil deposits. The microbes were introduced to the sand specimens in a liquid growth medium amended with urea and a dissolved calcium source. The results of both MICP and gypsum-cemented specimens were assessed nondestructively by measuring the shear wave velocity



with bender elements. A series of isotropically consolidated undrained compression (CIUC) triaxial tests indicated that the MICP-treated specimens exhibit a non-collapse strain softening shear behaviour, with a higher initial shear stiffness and ultimate shear capacity than untreated loose specimens.

**Ivanov and Chu (2008)** concluded the majority of the studies on Microbial Geotechnology at present are at the laboratory stage. Due to the complexity, the applications of microbial geotechnology would require an integration of microbiology, ecology, geochemistry, and geotechnical engineering knowledge. The aim of these applications was to improve the mechanical properties of soil so that it would be more suitable for construction or environmental purposes. Two notable applications, bioclogging and biocementation, had been explored.

**Natarajan et al. (2008)** studied various types of *Acidithiobacillus* group of bacteria which are responsible for acid mine drainage that was isolated from different Indian mines. Native bacteria such as *Thiomonas* and *Bacillus* spp exhibited higher arsenic tolerance and were capable of oxidizing arsenite to arsenate. Biological methods of remediation of acid mine drainage and bio removal of copper, zinc, iron and arsenic are illustrated. Sulphate Reducing Prokaryotes could effectively precipitate all the above-dissolved species as sulfides.

**Kavazanjian Jr et al. (2009)** investigated the application of biopolymers (xanthan gum and chitosan gum) as soil stabilizers to mitigate wind-induced erosion, either by spraying biopolymer solutions at different concentrations on the surface of the soil or mixing the solutions with soil prior to compaction. The results showed that both methods were effective in mitigating wind-induced soil erosion. The enhanced wind erosion resistance by surface-spraying came from the formation of crust on the surface of the treated soil. The mixing and compaction method could achieve similar improved resistance results but was more expensive. The effectiveness of the biopolymer treatment lasted for at least two weeks when exposed to sunlight and summer temperature.

**Dejong et al. (2010)** observed that bio-induced mineralization in soils may reduce the pore space of soil and strengthen the particle contacts, leading to increased strength and decreased permeability and compressibility.

**Landa and Santamarina (2012)** discussed sands, silts, and clayey sands inoculated with *Paracoccus denitrificans* when monitored to assess the effects of nutrient availability,

finer content, and pressure-diffusion on the evolution of nitrogen gas generation and bulk stiffness. Results show clear evidence of biogas bubble formation, earlier gas generation and entrapment in specimens with higher fines content, and a strong correlation between biogas volume and P-wave velocity. The volume of gas is correlated with the specific surface, suggesting that biogas bubble formation develops as heterogeneous nucleation and that it is directly linked to the availability of nucleation sites on mineral surfaces, which in turn also affect the degree of attainable supersaturation. Biogenic gas generation (nitrogen gas in this study) effectively reduces the bulk stiffness of the pore fluid, the P-wave velocity, Skempton's B parameter (relative to the soil shear stiffness), and the susceptibility to liquefaction

**He et al. (2013)** developed a biogas method to overcome this difficulty in injecting bacteria into soil pores. In this method, denitrifying bacteria are used to generate tiny, inert nitrogen gas bubbles in the sand. Shaking table tests using a fully instrumented laminar box are conducted on both saturated sand and sand containing microbially generated nitrogen gas bubbles. Test results showed that liquefaction occurred for saturated samples at loose states under  $a_{\max}^{1/4}$  ( $0.5 \text{ m/s}^2$ ) and at medium dense states under  $a_{\max}^{1/4}$  ( $1.5 \text{ m/s}^2$ ). The model tests have demonstrated that the biogas method is effective in lowering the degree of saturation and reducing significantly the liquefaction potential of saturated sand deposit.

**Chen et al. (2013)** studied xanthan gum and guar gum, two biopolymers that are naturally occurring and inexpensive, to stabilize mine tailings (MT). They found out that guar gum is more effective than xanthan gum in increasing the liquid limit and undrained shear strength of MT, because the guar gum solution is more viscous than the xanthan gum solution at the same concentration, the guar gum–MT particle bonding is stronger than the xanthan gum–MT particle bonding and guar gum causes a lower degree of aggregation of MT particles than xanthan gum. By comparing the undrained shear strength data with empirical equations in the literature, two new equations were proposed for predicting the undrained shear strength of the MT mixed with a biopolymer for water contents near the liquid limit, based on the liquid limit and water content, and the liquidity index.

**Chen et al. (2015)** investigated the effectiveness of xanthan gum and Guar gum, to control the dust due to mine tailing. Based on water retention test, surface resistance and wind tunnel test, as they observed that both XG and GG are effective in dust control.

**Morales et al. (2014)** analyzed the possibility of stabilizing compacted soils by a soft bio-mediated treatment. The treatment consists in adding microorganism of Bacillaceae family to the compaction water content and relying on the natural availability of urea and  $\text{Ca}^{+2}$  in the superficial soils used in the construction. Adding microorganism to the soil promotes the formation of an aggregated structure, which remains after compaction. The precipitated crystals filled the pores in the range 3–50  $\mu\text{m}$  and the pore volume of the material tends to decrease as a consequence of the progressive filling of the inter-grain/inter-aggregate porosity. The change in the pore size density function was reflected consistently in the hydraulic and mechanical behaviour of the treated soil, which presents typical features of a denser soil with respect to the untreated one. Filling part of the soil macroporosity of the treated samples affected the water retention properties inducing slightly higher air-entry value and lower water permeability at comparable void ratios. Treated soils displayed a slightly higher friction angle with no cohesion in the shear envelope, consistently with the pattern of a denser granular soil. The small-strain shear stiffness was increased, and collapse on wetting for a given initial void ratio reduced together with the post-yield compressibility on loading.

A comprehensive study on the biopolymer stabilization of soil is presented in Tables 2.1.

**Table 2.1:** Literature review in bioremediation of various soils.

SL. No	Reference	Soil or bacteria type	Investigation	Findings
1.	Lovley et al. (1995)	Soils, vanadium, molybdenum, copper, gold, and silver.	Microbial metal reduction	Microorganisms enzymatically reduce other metals for bio restoration of environments.
2.	Dejong et al. (2006)	Sand, <i>Bacillus pasteurii</i>	CIUC test, MICP	Non-collapse strain softening shear behaviour, higher initial shear stiffness and ultimate shear capacity of sand than untreated loose specimens.
3.	Ivanov and Chu (2008)	Microorganisms, natural soil	Microbial Geotechnology in bioclogging and biocementation	Application of microorganism in pore filling, particle binding reduction in hydraulic conductivity and increase in stiffness.
4.	Natarajan et.al (2008)	Mining, <i>Acidithiobacillus</i>	remediation of acid mine drainage	Bio removal of copper, zinc, iron and arsenic from mine areas.
5.	Kavazanjian Jr et al. (2009)	Soil, biopolymers (xanthan gum and chitosan gum)	Compaction, surface-spraying	Mitigating wind-induced soil erosion.

6.	Dejong et al. (2010)	Soils	bio-induced mineralization	Reduction in pore space of soil and strengthen the particle contacts, increased strength and decreased permeability and compressibility.
7.	Landa and Santamarina (2012)	sands, silts, and clayey sands, <i>Paracoccus denitrificans</i>	biogas bubble formation, bulk stiffness	Reduction in the bulk stiffness of the pore fluid, the P-wave velocity, Skempton's B parameter (relative to the soil shear stiffness), and the susceptibility to liquefaction
8.	He et al. (2013)	Sand, denitrifying bacteria	Biogas, Degree of saturation	Lowering the degree of saturation and reducing the liquefaction potential of saturated sand deposit.
9.	Chen and Zhang(2013)	Mine tailings, xanthan gum, guar gum	Liquid limit, water content, undrained shear strength, stabilization	Liquid limit and undrained shear strength increases on use of biopolymer. Guar gum–MT particle bonding is stronger than the xanthan gum–MT particle bonding, and causes a lower degree of aggregation of MT particles than xanthan gum.
10.	Morales et al. (2014)	Sand, microorganism (Bacillaceae family)	Compaction, hydraulic and mechanical behaviour	Higher friction angle with no cohesion in the shear envelope. Increase in small-strain shear stiffness, lower water permeability.

## 2.5 Summary and Critical Review

This Chapter pertains to the discussion of the sustainable material, controlled low strength material (CLSM), bio-modified cementitious material and geopolymer/ alkali activated material which can be summarized as follows:

### 2.5.1 Summary and Critical Review for CLSM

1. CLSM was first introduced in the US in 1964 and now has been widely used as a backfill material for utility trenches by many other countries. The high volume of various industrial by-products and waste materials can be utilized in CLSM to control the low strength and reduce the environmental concerns related to the disposal of these waste materials.
2. The advantages of CLSM over traditional soil-compacted method are less on-site labour and equipment requirements, fast construction speed as well as feasibility to use in tight or restricted-access areas.
3. But, there is no standard method used for proportioning CLSM, and it is generally based on previous experiences and trial-error methods.
4. The characteristics of the constituent materials and their proportions in the mixtures are the main parameters controlling the properties of CLSM including the high flowability and controlled low strength.
5. However, more research is still needed to refine the mix designs for different kinds of application (in particular incorporating with various kind of wastes) and standardized the testing methods for CLSM.
6. A limited attempt has been made to use mine tailing as a CLSM base material and no effort has been made using coal mine overburden and ferrochrome slag.

### 2.5.2 Summary and Critical Review for biopolymer modified material

1. From various researches, it has been found that microorganisms produce exopolysaccharides which have cementitious properties that help in soil aggregation, bioclogging, biocementation and can be helpful in stabilization, mitigation of liquefaction potential, strengthening tailing dams, binding etc.

2. Natural occurring biopolymers xanthan gum and guar gum are effective to stabilize the mine tailings with an increase in liquid limit and undrained shear strength of MT.
3. The guar gum is more effective due to its higher viscosity with stronger bonding with the MT particle bonding, which helps in increase in surface strength and water retention.
4. The bio-induced mineralization in soil reduces the void space thereby increasing strength, reduce the permeability and compressibility.
5. The biopolymer treatment is effective in mitigating air induced soil erosion and could last for two weeks when exposed to summer sunlight.
6. The covering fly ash with suitable soil for dust control is valid only for closed impoundments, but active fly ash pond is an important issue. Some studies have been made to stabilize the mine tailing using biopolymer, but, the study is limited to the coarse-grained mine tailing.

### **2.5.3 Summary and Critical Review for Geopolymer**

1. Geopolymer based material is environment friendly and is gaining increasing recognition and interest in its relation to the potential reduction up to 80% CO<sub>2</sub>emission in comparison to Portland cement-based materials.
2. Pozzolanic compound or alumina and silica source materials are the basic material for synthesis of geopolymer under alkali solution.
3. Compositions of raw material play a major role in the formation of geopolymer, with Si-rich materials and Al-rich are the primary raw materials. These raw materials are broadly classified as calcinated and non-calcinated with higher reactivity is observed from the calcined source material than non-calcined material due to the storage of extra energy during conversion of crystalline structure to an amorphous structure.
4. With limited use of natural pozzolanas like volcanic ash and burnt clay, the most common base materials used are industrial wastes, fly ash, bottom ash, blast furnace slag and cement kiln dust. Recently attempts are being made to use other industrial wastes like mine wastes, red mud, ferrochrome slag etc.

5. Curing temperature is the important factors in setting and compressive strength of geopolymer. High reactive silica content leads to the formation of a high amount of alkali alumino-silicate gel and results to better mechanical strength.
6. The appreciable silicon and aluminium content in the slag is responsible for its use as an ideal base material for geopolymer. High early strength with greater acid resistance is observed in slag based geopolymer compared to metakaolin and fly ash based geopolymers. At an early age (3 days), slag activated by NaOH has better strength than that activated with  $\text{Na}_2\text{CO}_3$ .
7. Applications of geopolymer as a cementitious material in soil stabilization and development of CLSM are limited.



## **CHAPTER 3**

# **BASIC MATERIAL CHARACTERIZATION**

### **3.1 Introduction**

The development of sustainable material lies in the development of suitable material from the industrial and mining wastes and has a minimum or no adverse effect on the geoenvironment (Jayanthi and Singh 2016). The present chapter describes the basic material characterization of the industrial wastes; ferrochrome slag, fly ash, granulated blast furnace slag and mining wastes; coal mine overburden and iron ore tailings. The fly ash and ferrochrome slag (FS) are rich in alumina and silica (pozzolanic material) with the very high amount of MgO and chromite percentage in FS. The granulated blast furnace slag is a non-metallic and non-toxic material consisting of silicates, aluminosilicates of calcium (Cheng and Chiu, 2003; Song and Saraswathy, 2006), having an adequate quantity of calcium, is being widely used as the cementitious material in blended cement. The coal mine overburden consists of topsoil, soft rock shale and siltstone and sandstone. In the present study, only the shale is considered. Though tailings in the iron ore mining's are less in comparison to coal mines, but still needs lots of space for its disposal. In the present study, only white and red shales are considered.

Various material properties of above waste materials have been investigated and characterized in terms of (i) physical, (ii) chemical, (c) mineralogy and (d) morphology. The results and discussion thereof are presented according to above group in different sections.

### **3.2 Material Collection and Material Characterization**

#### **3.2.1 Basic Materials Collection**

The coal mine overburden, which is predominantly shale, was collected from the coal mines, from Raigarh, Chhattisgarh, India. The iron ore mine tailings are collected from Tensa, Odisha and named as white shale for white colour overburden and red shale for red

colour overburden. For the development of CLSM, as the coal mine overburden is a very soft rock, it is crushed in a laboratory crusher machine to get both the coarse ( $> 4.75$  mm) and fine-grained ( $< 4.75$  mm) aggregate. The development of AAM was done after the collected samples were dried in an oven at 100 to 110°C and then processed in a crusher or ground in a ball mill, and a fine particle size less than 150  $\mu\text{m}$  is used for the alkali activation. Ferrochrome Slag (FS) is collected from Ferro Alloys Corp. Ltd. (FACOR), Bhadrak, Odisha, India. The FS is disposed off in the granular form of both coarse-grained ( $> 4.75\text{mm}$ ) and fine-grained aggregate ( $< 4.75\text{mm}$ ). Three types of fly ashes were collected from hoppers of the power plants of Jindal Power plant, Raigarh Chhattisgarh, NALCO, Angul, Odisha and Essar Power, Paradeep Odisha, India.

The ground granulated blast furnace slag (GGBS) was collected from Rourkela Steel Plant (RSP), Sundergarh district, Odisha, India. It was available in the granulated form, hence called as granulated slag or simply slag.

### 3.2.2 Alkali Activators

In the present study two sodium based activators, sodium hydroxide (NaOH) also named as caustic soda or white soda and sodium silicate ( $\text{Na}_2\text{SiO}_3$ ) are used. Sodium hydroxide solution is prepared from NaOH / KOH pellets (EMPLURA, Merck Socialization,  $> 97\%$  purity) and sodium silicate solution is prepared from the sodium silicate powder ( $\text{Na}_2\text{SiO}_3 \cdot 9\text{H}_2\text{O}$ ) (LOBA Chemie, Extra pure sodium metasilicate) by distilled water. NaOH has greater capability to discharge the silicate and aluminate monomers (Singh *et al.* 2015). Sodium silicate accelerates the geopolymerization process and develops geopolymer products with high mechanical strength (Hafid *et al.* 2017).

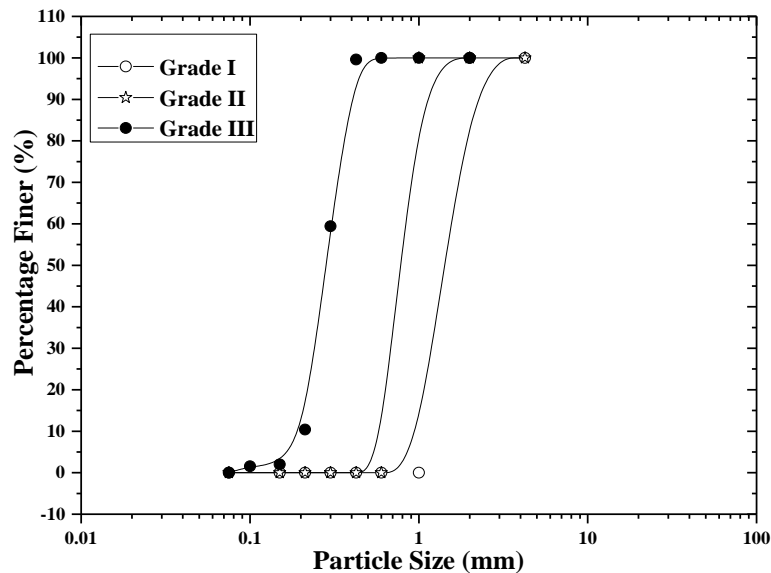
### 3.2.3 Biopolymers

In the present study three types of commercially available biopolymers, Xanthan gum (XG), guar gum (GG) and Carboxymethyl cellulose sodium salt (CMC) are used. Xanthan gum is a microbial exopolysaccharide produced by the Gram-negative bacterium *Xanthomonas Campestris* by fermenting glucose, sucrose, or other carbohydrate sources. The Guar or cluster bean (*Cyamopsis Tetragonoloba*) is an annual legume and the source of guar gum (GG). It is also known as Gavar, Guwar or Guvar bean. Guar as a plant has a multitude of different functions for human and animal nutrition but its gelling agent containing seeds (guar gum) today finds the most important use (Das *et. al.*, 2015). Both guar gum and xanthan gum used in the present study are commercially available.

Carboxymethyl cellulose sodium salt is used in drilling muds, in detergents as a soil-suspending agent, in resin emulsion paints, adhesives, printing inks, textile sizes, as a protective colloid in general. Its use in civil engineering application is very limited as an anionic polymer and found to be ineffective in reducing the expansiveness of Na-montmorillonite (Inyang et al. 2007).

### 3.2.4 Standard Sand

The Indian standard sand is available as Grade I, Grade II and Grade III and the corresponding grain size distributions are shown in Figure 3.1. To prepare mortar, Indian standard sand is collected from Pinal Corporation, Ahmedabad in India which is named as Quartzanium™ as per IS 650:1999. Figure 3.1 shows that the particle size of Grade I sand varies from 2 to 1 mm. Grade II sand varies from 1 to 0.5 mm. Grade III varies from 0.5 to 0.09 mm where 60% particles are 0.3 mm in size, 10% particles are 0.212 mm in size, and 1% particles are 0.15 mm in size. The particle size distribution of the standard sand is also discussed in terms of coefficient of uniformity ( $C_u$ ) ( $D_{60}/D_{10}$ ) and coefficient of curvature ( $C_c$ ) ( $D_{30}^2/D_{60} \times D_{10}$ ). The effective size ( $D_{10}$ ) of Grade I, Grade II and Grade III sands are 0.93, 0.58 and 0.18 respectively. The  $C_u$  of Grade I, Grade II and Grade III sands are found to be 1.69, 1.43 and 1.64 respectively. The  $C_c$  of Grade I, Grade II and Grade III sands are found to be 0.98, 0.94 and 1.02 respectively.



**Figure 3.1:** Particle size distribution of standard sand used in the present study.

### 3.2.5 Material characterizations

The chemical analysis of the basic materials (industrial wastes) is done using X-ray fluorescence (XRF) spectrometer of **PANalytical Axios** model to calculate the chemical composition in oxide form as weight percentages. The Fourier transform infrared spectroscopy (FTIR) of model **PerkinElmer Frontier made of Spectrum Two** is to identify the chemical bonds. The mineralogical analysis of the basic and developed material is investigated using X-ray diffraction instrument of the model – **Rigaku Ultima-IV, Japan** using Cu K $\alpha$  radiation and scanning range from 10 to 50 degrees / 10-70 degrees with 0.05 as the step size

The micromorphological analysis of the basic and developed materials is done using scanning electron microscope (SEM) fitted with electron dispersive X-ray (EDX) analyzer of the model - **JEOL JSM-6480LV** or FESEM of Nova Nano SEM 450 model. Energy-dispersive X-ray spectroscopy (EDS, EDX) is used for elemental analysis or chemical characterization of the surface chemistry of the material. Optical microscope of ZEISS make fitted with particle size analyzer is also used for shape analysis of FS.

## 3.3 Results and Discussion

### 3.3.1 X-Ray Fluorescence Analysis

The chemical analysis of all basic industrial wastes, i.e., NALCO fly ash, Paradeep fly ash, GGBS, and ferrochrome as per XRF analysis is presented as follows.

The chemical composition of NALCO fly ash and Paradeep fly ash is presented in Table 3.1 along with the chemical composition of other fly ashes from literature, which has been used for alkali activation. As per ASTM C618-15, NALCO fly ash and JSPL fly ash (chemical composition not presented here) belongs to Class F ( $\text{SiO}_2 + \text{Al}_2\text{O}_3 + \text{Fe}_2\text{O}_3 > 70\%$ ) with low calcium content (0.70%). But the Paradeep fly ash belongs to Class C as ( $\text{SiO}_2 + \text{Al}_2\text{O}_3 + \text{Fe}_2\text{O}_3 < 70\%$ ), but the CaO content is less than 15% (14.20%). Hence, Paradeep fly ash is termed as HCFA. It may be mentioned here that, most of the Indian fly ash belongs to Class F fly ash (Das and Yudhbir 2005). This type of fly ash is considered as a pozzolanic material due to the presence of aluminium oxide and silica content. It can be seen that for geopolymer synthesis, Class F fly ash is most widely used as the role of glass chemistry in fly ash is most necessary for pozzolanic activity (Duxson and Provis, 2008; Oh *et al.*, 2010).

**Table 3.1:** Chemical composition of fly ashes

Oxide Weight (%)	SiO <sub>2</sub>	Al <sub>2</sub> O <sub>3</sub>	Fe <sub>2</sub> O <sub>3</sub>	CaO	MgO	K <sub>2</sub> O	Na <sub>2</sub> O	TiO <sub>2</sub>	SO <sub>3</sub>	LOI
<b>NALCO FA</b>	60.36	29.48	4.51	0.70	0.63	1.36	0.15	1.80	0.27	0.74
<b>Paradeep FA</b>	36.10	15.18	14.97	14.20	8.05	1.12	0.51	0.75	8.24	0.88
<b>Typical range (Literature)</b>	27.69-63.09	17.28-32.97	3.02-13.7	1.15-30.28	0.0-8.39	0.0-3.78	0.0-4.74	-	0.0-4.1	0.0-8.06

Vassilev and Vassileva, (2007) further classified the fly ash as a pozzolanic material to Sialic (S), Calsialic (C), Ferrisialic (Fs) and Ferricalsialic (FCS), considering both Class C and Class F fly ash. The NALCO fly ash belongs to a Sialic group of highly acidic, with low calcium content and Paradeep fly ash belong to Calsialic group.

Table 3.2 shows the chemical composition of RSP blast furnace slag in oxide form along with the typical values, used for the alkali activation. The RSP slag contains 34.75% of CaO followed by 32.44% of SiO<sub>2</sub> and 17.06% of Al<sub>2</sub>O<sub>3</sub>. It also contains 11.22% of MgO, which may play a critical role in the cementitious reaction, hydration. The composition of blast furnace slag depends on – ores, fluxing stones, and impurities in the coke fed into the blast furnace (Özbay *et al.* 2016).

**Table 3.2:** Chemical composition of RSP slag

Oxide Weight (%)	SiO <sub>2</sub>	Al <sub>2</sub> O <sub>3</sub>	Fe <sub>2</sub> O <sub>3</sub>	CaO	MgO	K <sub>2</sub> O	Na <sub>2</sub> O	TiO <sub>2</sub>	LOI
<b>Present GGBS</b>	32.44	17.06	0.40	34.75	11.22	0.93	0.24	0.81	2.15
<b>Typical range</b>	21.00-41.86	5.74-21.60	0.00-5.80	33.50-56.10	0.00-12.09	0.00-1.47	0.00-1.06	0.00-1.90	0.00-2.72

Chemical composition, structure, and properties of the slag depend on source materials, which is of hydraulic type. The hydraulic activity of slag can be measured by its basicity coefficient, which can be expressed by following equations (Adam, 2009) –

$$K_b = \frac{(CaO + MgO + Fe_2O_3 + K_2O + Na_2O)}{(SiO_2 + Al_2O_3)} \quad (3.1)$$

According to basicity coefficient, slag is classified into three groups –

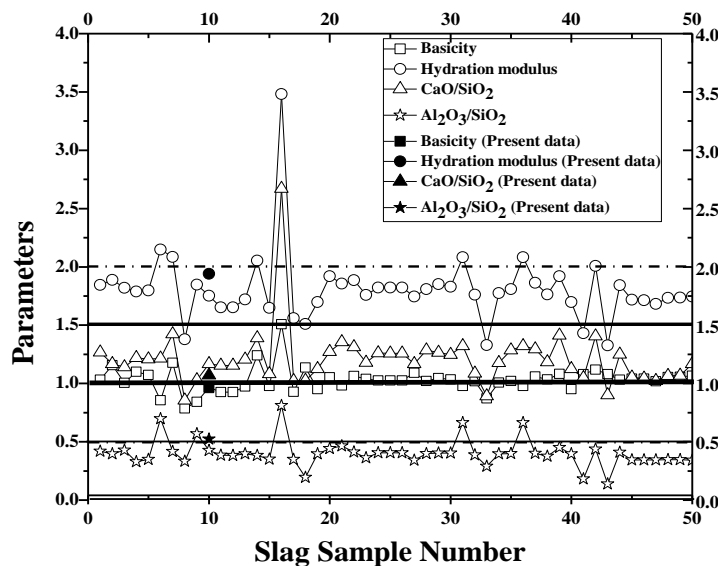
- (a) Acidic when  $K_b < 1$  (b) Neutral when  $K_b = 1$  and (c) Basic when  $K_b > 1$

Another parameter used to measure the hydraulic activity of slag is hydration modulus (HM) which is expressed as (Adam, 2009).

$$HM = \frac{(CaO + MgO + Al_2O_3)}{SiO_2} \quad (3.2)$$

For good hydration property, HM of slag should exceed 1.4 (Adam, 2009). Figure 3.2 shows the different parameters of the slag and the limits as proposed by different investigators as collected from different kinds of literature including the present slag. Though as per basicity coefficient ( $K_b = 0.96$ ), the present slag is considered as acidic type (Adam, 2009) and has a good hydration modulus (HM) as 1.94, which is greater than 1.4. The slag can act like both cementitious and pozzolanic material. The  $CaO/SiO_2$  ratio as  $1.07 > 1.0$  and the  $Al_2O_3/SiO_2$  ratio of 0.52, indicate the suitability of present slag as a suitable material for alkali activation (Tailing and Brandstetr, 1989; Adams, 2009). It is also found that most of the slag used for alkali activation satisfies the conditions,  $0 < CaO/SiO_2 < 2.0$  and  $0.1 < Al_2O_3/SiO_2 < 0.6$  (Tailing and Brandstetr, 1989).

Basicity and alkalinity are different. Basicity directly depends on pH scale whereas alkalinity is how much acid is needed to lower the pH into a significant acid value. But generally, these values are used interchangeably.



**Figure 3.2:** Different parameters of the slag used for the alkali activation along with the present slag

Table 3.3 shows the chemical composition of ferrochrome slag (FS) in oxide form along with the maximum, minimum, and average values of the limited data available in the literature. The present FS has MgO-24.94% as the major compound followed by alumina-

21.58% and silica-21.28%, and  $\text{Cr}_2\text{O}_3$ -19.46%. The utilization of the present ferrochrome slag is limited due to high MgO and  $\text{Cr}_2\text{O}_3$  content. It also has calcium and iron contents as 4.07% and 5.89%, respectively. The chemical composition of present FS is within the limits of the data available (Table 3.3). Most of FS are biased towards  $\text{SiO}_2 + \text{Al}_2\text{O}_3$  with a good amount of  $\text{CaO} + \text{MgO}$ . Karakoç *et al.* (2014) used FS from Turkey, with MgO content of 35.88% and Chromium oxide of 2.12% with 33.80+25.48% of  $\text{SiO}_2 + \text{Al}_2\text{O}_3$  for alkali activation. Elibol and Sengul (2016) used FS with 23.2% of CaO, 5.7 % of MgO and 7.90+ 59.70% of  $\text{SiO}_2 + \text{Al}_2\text{O}_3$  for activation with different activators. As the  $\text{CaO}/\text{SiO}_2$  ratio is  $0.19 < 2.0$ , Cr exist as magnesiochromite spinel phase (Sahu *et al.* 2016), which is stable against oxidation and is resistant to dissolution in aqueous media (Cabrera *et al.* 2012; Kilau *et al.* 1984).

**Table 3.3:** Chemical Composition of Ferrochrome Slag

Constituents	Present study (% by Weight)	Literature Values		
		Max	Min	Average
$\text{Al}_2\text{O}_3$	21.58	26.39	5.86	16.98
$\text{SiO}_2$	21.28	59.7	19.6	32.89
MgO	24.94	35.88	5.70	20.35
CaO	4.07	47.35	1.10	21.22
$\text{Cr}_2\text{O}_3$	19.46	47.35	2.00	10.71
$\text{FeO}/\text{Fe}_2\text{O}_3$	5.89	19.53	2.12	9.95

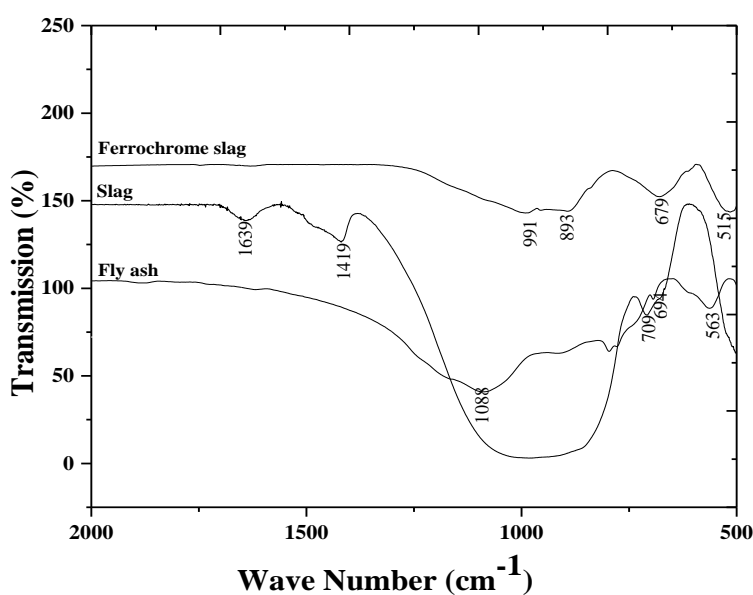
### 3.3.2 Fourier Transform Infrared Analysis

The FTIR analysis of fly ash, slag, and ferrochrome slag using samples of 13 mm pellet diameter, mixed with potassium bromide (KBr) and tested in the range of 2000 to 500  $\text{cm}^{-1}$  is presented in Figure 3.3. In fly ash, very thin and small bands are detected at  $\sim 1619 \text{ cm}^{-1}$  indicating absorbed water on the surface of the sample. The band at  $\sim 1088 \text{ cm}^{-1}$  represents the presence of silicate ions (Derrick *et al.* 1995) which signify the presence of quartz (Gao *et al.* 2015). However, band observed at  $\sim 798 \text{ cm}^{-1}$ ,  $\sim 692 \text{ cm}^{-1}$  and  $\sim 564 \text{ cm}^{-1}$  signify the presence of amorphous Si–O–Si and O–Si–O bond (Coates, 2000; Mužek *et al.* 2012). The band at  $\sim 564 \text{ cm}^{-1}$  is an indication of mullite due to the formation of the octahedral aluminium bond (Fernández-Jiménez and Palomo, 2005; Mužek *et al.* 2012).

Similarly, the tetrahedral aluminium bond is observed at  $\sim 915\text{ cm}^{-1}$  (Fernández-Jiménez and Palomo, 2005).

In granulated slag, bending band at  $1639\text{ cm}^{-1}$  indicates water molecule adsorbed on the surface of a sample consisting of a single band (Derrick *et al.* 1995). The narrow band at  $\sim 1419\text{ cm}^{-1}$  in slag conforms to the presence of calcite ( $\text{CaCO}_3$ ) or calcium carbonate due to the formation of O–C–O and is observed to be smooth, symmetrical type (Derrick *et al.* 1995; Bernal *et al.* 2012). In raw granulated slag, partial carbonation is identified due to the consequence of weathering during storage (Bernal *et al.* 2012). The wide stretching band at  $\sim 981\text{ cm}^{-1}$  indicates the presence of silicate ion (Coates, 2000). The narrow bending band at  $\sim 709\text{ cm}^{-1}$  is observed due to the presence of carbonate (Derrick *et al.* 1995). It also signifies T–O bond which consists of double or single rings of tetrahedral bond represented by  $\text{TO}_4$  (T refers to Si and Al) (Fernández-Jiménez and Palomo, 2005).

In ferrochrome slag, narrow stretching band at  $\sim 991\text{ cm}^{-1}$  and  $\sim 893\text{ cm}^{-1}$  are gradually lowered and bending vibration type at  $\sim 679\text{ cm}^{-1}$  and  $\sim 515\text{ cm}^{-1}$  which signify the presence of Si–O bond (Derrick *et al.* 1995).



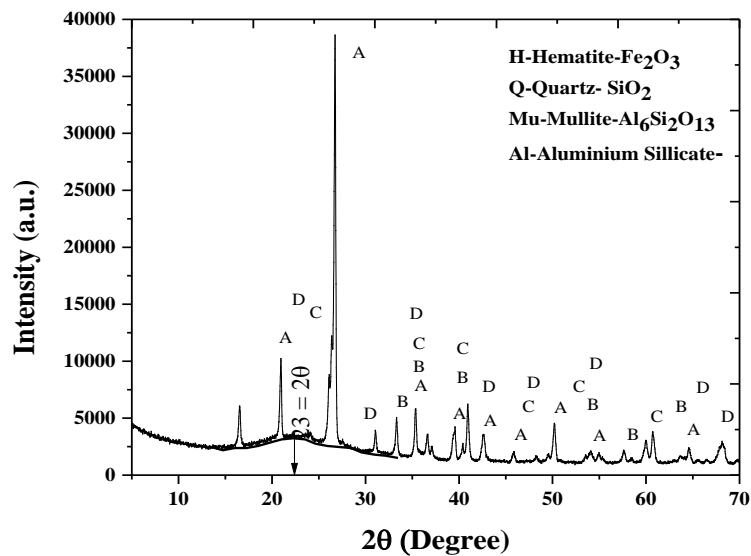
**Figure 3.3:** FTIR spectra of red mud, fly ash, granulated slag, and ferrochrome slag

### 3.3.3 X-Ray Diffraction Analysis

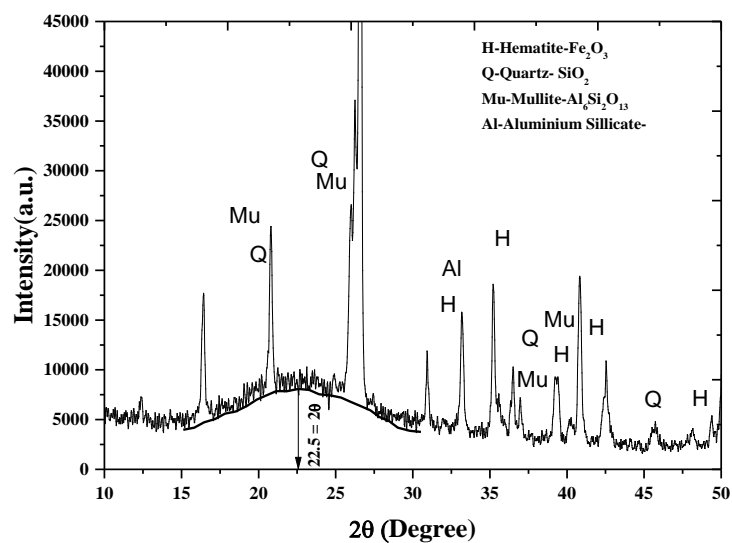
Figure 3.4 shows the XRD analysis of NALCO fly ash which contains quartz ( $\text{SiO}_2$ ), mullite ( $\text{Al}_6\text{Si}_2\text{O}_{13}$ ), and hematite ( $\text{Fe}_2\text{O}_3$ ) as the major minerals with calcite ( $\text{CaCO}_3$ ), albite ( $\text{NaAlSi}_3\text{O}_8$ ), and anorthite ( $\text{CaAl}_2(\text{SiO}_4)_2$ ) as minor compounds. Similar compositions are observed in JSPL fly ash. XRD pattern of NALCO fly ash with a broad



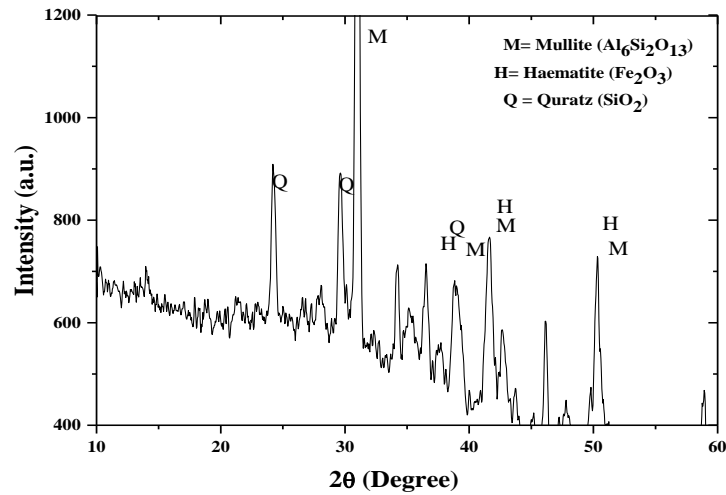
amorphous hump (Bignozzi *et al.* 2014) in between  $15^\circ$  to  $30^\circ$  and hump position at  $22.5^\circ$  ( $2\theta$ ) and for JSPL fly ash at hump position at  $23^\circ$  ( $2\theta$ ) indicates the presence of an alumino-silicate type of glassy phase (Das and Yudhbir, 2006). Though, the Paradeep fly ash shows quartz ( $\text{SiO}_2$ ), mullite ( $\text{Al}_6\text{Si}_2\text{O}_{13}$ ), and hematite ( $\text{Fe}_2\text{O}_3$ ) as the major mineral phases, the broad amorphous hump in between  $25^\circ$  to  $35^\circ$  with peak of the hump 27 shows the presence of both alumino-silicate and calcium- aluminate type of glassy phase (Das and Yudhbir, 2006).



(a)



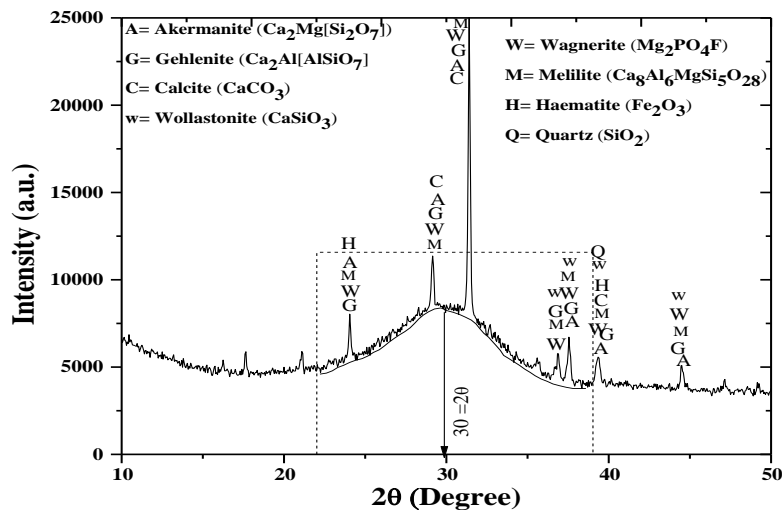
(b)



(c)

**Figure 3.4:** XRD analysis of (a) NALCO fly ash (b) JSPL fly ash and (c) Paradeep fly ash.

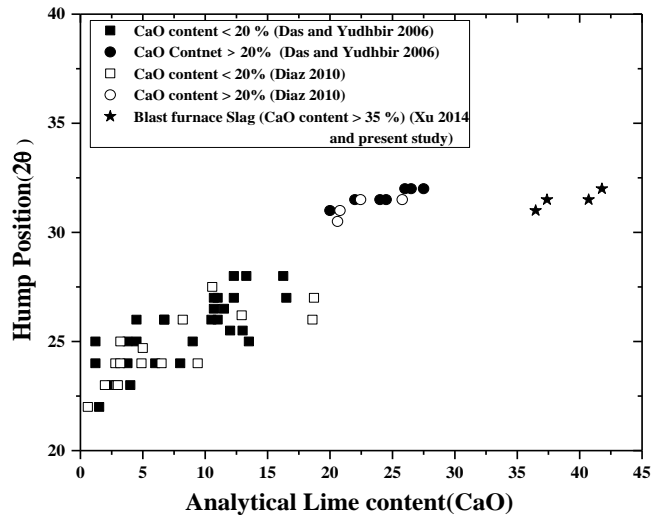
Similarly, GGBS contains minerals, Akermanite ( $\text{Ca}_2\text{Mg}[\text{Si}_2\text{O}_7]$ ), Gehlenite ( $\text{Ca}_2\text{Al}[\text{AlSiO}_7]$ ), Wagnerite ( $\text{MgFe}_2\text{PO}_4\text{F}$ ), and Melilite ( $\text{Ca, Na}_2(\text{Al, Mg, Fe}^{2+})[(\text{Al, Si})\text{SiO}_7]$ ) (Figure 3.5). Wide humps are observed in between 20 to 40°, centred at 30° and conform to a significant number of amorphous phases. The presence of amorphous structure leads to the development of high pozzolanic activity and binding property which conforms in RSP slag (Karakurt and Topçu, 2012).



**Figure 3.5:** XRD analysis of RSP GGBS

Diamond (1984) and Das and Yudhbir (2006) suggested a relationship between the quality of glass content to that of hump position ( $2\theta$ ). Figure 3.6 shows the variation of analytical lime content ( $\text{CaO}$ ) and the hump position as per Das and Yudhbir (2006) with additional

data available in literature and present data. It can be seen that there are two distinct groups of fly ashes, one with  $< 20\%$  of CaO and other with  $> 20\%$  of CaO. It may be mentioned here that the location of hump position defines the quality of glassy phase, with the better quality glassy phase at higher CaO content ( $2\theta$  value) (Das and Yudhbir (2006). Hence, the present GGBS contains a good amount of glassy phase.



**Figure 3.6:** XRD plot of (a) FA and (b) GGBS

Figure 3.7 shows the XRD analysis of ferrochrome slag. It consists of predominantly forsterite, olivine, spinel, hematite and quartz and similar observations are made by Panda *et al.* (2013). It consists of a wide hump which lies in between  $20$  to  $35^\circ$  producing angle  $2\theta$  as  $27^\circ$ . The hump position of XRD plot of FS indicates the presence of the amorphous phase of aluminosilicate glass, which is good for the pozzolanic reaction. Niemela and Kauppi (2007) also presented similar observations. However, it can also be seen that there is no hump for the magnetically separated samples and quartz is absent, which indicates presence of iron-bearing minerals and amorphous phase. However, in the present study, the FS is considered as whole instead of any separation. The XRD analysis of Indian standard sand (Figure 3.8) shows the presence of pure quartz in it. The XRD analysis of coal mine overburden shows, the major minerals present are quartz, kaolinite and calcite and it is denoted as black shale. Other details about the same are presented in Chapter 5 and 6.

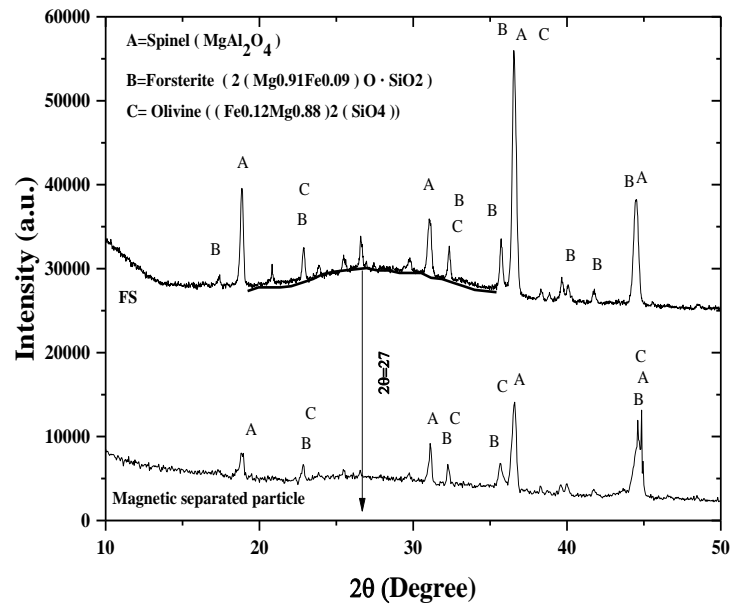


Figure 3.7: XRD plot of whole ferrochrome slag and magnetically separated particles.

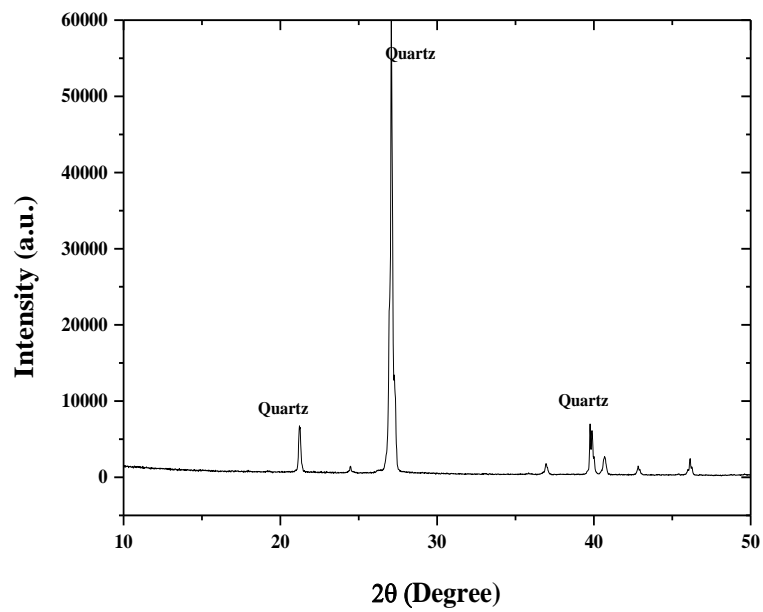


Figure 3.8: XRD plot of Indian standard sand.

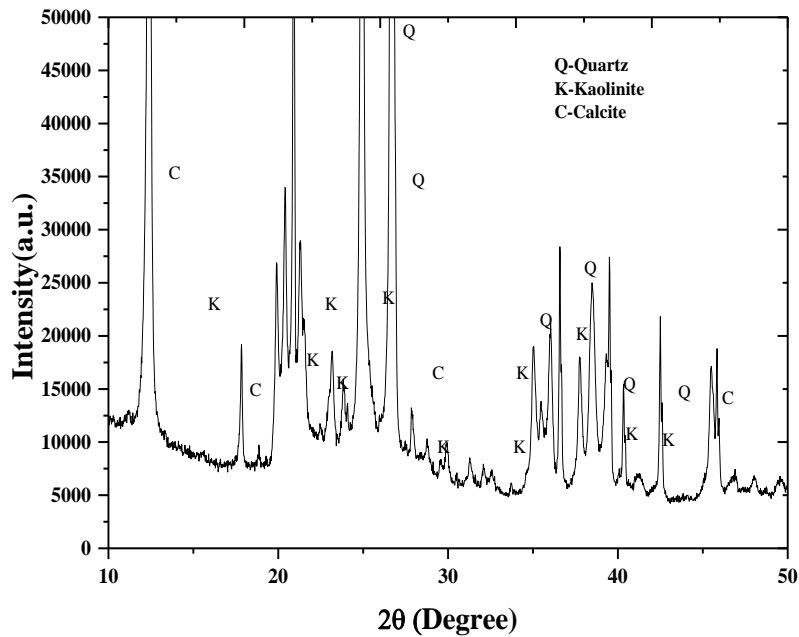
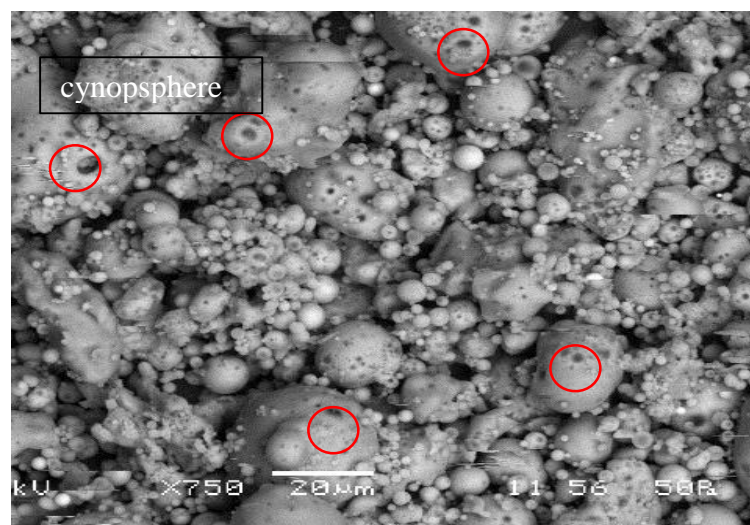


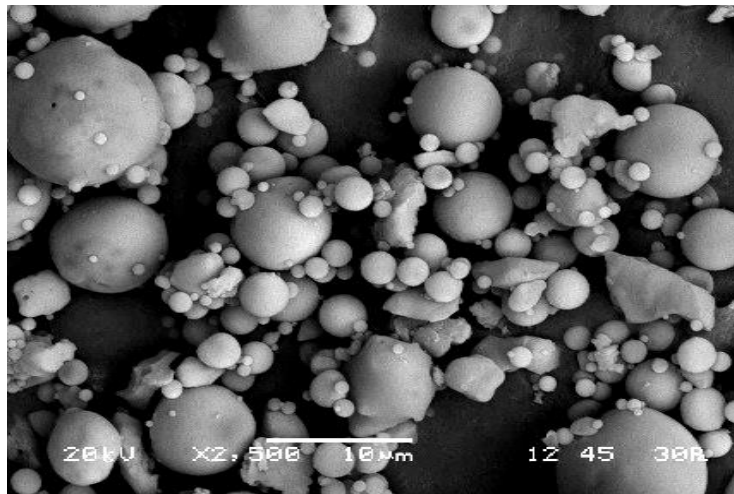
Figure 3.9: XRD plot of coal mine overburden shale.

### 3.3.4 Scanning Electron Microscope Analysis

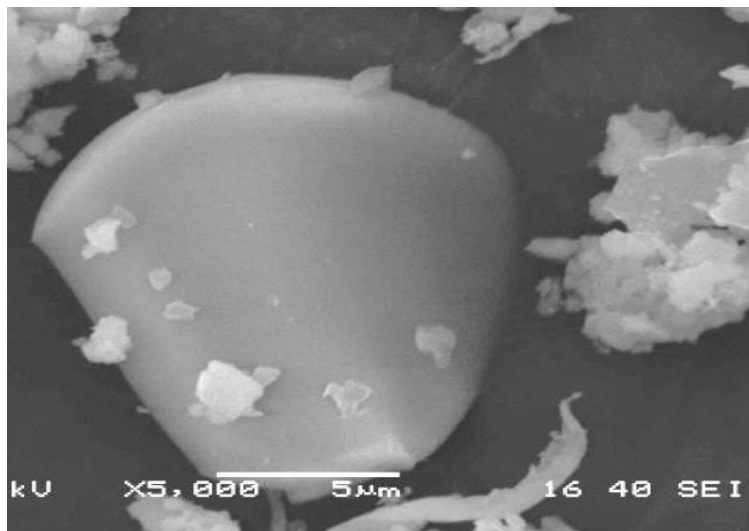
Figure 3.10 a and b show the particle morphology of JSPL and NALCO fly ash, respectively and particles are mostly spherical with a smooth surface known as cenospheres, with particle size varying from 1- 100 $\mu$ m (Das and Yudhbir 2005). The morphology of Paradeep fly ash shows the presence of irregularly shaped particles along with smooth spherical particles. Figure 3.10 (d) shows the particle morphology of RSP slag showing an angular shape with sharp edges, smooth surface, and exhibits an irregular pattern which is retained after ball mill grind with no agglomeration of particles (Kumar *et al.* 2005).



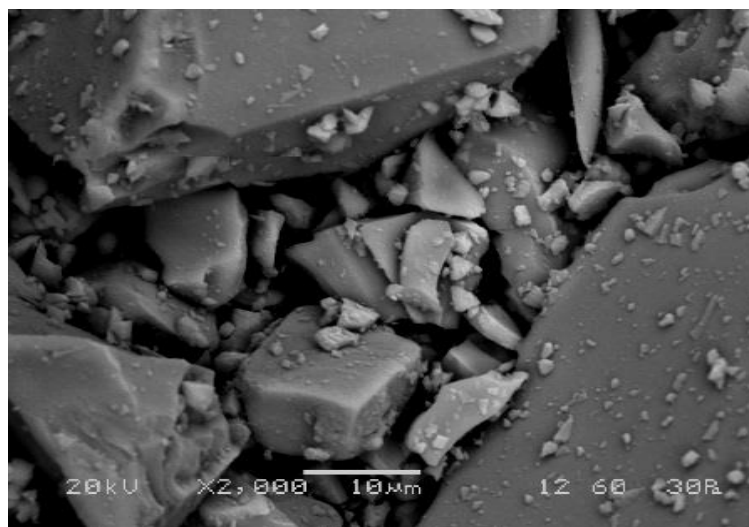
(a)



(b)



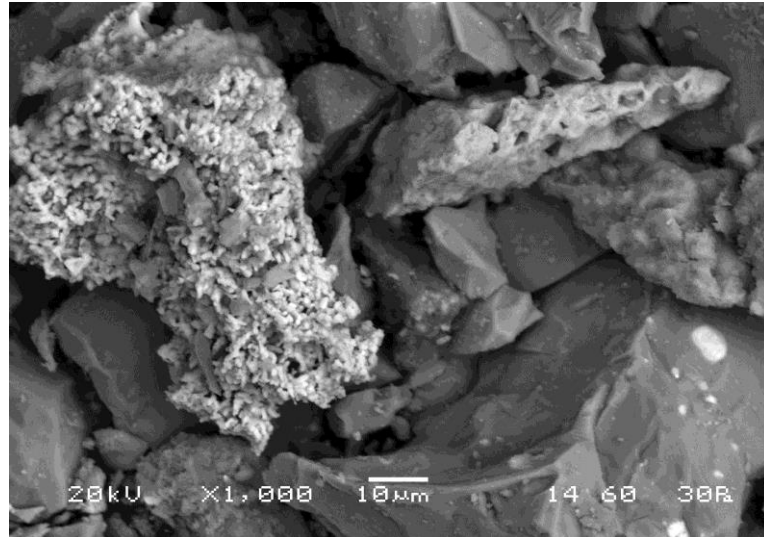
(c)



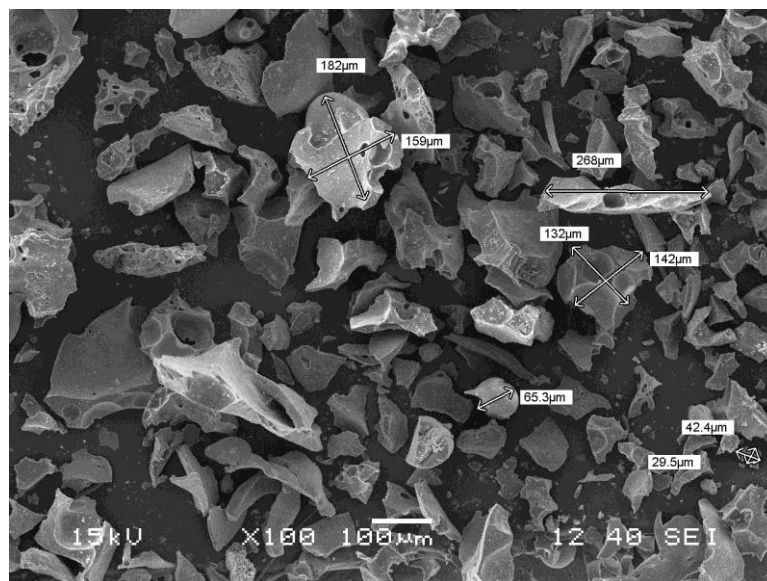
(d)

**Figure 3.10:** SEM micrograph of (a) JSPL fly ash (b) NALCO fly ash, (c) Paradeep fly ash (d) ground granulated blast furnace slag (GGBS)

Figure 3.11 represents SEM image of FS, which indicate that FS particles are irregular in shape with agglomerated particles. However, the magnetic part of the FS contains mostly angular particles of different sizes and typical size ranges varying from 63  $\mu\text{m}$  to 150 $\mu\text{m}$ .



(a)



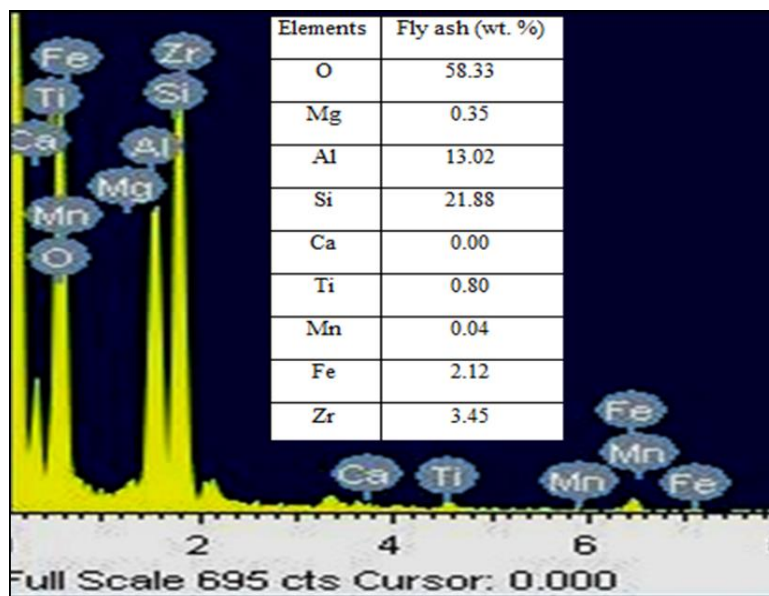
(b)

**Figure 3.11:** SEM microphotograph of (a) Ferrochrome slag and (b) magnetic part.

### 3.3.5 Energy Dispersive X-Ray Analysis

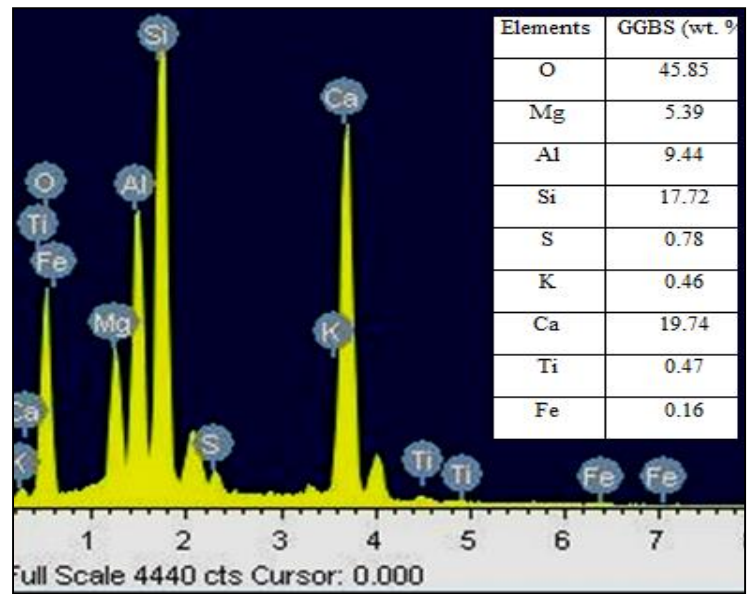
Figure 3.12 (a) shows the weight percentages of different elements and EDX image of NALCO fly ash. It shows that fly ash particles are abundant in Si (21.88%) and Al (13.02%) with minor constituents of Mg (0.35%), Ti (0.80%), Fe (2.12%), Zr (3.45%), and Mn (0.04%) (Marrero *et al.* 2007). As the surface chemistry is very important for alkali activation reaction, the presence of a higher percentage of alumina and silica on the

surface of fly ash will help in developing pozzolanic properties. Figure 3.12 (c) shows the weight percentages of different elements and EDX image of RSP slag particles. It consists of Ca (19.74%), Si (17.72%), Al (9.44%), and Mg (5.39%) as the major constituents and Fe (0.16%), S (0.78%), K (0.46%), and Ti (0.47%), as the minor constituents. The surface chemistry is close to the overall chemistry of the slag. The presence of higher amount of Ca leads to the enhancement of binding properties. In general, EDX spectrum of FS was found to vary with particles. The energy-dispersive X-ray (EDX) test analysis of whole FS (Fig. 3.13a) and the magnetically separated FS (Fig. 3.13b) are different. It can be seen that though, Fe (iron) and chromium (Cr) content are more in magnetically separated FS, other elements like Mg, Al, Si and Ca are also present in it. This is due to the presence of different spinel structure of FS containing Mg, Al, etc. as discussed earlier and also shows the heterogeneous nature of the FS particles. Hence, an optical microscope photograph of magnetic separated FS is presented in Fig. 3.14 and bright and glossy surface represent the position of light alkali metals like Mg, Al and Si. This is a good sign of pozzolanic reactivity of FS, which will be discussed in Chapter 4.



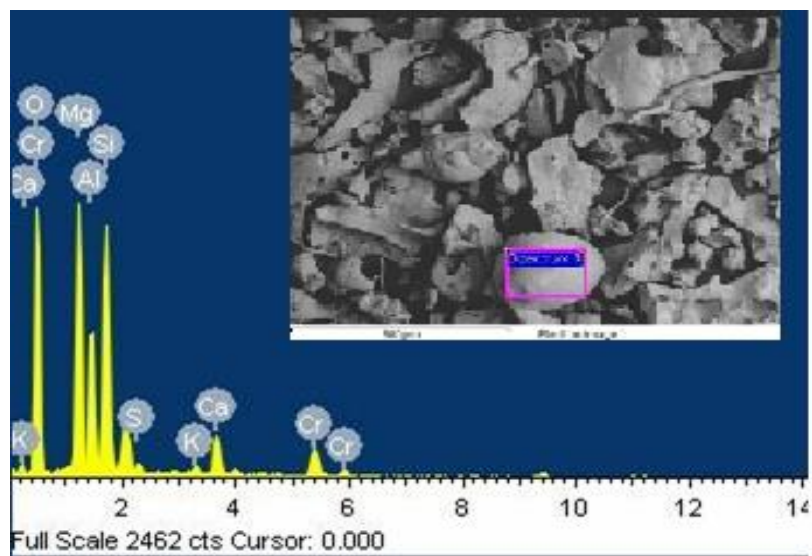
(a)





(b)

Figure 3.12: EDX analysis of (a) NALCO fly ash and (b) GGBS particles



(a)

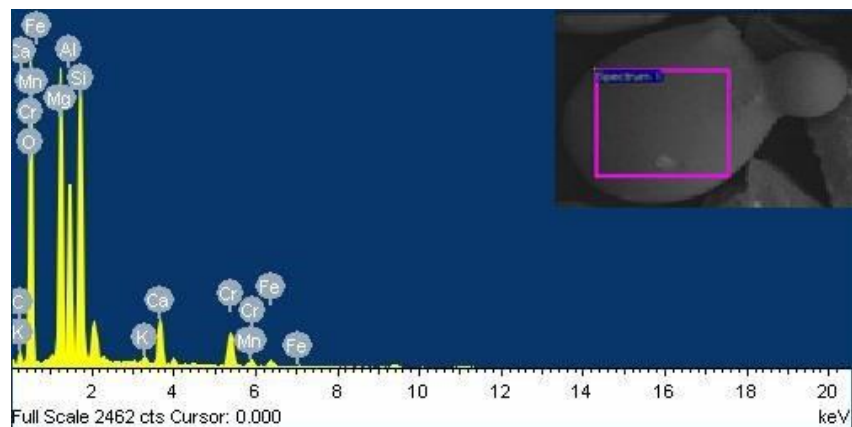
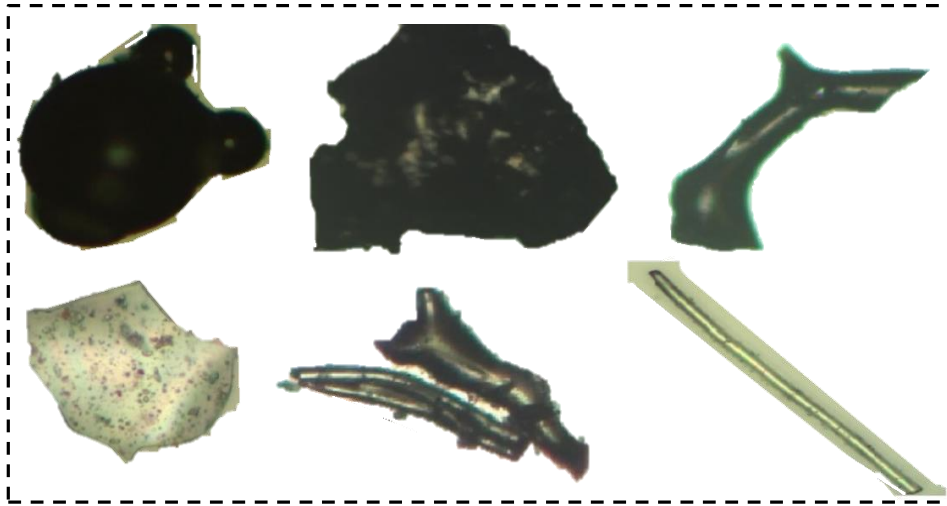


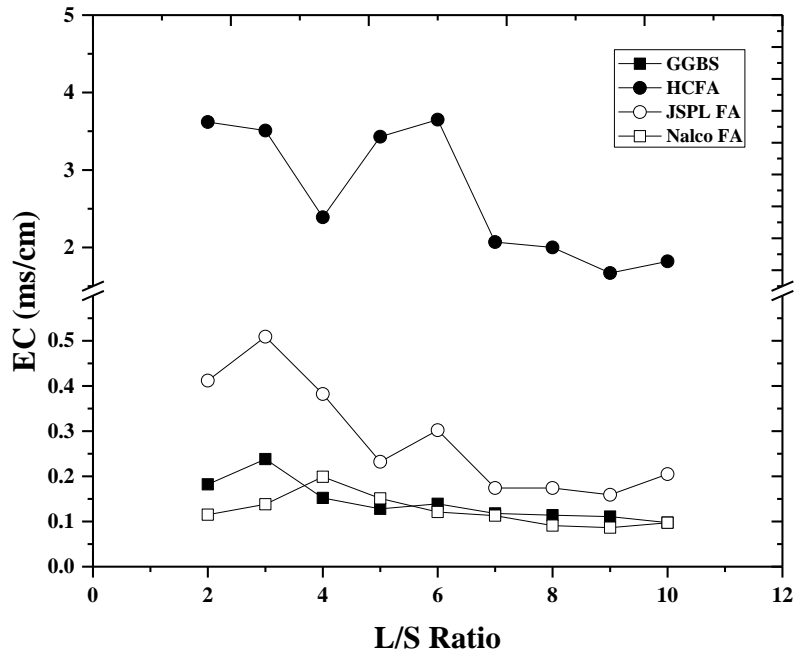
Figure 3.13: EDX analysis of (a) typical ferrochrome slag sample (b) magnetic separated particles



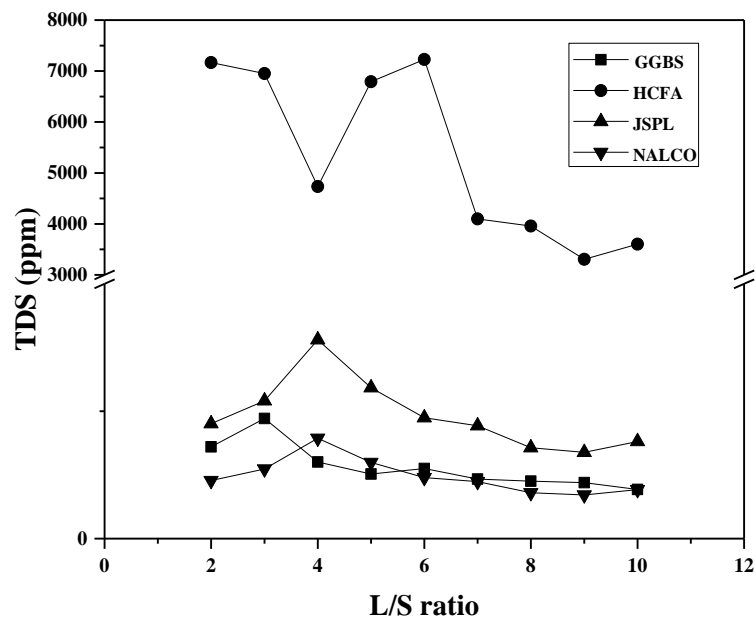
**Figure 3. 14:** Optical microscope analysis of magnetically separated part.

The electrical conductivity (EC) total dissolved solids (TDS) and pH of different fly ashes and GGBS are also studied at different L/S using HACH HQ40d and shown in Figures 3.15, 3.16, 3.17, respectively. It can be seen that both EC and TDS of the materials decreased as the L/S increases. Similar trends are observed for TDS as EC and TDS are related. For the same L/S value, HCFA shows the higher value of EC and TDS than GGBS, JSPL and NALCO fly ash. Though based on chemical content, GGBS contains higher CaO content than HCFA. High TDS and EC may be due to the presence of free lime and sulphate content.

The variations of EC, TDS and pH of coal mine overburden (black shale) and iron ore tailings (white and red shale) are shown in Figures 3.18, 3.19 and 3.20, respectively. It can be seen that EC of black shale is higher than that of white and red shale (Figure 3.18). Similar, trend is observed for TDS (Figure 3.19) of all samples. It may be mentioned here that white and red shale is from the iron ore mines. The black shale is highly acidic, whereas white and red shale is basic. The variations of EC, TDS and pH are very sensitive to L/S ratio for black shale, but the variations for white and red shale is negligible. This aspect will be discussed in the following chapters.



**Figure 3.15:** Variation of EC of GGBS, HCFA, JSPL fly ash and NALCO fly ash with liquid to solid (L/S) ratio.



**Figure 3.16:** Variation of TDS of GGBS, Paradeep fly ash (HCFA), JSPL fly ash and NALCO fly ash with liquid to solid (L/S) ratio.

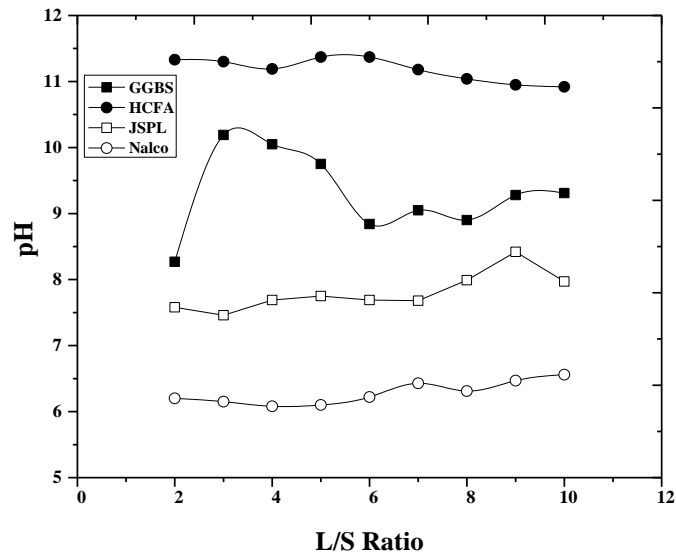


Figure 3.17: Variation of pH of GGBS, Paradeep fly ash (HCFA), JSPL fly ash and NALCO fly ash with liquid to solid (L/S) ratio.

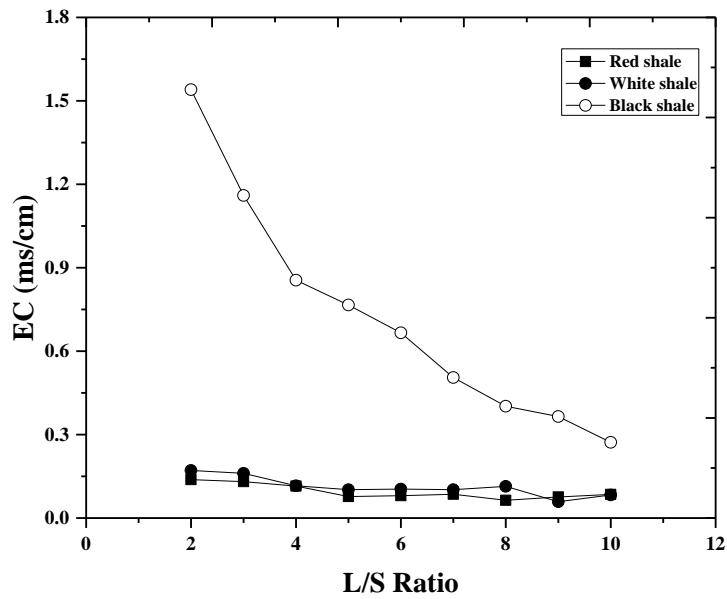
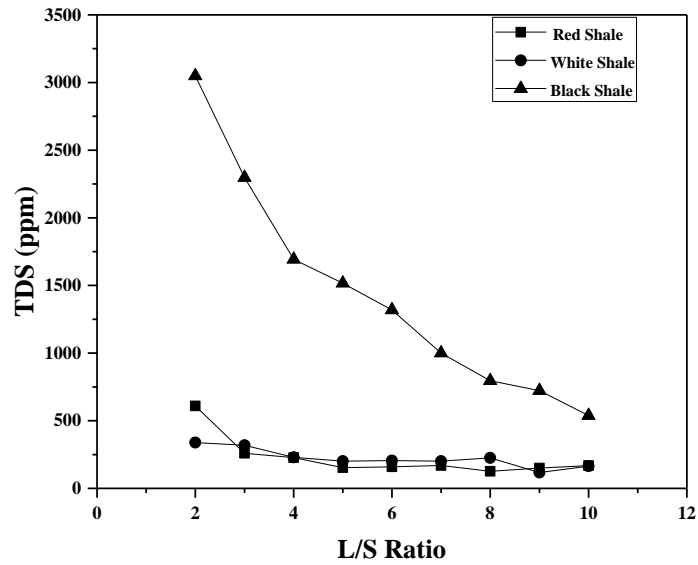
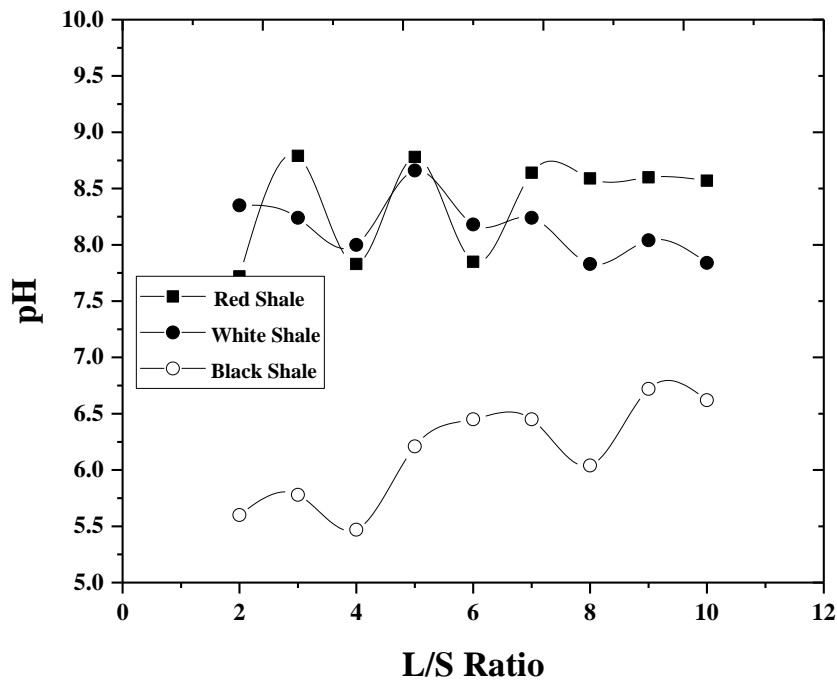


Figure 3.18: Variation of EC of red shale, white shale and black with liquid to solid (L/S) ratio.



**Figure 3.19:** Variation of TDS of red shale, white shale and black with liquid to solid (L/S) ratio.



**Figure 3.20:** Variation of pH of red shale, white shale and black with liquid to solid (L/S) ratio.

### 3.4 Summary

The present chapter describes the basic material characterization of the industrial wastes; fly ash, ferrochrome slag, granulated blast furnace slag. The material characteristics regarding chemical, morphological, mineralogical and physical characteristics of the above materials are discussed. The chemical compositions of the industrial wastes are investigated using X-ray fluorescence (XRF) of PAN Analytical Axios, and the mineral compositions are detected by XRD instrument of the model - RigakuUltima-IV, Japan with Cu target. The microstructure images are observed by SEM instrument fitted with electron dispersive X-ray (EDX) analyzer of the model - JEOL JSM-6480LV or FESEM of Nova Nano SEM 450 model. The fineness of the materials is found out using both laser diffraction particle size analyzer (LDA) (MASTERSIZER S, Malvern, UK model) and the Brunauer–Emmett–Teller (BET) apparatus and the results are compared. Based on the above results, the materials are characterized as follows.

1. NALCO fly ash and JSPL fly ash belongs to Class F ( $\text{SiO}_2 + \text{Al}_2\text{O}_3 + \text{Fe}_2\text{O}_3 > 70\%$ ) with low calcium content (0.70%). But the Paradeep fly ash belongs to Class C as ( $\text{SiO}_2 + \text{Al}_2\text{O}_3 + \text{Fe}_2\text{O}_3 < 70\%$ ), but the CaO content is less than 15% (14.20%). The NALCO and JSPL fly ashes belong to a Sialic group of highly acidic, with low calcium content and Paradeep fly ash belong to Calsialic group.
2. The RSP slag contains 34.75% of CaO followed by 32.44% of  $\text{SiO}_2$  and 17.06% of  $\text{Al}_2\text{O}_3$ . The present slag has a good hydration property with hydration modulus HM (1.94) is greater than 1.4. The CaO/ $\text{SiO}_2$  ratio as  $1.07 > 1.0$  and the  $\text{Al}_2\text{O}_3/\text{SiO}_2$  ratio of 0.52, indicate the suitability of present slag as a pozzolanic and cementitious material.
3. The Ferrochrome slag contains about 43% of aluminosilicate compound, 24.99 % of MgO and 19.53% of chromium oxide ( $\text{Cr}_2\text{O}_3$ ) as the major components. As the CaO/ $\text{SiO}_2$  ratio is  $0.19 < 2.0$ , Cr exist as magnesiochromite spinel phase, which is stable against oxidation and is resistant to dissolution in aqueous media. The minerals like forsterite, olivine, spinel, hematite and quartz, and the hump position at 26 degrees indicates the presence of aluminosilicate glass. The magnetic part consists of different types of minerals of different shape, colour and transparency with surface chemistry showing the presence of Mg, Si, Al and Ca.

4. The present FS contains MgO (24.94%) as the major compound followed by alumina 21.58%, silica 21.28%, and Cr<sub>2</sub>O<sub>3</sub> of 19.46% as the minor compounds. The utilization of the present ferrochrome slag is limited due to high MgO and Cr<sub>2</sub>O<sub>3</sub> content.
5. NALCO fly ash contains quartz (SiO<sub>2</sub>), mullite (Al<sub>6</sub>Si<sub>2</sub>O<sub>13</sub>), and hematite (Fe<sub>2</sub>O<sub>3</sub>) as the major compounds. A broad hump in between 15° and 30° with hump position at 22.5° (2θ) indicates the presence of alumino-silicate type of glassy phase. Though the Paradeep fly ash shows quartz (SiO<sub>2</sub>), mullite (Al<sub>6</sub>Si<sub>2</sub>O<sub>13</sub>), and hematite (Fe<sub>2</sub>O<sub>3</sub>) as the major mineral phases, the broad amorphous hump in between 25° to 35° with a peak of the hump 27° shows the presence of both alumino-silicate and calcium-aluminate type of glassy phase.
6. GGBS contains minerals, akermanite (Ca<sub>2</sub>Mg [Si<sub>2</sub>O<sub>7</sub>]), gehlenite (Ca<sub>2</sub>Al [AlSiO<sub>7</sub>]), wagnerite (MgFe)<sub>2</sub> PO<sub>4</sub>F, and melilite (Ca, Na)<sub>2</sub>(Al, Mg, Fe<sup>2+</sup>) [(Al, Si) SiO<sub>7</sub>]. Wide humps are observed in between 20° and 40°, centred at 30° which confirm the significant amount of amorphous phases.
7. The FS consist of quartz (SiO<sub>2</sub>), gismondine (CaAl<sub>2</sub>Si<sub>2</sub>O<sub>8</sub>.4H<sub>2</sub>O), gypsum (CaSO<sub>4</sub>.2H<sub>2</sub>O), spinel (MgAl<sub>2</sub>O<sub>4</sub>), enstatite-ferroan (Mg, Fe) SiO<sub>3</sub>, fayalite (Fe<sub>2</sub>SiO<sub>4</sub>), and Cochromite- syn (CoCr<sub>2</sub>O<sub>4</sub>). It shows a wide hump that lies in between 20° and 35° producing angle 2θ as 27°. The FTIR analysis of the above industrial wastes shows the bonds of the materials as per chemical compound and confirms the presence of the glassy and amorphous phase as observed in XRD analysis.
8. The particle texture of NALCO fly ash shows that particles are mostly spherical with a smooth surface known as cenospheres, with particle size varying from 1- 100µm. The RSP slag shows an angular shape with sharp edges and exhibits an irregular pattern, and ferrochrome slag shows the irregular plate-like structure of different sizes.
9. Based on EDX analysis and optical microscope photograph of magnetically separated FS, bright and glossy surface represent the position of light alkali metals like Mg, Al and Si on the surface of FS particles, which is a good sign of pozzolanic reactivity of FS.

10. The XRD analysis of coal mine overburden shows, the major minerals present are quartz, kaolinite and calcite and it is denoted as black shale.
11. The black shale is highly acidic, whereas white and red shale is basic. The variations of EC, TDS and pH is very sensitive to liquid/solid (L/S) ratio for black shale, but the variations for white and red shale is negligible. For the same L/S value, HCFA shows the higher value of EC and TDS than GGBS, JSPL and NALCO fly ash.

As discussed in Chapter 2, development and characterization of three types of sustainable materials are studied in the present thesis. After a discussion about the basic material properties of different industrial wastes in this chapter, the development and characterization of controlled low strength material using less explore industrial waste ferrochrome slag and coal mine overburden are discussed in Chapter 4 and 5 respectively. The biopolymer treated fly ash and a fine fraction of coal mine overburden using different biopolymers for erosion control are discussed in Chapter 6 and development of alkali-activated material using mine overburden is discussed in Chapter 7.



## CHAPTER 4

# CHARACTERIZATION OF FERROCHROME SLAG AS A CONTROLLED LOW STRENGTH MATERIAL

### 4.1 Introduction

As discussed in Chapter 2, though several attempts have been made for the development of CLSM with cement and the industrial wastes, depending upon the availability of marginal material in the vicinity, there is no work related to characterization of CLSM using ferrochrome slag. In the course of manufacturing of ferrochrome alloy, a huge amount of ferrochrome slag is produced from submerged electric arc furnaces, and it is considered as waste or spoil. Globally, generation of ferrochrome slag is 6.5 to 9.5 million tons and increased by 2.8 to 3 % per annum Niemela and Kauppi (2007). It consists of  $\text{SiO}_2$ ,  $\text{MgO}$ ,  $\text{Al}_2\text{O}_3$ ,  $\text{CaO}$ ,  $\text{Cr}_2\text{O}_3$ ,  $\text{Fe}_2\text{O}_3/\text{FeO}$  and other minerals. Leaching tests with salt seawater and pH adjusted water Yilmaz and Karasahin (2010), revealed low leachability from the slag for most elements. The ferrochrome slag products are chemically very stable with a significant amount of amorphous glass Niemela and Kauppi (2007). In comparison to efforts on characterization and use of industrial wastes like fly ash, blast furnace slag and red mud, very little efforts have been made to use ferrochrome slag as a construction material (Yilmaz and Karasahin 2010; Panda et al. 2013); Sathwik et al. 2016). Panda et al. (2013) observed that ferrochrome slag could be used as coarse aggregate in the preparation of concrete. Yilmaz and Karasahin (2010) discussed the experimental results to use ferrochromium slag as an aggregate for granular layers of flexible pavements. The results show that the mechanical and physical properties of air-cooled ferrochromium slag are almost same or better than those of natural aggregates. It can be seen that very limited efforts have been made worldwide to use ferrochrome slag as an alternate construction material. But the findings based on the limited laboratory tests of the basic material

properties, suggest that ferrochrome slag has the potential to be used as an alternate construction material (Sathwik et al. 2016).

Therefore, in the present chapter, an attempt has been made to characterize locally available ferrochrome slag as a construction material in general and to develop CLSM using ferrochrome slag as the base material with cement and fly ash as binding material. In the 1<sup>st</sup> stage, the FS is characterized in terms of morphology, mineralogy, chemical properties, electrical conductivity (EC) total dissolved solids (TDS) along with other geotechnical properties. The thermal resistivity of the developed CLSM is also studied using indigenously developed thermal probe. Then flowability, fresh density, bleeding, unconfined compressive strength (UCS), California bearing ratio (CBR) and settlement values as per relevant ASTM standards of the developed CLSM material using FS as a base material with fly ash and cement as the binding material is discussed. Limited leachate analysis was also done to study the effect of CLSM on the environment.

### **4.2 Materials and Methods**

For the present work ferrochrome slag (FS) was collected from Ferro Alloys Corporation Ltd (FACOR), Bhadrak, Odisha, India. The FS from the plants disposed off in the solid form as fine-grained and coarse-grained material. The basic material property of the coarse-grained FS is presented in Table 4.1. Based on the physical properties like impact value (10.01%), crushing value (16%) and abrasion value (16.84) and flakiness index (4.32), elongation index (12.51) and angularity number (1.22), it is suitable as a construction material. The soundness value is 11.89 and less than the permissible limit of 12 as per ASTM C 88- 13(2013). However, in the present study detailed study of the fine aggregate is considered to compare its results with standard fine aggregate, Indian standard sand SS1 and SS2.

Chemistry, particle morphology and mineralogy are made to explain some of the macro properties of FS. The mineralogical and morphological analysis of magnetically separated particles is also done and have been presented in Chapter 3.

The particle morphology of the aggregate plays an important role towards the density, shear strength and flowability of the material (Yudhbir and Abedinzadeh1991). In the present study, an attempt has been made to make particle shape analysis of the ferrochrome slag using optical microscope fitted with particle size analyzer to describe

shape parameters of FS. Particle shape analysis provides quantitative parameters like elongation ( $E_R$ ), Flakiness (FR), sphericity ( $\psi$ ), shape factor (SF) and roundness index (Ri) (Yudhbir and Abedinzadeh1991).

Table 4.1: Mechanical properties of coarse-grained ferrochrome slag

Material/ Standard values	Specific gravity	Bulk Density (kg/lit)	Water absorption (%)	Percentage of Void	impact value (%)	Crushing Value (%)	Abrasion value (%)	Flakiness Index (%)	Elongation Index (%)	Angularity Number (%)
FS	2.92	1.959 (19.21 kN/m <sup>3</sup> )	0.66	32.89	10.01	16	16.84	4.32	12.51	1.22
Acceptable value as per IS: 2386-1963	2.4 to 2.9		Max. 2		Max. 30 for wearing course, 35 for bituminous macadam and 40% of water bound macadam base course.	Max. 45 for base course, and 30 for surface course	Max. 30 for water bound and 50 for bituminous macadam base courses	15	20	0 to 11

The FS samples subjected to optical microscope analysis were separated prior according to their size by sieve analysis and minimum 10 particles from each fraction were subjected to the optical microscope analysis (Yudhbir and Abedinzadeh1991).

Then particle shape parameters; elongation ( $E_R$ ), Flakiness ( $F_R$ ), sphericity ( $\psi$ ), shape factor ( $S_F$ ) and roundness index ( $R_i$ )of the ferrochrome slag particle is calculated as per the following equations (Yudhbir and Abedinzadeh1991).

$$E_R = \frac{d_L}{d_I} \dots\dots\dots (4.1)$$

$$F_R = \frac{d_S}{d_I} \dots\dots\dots (4.2)$$

$$\psi = \sqrt[3]{\frac{d_S \times d_I}{d_L^2}} \dots\dots\dots (4.3)$$

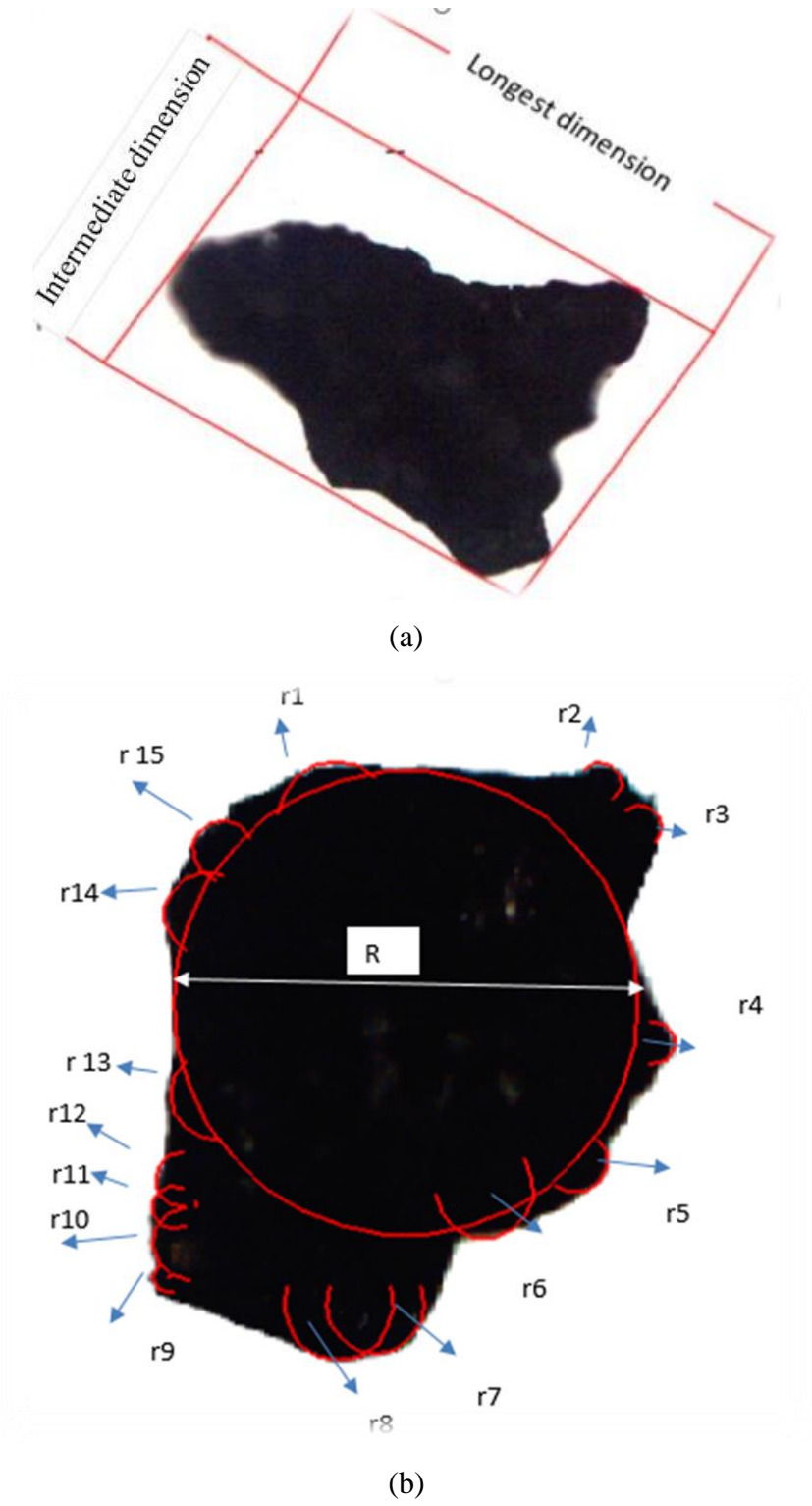
$$S_F = \frac{d_S}{\sqrt{d_L \times d_I}} \dots\dots\dots (4.4)$$

Where,  $d_L$ = the longest particle dimension,  $d_I$ = the intermediate particle dimension, and  $d_S$ = the shortest particle dimension (found from Vernier scale reading of the optical microscope). For a typical irregular particle, the determination of longest dimension and intermediate dimensions are shown in Figure4.1 (a). The roundness index ( $R_i$ ) is defined in Equ. 4.5.

$$R_i = \frac{\sum(\frac{r}{R})}{N} \dots\dots\dots (4.5)$$

Where  $r$  is the radius of corners of a sand grain,  $R$  is the radius of inscribed circle and  $N$  is the number of the corner. A typical diagram showing the radius of the corner ( $r$ ) for 15 ( $N$ ) corners and the radius of inscribed circle  $R$  is shown in Figure 4.1(b). The above procedure is repeated for all individual particles to find out the  $E_R$ ,  $F_R$ ,  $\psi$ ,  $S_F$  and  $R_o$ of the ferrochrome slag particle.

As FS contains a high percentage (24.99%) of MgO, the soundness and expansion test was also conducted as per ASTM C 88-13 (2013) and ASTM D 4792(2013), respectively. The pH values of FS and FA was tested using a Hach, HQ40d portable pH meter, corresponding to liquid to solid ratio L/S, varying between 2 and 10. The electrical conductivity (EC) and total dissolved solids (TDS) are also measured using the above instrument with automatic temperature compensator.



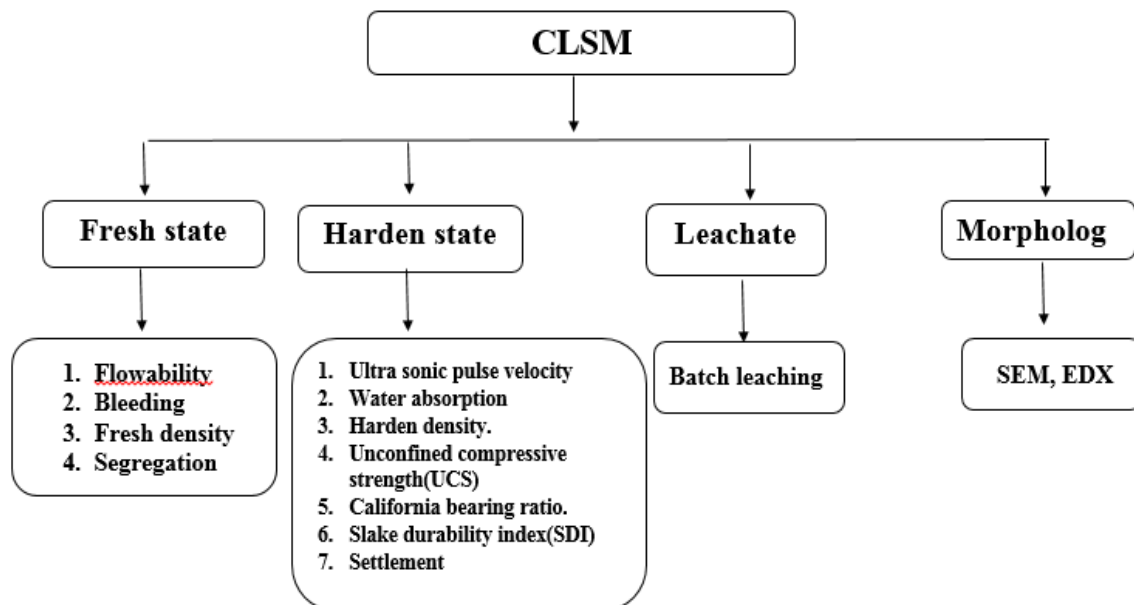
**Figure 4.1:** Particle shape analysis (a) longest dimension, shortest dimension (b) largest radius and corner radius of the circle.

The zeta potential describes the influence of pore fluid on the particle to particle interaction in the sample can be explored by the change in the surface charge potential (Padmakumar 2012). In the present study, zeta potential was measured by Zetasizer Nano ZS90 (make, Malvern, UK). Atomic absorption spectroscopy (AAS) test was conducted to

get the leaching behaviour of FS in terms of cumulative Cr, Fe, Si, Mg, Al and Ca elements for 14 days. The leaching behaviour of FS was also studied in terms of hexavalent chromium using ultraviolet spectroscopy studied.

Different geotechnical engineering properties like specific gravity, grain size, classification, compaction characteristic and direct shear test on FS was also conducted as per relevant ASTM standards.

Figure 4.2 shows the experimental flow diagram of CLSM. In present section of the study, CLSM is developed by using FS, fly ash (JSPL), cement and water. The experiments are conducted both in the fresh state and harden state. The flowability, fresh density, bleeding and segregation are measured in its fresh condition. The unconfined compressive strength (UCS), California bearing ratio (CBR) and settlement analysis are conducted on harden state of CLSM. Leaching behaviour of the CLSM is conducted by AAS atomic absorption spectroscopy) by the batch leaching process. The morphology of the design material is also studied by SEM and EDX analysis.



**Figure 4.2:** Flow diagram showing the details of the experimental investigation on CLSM using ferrochrome slag.

### 4.3 Result and Discussion

The results of the experimental investigations are presented describing the basic material characterization of ferrochrome slag and comparing the results with that of Indian standard sand (SS1 and SS2), which are considered as a standard fine aggregate.

#### *Basic material characterization*

The chemical analysis of ferrochrome slag as presented in Chapter 3 consist of 21.63% aluminum oxide ( $\text{Al}_2\text{O}_3$ ), 21.33% of silicon oxide ( $\text{SiO}_2$ ), 24.99% of magnesium oxide ( $\text{MgO}$ ) and 19.53% of chromium oxide ( $\text{Cr}_2\text{O}_3$ ) with forsterite, olivine, spinel, hematite and quartz as the major minerals. Similar observations have been made by Panda et al. (2017). Based on SEM analysis, the FS particles are irregular in shape with agglomerated particles, but, the magnetic part of the FS contains mostly angular particles of different sizes varying from 63  $\mu\text{m}$  to 150 $\mu\text{m}$  as discussed in Chapter 3. The presence of Al, Si and Mg elements on the surface of FS are the attractions for its use as a pozzolanic material.

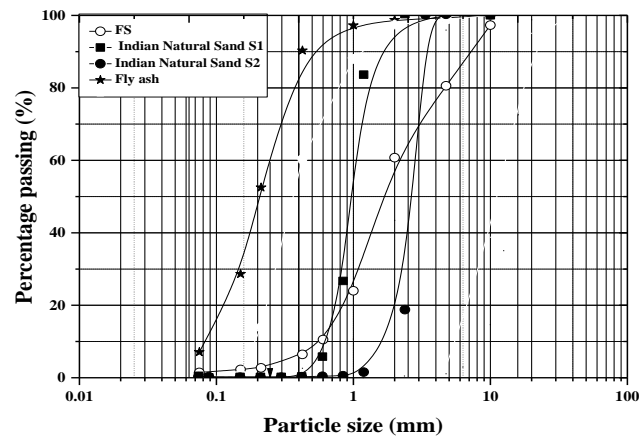
The FS and FA are slightly alkaline and slightly acidic, with pH values as 7.94 and 6.62, respectively. Though FS contains an appreciable amount of iron and chromium oxide, alkalinity nature may be due to high MgO content. The specific gravity of ferrochrome slag is found to be 2.90. The high specific gravity of FS of 3.01 (Yukselen and Kaya2003) and 2.90 of the present study are due to the presence of iron-bearing minerals (Spinel) as discussed earlier and low specific gravity of FA is due to the presence of cenospheres (Das and Yudhbir 2006; Mahamaya and Das 2017). The grain size distribution curves for the ferrochrome slag and sand are shown in Figure. 4.3 with  $C_u$  and  $C_c$  values of FS are found to be 3.33 and 1.00, respectively and can be classified as a poorly graded sand. As per the chemical analysis, FS contains 24.99 % of MgO, hence to measure the resistance to the disintegration of FS soundness test was conducted using sodium sulfate solution as per ASTM C88 (2013). Based on soundness test, the value is observed as 11.89%, which is within the permissible limit (12%).

#### *Particle shape parameters*

The particles shape parameters elongation, sphericity, shape factor and roundness index (Ri) are calculated as per the methodology discussed earlier and are presented in Table 4.2. The range of elongation ratio, flakiness ratio, and sphericity was found to be in the range of 1.0-2.05, 0.01-0.97 and 0.17-0.98, respectively. The roundness index is measured



(Equ. 4.5) and the quantitative index of roundness is more conveniently expressed in terms of Powers' roundness criteria (Yudhbir and Abedinzadeh1991) as presented in Table 4.3. Different shapes of FS particles belonging to different groups are also represented in Table 4.3. It can be seen that 75% of the particles are very angular and 20% of the particles are angular, hence supposed to have better interlocking,i.e., higher angle of internal friction ( $\phi$ ) value. However, other shape parameters, which also affect the properties of the material are flakiness, elongation, etc.



**Figure 4.3:** Grain size analysis of ferrochrome slag, fly ash and Indian natural sand.




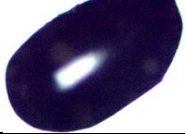
The coefficient of uniformity ( $C_u$ ) of FS, fly ash, Indian natural sand I and Indian natural sand II are found to be 1.88,3, 1.61 and 0.73 respectively. The coefficient of curvature ( $C_v$ ) of FS, fly ash, Indian natural sand I and Indian natural sand II are found to be 1.81, 1.02, 0.05 and 0.66 respectively. Similarly effective size ( $D_{10}$ ) of FS, fly ash, Indian natural sand I and Indian natural sand II are found to be 0.59,0.08 0.62 and 1.60 respectively.

**Table 4.2:** Particle shape parameters of FS and Indian standard sand

Properties	Values(Range)		
	FS	SS1	SS2
Elongation ratio ( $E_R$ )	1.0-2.05	1.14-1.59	1.03-1.92
Flakiness ratio ( $F_R$ )	0.01-0.97	0.13- 0.38	0.12-0.49
Sphericity ( $\Psi$ )	0.17-0.98	0.47-0.55	0.36-0.66
Shape factor (SF)	0.008-0.95	0.13-0.32	0.09-0.40
Roundness index ( $R_I$ )	0.06-0.58	0.25-0.50	0.16-0.50

Hence, for more elaborate shape analysis, two-shape indices in terms of ratios  $d_i/d_l$  and  $d_s/d_i$ , are used to construct Zingg diagram (Yudhbir and Abedinzadeh1991). According to Zingg diagram, FS particles are classified as an oblate (disk), equant, prolate (roller) and bladed. There are 66.25% of oblate, 7.5% equant, 6.25% of prolate and 20% of blade-shaped particles as found in FS (Figure.4.4). This affects the overall physical properties of the material. Based on the grain shape parameters, sphericity and shape factor using the particle dimensions'  $d_L$ ,  $d_i$ ,  $d_s$ , (Yudhbir and Abedinzadeh1991), Figure. 4.5 shows, 72.5% of FS are flaky grains, 20% are bulky elongated, and 7.5% are bulky rounded particles. The maximum void ratio ( $e_{max}$ ) and the minimum void ratio ( $e_{min}$ ) of the FS were found to be 0.945 and 0.650, respectively and the corresponding angle of internal friction  $\phi$  (at  $e_{max}$ ) and  $\phi$  (at  $e_{min}$ ) values are  $34.42^\circ$  and  $41.18^\circ$ , respectively.

**Table 4.3:** Classification of particles based on Powers' roundness criteria (Yudhbir and Abedinzadeh 1991)

Type	Percentage	Shape
Very angular	75	
Angular	20	
Sub-angular	2.5	
Rounded	2.5	

The average roundness index of FS and Indian standard sand SS1 and SS2 sands as shown in Table 4.2, it can be seen that the average roundness index of RS is higher than that of SS. Cortes et al. (2008) studied the effect of roundness index on the flowability of fresh mortar and found that for the same water to cement ratio and fine aggregate to cement ratio, aggregate having higher value of  $R_i$  gives higher flowability. The sphericity of the red sands (NRS and HRS) is found to be higher than that of standard sand (SS1 and SS2) (Table 4.2). However, HRS shows the higher value of sphericity as compared to NRS. Goncalves et al. (2007) studied the effect of particle shape on cement mortar and found

that at the lower water to cement ratio (0.4), particles with higher  $\psi$  gives better workability.

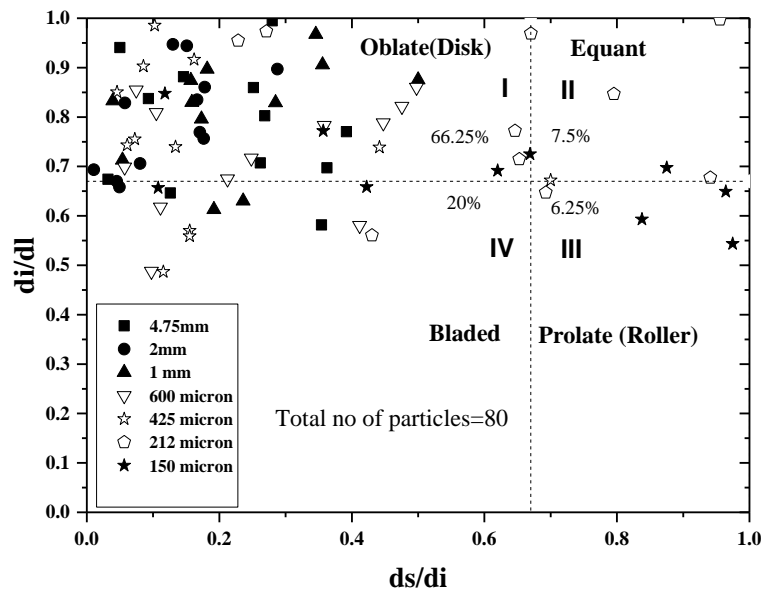


Figure 4.4: Particle shape classification using Zingg diagram.

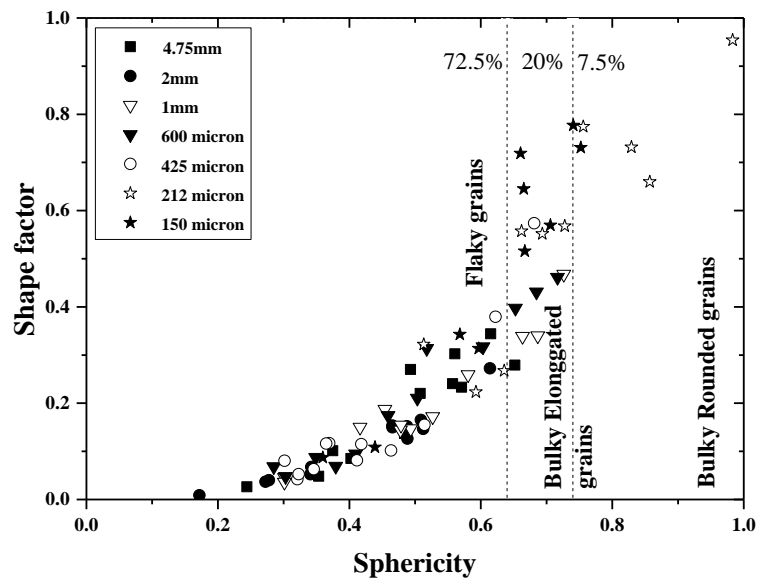
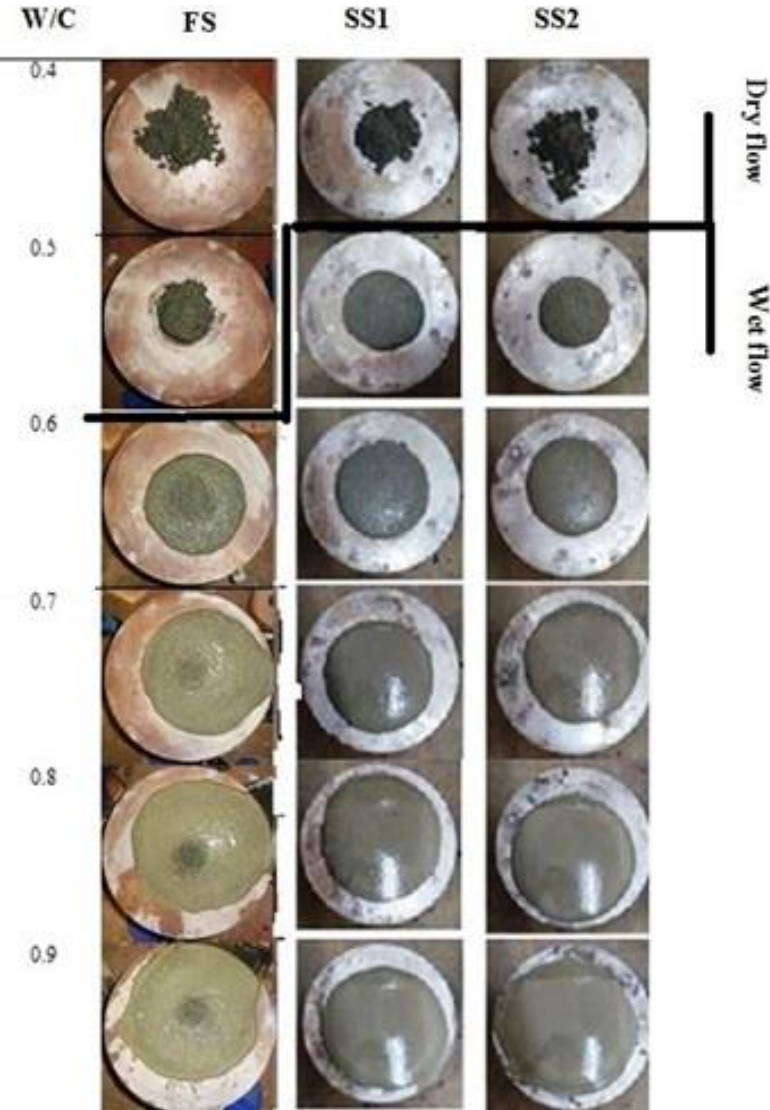


Figure 4.5: Relationship between Shape factor and Sphericity.

Hence, the flowability of the mortar, prepared using RS and SS with sand to cement ratio of 2 and at a different water-cement ratio (w/c), has been studied. It is found that for a particular water-cement ratio, the mortar prepared using SS is more flowable compared to RS as shown in Figure 4.6. The study reveals that along with the angularity of the fine aggregate, there are some other factors which affect the flowability of mortar. One of the factors may be the specific surface area of the fine aggregate. So, the surface area of sands

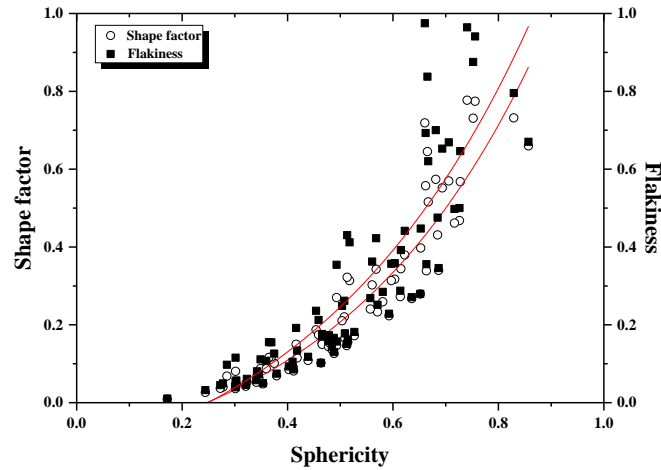
is investigated using ethylene glycol monoethyl ether (EGME) method (Cerato and Lutenegeger, 2002). It was found that the surface area of SS1 and SS2 are  $0.847\text{m}^2/\text{g}$  and  $0.866\text{m}^2/\text{g}$  respectively while the surface area of NRS and HRS are  $23.45\text{m}^2/\text{g}$  and  $20.40\text{m}^2/\text{g}$  respectively. For the same water-cement ratio, the lower flowability of the RS may be due to its higher surface area as compared to SS. However, the effect of water to cement ratio on the strength properties of mortar prepared using red sand needs to be investigated.



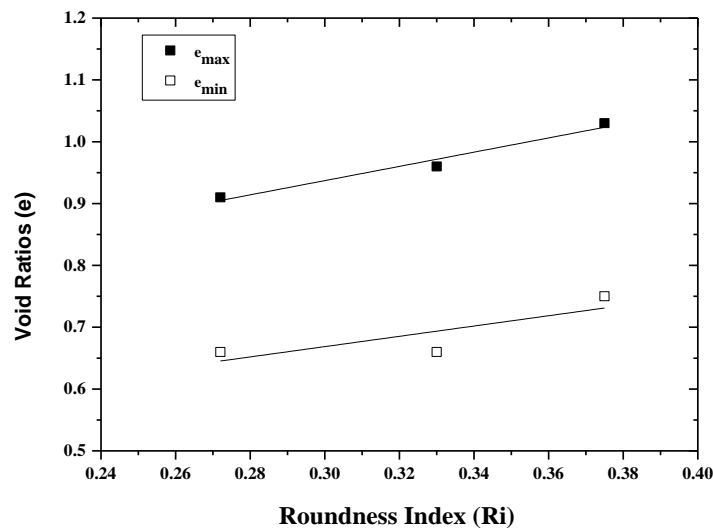
**Figure 4.6:** Flowability of FS with different water cement ratio

The variation of flakiness with shape factor shows similar trend like that of sphericity (Figure.4.7) with a nonlinear relationship. A higher value of flakiness is observed in comparison to sphericity, irrespective of sphericity and the particle size. It may be mentioned here that higher sphericity refers to higher variations in  $d_s$ ,  $d_l$  and  $d_L$ . The result

of the particle size analysis is correlated to the index properties of FS, the relationship between the roundness index and void ratio of FS is shown in Figure 4.8 along with the results of Indian standard sand samples (SS1, SS2). It can be seen that there is a linear relationship between the void ratio and roundness index. Similar patterns have been observed for coarse aggregate and red sand (Alam et al. 2017).



**Figure 4.7:** Relationship between Shape factor, Sphericity and flakiness.

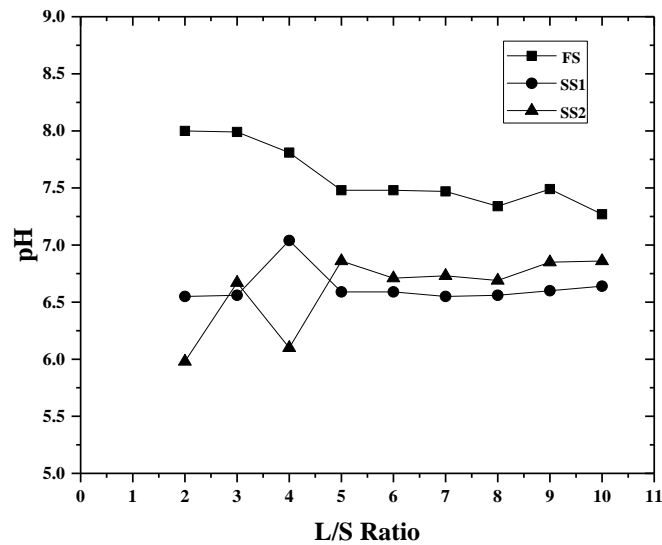


**Figure 4.8:** Relationship between roundness index and void ratio.

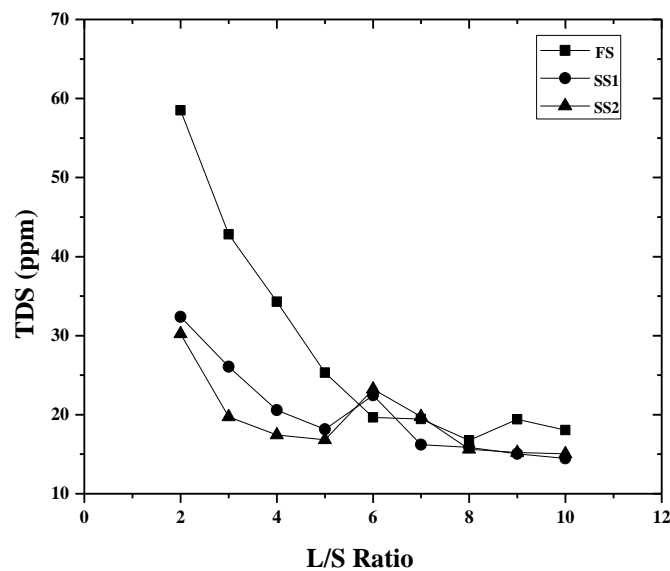
### ***Chemical Properties***

The variations of pH and EC (chemical properties) of FS are also determined using HACH HQ40d at different liquid to solid ratio (L/S) ratio as shown in Figure. 4.9, and Figure 4.10, respectively. The pH and EC values follow the similar trend and decrease with increase in L/S ratio (dilution). The results are compared with Indian standard sands (SS1 and SS2). The variation of pH with dilution is studied by varying the L/S from 2 to 10

with each data point is as the average of three data. The pH of FS is slightly alkaline varying from 8.0 to 7.27 with dilution, though standard sand is always acidic varying from 5.98 to 7.0 (Figure. 4.9). The EC value of FS is found the maximum (123.7  $\mu\text{s}/\text{cm}$ ) in comparison to 64.1 and 59.8  $\mu\text{s}/\text{cm}$  for SS1 and SS2 at L/S ratio of 2 as shown in Figure. 4.10. Higher EC value of FS than SSs due to the presence of dissolved metallic oxides (magnesium, chromium, iron and aluminium oxide). However, with an increase in L/S ratio, the EC value of FS decreased up to 39.9  $\mu\text{s}/\text{cm}$  and is comparable to that of standard sands (28.6 and 29.8  $\mu\text{s}/\text{cm}$ ). Hence, FS can be used as a substitute for natural sand.



**Figure 4.9:** Variation of pH of FS, SS1 and SS2 with liquid to solid ratio (L/S).



**Figure 4.10:** Variation of EC of FS, SS1 and SS2 with liquid to solid ratio (L/S).

The variation of zeta potential ( $\zeta$ ) with pH (adjusted using NaOH and HCl) of ferrochrome slag after 30, 60 and 120 minutes are shown in Figure. 4.11. It can be seen that the  $\zeta$  is highly dependent on the pH value. It was found that at lower pH value,  $\zeta$  is positive but at higher pH value,  $\zeta$  is negative as shown in Figure. 4.11. Kosmulski et al. (1999) and Alam et al. (2017) also observed similar results for Anatase and red mud respectively. Depending upon the waiting period,  $\zeta$  of ferrochrome slag is zero at a certain pH value, and the corresponding point is called as a point of zero charge (PZC). It can also be seen that the PZC of FS exists in the acidic region. The PZC of FS lies between the pH values of 2.2 to 3.4, as the time increased from 30 min to 120 min. At any pH value, the zero charge on the particle will cause only attractive force causing flocculation of the particles (Yukselel and Kaya 2003). It is also found that there is a sudden decrease in  $\zeta$  of FS beyond the PZC. Nagela and Schneider (1989) found a similar pattern for solid waste material such as low calcium fly ash, blast furnace slag, and blast furnace slag cement. There is a significant variation in  $\zeta$  on the acidic side while beyond pH 7, variation is marginal. Alam et al. (2017) observed a large variation also in the alkali environment red mud, may be due to its high alkaline nature.

As chromium is a hazardous mineral, particularly the hexavalent chromium in the chrome ore. The FS was subjected to leaching analysis and based on UV spectroscopy no hexavalent chromium was observed. However, for other elements using atomic absorption spectroscopy (AAS) and tests were conducted after 1<sup>st</sup> day, 2<sup>nd</sup> day, 3<sup>rd</sup> day, 7<sup>th</sup> day and 14 days of leaching analysis. The outcome of the AAS test (not presented here) showed that leaching of Si, Cr and Al are negligible and leaching of Fe, Ca and Mg is moderate, and decreasing with time except for Mg, but the values are within acceptable limit.

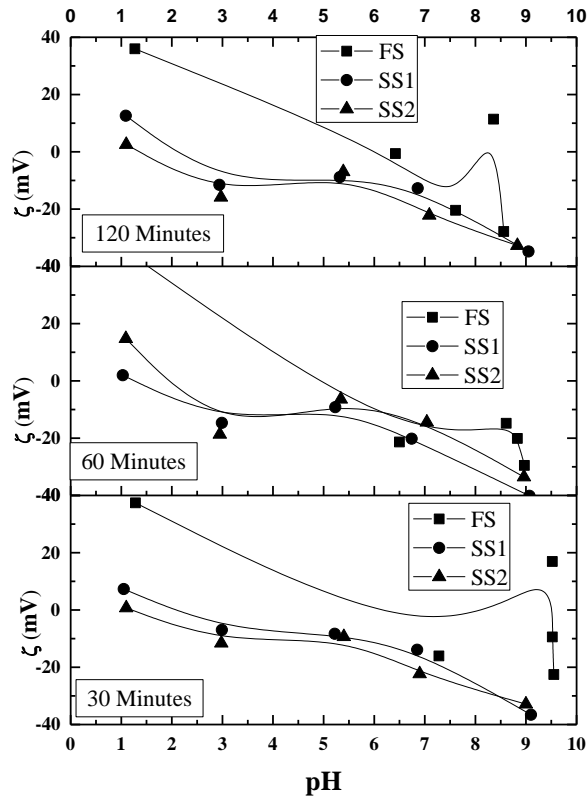


Figure 4.11: Variation of zeta potential with pH of ferrochrome slag and Indian standard sand.

Thermal resistivity test of ferrochrome slag was also conducted at its loose and dense states. The test was also conducted on different CLSM mixtures at its fresh state and after 7days of curing, an average of three tests was taken as a final result. The results of the thermal resistivity test of ferrochrome slag and different CLSM mixtures are presented in Figure 4.12. This will help in deciding the present CLSM for bedding and trench filling.

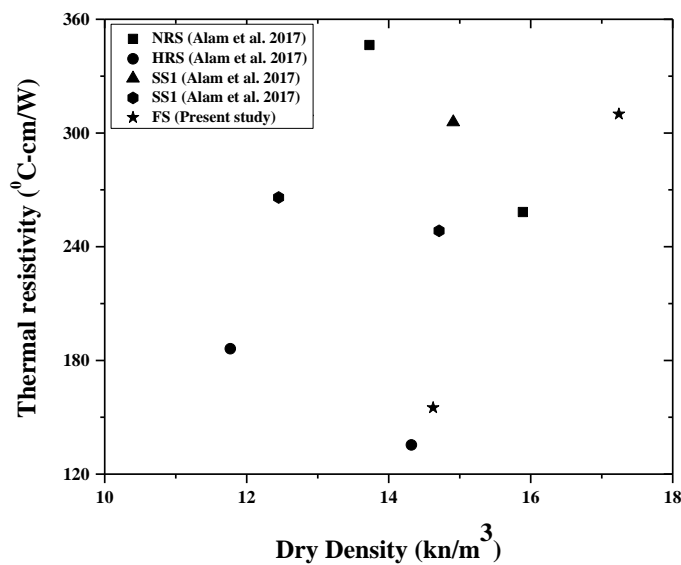


Figure 4.12: Relationship between density and thermal resistivity



After getting mineralogical, morphological, physical and geotechnical characteristics of FS and FA, several trials are made to prepare CLSM using FS, FA, and cement with different water to binder ratio. The cement used in the mixture has consistency 38%, specific gravity 3.01, initial and final setting time are 3h 36 min and 10h 11 min, respectively. The final proportion of CLSM mixture is represented in Table 4.4. The flowability, fresh density, and bleeding properties of fresh CLSM mixture are also presented in Table 4.4.

The spread diameter increases with increase in water content and flow diameter vary from 85mm to 390mm (Table 4.4), which have self-flowing and self-levelling consistency as needed for CLSM and bleeding took place at higher water content. Bleeding defines as the potential of the particles to remain in suspension (Naganathan *et al.* 2009) and also a parameter to measure stability, permeability and leaching properties of CLSM. The additional water added to the mixture hail out as bleed and the bleed water is expressed by the percentage of the original volume of CLSM sample as bleeding (%). The bleeding value of presently used CLSM varies from 1.55% to 11.75%. The bleeding is found to be minimum for M3S1 and maximum for the M6S4 mix. The CLSM having a bleeding value of less than 5% in 2 hours considered as stable mixture (Gabr and Bowders 2000). It can be seen that for fly ash/cement (F/C) ratio up to 3.5, the bleeding values are close to 5% upto binder ratio of 0.6. It is also observed that replacement of fly ash with additional finer FS increased the bleeding value even with F/C ratio of 2.66. Hence, fly ash percentage plays an important role in the properties of CLSM (Folliard et al. 2008) due to its spherical particles. The density of freshly prepared CLSM samples gradually reduced with the increase the water content as presented in Table 4.4. The fresh density of CLSM is found to be minimum for M3S4 is (18.25 kN/m<sup>3</sup>) and maximum for M5S1 is (20.89 kN/m<sup>3</sup>). The low density is due to higher percentage of fly ash and density increased with a decrease in fly ash content. The fresh density of CLSM without air entraining varies from 16.16 kN/m<sup>3</sup> to 22.47 kN/m<sup>3</sup> (Folliard et al. 2008). Fresh CLSM slurry is poured into a cylindrical mould of size 50mm diameter and 100mm height. After 24h the samples are demoulded and then covered by thin cling wrap up to desired curing period. In the present study, unconfined compressive strength (UCS) is conducted after 7, 28 and 56 days of curing.

The typical stress-strain curve corresponding to the minimum (M5S4) and maximum (M4S1) compressive strength after 7, 28 and 56 days of curing are shown in Figures 4.13

and 4.14, respectively. For sample M5S4, with least amount of cement content corresponds to 2.78% strain at peak stress of 0.6710 MPa, and could sustain up to 3.72% strain at failure after 7 days. The strain corresponding to peak stress at 28 days is 2.18% at a stress of 1.933 MPa, and failure strain is 2.81% and the corresponding values at 56 days are 3.03% at a stress of 3.79 MPa, and stress(1.526MPa) sustain to 3.66% The strain varies 2.7% to 3.03% for peak stress. The strain at peak stress corresponds to that of soft to medium clay (Nataraja and Nalanda 2008). The 7 days' strain corresponding to peak stress is varying to 2.78% to 4.91%. The 28 days' strain corresponding to peak stress is varying from 2.18% to 3.37% and the corresponding value after 56 days varies from 3.03% to 3.36%. It may be mentioned here that Nataraj and Nalanda (2009) observed 60 days strain varying from 4 to 6% for the CLSM using cement and fly ash. In the present study lower strain value corresponding to the peak, stress is due to coarse grain material FS.

The UCS of different mixture samples prepared in the present study after 7, 28 and 56 days of curing are presented in Figure4.15. The UCS after 7days of curing varies from 0.67N/mm<sup>2</sup> to 7.53 N/mm<sup>2</sup> and maximum and minimum UCS are achieved for mixture M4S1 and M5S4, respectively as shown in Figure4.15(a). The minimum and maximum UCS after 28 days of curing are 1.93 and 13.42 N/mm<sup>2</sup> for mixture M5S4 and M4S1 respectively as shown in Figure4.15(b). Similarly, after 56 days of curing the minimum UCS (3.83 N/mm<sup>2</sup>) value is obtained for M5S4 and the maximum value (18.32 N/mm<sup>2</sup>) was achieved for M4S1 as shown in Figure4.15(c). The UCS values increased with increase in cement content and decreased with increase in water content, similar observations have been made for CLSM using ground granulated blast furnace slag (GGBS) (Udayashankar and Raghavendra 2014). The UCS value less than 2.1 N/mm<sup>2</sup> are appropriate to use in nonstructural excavation applications such as backfilling, pipe trench refilling, control density filling and for erosion control, and mixtures having a higher value of UCS can be utilized in structural and non-excavation applications such as in foundation (ACI, 1999). Hence, the CLSM used in the present investigation can be used in structural and non-excavation applications. Hence, to assess the use of developed CLSM as a subbase and subgrade material, CBR test was conducted on the six CLSM mixtures with 0.65 water binder ratio, which corresponds to the minimum UCS value of the corresponding mix (Figure. 4.15). The soaked CBR values were conducted after 7 days of curing under ambient condition followed by four days (96 h) of soaking period and

presented in Table 4.5. The CBR values are found to vary from 57.8% to 184.3% with a maximum value for M4S4 and minimum for M5S4. Hence, the CLSM using FS can be used as suitable as a subgrade or subbase material.

To know the subsidence of the prepared CLSM mix, the settlement test on different CLSM mixture was also conducted by using an acrylic mould of 40mm diameter and 80mm height. The freshly prepared CLSM mixture was poured into the mould and settlement of CLSM was measured as the reduction of sample height with time after 7, 28 and 56 days. The mixtures M1S4, M2S4, M3S4 show no settlement whereas M4S4, M5S4 and M6S4 show 1 mm settlement in 7days of curing no further change were observed up to 56 days (Table 4.6). Raghavendra and Udayashankar (2014) observed settlement up to 4mm for CLSM with fly ash and waste gypsum board. The pH of different CLSM mixture was measured after seven days are represented in Table 4.7 and found that the mixture is alkali condition; hence reaction is expected to continue beyond 7 days. Thermal resistivity test was also conducted on different CLSM mixtures at its fresh state and its 7days of curing, an average of three tests was taken as a final result. The results of the thermal resistance of ferrochrome slag and different CLSM mixtures are presented in Table 4.8. It can be seen that the thermal resistivity depends upon the moisture content and density of the CLSM and decreased with the decrease in the cement content. The CLSM can be designed keeping in mind the thermal resistivity requirement of the bedding and trench filling. The leachate analysis made on a typical CLSM mix (M4S1) shows the values of heavy metals as 0.049, 0.00, 0.260, 0.005 ppm for Zn, Pb, CR, Ni and Cu, respectively. Similarly, the concentration of heavy metals As and Hg are 0.00 and 0.409 ppb and the values are within permissible limit.

Table 4.4: Mix design of CLSM using FS+fly ash +cement.

SL NO	SERIES	Sample Name	W (%)	W/B Ratio	Cement (gm)	FA (gm)	Water ( ml)	FS (gm)	FS (gm)(as binder)	Flow diameter (mm)	Fresh density (Kg/m <sup>3</sup> )	Bleeding (%)
1	F/C=3.5	M1S1	20	0.50	200	700	450	1350	-	167	1970	2.83
		M1S2	22	0.55	200	700	495	1350	-	174	1950	3.70
		M1S3	24	0.60	200	700	540	1350	-	260	1930	5.15
		M1S4	26	0.65	200	700	585	1350	-	320	1890	5.82
2	F/C=2.8	M2S1	20	0.50	250	700	475	1425	-	110	1980	1.60
		M2S2	22	0.55	250	700	523	1425	-	240	1970	3.32
		M2S3	24	0.60	250	700	570	1425	-	285	1900	5.58
		M2S4	26	0.65	250	700	618	1425	-	335	1880	6.36
3	F/C=2	M3S1	20	0.50	350	700	525	1575	-	130	1990	1.55
		M3S2	22	0.55	350	700	578	1575	-	255	1970	2.24
		M3S3	24	0.60	350	700	630	1575	-	320	1900	4.43
		M3S4	26	0.65	350	700	683	1575	-	390	1860	6.84
4	F/C=1.75	M4S1	20	0.50	400	700	550	1650	-	85	2000	2.33
		M4S2	22	0.55	400	700	605	1650	-	140	1970	3.71
		M4S3	24	0.60	400	700	660	1650	-	240	1920	5.09
		M4S4	26	0.65	400	700	715	1650	-	280	1890	6.66
5	F/C=8	M5S1	20	0.50	100	200	450	1350	600	105	2130	5.92
		M5S2	22	0.55	100	200	495	1350	600	145	2080	8.51
		M5S3	24	0.60	100	200	540	1350	600	240	2040	9.33
		M5S4	26	0.65	100	200	585	1350	600	250	2010	11.09
6	F/C=2.66	M6S1	20	0.50	300	200	550	1650	600	110	2120	5.86
		M6S2	22	0.55	300	200	605	1650	600	140	2080	7.93
		M6S3	24	0.60	300	200	660	1650	600	260	2000	9.73
		M6S4	26	0.65	300	200	715	1650	600	330	1970	11.75

Note: C: Cement, F: Fly ash, W: Water content, B: Binder. FS as binder: size less than 150 micron

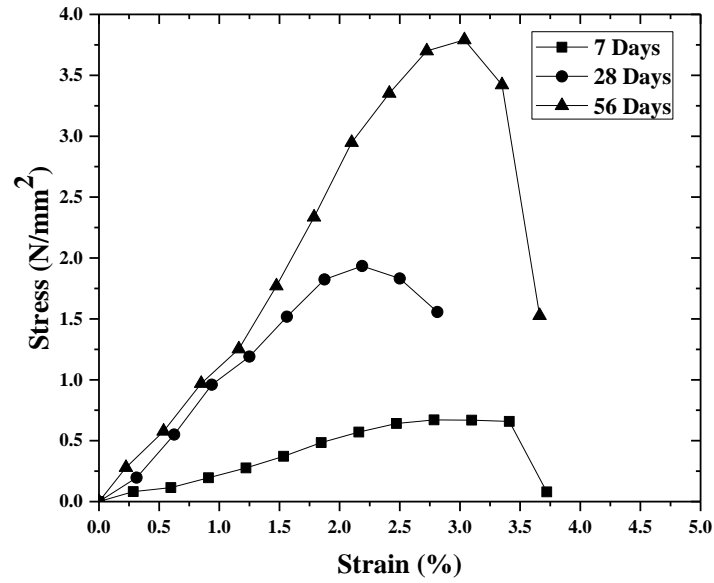


Figure 4.13: Stress- strain curves for M5S4 after 7, 28 and 56 days of curing period.

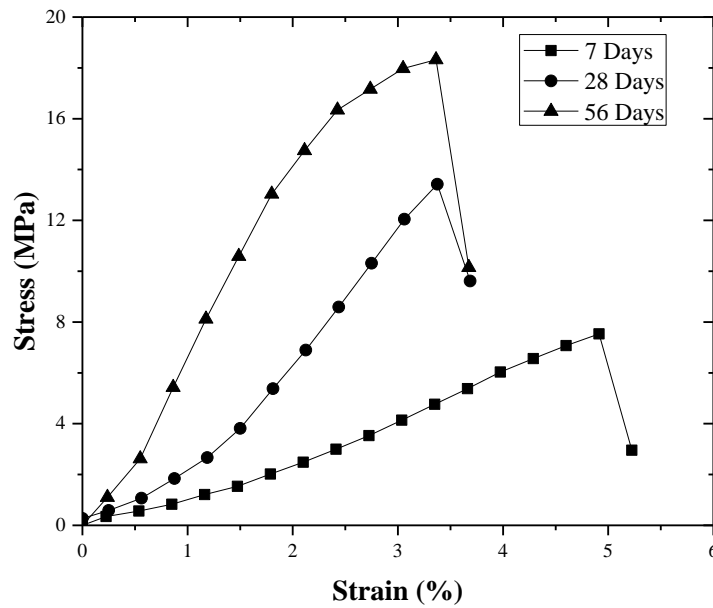
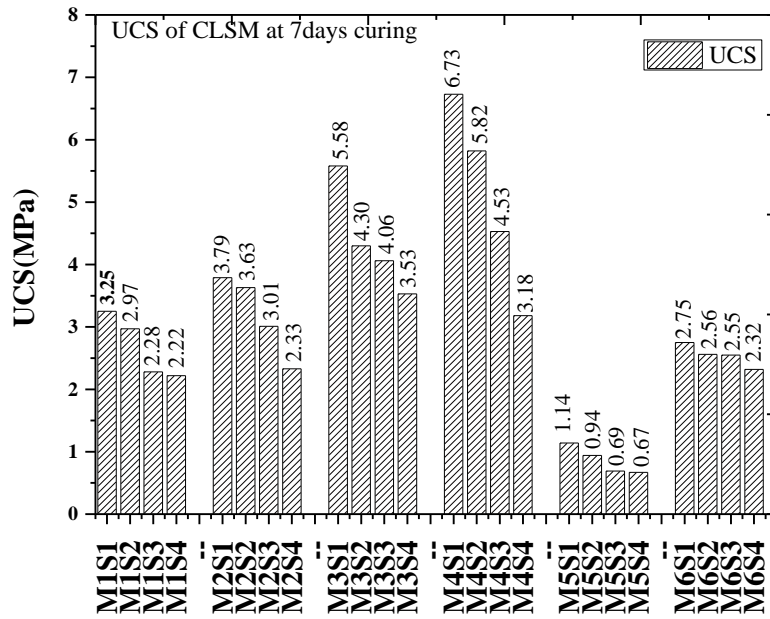
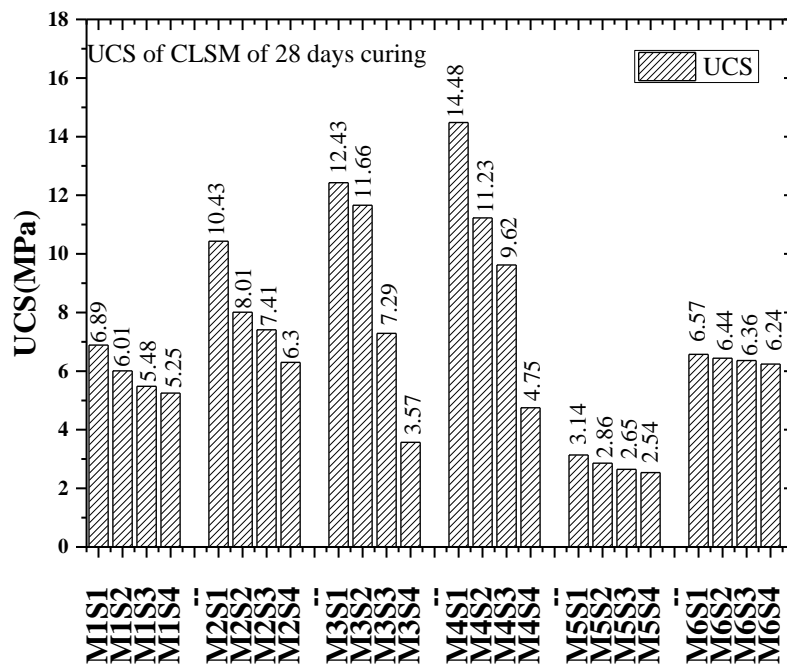


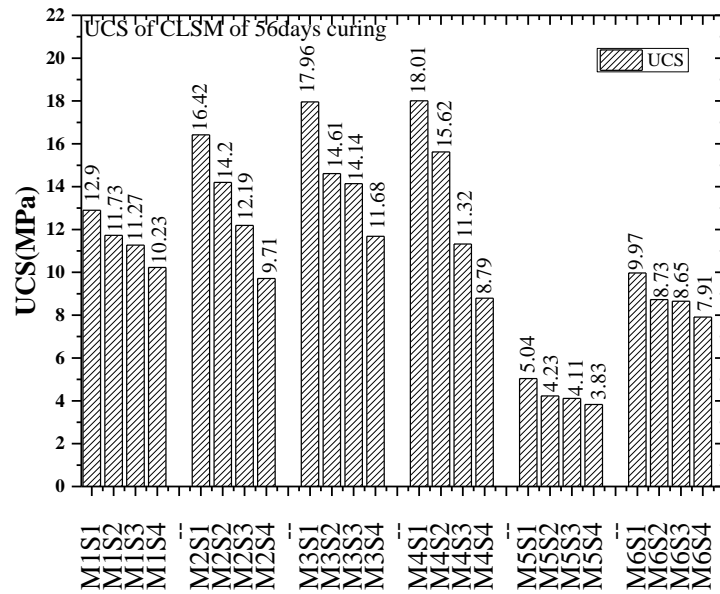
Figure 4.14: Stress- strain curves for M4S1 after 7, 28 and 56 days of curing period.



(a)



(b)



(c)

Figure 4.15: Unconfined compressive strength of CLSM mixtures (a) 7 days (b) 28 days (c) 56 days.

Table 4.5: CBR of Different CLSM Mixtures (7 days of curing + 4 days of soaking)

Sample	CBR value (%)
M1S4	109.0
M2S4	162.0
M3S4	174.0
M4S4	184.0
M5S4	58.0
M6S4	111.0

Table 4.6: Settlement Analysis of Different CLSM Mixtures.

Sample No.	Settlement		
	7days	28 days	56 days
M1S4	No settlement	No settlement	No settlement
M2S4	No settlement	No settlement	No settlement
M3S4	No settlement	No settlement	No settlement
M4S4	1mm	1mm	1mm
M5S4	1mm	1mm	1mm
M6S4	1mm	1mm	1mm

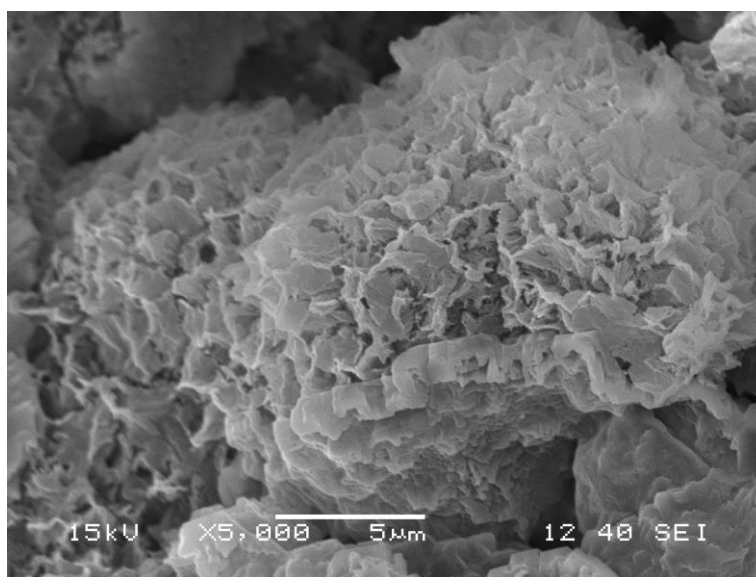
**Table 4.7:** pH Value of CLSM Mixtures

CLSM Sample	pH Value(7 days)
M1S4	11.17
M2S4	11.02
M3S4	11.21
M4S4	11.15
M5S4	10.73
M6S4	11.02

**Table 4.8:** Thermal Resistivity of Ferrochrome Slag and Different CLSM Mixtures

Material	RT (°C-cm/W) (Fresh state)	RT (°C-cm/W) (7days curing)
M1S4	58	343
M2S4	105	226
M3S4	62	111
M4S4	53	208
M5S4	50	156
M6S4	86	107

The SEM micrograph of the CLSM after 28 days is shown in Figure 4.16, depicting the development the C-S-H gel, which is responsible for gain in strength.



**Figure 4.16:** SEM morphology of the FS CLSM



**Table 4.9:** Leachate analysis of base material and FS CLSM

<b>Materials</b>	<b>Zn (ppm)</b>	<b>Pb (ppm)</b>	<b>Cr (ppm)</b>	<b>Ni (ppm)</b>	<b>Cu (ppm)</b>	<b>As (ppb)</b>	<b>Hg (ppb)</b>
JSPL FA	0.049	0	0	0.042	0	2.211	0
FS	0.085	0	0	0.050	0	10.00	0
CLSM	0.049	0	0.026	0.026	0.005	0	0.063
Permissible Limit	15.0	0.10	0.05	-	0.10	20.0	10.0

## 4.4 Conclusions

The chief deliverable emanating based on outcomes of the limited laboratory tests was observed that ferrochrome slag is a potential construction material. Some of the important findings are presented as follows.

1. The specific gravity of FS is high (2.90) due to iron and chromium-bearing minerals. Though FS contains a good amount of MgO, based on sodium sulfate soundness test; the percentage loss value comes as 11.89%, which is within the permissible limit (12%).
2. The FS contains 66.25% of oblate, 7.5% equant, 6.25% of prolate and 20% of bladed shaped particles, as obtained from image analyzer test, and a linear relationship between sphericity and void ratio was also obtained.
3. Based on the present investigation on FS along with that of Indian standard sand, the FS can be used as an alternate fine aggregate. Characterization of CLSM using FS suggests, the FS can be used in large quantities for infrastructure development thereby conserving the natural resources, utilizing the industrial wastes and helping in sustainable development.
4. In CLSM for every mixture, flow is a linear function of water content, there is limiting water content beyond which bleeding takes place. The bleeding value of presently used CLSM varied from 1.55% to 11.75%. The fly ash helps in giving a stable mix and the bleeding increases with increase in FS quantity.

5. The 7 days' strain corresponding to peak stress is varies from 2.78% to 4.91%. The 28 days' strain corresponding to peak stress is varying from 2.18% to 3.37% and the corresponding value after 56 days varies from 3.03% to 3.36%.
6. The UCS of 7days of curing varies from 0.67N/mm<sup>2</sup> to 7.53 N/mm<sup>2</sup> and after 56 days of curing the UCS value increased up to 18.32 N/mm<sup>2</sup> with minimum UCS value of 3.79 N/mm<sup>2</sup>. Hence, the developed CLSM can be used in structural and non-excavation applications. The CBR values after 56 days are found to vary from 57.8% to 184.3%, hence can be used for sub base and base course of the pavement. The settlement of the CLSM mixes is 1mm after 56 days.
7. The C-S-H gel is responsible for gain in strength of CLSM mixes as per SEM micrograph.
8. The leachate analysis of CLSM confirmed that the heavy metals are within the limit as per environmental norms.
9. Based on the present investigation on FS, it can be used as an alternate fine aggregate. Characterization of CLSM using FS suggests that FS can be used in largely in structural fill for infrastructure development thereby conserving the natural resources, utilizing the industrial wastes and helping in sustainable development.

This chapter discussed the development of CLSM using a less explored industrial waste, FS. Though the chemical content (MgO) is a constraint to use, the materials have the physical properties, which qualifies it to be used as a base course in the pavement and in concrete. Hence, in the next chapter a material with low physical strength, coal mine overburden, is considered for development of CLSM.

## CHAPTER 5

# COAL MINE OVERBURDEN AS A CONTROLLED LOW STRENGTH MATERIAL

### 5.1 Introduction

India is the third largest producer of coal in the world and has the fourth largest reserves of coal in the world (approx. 197 billion tonnes) (Rai et al., 2011). Though underground mining is the oldest method of excavation, surface mining has come to force in recent years for its manifold advantages to meet the increasing demand for coal. In 1974-75 the share of total coal production from opencast mines was only 11%, whereas in 2009-10 and 2010-11 this has risen to 72.61% and 85% respectively. The coal mine overburden is highly heterogeneous, consisting of a fine and coarse fraction of alluvium, laterite, sandstone, carbonaceous shale, coal bands, clays, between coarse to medium-grained highly ferruginous sandstone, thymide, turbidite, etc. (Ulusay et al., 1995). The storage of unutilized mine overburden is associated with occasional landslides, loss of topsoil, soil erosion, water and air pollution. The mine overburden including topsoil is approximately 2.0 times the amount of coal mined, which is going to increase every year with, an increase of depth of coal seam and coal production. The poor strength and hardness of the coal mine overburden (OB) make its unsuitable as a construction material in base course and concrete.

Figure 5.1 shows a typical open cast coal mine with the thermal power plant in the vicinity. This is very common now a day with the introduction of the central grid for the electricity distribution. The current annual production of coal ash is estimated around 600 million tons worldwide, which constitutes about 500 million tons of fly ash at 75-80% of the total ash produced (Ahmaruzzaman, 2010).



**Figure 5.1:** Power plant present vicinity of mines area.

Construction of high embankments has become an integral part of major roadworks in the construction of National highways, expressways and other connectivity. Presence of expansive soils, shortage of borrow area soil creates lots of hindrance to such projects. From environmental consideration vast use of topsoil in the available area is also matter of concern as it takes thousands of years to form the natural topsoil. Hence in the present study, an attempt has been made to develop CLSM using the coal mine overburden as the base material with cement and fly ash the cementitious material. The development and characterization of the CLSM using coal mine overburden are presented similar to that of CLSM using FS as described in Chapter 4.

## 5.2 Materials and Methods

### 5.2.1 Materials

Figure 5.2 shows a typical coal mine overburden consisting of soft rock of different size fractions. For the present study, the coal mine overburden and fly ash were collected from Raigarh, Chhattisgarh, India and the power plant is in close proximity to the coal mine. The collected OB was crushed in a laboratory crusher. The coarse fraction (size more than 4.75mm) of the coal mine overburden (shale) are subjected to the aggregate test such as specific gravity, bulk density, water absorption, the percentage of the void, crushing value, abrasion, flakiness index, elongation index, angularity number and soundness tests. Table 5.1 shows the aggregate test results of the shale aggregate and accept value as per IS code. The specific gravity of shale aggregate found to be 2.07 whereas acceptable value is within 2.4 to 2.9 and the bulk density is 1.286kg/ltr (12.61 kN/m<sup>3</sup>). The water absorption of

shale aggregate is found to be 8.87% where the permissible limit of aggregate is maximum 2% and the percentage void is 37.86%. The impact value, crushing value, abrasion value, flakiness index, elongation index and angularity number of the shale aggregate are found to be 37.13%,36%,56.43%,23.01%,25.63% and 1.71% respectively and not suitable for roads and pavements and the OB are being dumped near the mine. Hence, in the present study, an attempt is made to develop CLSM using coal mine overburden.



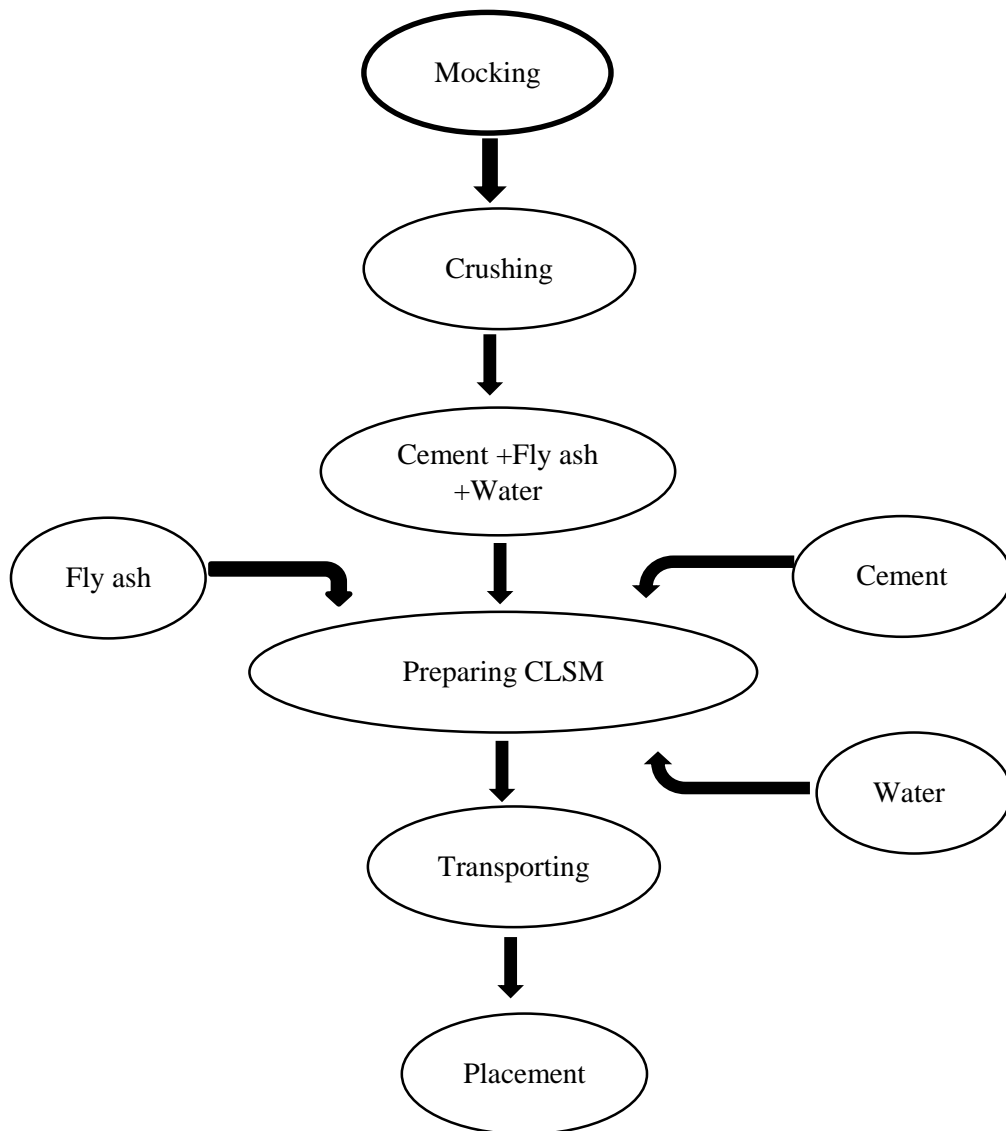
**Figure 5.2:** Overburden at coal mine area.

### 5.2.2 Preparation of CLSM

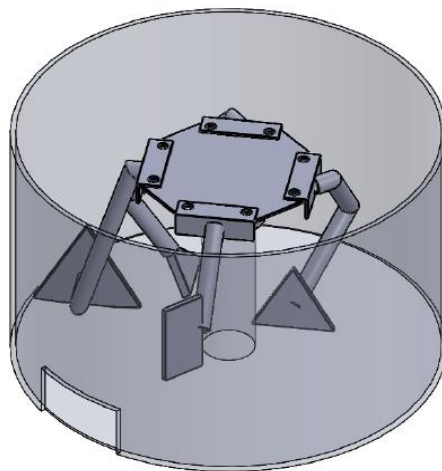
The product materials can be used for structural fill, embankment, pavement and void filling. The proposed process of preparing the CLSM in the field condition is shown in Figure 5.3, wherein the methods include the collection of shale boulders, crushing, mixing with the appropriate amount of fly ash, cement and water and transportation of the developed CLSM to the application site and placed the fresh mixture in the appropriate area. In the present study, a laboratory scale model mixture machine is fabricated, whose schematic diagram is shown in Figure 5.4a. The mixture machine is fabricated keeping in mind the low cement content, soft and fine aggregate and shown in Figure 5.4b.

Table 5.1: Aggregate test reports of the coal mine overburden

Material	Specific gravity	Bulk Density (kg/lit)	Water absorption (%)	Percentage of Void	impact value (%)	Crushing Value (%)	Abrasion value (%)	Flakiness Index (%)	Elongation Index (%)	Angularity Number (%)
Shale	2.07	1.286 (12.61 kN/m <sup>3</sup> )	8.87	37.86	37.13	36	56.43	23.01	25.63	1.71
Acceptable value as per IS: 2386-1963	2.4 to 2.9		Max. 2		Max. 30 for wearing coarse, 35 for bituminous macadam and 40% for water bound macadam base coarse.	Max. 45 for base coarse, and 30 for surface coarse	Max. 30 for water bound and 50 for bituminous macadam base courses	15	20	0 to 11



**Figure 5.3:** Process of development of CLSM using mine overburden.



(a)



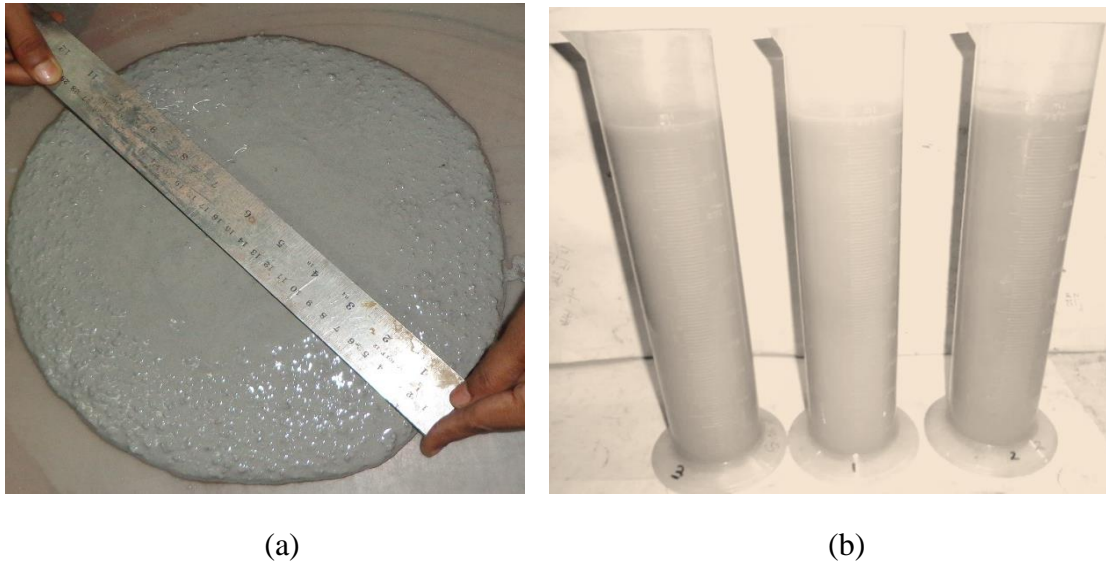
(b)

**Figure 5.4:** Fabricated soil based mixture machine (a) pictorial diagram. (b) developed mixture machine.

In the absence of proper standards and guidelines for development of CLSM, physical and chemical property of the base material is important to go for a trial mix. In the present study, CLSM mixture is developed by using coal mine overburden (black shale), JSPL fly ash, cement and water. Table 5.2 shows different trial mix design of CLSM developed in the present study. Firstly, the dry basic materials are mixed thoroughly for 3 minutes and then half of the required water added to the dry mixture, and mixed it for a period of 2 minutes, followed by 2 minutes of elapsed time. After 2 minutes of elapsed time remaining water is added to the prepared mixture and mixed it thoroughly again for 2 minutes. Total mixing time of the design material is 9 minutes. Flowability, bleeding, fresh density and segregation test are conducted on the fresh sample.

Figure 5.5(a) shows typical measurement of flow diameter of the CLSM, and Figure.5.5 (b) shows the lab set up for measuring fresh density and bleeding of the freshly prepared CLSM samples.





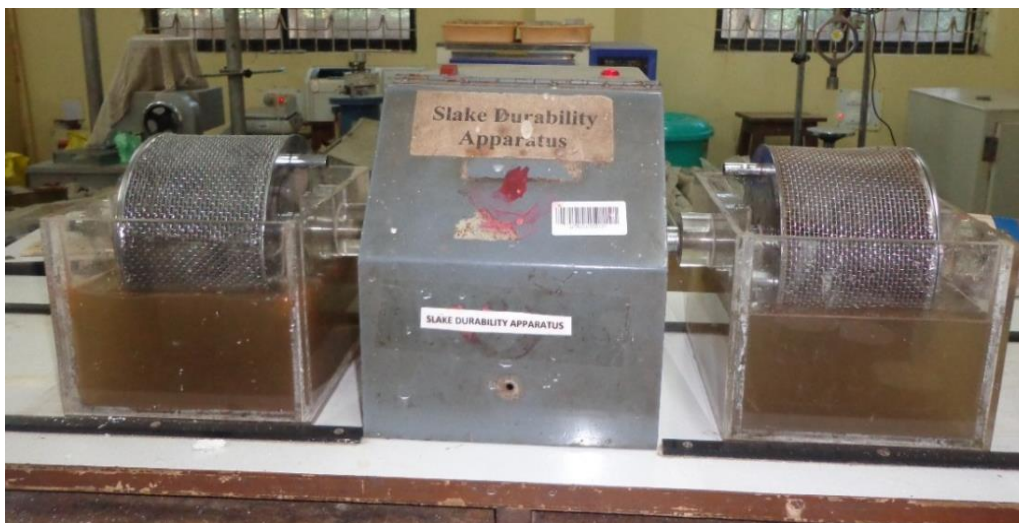
**Figure 5.5:** (a) Measuring flow diameter of CLSM. (b) The test set of for measuring bleeding of CLSM.

### 5.2.3 Preparation of Test Cylinders

For each CLSM mixture, the specimen cylinder of size 75mm diameter and 150mm height are prepared for measuring the compressive strength, water absorption and ultrasonic pulse velocity and other properties of the CLSM. It is necessary to handle the specimen cylinder samples very carefully because of their low strength. A number of plastic cylinders are fabricated which are laterally detachable and both opening ends are covered to prevent leakage. Special care was taken during stripping of mould. The freshly prepared CLSM mixture filled into the fabricated cylindrical mould after 30 minutes of its mixing and gently tapped to eliminate the entrapped air voids. Three number of the specimen is prepared for each type of mixture sample. The specimen samples are removed from the mould within 24-48 hours of its preparation and wrapped with cling wrapper to avoid moisture loss. The samples are cured at ambient temperature for a period of 7 days and 28 days. After the specific curing period, the samples are tested and the average of three results is taken as the final result of the sample. Prior to unconfined compressive strength test, the test samples are subjected to the water absorption and ultrasonic pulse velocity test. The test samples are initially weighed and data is recorded, followed by immersing them in water for 30 minutes. After 30 minutes of absorption of water, samples are removed and exposed to the environment for attaining surface dry condition. The samples are weighed again to get the water absorption values of the corresponding samples.

### 5.2.4 Slake Durability Index (SDI)

Exposure to short-term weathering processes may cause wearing, fragmentation, or a combination of the two processes in soft rocks and rock-like materials that include stabilized materials. The susceptibility to short-term weathering process is essential in assessing the durability of stabilized materials for engineering projects (Franklin 1981) and the slake durability test has emerged as the most effective durability test (Lovell 1983). The quantitative estimate of the durability of weak rocks and rock-like substances in the service environment are determined by the slake durability index (SDI) after two drying and wetting cycles with abrasion. The SDI is defined as the percentage, by dry mass, of the material retained on a 2.00 mm sieve after two cycles of oven drying and 10 min of soaking in water with a standard tumbling and abrasion action. In the present investigation, the test was conducted in accordance with ASTM D 4644-87 (ASTM 1992b) using a standard slake durability test apparatus. Oven-dried fragments were placed in drums mounted in the respective troughs filled with water. The drums were rotated at 20 rpm for a period of 10 min. All fragments retained in the drums were carefully removed and put in the oven for 24 h, and the oven-dried weight was taken. The fragments were again put in the drums and the whole process was repeated. The final oven-dried weight of the retained fragments after the second cycle was recorded. The data were used to calculate the SDI after the first and second cycles. Figure 5.6 shows a typical set up for slake durability test set up.



**Figure 5.6:** Slake durability set up.

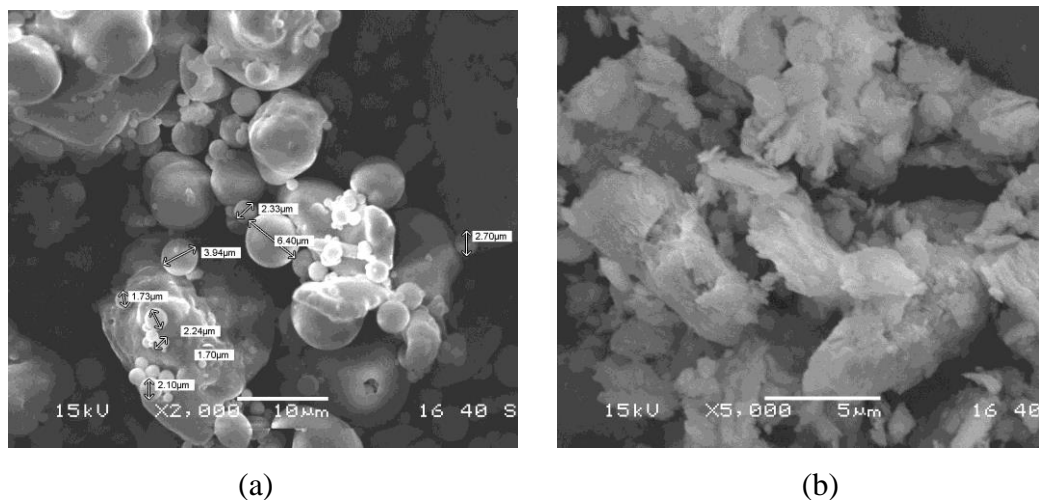
**Table 5.2:** Mix design of CLSM using shale (coal mine overburden, all in aggregate), fly ash, cement and water.

Mix	SERIES	W/B Ratio	Sample Name	Water (%)	Cement (%)	Cement (gm)	FA (gm)	Water	Shale (gm)	Shale as binder (gm)
1	F/C=3.5	0.65	ScM1S1	26	8.88	200	700	585	1350	
		0.70	ScM1S2	28	8.88	200	700	630	1350	
		0.75	ScM1S3	30	8.88	200	700	675	1350	
		0.80	ScM1S4	32	8.88	200	700	720	1350	
2	F/C=2.8	0.65	ScM2S1	26	10.52	250	700	618	1425	
		0.70	ScM2S2	28	10.52	250	700	665	1425	
		0.75	ScM2S3	30	10.52	250	700	713	1425	
		0.80	ScM2S4	32	10.52	250	700	760	1425	
3	F/C=2	0.65	ScM3S1	26	13.33	350	700	683	1575	
		0.70	ScM3S2	28	13.33	350	700	735	1575	
		0.75	ScM3S3	30	13.33	350	700	788	1575	
		0.80	ScM3S4	32	13.33	350	700	840	1575	
4	F/C=1.75	0.65	ScM4S1	26	14.54	400	700	715	1650	
		0.70	ScM4S2	28	14.54	400	700	770	1650	
		0.75	ScM4S3	30	14.54	400	700	825	1650	
		0.80	ScM4S4	32	14.54	400	700	880	1650	
5	F/C=2	0.65	ScM5S1	26	4.44	100	200	585	1350	600
		0.70	ScM5S2	28	4.44	100	200	630	1350	600
		0.75	ScM5S3	30	4.44	100	200	675	1350	600
		0.80	ScM5S4	32	4.44	100	200	720	1350	600
6	F/C=0.66	0.65	ScM6S1	26	10.90	300	200	715	1650	600
		0.70	ScM6S2	28	10.90	300	200	770	1650	600
		0.75	ScM6S3	30	10.90	300	200	825	1650	600
		0.80	ScM6S4	32	10.90	300	200	880	1650	600

Note: F: fly ash, C: Cement, W: Water, B: Binder.

### 5.3 Results and Discussion

Scanning electron micrograph (Figure 5.7a) shows that fly ash consists of mostly spherical particles of a varying size from 1  $\mu\text{m}$  to 100  $\mu\text{m}$ . Similar results have been presented by Das and Yudhbir (2005) and Mahamaya and Das (2016). The shale consists of flaky and plate-like particles shown in Figure 5.7 (b). The spherical fly ash particle will help in lubricating the claimed fill material thereby reducing the water demand.



**Figure 5.7:** Scanning electron micrograph of (a) fly ash (b) shale.

As discussed in Chapter 3, fly ash contains quartz, mullite and haematite along with aluminosilicate in glassy phase and does not have common clay minerals, like kaolinite, illite, chlorite, smectite etc., and particles are spherical (Das and Yudhbir 2005). Hence, fly ash is considered as non-plastic geomaterial (Sridharan and Prakash, 2007). The major minerals found in shale are quartz, calcite and kaolinite shown in Figure 5.8. Mahamaya and Das (2016) also found similar minerals in shale in coal mine overburden. Figure 5.9 illustrates a typical FTIR spectroscopy of shale showing the presence of Si-O-Si and other bonds. The overall chemistry in terms of pH was determined and found that both fly ash (pH = 6.62) and shale (pH = 3.56) are acidic in nature.

Figure 5.10 illustrates a typical grain size distribution curves for the crushed shale and fly ash which is used as the basic material. The boundary of all-in-aggregate shows the importance of the particular crushing machine, thereby giving both fine and coarse aggregate at the same time.

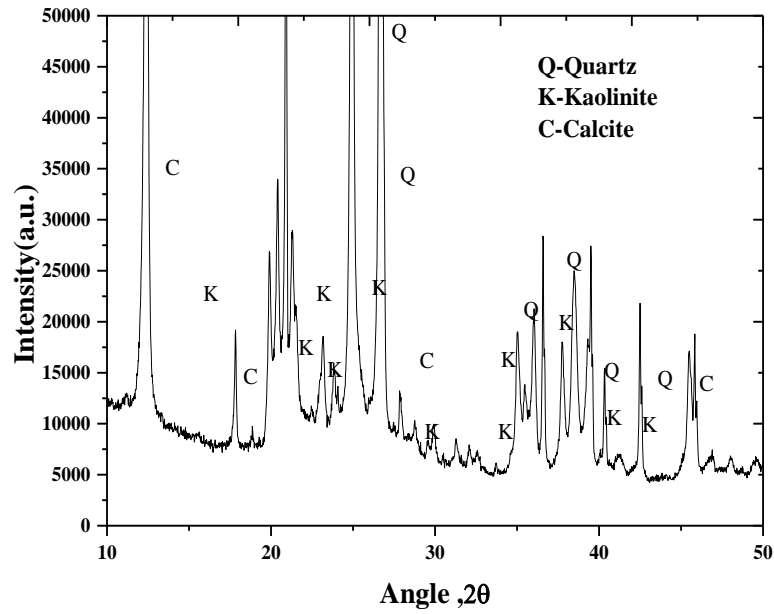


Figure 5.8: XRD analysis of Shale.

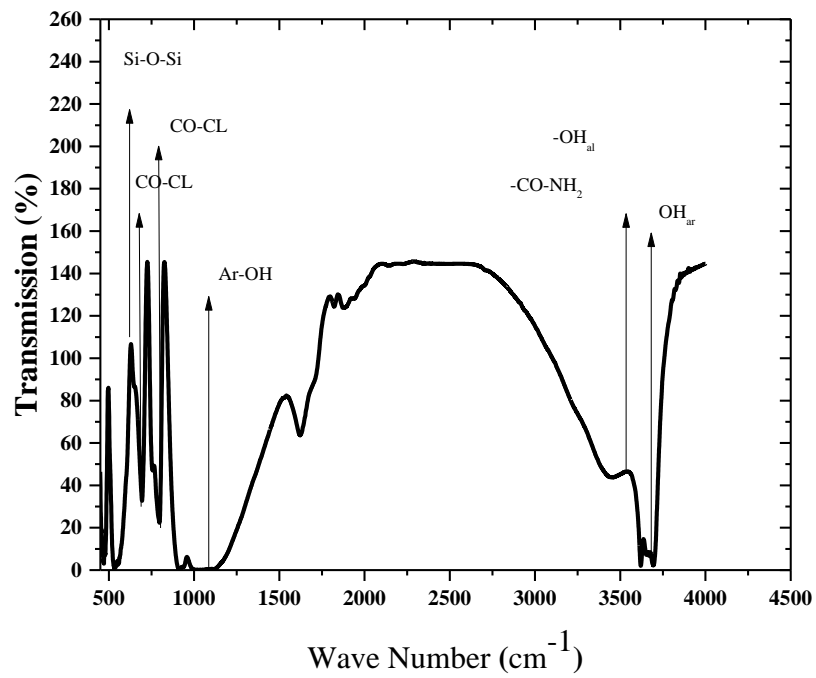


Figure 5.9: FTIR spectroscopy of shale

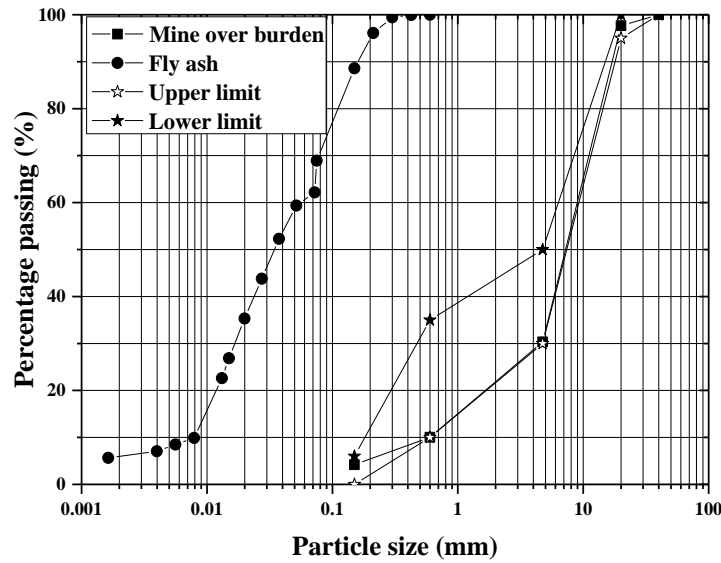


Figure 5.10: Grain size distribution curves for the crushed shale and fly ash.

The heavy compaction (modified Proctor) was conducted as per ASTM D1557 and the maximum dry density (MDD) of fly ash is 12.60 kN/m<sup>3</sup> at optimum moisture content (OMC) of 22.02%, as shown in Figure 5.11. Similarly, the MDD and OMC values for shale are 19.34 kN/m<sup>3</sup> and 9.13%, respectively (Figure 5.11).

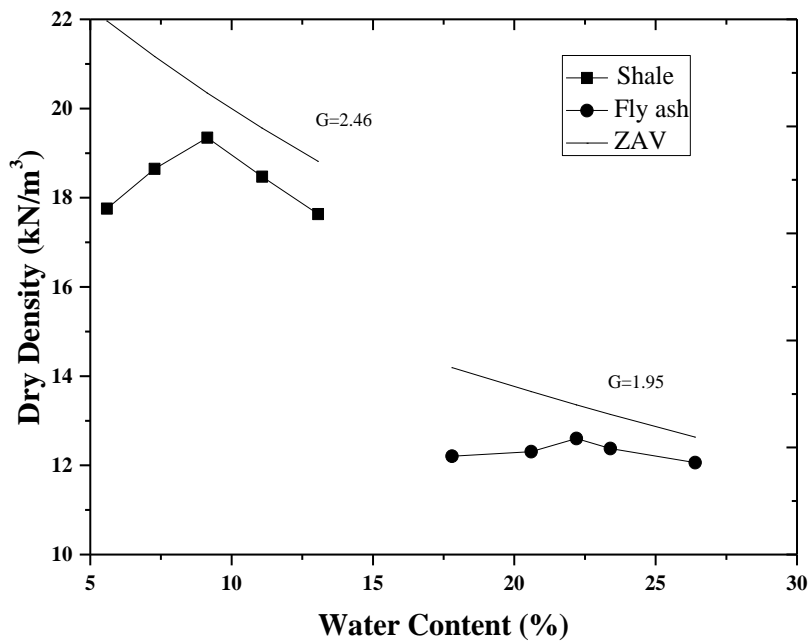


Figure 5.11: Compaction characteristics of fly ash and shale.

There is six number of mixtures and each mixture has four different samples. Each sample of a particular type of mixture varies from other samples only by its water content. The

water to binder ratio is fixed to 0.65 to 0.80. The percentage of cement used in the mixture varies from 8% to 14%. In the mixture 5 and 6, the finer fraction of shale is added as (150 microns) to check the effect of fineness. The cement used in the mixture has consistency 38%, specific gravity 3.01, initial and final setting time are 3h 36 min and 10h 11 min, respectively as described in Chapter 4. The mix design of CLSM mixture is represented in Table 5.2.

The spread diameter increases with increase in water content and flow diameter vary from 128mm to 320mm (Figure 5.12), which have self-flowing and self-levelling consistency as needed for CLSM and bleeding took place at higher water content. The bleeding value of presently used CLSM varies from 0.01% to 2.90%. The bleeding is found to be minimum for ScM2S1 and maximum for the ScM5S4 mix, may be due to reduction in fly ash content. The CLSM having a bleeding value less than 5% at 2h is considered as stable (Gabr and Bowders 2000).

It is also observed that replacement of fly ash with additional finer shale decreased the flow diameter and bleeding, as fly ash percentage plays an important role in the properties of CLSM (Folliard et al. 2008) due to its spherical particles. The fresh density and harden density at 7 days and 28 days of curing of CLSM samples are shown in Figure 5.13. The segregation was not found in any of the mixture as per visual observation.

The fresh density of CLSM is found to be minimum for ScM3S4 is ( $17.18 \text{ kN/m}^3$ ) and maximum for ScM6S1 is ( $18.92 \text{ kN/m}^3$ ). The fresh density of CLSM without air entraining varies from  $16.16 \text{ kN/m}^3$  to  $22.47 \text{ kN/m}^3$  (Folliard et al. 2008). Then CLSM slurry is poured into a cylindrical mould of size 75mm diameter and 150mm height. After 24h the samples are demoulded and then covered by thin cling wrap up to desired curing period. The harden density of the CLSM at 7 days and 28 days of ambient curing was found to be within  $14.96 \text{ kN/m}^3$  to  $16.70 \text{ kN/m}^3$  and  $15.17 \text{ kN/m}^3$  to  $14.47 \text{ kN/m}^3$  respectively. The low density is due to higher percentage of fly ash and density increased with a decrease in fly ash content. The UCS is the pivot test for CLSM (Kuo et al. 2013) and in the present study, unconfined compressive strength (UCS) is conducted after 7 and, 28 days of curing.

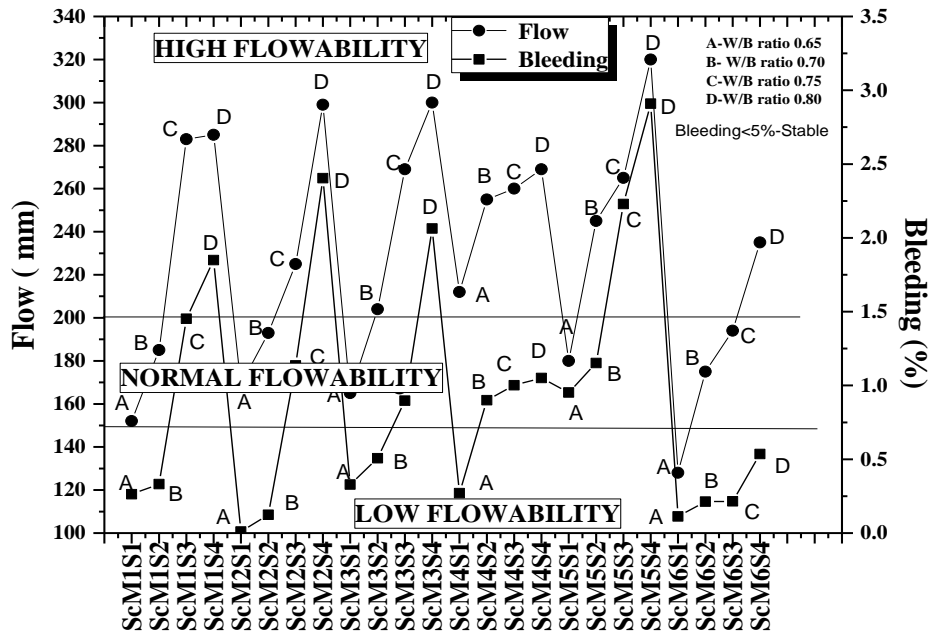


Figure 5.12: Flow and bleeding characteristics of CLSM.

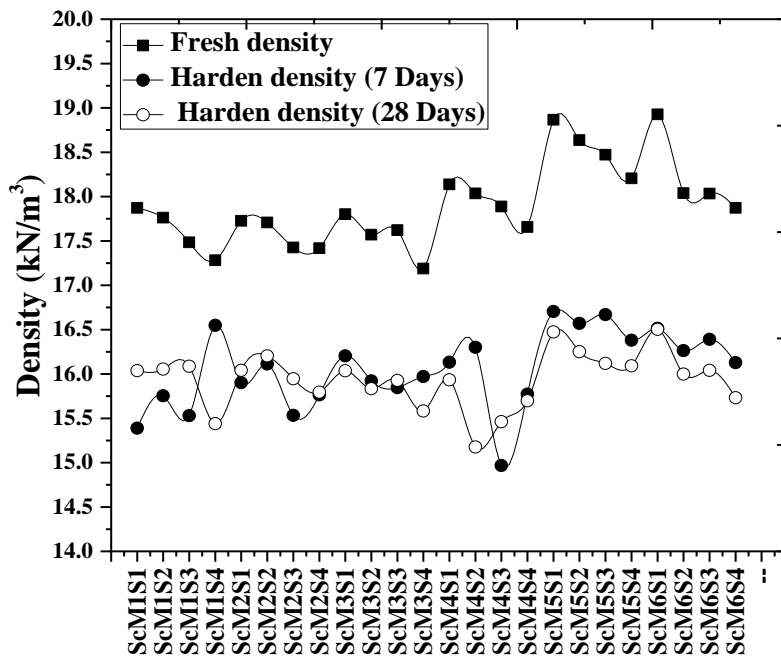


Figure 5.13: Fresh and harden density of CLSM.

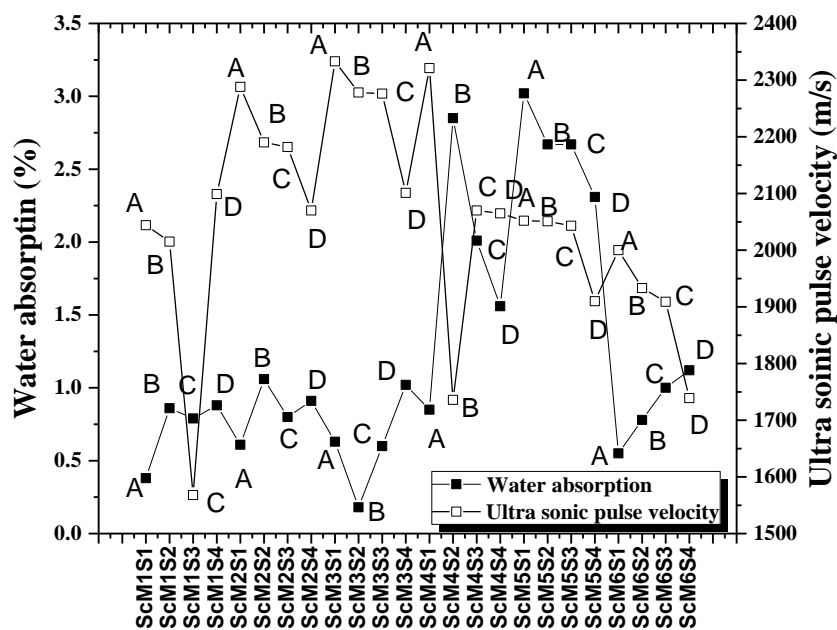
Figure 5.14 shows the measurement of ultrasonic pulse velocity of the CLSM sample and the variations of water absorption of the CLSM samples and their corresponding ultrasonic pulse velocity is Figure 5.15. The water absorption of the CLSM samples are varied within 0.18% to 3.02% and ultrasonic pulse velocity varies from 1568m/s to 2333m/s depending on the voids present in the samples. Low cementation was used in designing the mix proportion of the CLSM, so the C-S-H gel was weak, lacking colloids to fill the internal



pores. Therefore, the measured ultrasonic pulse velocity (UPV) was much lower than that of normal concrete. Higher wave velocity indicates a denser internal structure of concrete as well as higher compressive strength (Kuo et al. 2013).



**Figure 5.14:** Ultrasonic pulse velocity measurement of CLSM sample.

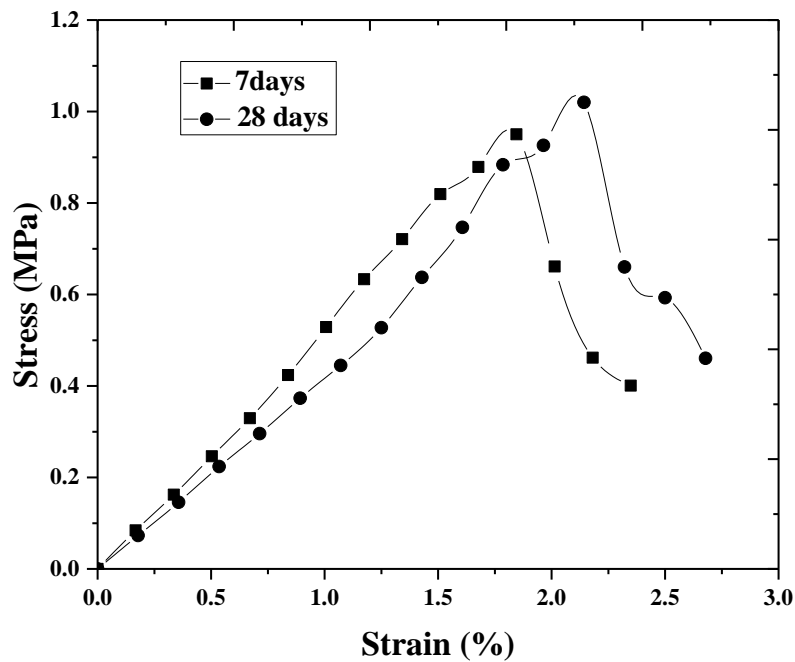


**Figure 5.15:** Ultrasonic pulse velocity and water absorption of different CLSM samples.

The typical stress-strain curve corresponding to the samples ScM5S4 (low F/C ratio) and ScM1S1 (high F/C ratio) after 7 and 28 days of curing are shown in Figures 5.16 and 5.17, respectively. For ScM5S4, the strain corresponding to peak stress (0.95 MPa) is 1.84% and sustained upto 2.34% for 7 days cured sample and the corresponding values at 28 days are 2.14% and 2.67%, respectively. Similarly, ScM1S1, the 7 days peak stress (1.48MPa) and corresponding strain is 1.32% and stand upto 1.82% and the corresponding values at

28 days are 1.85% and 2.36%. Hence, the decrease in fly ash content, decreases the ductility, with small increase in stress, may be due to spherical shape of the fly ash. The stress – strain curve for ScM5S4, corresponds to soft to medium clay (Nataraja and Nalanda, 2008).

The unconfined compressive strength (UCS) of CLSM samples varies from 0.17MPa to 2.44MPa at 7days of curing and 0.58MPa to 2.85MPa after 28 days of curing (Figure 5.18). The maximum compressive strength is found for the sample for ScM3S2 and minimum compressive strength is for ScM6S3 at 28 days of curing. The CBR test was conducted on CLSM sample with soaked condition (7days +4days soaking=11days) and CBR values vary from 32% to 176%.The maximum and minimum CBR values are found for ScM4S2 and ScM5S3 as shown in Figure 5.19. A linear relationship between UCS value and UPV value suggest the compactness is important for the UCS values (Figure 5.20).



**Figure 5.16:** Stress-strain characteristics of sample ScM5S4.

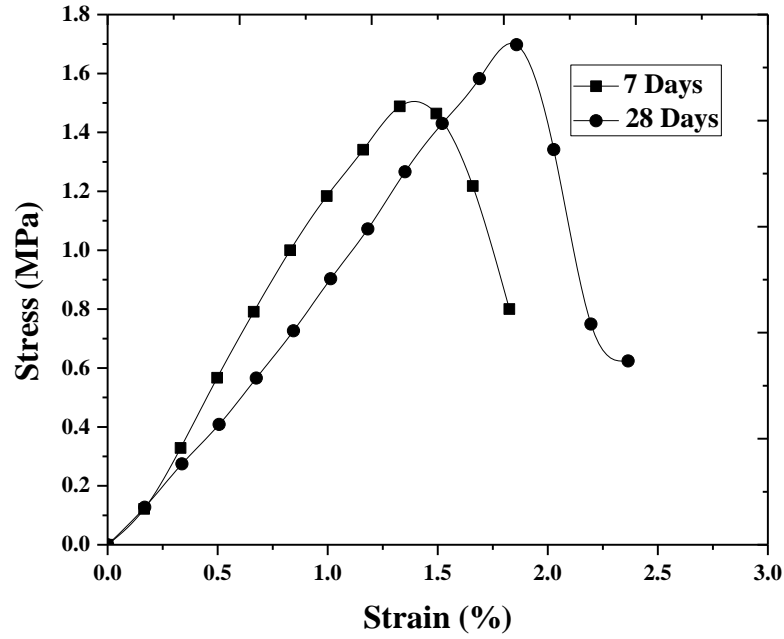


Figure 5.17: Stress-strain characteristics of sample ScM1S1.

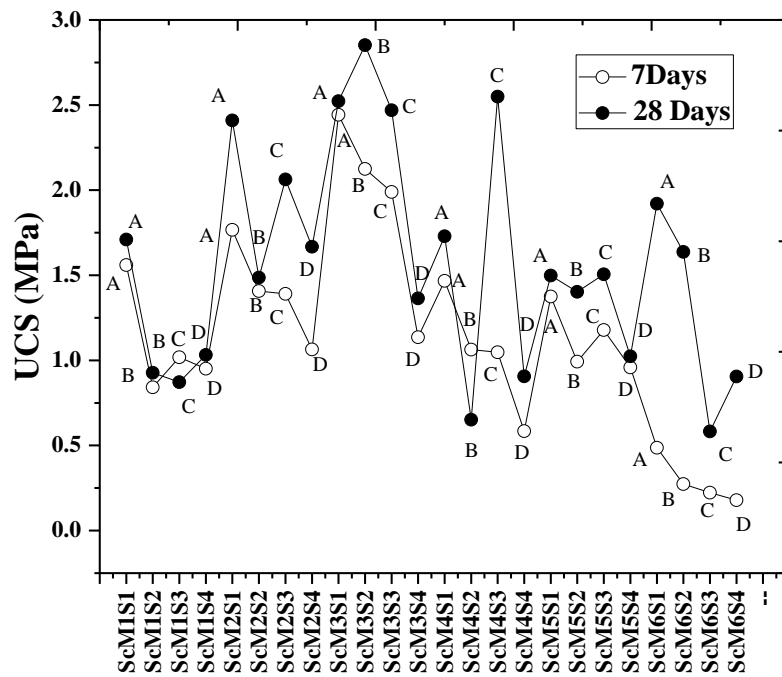


Figure 5.18: The unconfined compressive strength of shale CLSM at 7days and 28days of curing

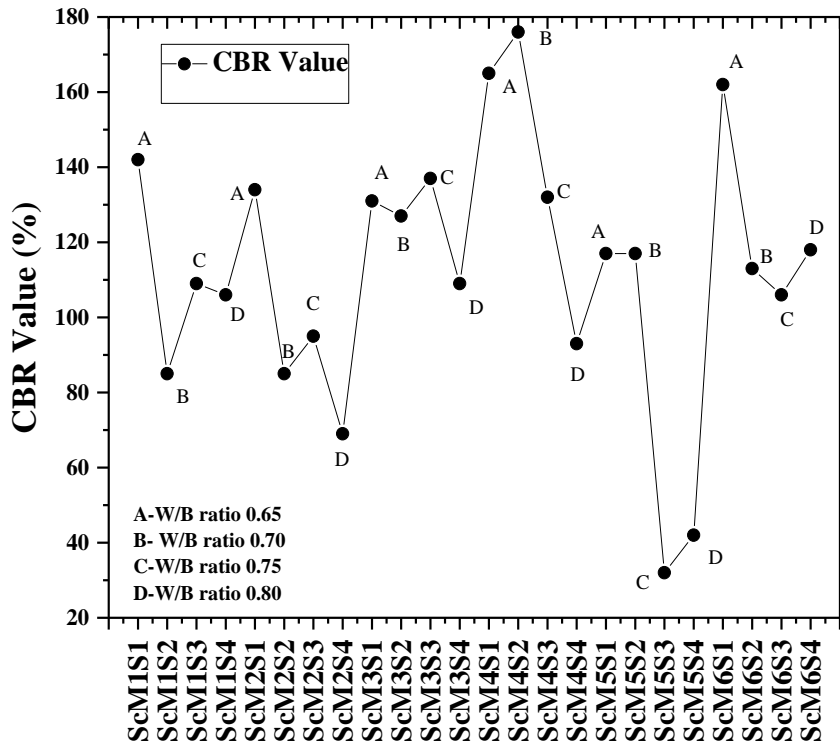


Figure 5.19: CBR values of different CLSM samples.

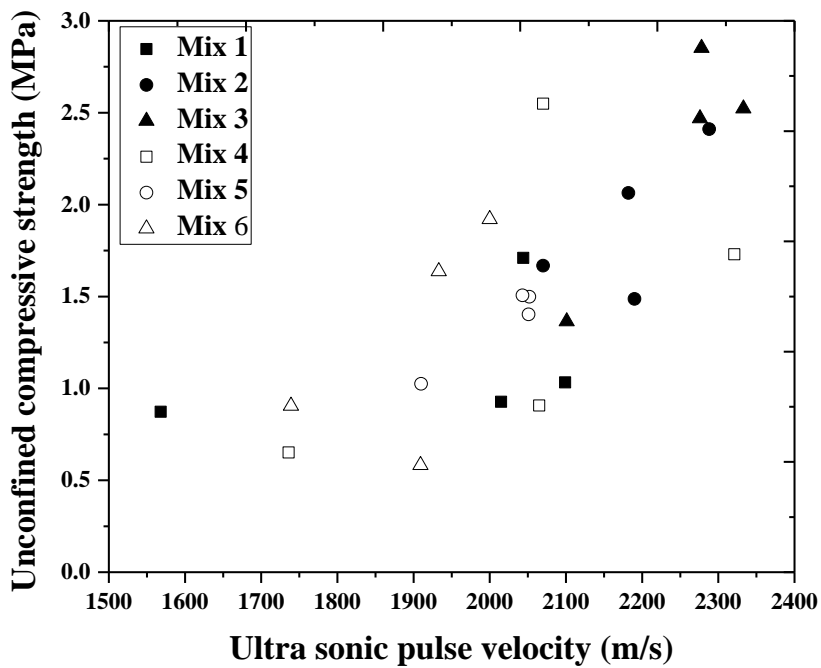
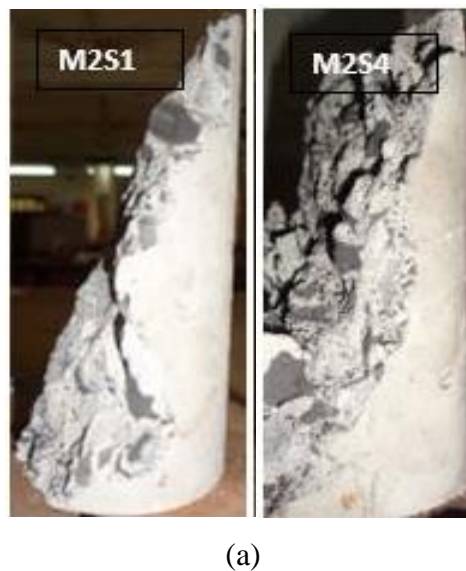


Figure 5.20: Relationship between ultra-sonic pulse velocity and unconfined compressive strength of CLSM samples.

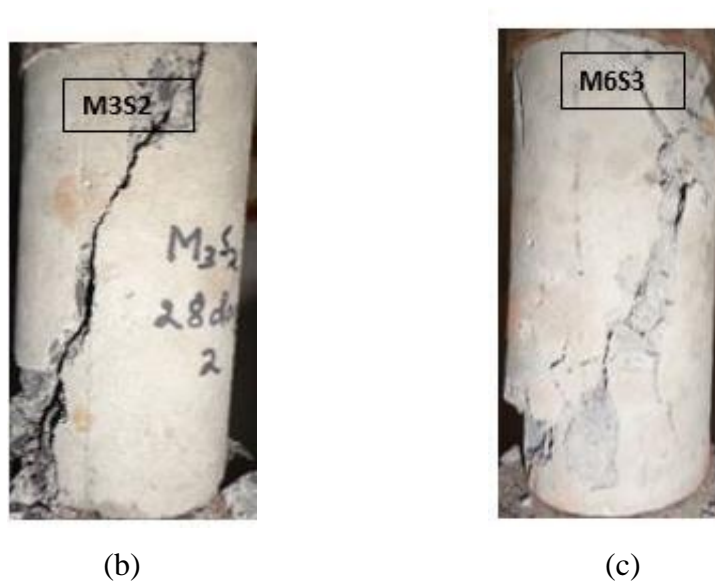
Figure 5.21 shows the cylindrical specimen samples before and after subjected to the unconfined compressive strength. The failure surface as presented in Figure 5.22a shows the aggregates. Figure 5.22b, corresponds to failure pattern of CLSM mix, ScM3S2 (maximum UCS value) and Figure 5.22c, shows that for sample ScM6S3 (minimum UCS value). Table 5.3 shows settlement analysis of presently prepared CLSM samples. The settlement of the samples varies from 0 to 3mm as discussed in Chapter 4, Raghavendra and Udayashankar (2014), observed settlement upto 4mm for gypsum based CLSM. .



**Figure 5.21:** Cylindrical specimen samples (a) before the test and (b) after the test.



(a)



**Figure 5.22:** Failure patterns (a) showing internal aggregates (b) sample ScM3S2 (maximum UCS) (c) sample ScM6S3 (minimum UCS) at 28 days of curing.



**Figure 5.23:** Settlement test set up for CLSM samples.













**Table 5.3:** Settlement test of CLSM (Cylinder size 10cm dia, 20cm height) (in mm from top)

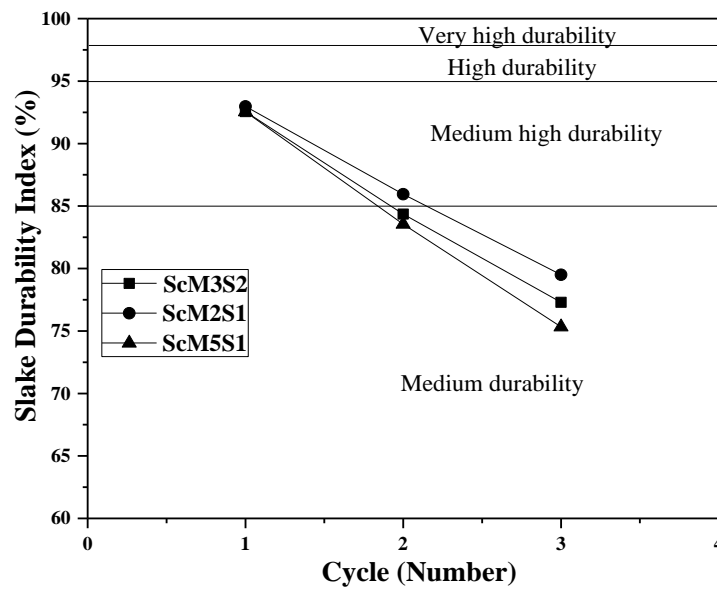
Sample	3days settlement	7days settlement	28days settlement
ScM1S4	3mm	3mm	3mm
ScM2S4	2mm	2mm	2mm
ScM3S4	3mm	3mm	3mm
ScM4S4	3mm	3mm	3mm
ScM5S4	2mm	2mm	2mm
ScM6S4	0	0	0



Some selective cylindrical specimen samples as shown in Table 5.4, after UCS test are subjected to the slake durability index (SDI) test. Figure 5.24 shows the SDI of the selected CLSM mixture and the sample ScM2S1 is of “medium high durability” and other two samples showed “medium durability”.

**Table 5.4:** Slake durability test on CLSM.

Sample	Initial stage	1 <sup>st</sup> Cycle	2 <sup>nd</sup> Cycle	3 <sup>rd</sup> Cycle
ScM3S2 (UCS= 2.85MPa)				
ScM2S1 (UCS= 2.41MPa)				
ScM5S1 (UCS= 2.49MPa)				



**Figure 5.24:** Slake durability index corresponding to the different cycle of some selected CLSM samples.

Leachate analysis of the hardened CLSM mixture is conducted by AAS (Atomic absorption spectroscopy) test through base leaching procedure, for the hazardous elements like zinc, lead, chromium, copper, arsenic and mercury. The Table 5.5 shows the details of leachate analysis of base material and developed materials. All the values of leachate of heavy metals are within the permissible limit.

**Table 5.5:** Leachate analysis of shale CLSM.

<b>Material/Limits</b>	<b>Zn ( ppm)</b>	<b>Pb ( ppm)</b>	<b>Cr ( ppm)</b>	<b>Ni ( ppm)</b>	<b>Cu ( ppm)</b>	<b>As ( ppb)</b>	<b>Hg ( ppb)</b>
Shale (B)	4.134	0	0	8.413	0.027	0.00446	0
JSPL FA	0.004	0	0	0.042	0	2.211	0
CLSM	0.092	0.095	0.039	0.118	0.027	0.01516	0

## 5.4 Summary

This chapter discussed about the development and characterization of CLSM using coal mine overburden using cement and fly ash as a binder. Different physical properties of the fresh and harden CLSM are discussed. Based on the experimental investigation and discussion thereof following conclusions can be made.

- 1 The water absorption of shale aggregate is higher (8.87%) than permissible limit of 2% and the percentage void of is 37.86%. The impact value, crushing value, abrasion value, flakiness index, elongation index and angularity number of the shale aggregate are found to be 37.13%,36%,56.43%,23.01%,25.63% and 1.71% respectively and not suitable for roads and pavements and the OB is being dumped near the mine. Hence, in the present study, an attempt is made to develop CLSM using coal mine overburden.
- 2 The crushing of shale rock resulted in giving both fine and coarse aggregate at the same time, which is termed as all-in-aggregate as per Indian standard.
- 3 The MDD of fly ash is 12.60 kN/m<sup>3</sup> at OMC of 22.02%, similarly, the MDD and OMC values for shale are 19.34 kN/m<sup>3</sup> and 9.13%, respectively as per heavy compaction test.
- 4 The spread diameter increases with increase in water content and flow diameter vary from 128mm to 320mm, which have self-flowing and self-levelling



consistency as needed for CLSM. The bleeding value of presently used CLSM varies from 0.01% to 3.28%. Increase in the finer content of shale and decrease of fly ash content decreased the flowability of CLSM.

- 5 The fresh density of CLSM is found to be minimum for ScM3S4 is ( $17.18 \text{ kN/m}^3$ ) and maximum for ScM6S1 is ( $18.92 \text{ kN/m}^3$ ). The harden density of the CLSM at 7days and 28 days of ambient curing was found to be within  $14.96 \text{ kN/m}^3$  to  $16.70 \text{ kN/m}^3$  and  $15.17 \text{ kN/m}^3$  to  $14.47 \text{ kN/m}^3$  respectively. The low density is due to higher percentage of fly ash and density increased with a decrease in fly ash content.
- 6 The strain corresponding to peak stress ( $1.02 \text{ MPa}$ ) is 2.14% and sustained upto 2.67% at 28 days, corresponding to soft to medium clay. Similarly, ScM1S1, at 28 days strain at peak stress ( $1.71 \text{ MPa}$ ) is 1.85% and sustained upto 2.36%. Hence, decrease in fly ash content, decreases the ductility, but increased in stress.
- 7 The unconfined compressive strength (UCS) of CLSM samples varies from  $0.17 \text{ MPa}$  to  $2.44 \text{ MPa}$  at 7days of curing and  $0.58 \text{ MPa}$  to  $2.85 \text{ MPa}$  after 28 days of curing. The CBR test was conducted on CLSM sample with soaked condition (7days +4days soaking=11days) vary from 32% to 176%. Hence, the material can be used as nonstructural and structural fill.
- 8 As per SDI value the durability of the developed shale CLSM varies from “medium durability” to “medium high durability”.
- 9 Leachate analysis shows that leaching of heavy metals of developed shale are within permissible limit. Hence, the developed CLSM is environmentally sustainable.

Though present chapter discussed about the utilization of coal mine overburden as CLSM, it may not be possible to utilize all the OB and the fly ash within a stipulated time. Hence, there is a need for short-term management of OB and fly ash on their effect on the environment in terms of air and water pollution. In the next chapter a short-term sustainable management of fly ash and coal mine OB using biopolymer.



## CHAPTER 6

# BIOPOLYMER BASED CEMENTITIOUS MATERIAL FOR ENVIRONMENTAL CONTROL

### 6.1 Introduction

Soils in which the clay particles will separate instinctively from each other and go into suspension in quiet water are called dispersive soils (Mitchell, 1993). Dispersivity is a physicochemical process which is mainly affected by the type of soil minerals and chemical properties of the soil pore fluid (Sherad et al., 1976). The dispersive soil (DS), in dry state, causes a dust problem. In saturated condition, piping occurs through this soil causing failure of dams and embankments (Sheard *et al.* 1976). The formation of dispersivity may cause the occurrence of piping phenomena in earth dams (Fell *et al.*, 1992), deterioration and demolition of roads (Nevels, 1993), and the erosion of the compacted soils of landfill clay liners (Tin, 1984). Thus dispersive soils erode under small seepage velocity leading to problems of stability of earth and earth retaining structures. These soils are also identified with negative differential free swell values. The attractive forces are less than the repulsive forces under saturated conditions and this will help the particle to segregate and to move in suspension.

The coal mine overburden mostly contains shale which is low plastic, fine-grained material, susceptible to erosion by both air and water. It decreases visibility and contaminates air and surface water, which seriously affect soil, water and air quality. This contamination causes harmful effect on human health and the quality of life in the surrounding areas. Hence, the most demanding task in these areas is to stabilize the material for wind mainly in semiarid regions and during dry weathers. Similarly, the water erosion of mine overburden is due to dispersive nature of the material. The overland disposal of mine-overburden is responsible for leaching of heavy metals into groundwater and possible transmission of trace metals into the food chain. The disposal of the fine

fraction of coal mine overburden is an issue. One of the major reasons for air pollution is the loss of moisture from the surface of the soil. In most of the mines, water is sprayed continuously to manage the air pollution, which is not cost effective. Figure 1 (a) shows cracking surface of mine overburden after evaporation of water which leads to dust pollution and Figure 1 (b) shows temporary stabilization of dust by sprinkling of water at mines areas. The commercially available chemical suppressants are mostly proprietary items and a costly alternative and may not be environmentally sustainable (Chen et al. 2015).



**Figure 6.1:** (a) Surface crack of a typical mine overburden, (b) Temporary stabilization of dispersive soil by a sprinkling of water.

As discussed in Chapter 5, many times, the thermal power plants are coming up in the vicinity of coal mines. The fly ash particles are spherical, does not contain common clay minerals and non-plastic (Das and Yudhbir 2005; Sridharan and Prakash 2007), hence susceptible to wind and water erosion. Similarly, shale is mostly silt-sized particle with low plasticity and susceptible to erosion by both air and water. In the mining areas, Fly ash and mine overburden particles decrease visibility and contaminate air and surface water, which seriously affect soil, water and air quality. This contamination results in a harmful effect on human health and the quality of life in the surrounding areas. When the fly ash is used to fill the mine, the wind and water erosion problem become compounded. Hence, the most demanding task in these areas is to stabilize the material for wind mainly in semiarid regions especially during dry weathers and water erosion during occasional heavy rain falls. The overland disposal of fly ash is responsible for leaching of heavy metals into groundwater and possible transmission of trace metals into the food chain, though, as a whole fly ash is not included in the hazardous waste group (Das et al. 2015).

As discussed in Das and Yudhbir (2005), fly ash fill and embankment needs to be protected against erosion as they have apparent cohesion, which is lost when they are dry. Then the particles get detached from the surface and transported away from its origin and make the embankment unsafe and environment polluted. One way is covering fly ash with suitable soil, but this can be implemented only for closed impoundments (Chen et al. 2015), but active fly ash pond is an important issue. Similarly, shale is also vulnerable to wind erosion (Figure 6.1b) and water erosion, due to its dispersiveness nature.

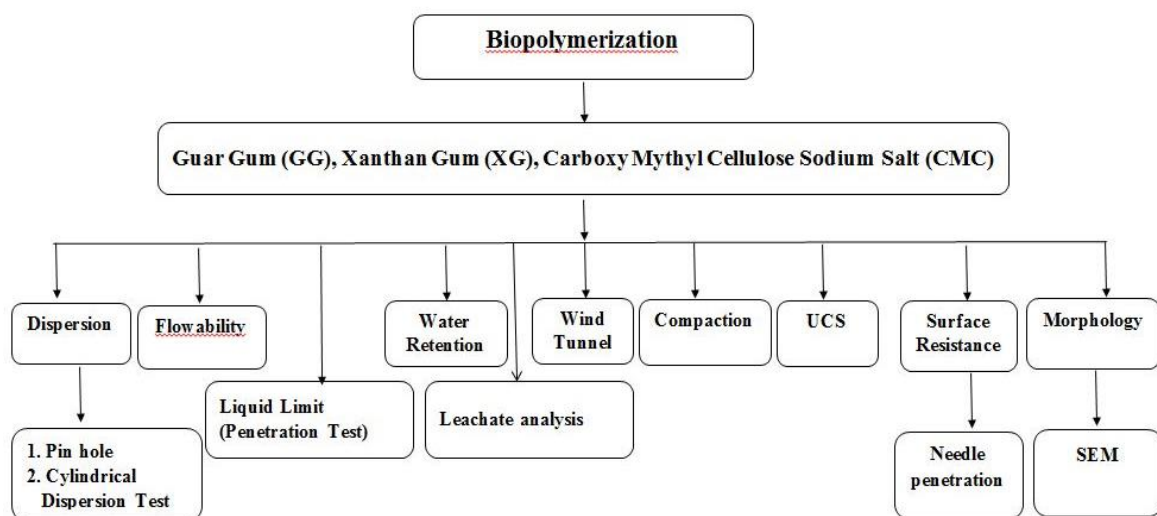
The alum (aluminium sulphate) was found to be effective to control the dispersivity of bentonite, which is a dispersive soil (Ouhadi and Goodarzi, 2006). Based on pinhole tests, double hydrometer and crumb test (Bhuvaneshwari and Soundara, 2007) observed that dispersive soil could be stabilized with lime and fly ash mixture. Lime and cement improves the strength and reduce the dispersivity of the soil (Umesh et al, 2009, Vakili et al., 2013) and chemical agents including sodium chloride, sodium carbonate, sodium sulfate and sodium polyphosphate are also found to be effective for reducing dispersivity of natural soil (Abbasi and Nazifi, 2013). The magnesium chloride ( $MgCl_2$ ) solution is effective in reducing dispersive and expansiveness of clay soils (Turkoz et al., 2014). The industrial by-product, granulated blast furnace slag (GBFS) and basic oxygen furnace slag (BOFS) also can be used to reduce the dispersivity of soil (Goodarzi and Salimi 2015). However, the chemicals used for such stabilization may not be suitable for the ecosystem. The erosion control of canal banks, due to dispersive soils using chemical admixtures may not be in coherence to sustainable development. The microorganisms present in the soil can be helpful to achieve some modification in soil (Ivanov and Chu, 2008). Some studies have been made to stabilize the mine tailing using biopolymer (Chen et al. 2013; Chen et al. 2015), but, the study is limited to the coarse-grained mine tailing.

Hence, in the present study focuses on stabilization of fly ash and mine overburden using biopolymer for wind and water erosion by incorporation of three natural biopolymers; guar gum (GG), xanthan gum (XG) and Carboxyl methylcellulose sodium salt (CMC) my. Biopolymers are produced by biological systems such as microorganisms, plants, and animals and are synthesized chemically. But they are originated from biological starting materials such as amino acids, sugars, natural fats, or oils. Because of their unique properties and the growing awareness of environmental sustainability and stability, biopolymers have been increasingly investigated for their potential use in soil stabilization (Martin et al. 1996; Karimi 1998; Ivanov and Chu 2008; Dejong et al. 2010). Both the fly

ash and coal mine overburden are fine-grained particles and pose a serious environmental problem in regards to air and water pollution. The stabilized material was prepared using various concentrations of GG, XG and CMC whose physical properties helps in binding the non-cohesive and dispersive materials fly ash and mine overburden with a considerable increase in strength. The effectiveness of stabilization using biopolymers is discussed in terms of both air and water erosion. Different measures like dispersiveness, surface resistance, water retention capacity and wind tunnel test are used to assess the effectiveness of biopolymer stabilization.

## 6.2 Materials

The mine overburden, which is predominantly shale, was collected from the coal mines and the fly ash was collected from the hopper of a thermal power plant near the coal mine, from JSPL, Raigarh, Chhattisgarh, India. It may be mentioned here that coal mine overburden mostly consists of shale (Bell 2007) with other rock/soil. In the present chapter, the finer fraction of coal mine overburden, which is black in colour is termed as shale. The basic properties of the shale, fly ash and the biopolymers, xanthan gum (XG), guar gum (GG) and Carboxymethyl cellulose (CMC) have been discussed in Chapter 3. Both XG and GG have been successfully applied for dust control and increase in the cohesion of mine tailings (Chen et al. 2013, 2015), but the use of CMC as an anionic polymer for control of Na- montmorillonite was not effective (Inyang et al. 2007). The flow chart of the experimental investigations of the present work is shown in Figure 6.2.



**Figure 6.2:** Flowchart of experimental investigations of the present chapter.

## **6.3 Methods**

Different geotechnical engineering properties like grain size (ASTM D422), liquid limit (ASTM D4318), plastic limit (ASTM D4318), and compaction characteristic (ASTM D1557) test were conducted as per relevant ASTM standards. The erosion of fly ash and mine overburden can be described either (1) due to water or (2) due to wind erosion. The susceptibility of fly ash and shale to water erosion (dispersiveness) was studied using pinhole test and cylinder dispersion test. The erosion susceptibility to wind was tested with surface resistance, water retention and wind tunnel test, and is discussed in this section.

### **6.3.1. Dispersion Test**

Different methods available to measure the dispersiveness of geomaterials are crumb test, double hydrometer test, pinhole test (ASTM D4647) and cylinder dispersion test (Atkinson et al. 1990). In the present study, pinhole test and cylinder dispersion test are used. Cylinder dispersion test is an advanced process of crumb test, which is considered to observe the characteristics of soil at zero effective stress by immersing a saturated sample in water (Atkinson et al. 1990). The cylindrical dispersion test erosion resistance is presented by true cohesion and influence of pore water dispersion characteristics of materials on their erosion resistance can be assessed. In the dispersive test, the quality of water in which the samples were immersed will give a colloidal suspension from which samples can be categorized as dispersive and non-dispersive. The procedures adopted for the cylinder dispersion test are simple and adopted using a measuring jar of 1000 ml. A sample of the geomaterial to be tested was dried, ground to a powder and remixed with de-aired water to form a cylindrical sample. The chemistry of the mixing water may be chosen to examine different initial condition and in the present study it is either water of the biopolymer solution. The sample was then gently lowered into a beaker containing water with the required chemical composition. Alternatively the sample may be placed in an empty beaker and water added. In both cases it is important to avoid excessive turbulence.

### **6.3.2. Water Retention and Wind Tunnel Test**

The water retention helps in binding the particles for dust control. Hence, in the present study, the effect of biopolymer on the water retention and dust control was studied.

The samples for the water retention and wind tunnel test were prepared using aluminium container size (15×18) cm and (30×30) cm, respectively. Firstly sundried samples are taken and subjected to minor compaction to attain field criteria, then a constant amount of normal water was added to similar kinds of sample and water is sprayed equally over the entire area (Chen et al. 2015). The biopolymer solution is prepared by dissolving biopolymer powder to normal water to a specific concentration of (0.5%, 1%, 1.5% and 2%) after getting a homogeneous solution. Different methods of application of biopolymer solution on the surface of the container were adopted. In the first attempt, prepared solution was directly spread over the entire area and exposed to sunlight, but it was observed that the thin layer of dry gum started to get removed from its surface with time and the bonding between gum layer and the surface of stabilize material get separated. To resolve the problem some amount of fly ash or shale mixed thoroughly with respectively prepared gum solution to a homogeneous slurry and spread over the surface of materials and it was found effective. The sundried samples were treated with biopolymer solution (GG, XG and CMC) at the rate of 2.5L/m<sup>2</sup> to cover the surface area in comparison to 1.9L/m<sup>2</sup> as per Chen et al. (2015). It may be mentioned that Chen et al. (2015) studied for the coarse-grained mine tailing whereas in the present study shale and fly ash is finer than the mine tailings, hence need more solution per surface area.

After completion of water retention test, the sample with container size 15cm×18cm was subjected to flat-ended cylindrical penetration test for measurement of surface resistance strength. The sundried sample of the container of size 30cm × 30cm was subjected to wind tunnel test. The samples subjected to wind tunnel tests are shown in Figure 6.3 (a). The setup of the wind tunnel is shown in Figure 6.3(b). It is fitted with anemometer slightly above the sample container and applied with a wind speed of 100km/h (27.77 m/s) for the duration of 10 min. The weights of the samples before and after the wind tunnel tests are measured. The weight loss during the wind tunnel test is considered as the estimate of dust resistance of each sample.



(a)





(b)

**Figure 6.3:** (a) Sample prepared for wind tunnel test (b) Wind tunnel set up.

### 6.3.3 Surface Resistance Test

There are different methods to assess the erosion resistance of soil like the surface resistance of soil, modulus of rupture method, needle penetrometer method, fall cone method, needle penetrometer method, torvane method, aggregate stability method (Rice et al. 1996). In the present study flat-ended cylindrical penetrometer technique is used as per Rice et al. (1996) and Chen et al. (2015) to determine the surface strength of fly ash and shale treated with different concentration of biopolymer. This method is more convenient as far as field application is concerned (Chen et al. 2015). Hence, in the present study, a flat-ended cylindrical penetrometer having diameter 6mm was fabricated and attached to loading machine to obtain the force penetration curve. The penetration test was conducted at a strain rate of 1.2 mm/min and up to 4mm depth of penetration.

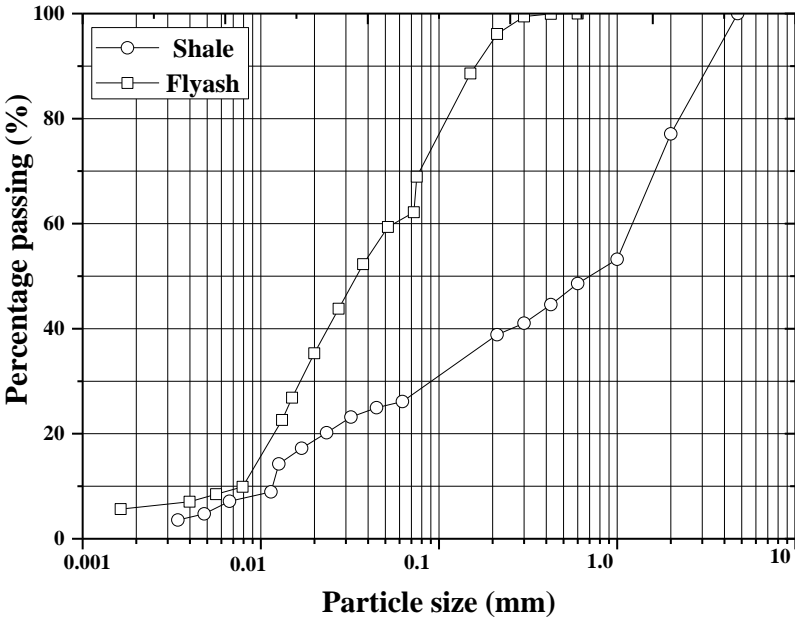
## 6.4 Results and Discussion

The results of the present study regarding material properties with and without biopolymer stabilization are presented in this section. The repeatability of the results is presented in terms of average value and coefficient of variance (COV). The COV is defined as the ratio of mean value to standard deviation and is presented in percentage. It was observed that the COV (%) values are within the range of different geotechnical parameters as presented in Phoon et al. (1995).

As presented in Chapter 5, fly ash consists of mostly spherical particles of a varying size from 1 $\mu$ m to 100  $\mu$ m and major minerals in shale are quartz, calcite and kaolinite and both fly ash (pH = 6.62) and shale (pH = 3.56) are acidic in nature.

**Grain Size Distribution, Plasticity and Specific Gravity**

The grain size distribution of fly ash and shale used in the present study are presented in Figure 6.4. It can be seen that fly ash is fine-grained with 70% being fine particles (< 75 μm) and shale is a coarse-grained material with 27% finer particles. It may be mentioned here that shale was ground mechanically to the coarse-grained size as a construction material. The liquid limit of shale was found to be 33% with plasticity index as 12, whereas the fly ash is non-plastic with LL of 32%. As per ASTM D2487 classification, shale can be classified as clayey sand (SC) and fly ash as non-plastic inorganic coarse silt-sized fractions (MLN) as per Sridharan and Prakash (2007). As discussed in Chapter 5, the specific gravity (*G*) values of the materials are found to be 1.95 for fly ash and 2.46 for shale as per ASTM D854, which is lower than the *G* value of the standard soil of 2.65-2.7. Sridharan and Prakash (2007) presented similar results of Indian fly ash *G* value varying 1.66 to 2.55. The lower *G* value of spherical particles and non-plastic nature of fly ash makes it vulnerable to wind and water erosion. Similarly, shale is with low plasticity, contains coarse-grained particle and low *G* value, hence needs investigation for wind and water erosion susceptibility.



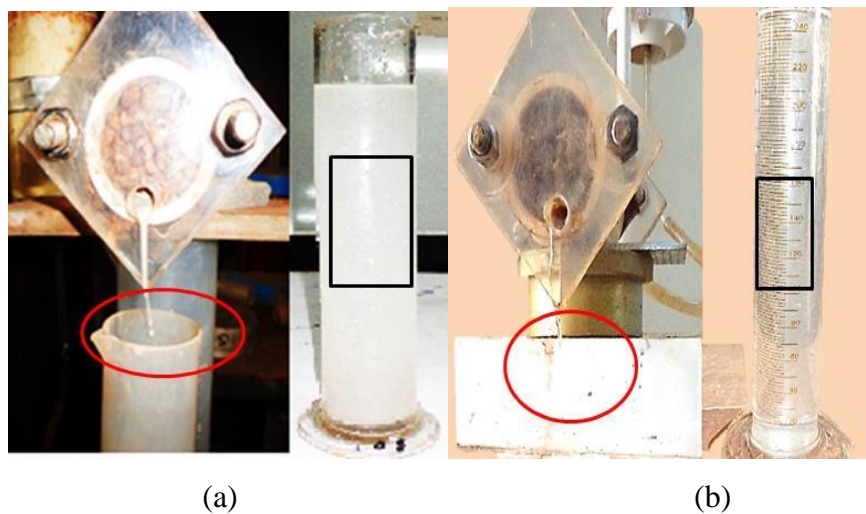
**Figure 6.4:** Grain size distribution of fly ash and shale.

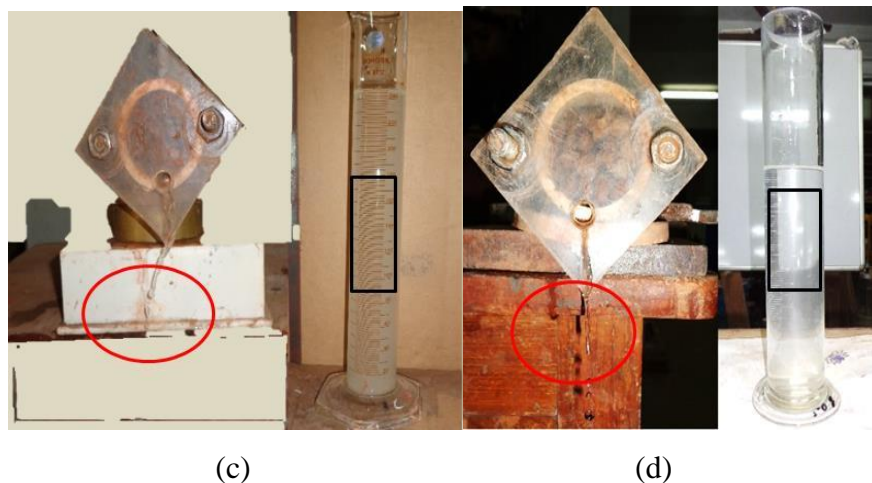
**Dispersion Test**

As discussed earlier, the dispersiveness was measured as per pinhole test and cylindrical dispersion test. Based on pinhole test as shown in Figure 6.5(a) it was observed that fly ash is highly dispersive as the water hail from the pinhole had turbidity and cloudiness of

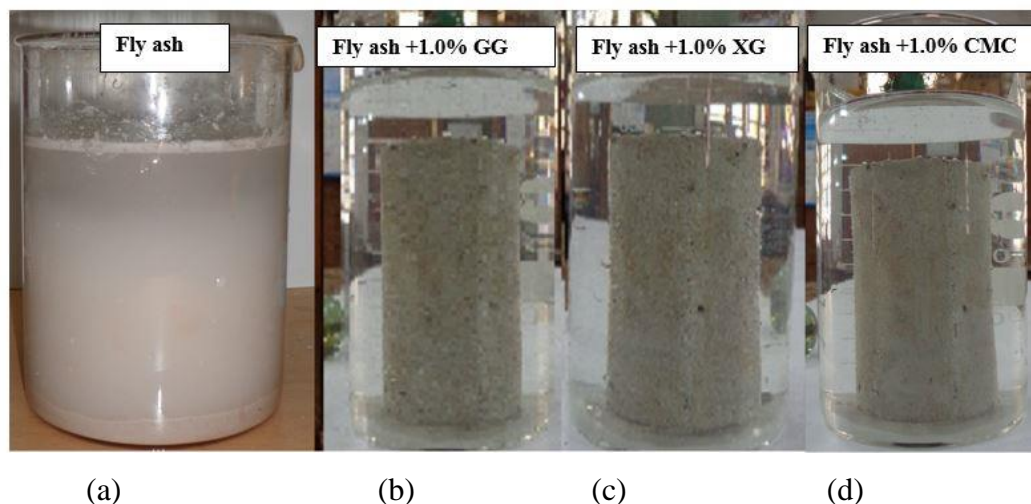
water are very dark (ASTM D4647). Hence, in the present study, fly ash was treated with different percentages (0.5%, 1.0%, 1.5% and 2.0%) of xanthan gum (XG), guar gum (GG) and carboxymethyl cellulose sodium salt (CMC). Fly ash treated with GG of 0.5% of concentration as per pinhole test (Figure 6.5b) showed that the water hail from the biopolymer treated sample had no turbidity and water quality is clear. Similar observations are made for the higher percentages (1.0%, 1.5%, and 2%) of guar gum. Pinhole test results of fly ash treated with different concentrations (0.5%, 1.0%, 1.5%, and 2%) of xanthan gum showed that water coming out from treated fly ash was moderately dark in colour, even with 2% of xanthan gum solution as shown in Figure 6.5c. The pinhole test was also conducted on the fly ash treated with 0.5% of CMC and it was observed that the water hails outlet of the pinhole was very clear as shown in Figure 6.5d compared to Figure 6.5b for GG. Hence, it may be concluded that CMC is more effective in reducing the dispersiveness of fly ash compared to XG and GG. This may be due to the fact that CMC is anionic and more viscous.

Figure 6.6 shows the cylindrical dispersion test on fly ash and fly ash with 1.0% concentration of GG, XG and CMC treated samples, respectively as 0.5% concentration was not effective. It can be observed that the fly ash without any biopolymer treatment shows puddle clay water surrounding the sample and some sediment gets deposited at the bottom of the beaker, whereas the water around bio-treated fly ash sample is clear. It can be seen that biopolymer treatment can reduce the dispersiveness of the fly ash as per cylindrical dispersion test. It may be mentioned here that though as per pinhole test, XG was not effective, as per cylindrical test it is effective in reducing the dispersiveness.





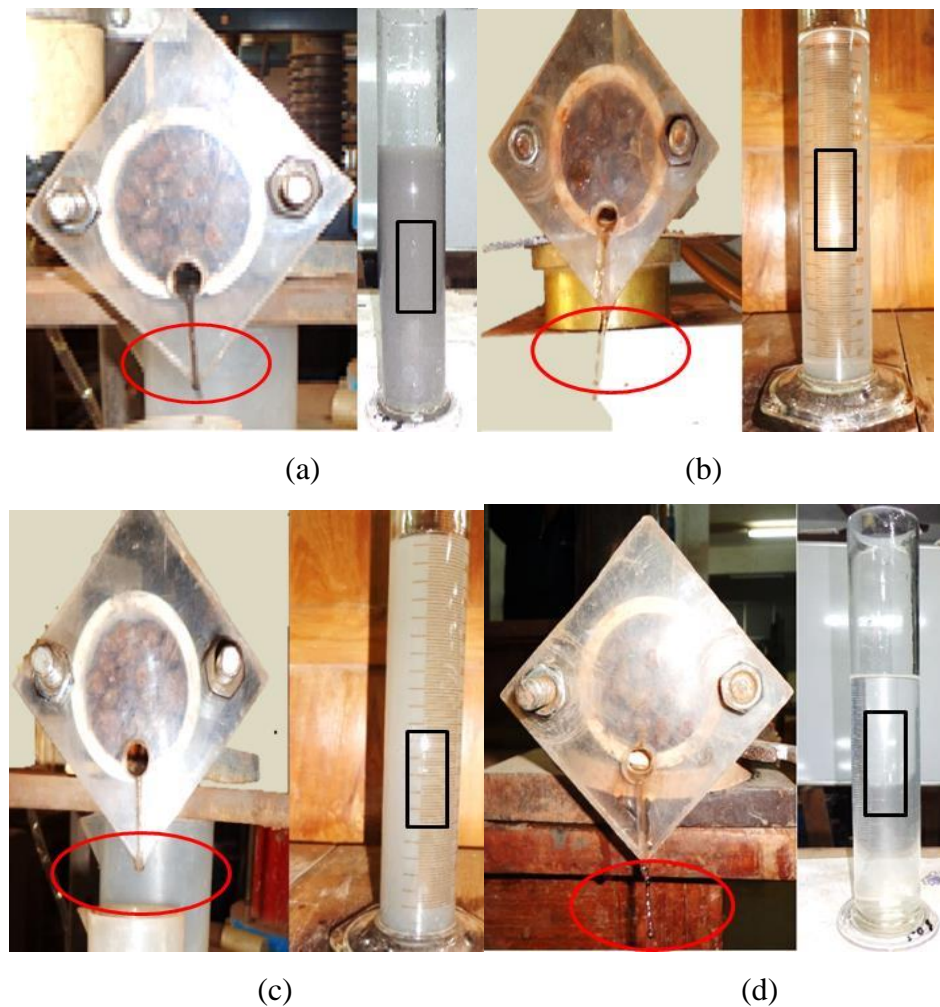
**Figure 6.5:** Pinhole test of (a) fly ash, (b) fly ash treated with 0.5% of GG, (c) fly ash treated with 2.0% of XG, and (d) fly ash treated with 0.5% of CMC.



**Figure 6.6:** Cylinder dispersion test of (a) fly ash (b) fly ash treated with 1.0% of GG and (c) fly ash treated with 1.0% of XG and (d) fly ash treated with 1.0% of CMC

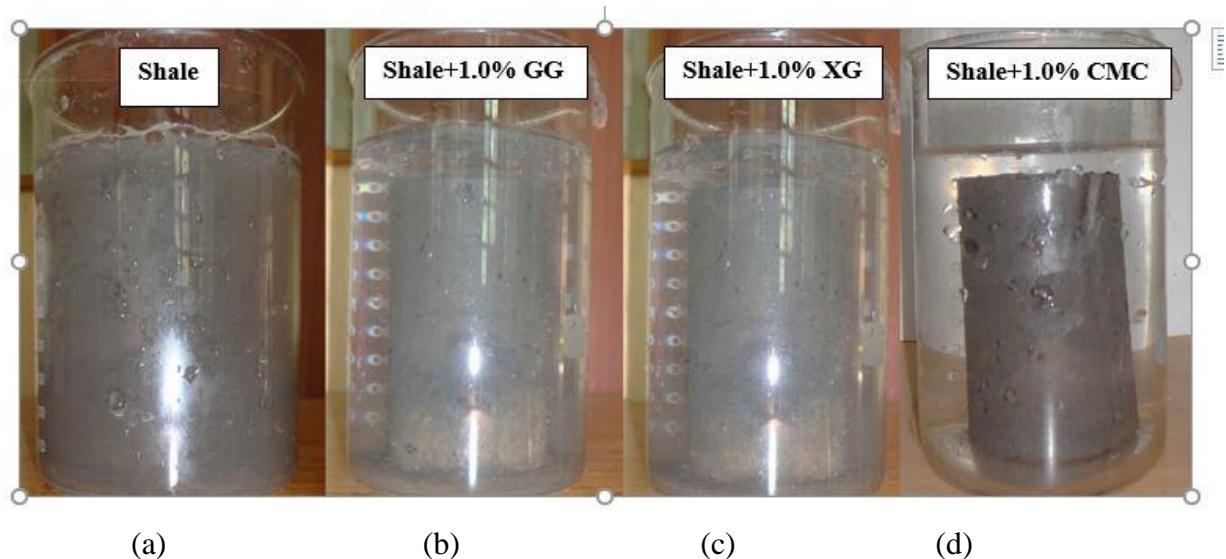
The pinhole test Figure 6.7a shows that shale is dispersive in nature as the water hail from the pinhole had cloudiness (ASTM D4647). The pinhole test with 0.5% GG (Figure 6.7b) had no turbidity and water quality is clear. The shale sample treated with different concentrations (0.5%, 1.0%, 1.5%) of xanthan gum solution was subject to same procedure and it was found that the water hail from the samples are moderately dark in color up to 1.5% of XG and the shale sample treated with 2% of XG solution is shown in Figure 6.7c. Similarly, the shale sample also treated with 0.5% of CMC and subjected to pinhole test and it was found that the water hails from the outlet of the pinhole was very clear (Figure 6.7d).

Similarly, based on the result of shale for cylinder dispersion test, the shale and shale with 1.0% concentration of GG, XG and CMC treated samples respectively is shown in Figure 6.8. It can be clearly visible that the shale without any biopolymer treatment shows puddle clay water surrounding the sample of the beaker whereas the water around biotreated shale sample is clear. As the cylindrical dispersion test presents the resistance due to true cohesion and depends upon the influence of pore water (Atkinson et.al, 1990), it may be considered as a better method compared to pinhole test. Hence, as per the cylindrical dispersive test both fly ash and shale becomes non-dispersive after stabilizing with GG, XG and CMC. However, CMC is found to be more effective in reducing the dispersiveness of the fly ash and shale.



**Figure 6.7:** Pin hole test of (a) shale, (b) shale treated with 0.5% of GG, (c) Shale treated with 2.0% of XG, and (d) Shale treated with 0.5% of CMC.





**Figure 6.8:** Cylinder dispersion test of (a) shale (b) shale treated with 1.0% of guar gum (c) shale treated with 1.0% xanthan gum and (d) Shale treated with 1.0% of CMC

### The Consistency of Biopolymer Treated Sample

The consistency test was conducted using cone penetration test to determine the consistency of biotreated samples as per BS: 1377 (British Standard Institution 1990; Chen et al. 2015). Variation of water content with a penetration depth of fly ash and fly ash treated with GG, XG and CMC are shown in Figure 6.9 and Figure 6.10 and Figure 6.11 respectively. The liquid limit corresponding to 20mm penetration found to increase with the concentration of biopolymer. The variations of water content and penetration depth treated with biopolymers (GG, XG and CMC) show irregular variation, though, Chen et al. (2015) observed increases in liquid limit with an increase in biopolymer concentration for the mine tailing. But it may be mentioned here that mine tailings are coarse-grained and non-cohesive, whereas fly ash is fine-grained but non-cohesive. Hence, the grain size and cohesion may play a role in determining the effectiveness of biopolymer and needs further investigations in this regards.

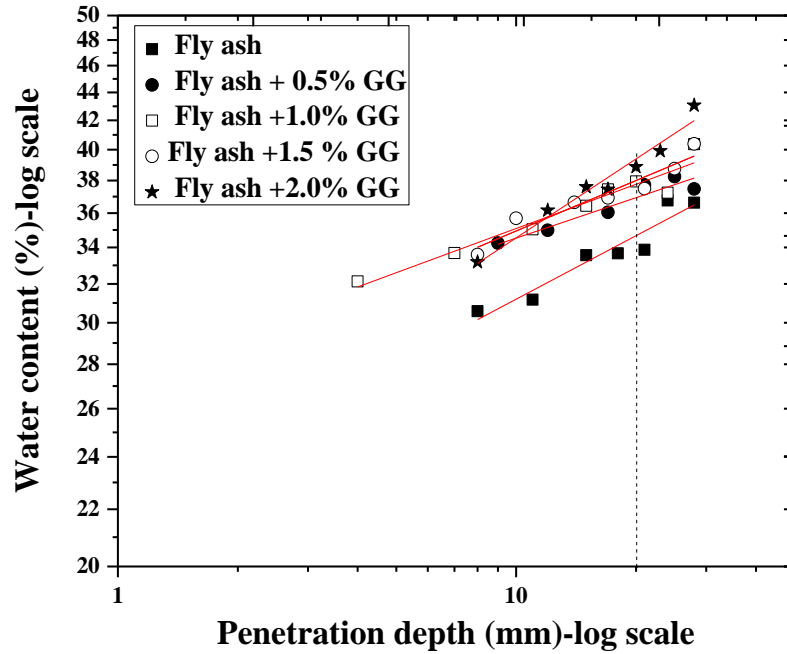


Figure 6.9: Log-log plot of penetration depth versus water content at different biopolymer concentrations for fly ash with GG

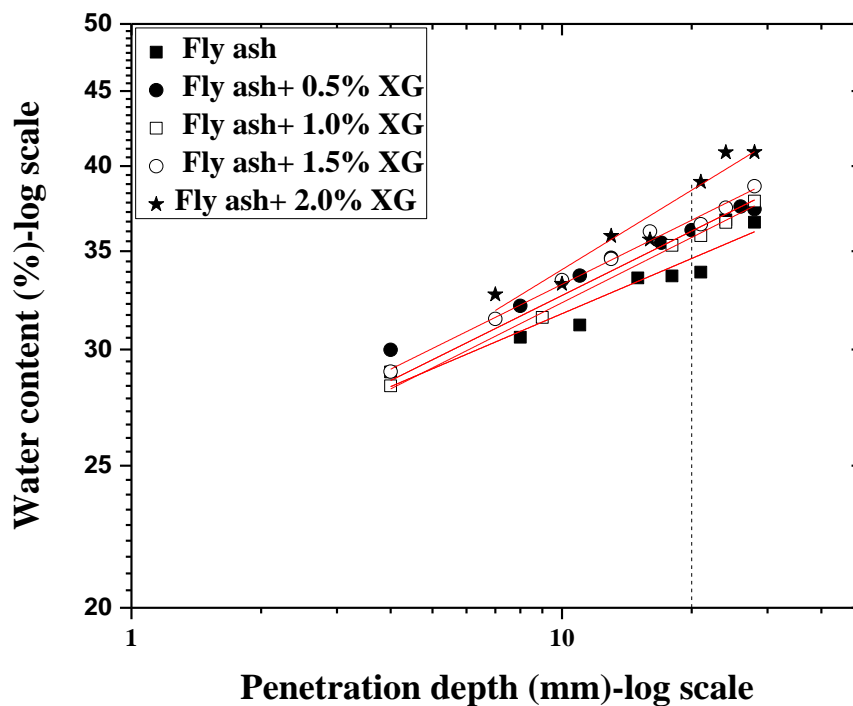


Figure 6.10: Log-log plot of penetration depth versus water content at different biopolymer concentrations for fly ash with XG

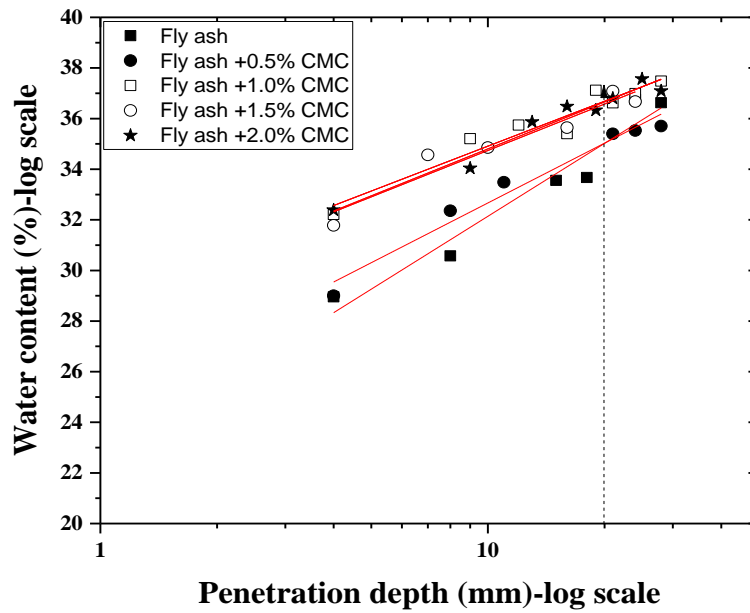


Figure 6.11: Log-log plot of penetration depth versus water content at different biopolymer concentration

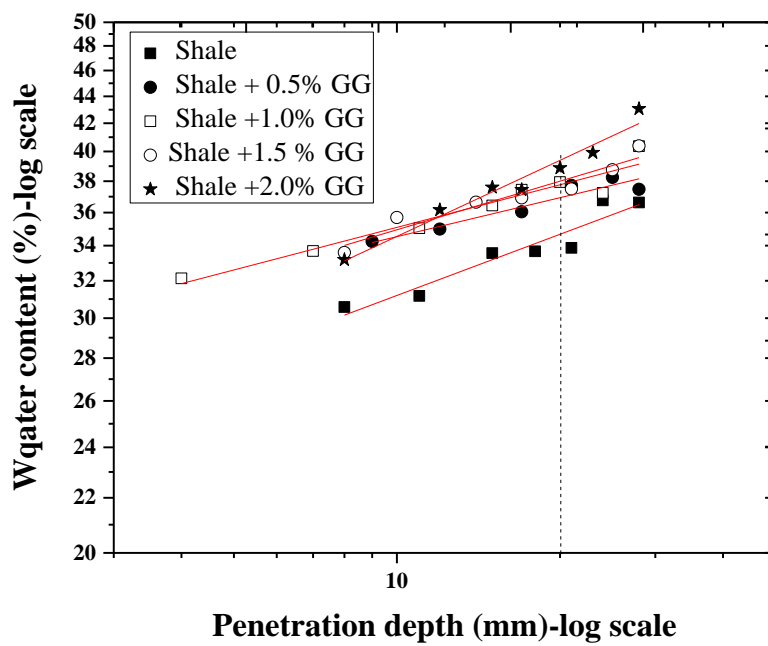
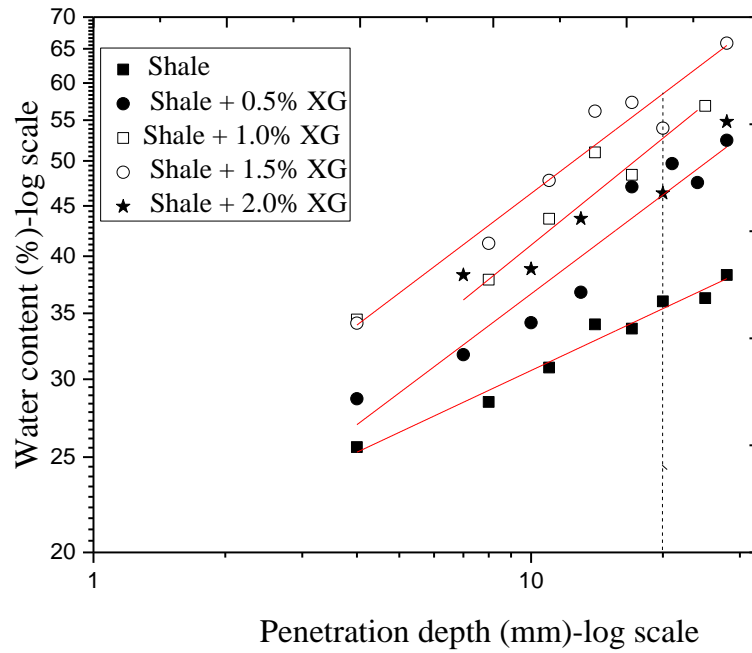
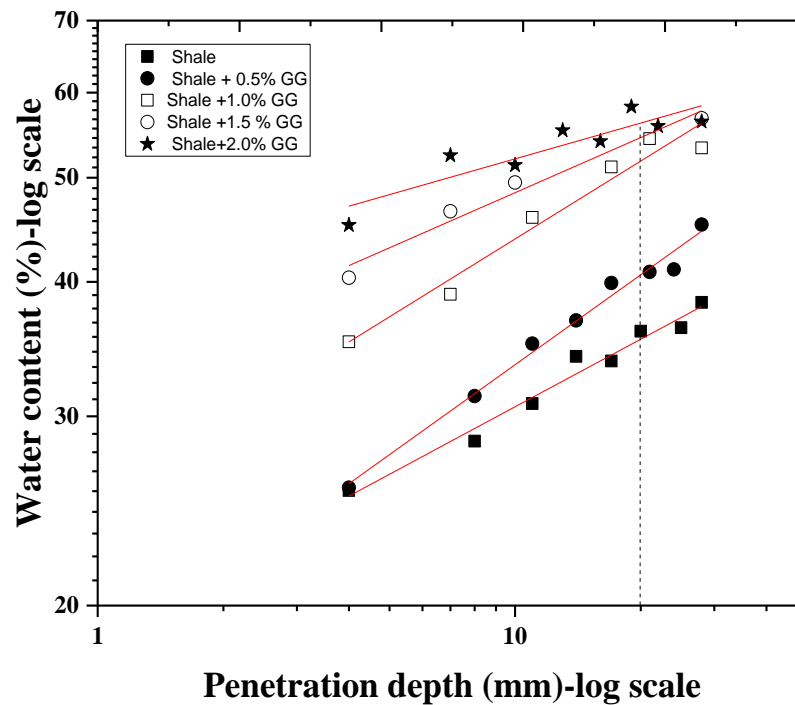


Figure 6.12: Log-log plot of penetration depth versus water content at different biopolymer concentrations for shale with GG





**Figure 6.13:** Log-log plot of penetration depth versus water content at different biopolymer concentrations for shale with XG



**Figure 6.14:** Log-log plot of penetration depth versus water content at different biopolymer concentrations for shale with CMC

Figure 6.15 shows biopolymer concentration of biopolymer treated fly ash and corresponding liquid limits. It can be observed that the liquid limit of biopolymer treated fly ash varies in a close range of 37.07 to 39.51% as GG varies from 0.5 to 2.0%.

Similarly, for XG, the liquid limit varies from 36.1 to 38.57% and for CMC it varies from 35.1 to 36.69%.

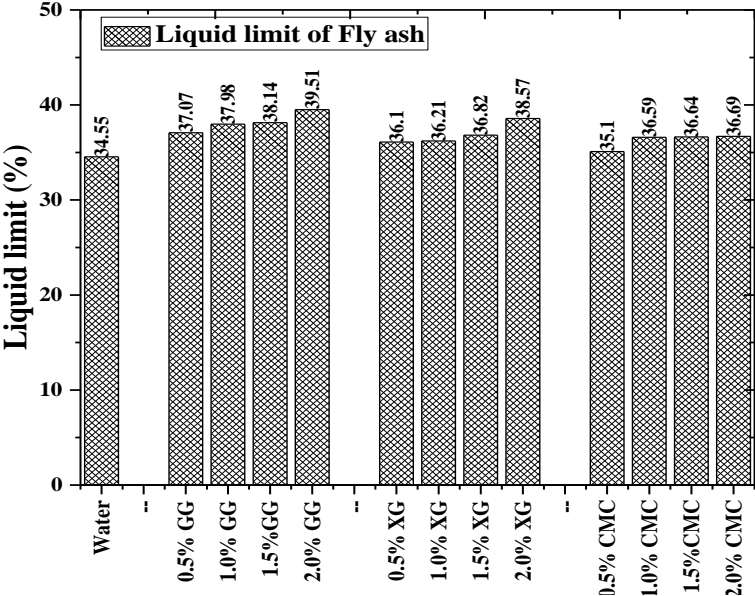


Figure 6.15: Biopolymer concentration versus the liquid limit of fly ash.

The liquid limit of shale was found to be 35.47, which varies as 36.99%,37.81%,38.23% and 39.34% respectively with 0.5%,1.0%,1.5% and 2.0% of GG (Figure 6.13). The variation of liquid limit for XG and CMC were also in a close range with maximum variations with CMC treated shale as 40.37%, 51.52%, 54.71% and 56.22% with 0.5%, 1.0%, 1.5% and 2.0%, respectively.

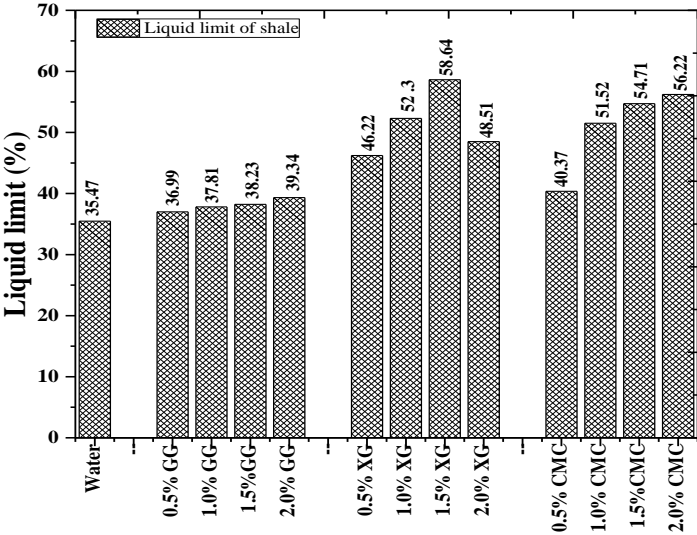
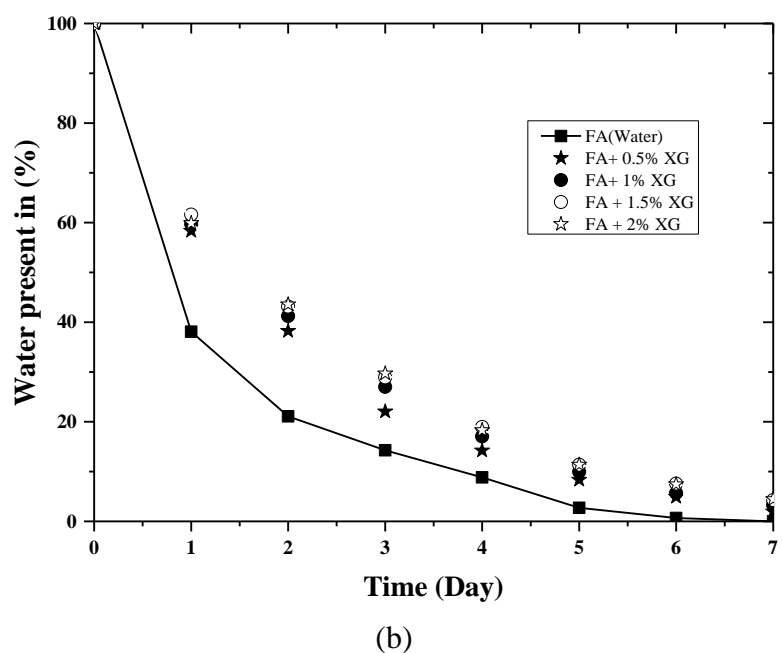
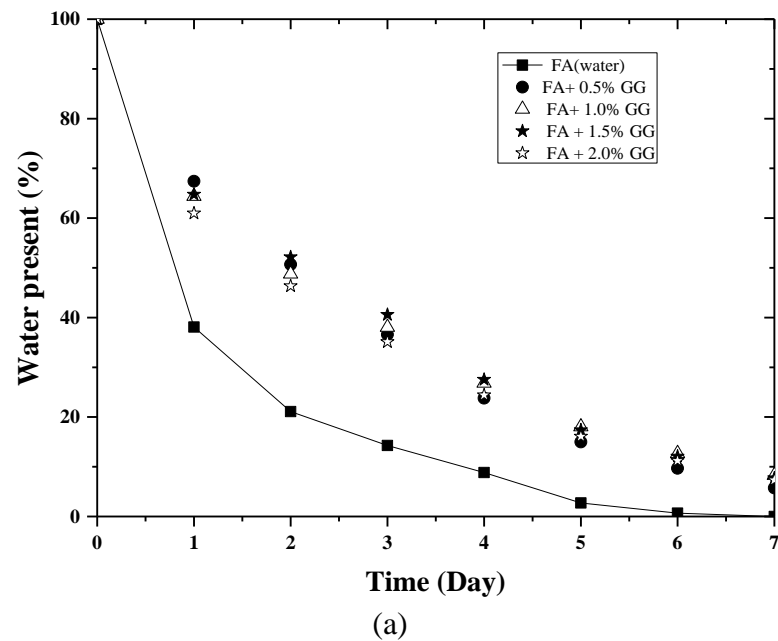
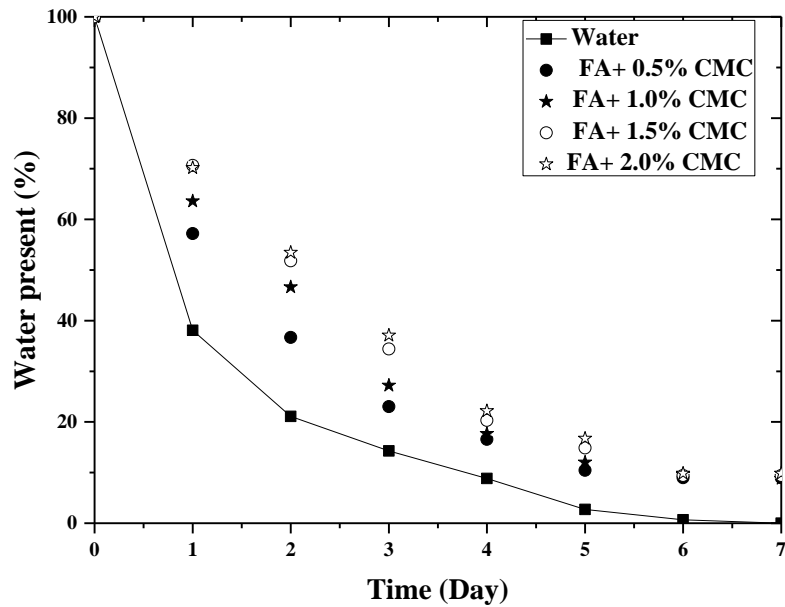


Figure 6.16: Biopolymer concentration versus the liquid limit of shale

### Water Retention Test

The water retention test of fly ash using GG, XG and CMC is shown in Figure 6.17. The water retention capacity found to increase with concentration and type of biopolymer. The water retention of the fly ash sample treated with guar gum and CMC show a similar pattern and higher retention than that of XG treated sample with xanthan gum. It may be mentioned that Chen et.al (2015) also obtained higher retention for GG than XG for mine tailing.

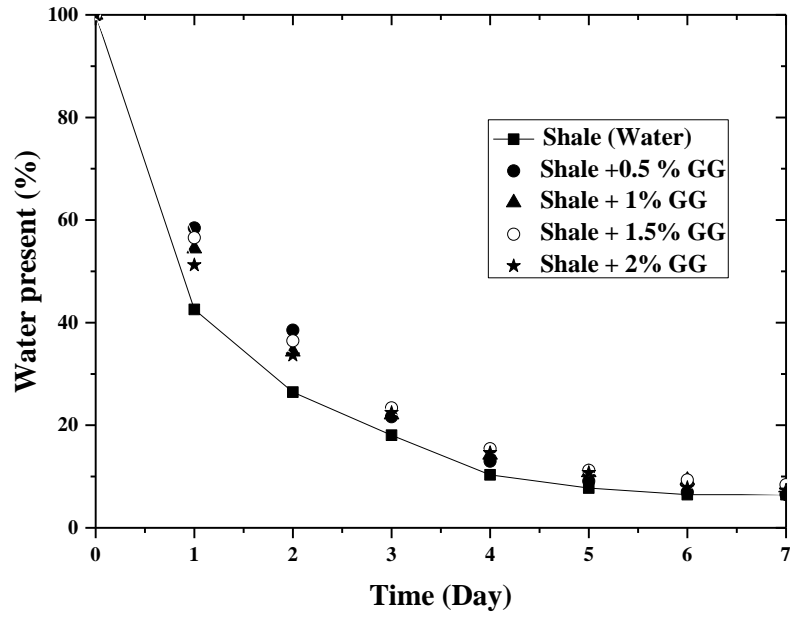




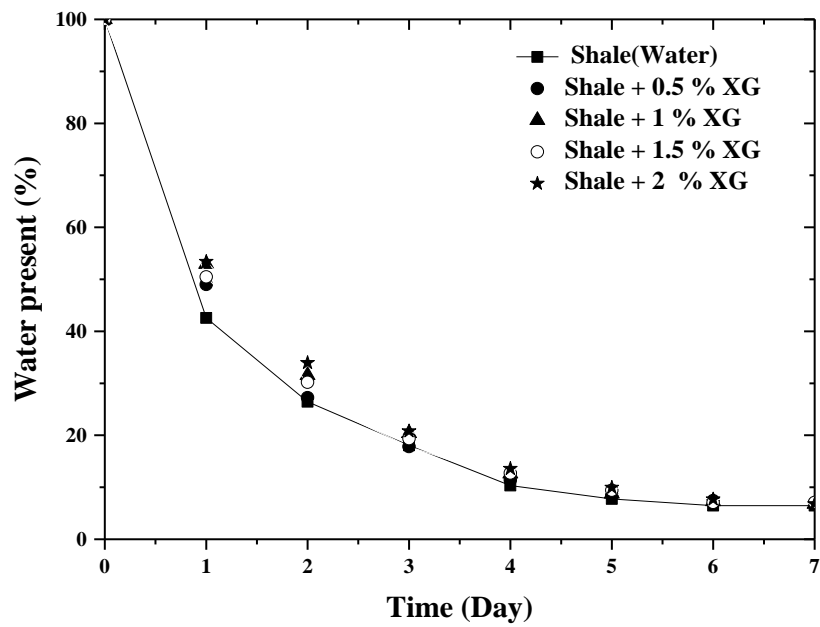
(c)

**Figure 6.17:** Water retention test of fly ash using 0.5%, 1.0%, 1.5% and 2.0% of (a) guar gum (b) xanthan gum and (c) CMC.

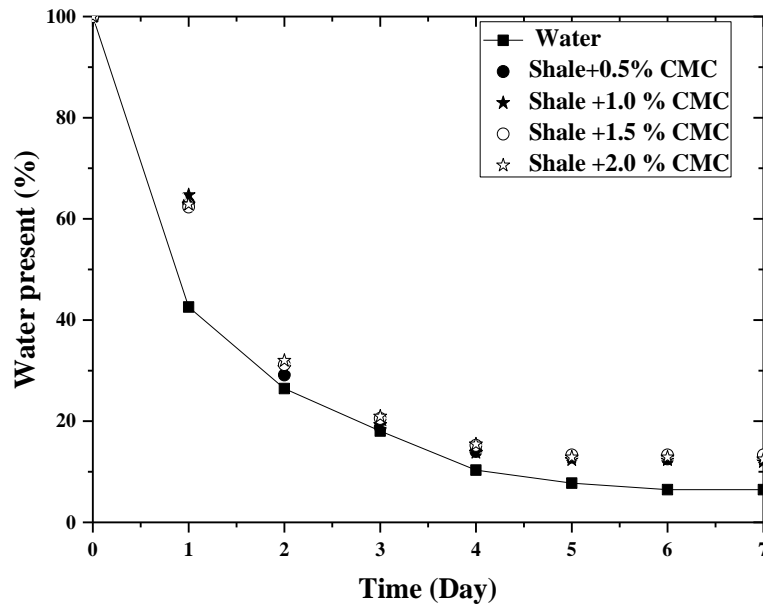
The results of water retention test of shale using GG, XG and CMC is shown in Figure 6.18. It can be seen that the shale treated with biopolymer solutions exhibited higher water retention capacity than that treated with only water. Similar to that of fly ash water retention capacity varies with the type of biopolymer and its concentration. The water retention capacity of shale treated GG increase up to 1% concentration and then almost remains constant (Figure 6.18 a). However, in case of XG water retention capacity increases with increase in concentration up to 2% (Figure 6.18 b). Similar results are obtained for CMC, with water retention capacity increasing with increase in concentration up to 2% (Figure 6.18 c). Hence, it is important to check with the optimum concentration after selecting a particular biopolymer.



(a)



(b)

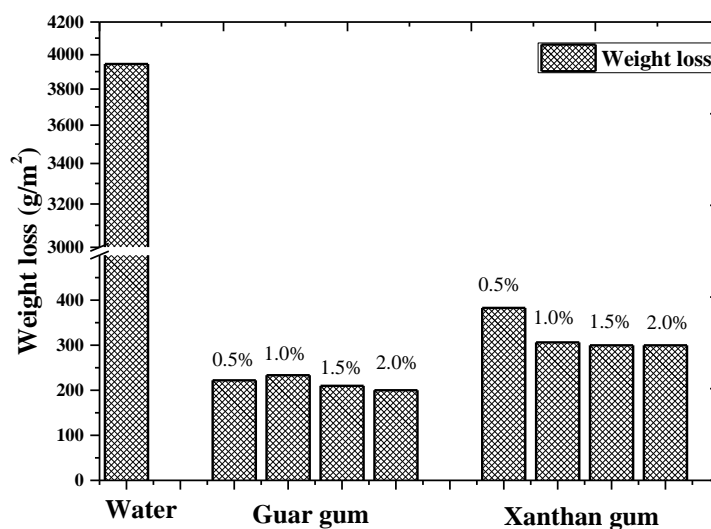


(c)

**Figure 6.18:** Water retention test of shale using 0.5%, 1.0%, 1.5% and 2.0% of (a) guar gum (b) xanthan gum and (c) CMC.

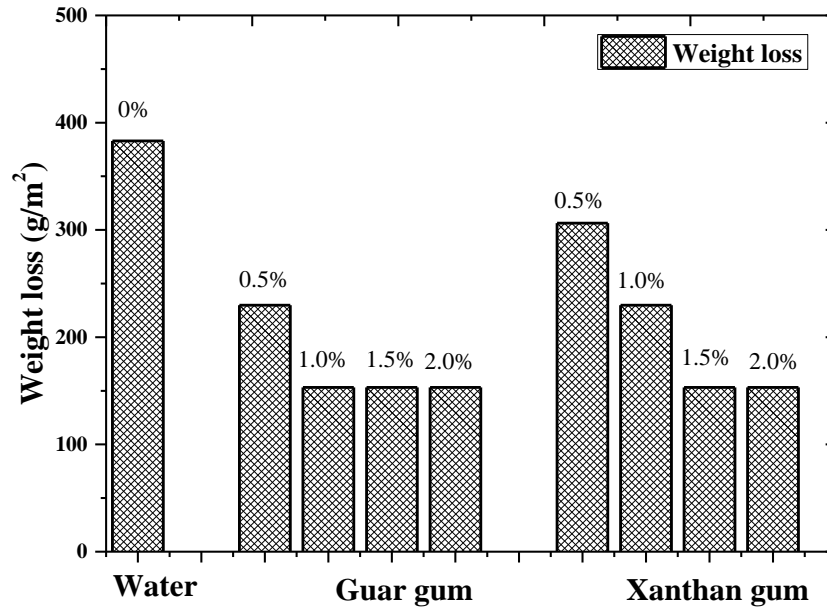
### Wind Tunnel Test

The weight loss during the wind tunnel test of the water and biopolymer treated fly ash samples are shown in Figure 6.19. It can be seen that the weight loss is dependent on the concentration of the biopolymer, but the weight loss is less in GG in comparison to XG, may be due to the fact that GG is more viscous than XG. Due to some technical difficulties, wind tunnel test could not be conducted for CMC treated FA and shale.



**Figure 6.19:** Wind tunnel test of fly ash sample and fly ash sample treated with different concentration of guar gum and xanthan gum.

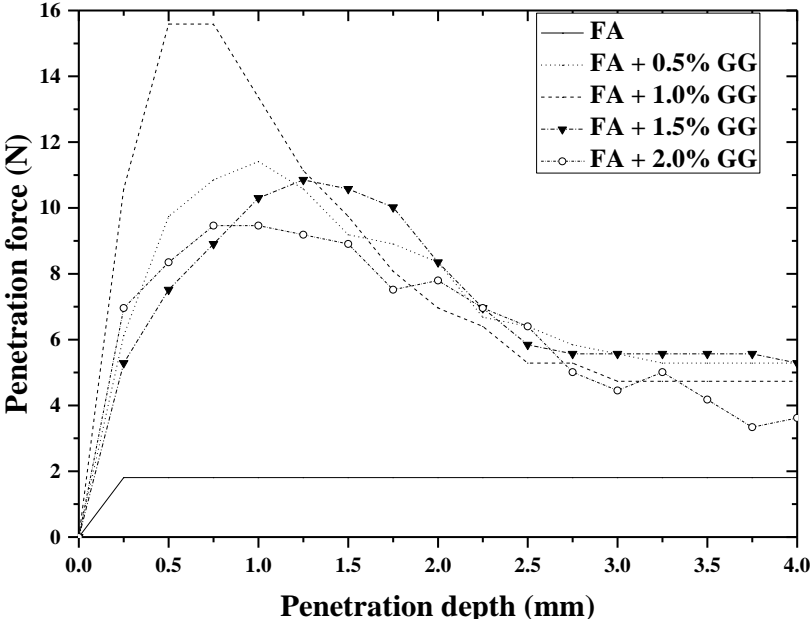
Figure 20 shows the weight loss of shale sample during wind tunnel test. Similar to that for FA, GG is found to be more effective and 1% concentration is optimum, but for XG treated shale 1.5% found to give minimum weight loss.



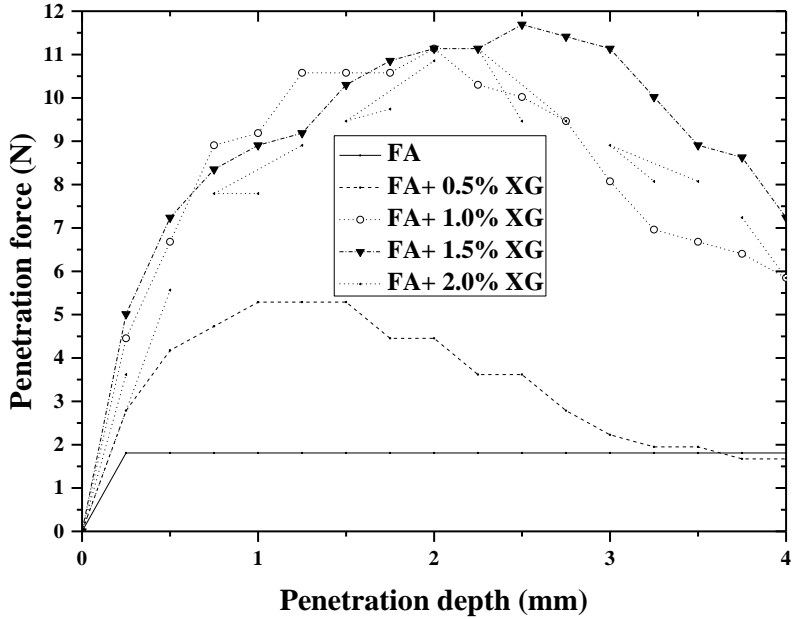
**Figure 6.20:** Wind tunnel test of shale sample treated with different concentration of guar gum and xanthan gum.

### Surface Strength Test

Figure 6.21 shows the typical penetration force (resistance) versus penetration depth curves for fly ash samples treated with (a) GG (b) XG and (c) CMC solution at different concentrations of 0.5%, 1.0%, 1.5% and 2.0%, after 7 days of drying cycle. It can be observed that the fly ash sample treated with biopolymer solutions exhibits higher surface strength than the fly ash treated with only water. Similar observations are also made for shale sample treated with different concentration of guar gum, xanthan gum and CMC as shown in Figure 6.22. As the shale is a cohesive material and fly ash is a non-cohesive material, the relationship between force and penetration are different. The penetration force for shale with guar gum treatment is more than that of fly ash. Similar observations are also made for the xanthan gum and CMC treated shale as shown in Figure 6.22 (b) and Figure 6.22 (c).

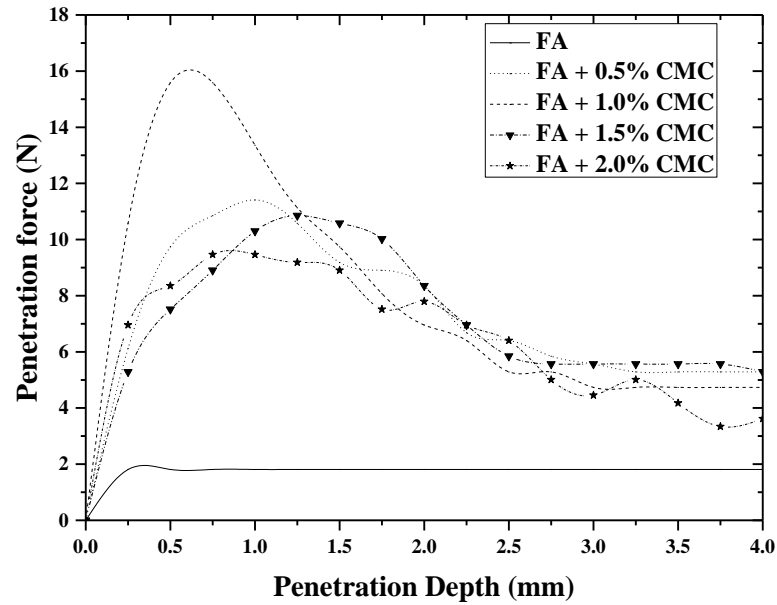


(a)



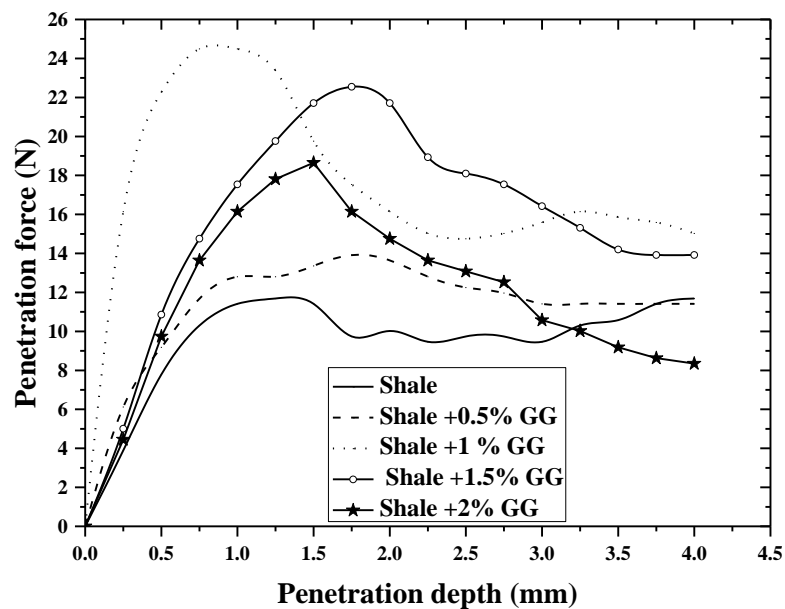
(b)



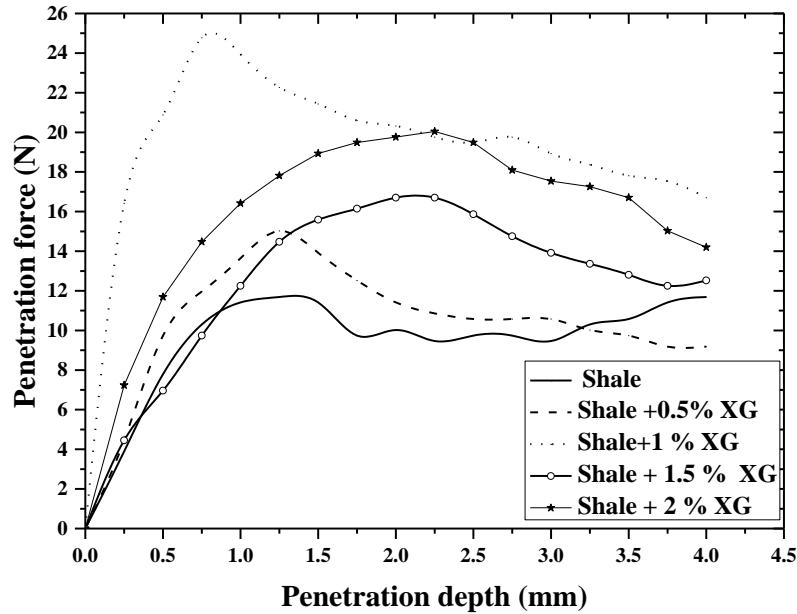


(c)

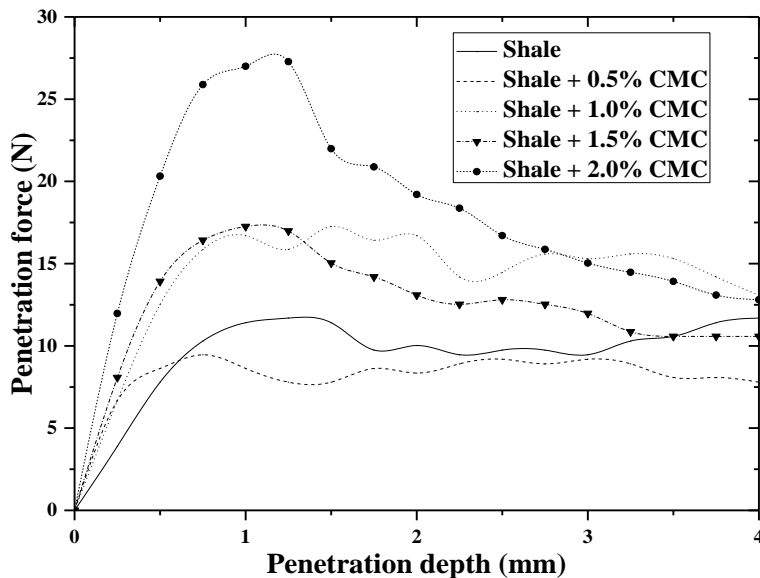
**Figure 6.21:** Typical penetration force versus penetration depth curve for fly ash treated with different concentration of (a) guar gum (b) xanthan gum and (c) CMC.



(a)



(b)

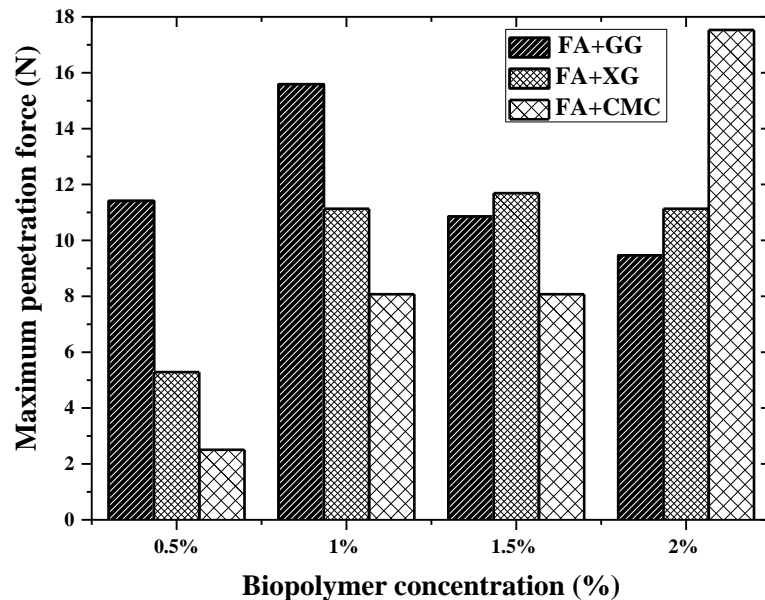


(c)

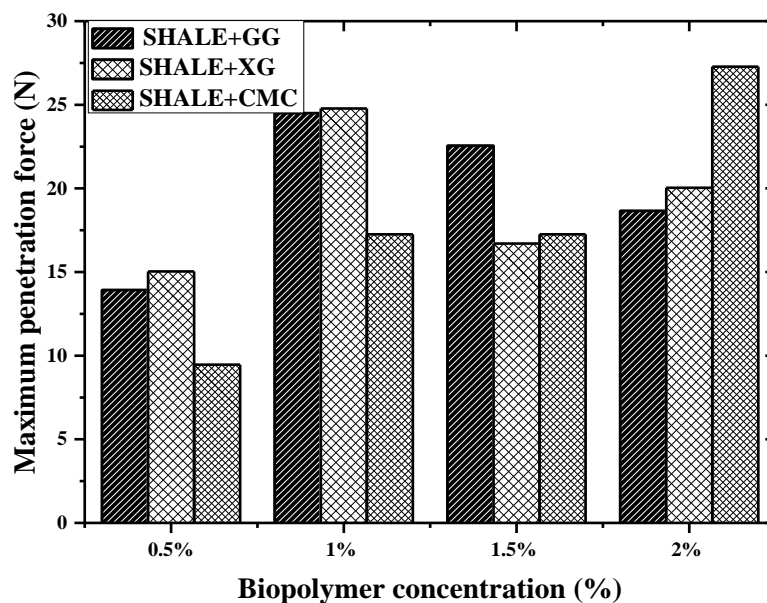
**Figure 6.22:** Typical penetration force versus penetration depth curve for shale treated with different concentration of (a) guar gum (b) xanthan gum and (c) CMC.

The variation of penetration force for fly ash with GG, XG and CMC of different concentration is shown in Figure 6.23. In case of GG, maximum penetration force was observed with 1% concentration, but for XG treated FA, the penetration force is same as 1%, 1.5% and 2% concentration. For the CMC treatment, the penetration force increased with increase in biopolymer concentration. The maximum penetration force (17.53N) was observed for CMC, though at an initial concentration (0.5%), the CMC is not effective like

XG and GG with minimum penetration force (2.50N). Similarly, for bio-treated shale, the optimum concentration for GG and XG is with 1% concentration with a maximum penetration force of 24.7N. For CM treated shale, maximum penetration force increase with the concentration of biopolymer with a maximum value of 27.27N at 2% concentration.



(a)



(b)

**Figure 6.23:** Average maximum penetration force for samples treated with guar gum, xanthan gum and CMC gum solutions at concentrations of 0.5, 1, 1.5, and 2%, respectively (a) fly ash (b) shale.

As a result of biopolymer treatment, the surface strength of fly ash and shale increased due to the bonding of particles and development of dense and strong surface layer. The surfaces of the fly ash treated with water and with 1% of guar gum concentration after penetration test are shown in Figure 6.24 (a) and Figure 6.24 (b), respectively. It indicates that biopolymer treated fly ash sample shows an undamaged surface cover after penetration test and water treated fly ash sample shows multiple cracks on the surface due to penetration. Similarly, Figure 6.24 (c) and Figure 6.24 (d) shows the undamaged surface of fly ash treated with 1.0% xanthan gum and CMC. This type of observations has been made by Chen et al. (2015) for mine tailing.



(a)



(b)



(c)



(d)

**Figure 6.24:** Penetration surface of fly ash sample treated with (a) water (b) 1.0% of guar gum solution (c) 1.0% of xanthan gum solution and (d) 1.0% of CMC gum solution.

The surface of water treated shale sample and shale with 1% of GG, XG and CMC are shown in Figure 6.25. Similar to the surface of fly ash sample, the shale sample treated with biopolymer indicates undamaged surface cover after penetration test, whereas the sample treated with only water shows cracked surface. Hence, it was observed that the tensile strength of fly ash and shale considerably increases with biopolymer stabilization (Khatami and O'Kelly, 2013, Chen et. al, 2015). It may be mentioned here that present study deals with fine-grained soil in comparison to coarse-grained materials of above two studies.

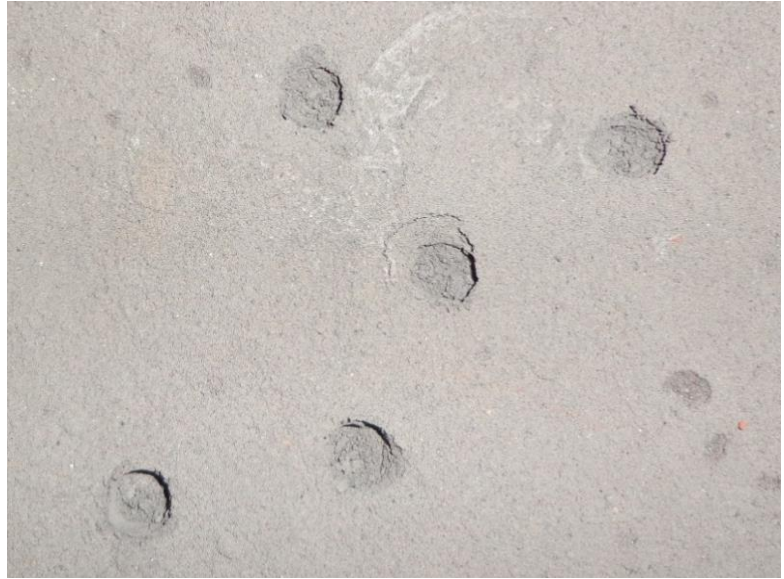




(a)



(b)



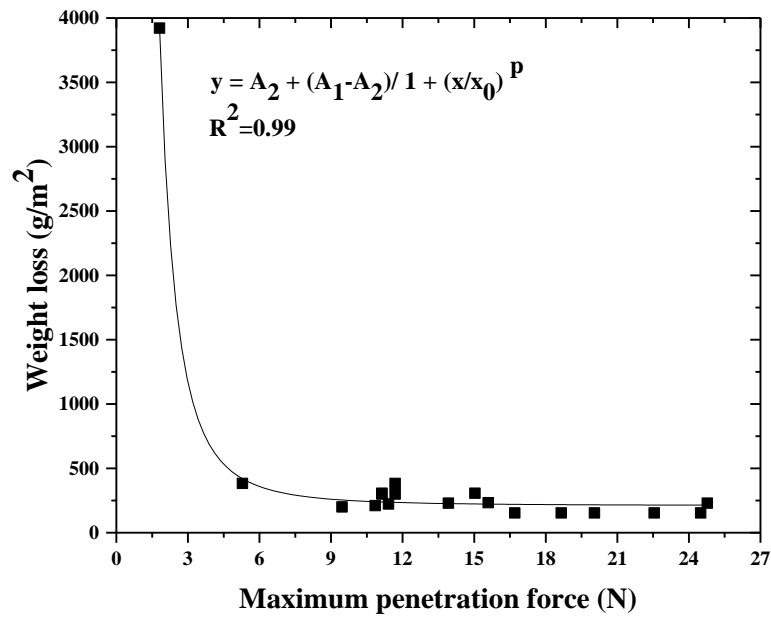
(c)



(d)

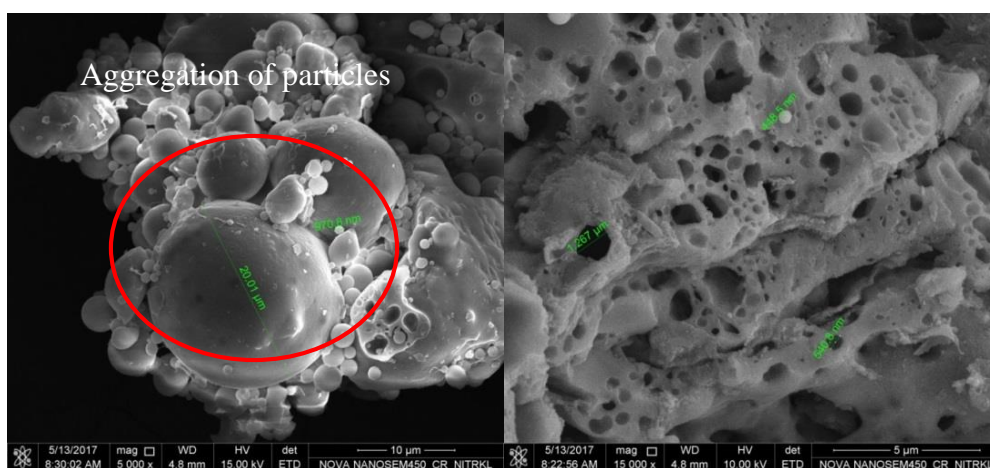
**Figure 6.25:** Penetration surface of shale sample treated with (a) water (b) 1.0% of guar gum solution (c). 1.0% of xanthan gum solution (d) 1.0% of CMC gum solution

An effort was also made to correlate the surface resistance in terms of weight loss during wind tunnel test. Figure 6.26 shows the weight loss of fly ash and shale sample after wind tunnel test versus the maximum penetration force. It can be seen that a strong relationship exists between the weight loss and the maximum penetration force. On the basis of best fitting analysis the relationship between weight loss and the maximum penetration force obtained with correlation coefficient ( $R^2$ ) value of 0.99. The strong relationship between weight loss and the maximum penetration force shows that the penetration test method can be a good approximation to characterizing the dust resistance of fly ash and mine overburden. Hence, though wind tunnel test could not be conducted for CM treated FA and shale, but as the penetration force is more for CMC treated sample, the weight loss for CMC treated sample will be less than that for XG and GG treated sample.



**Figure 6.26:** Weight loss of fly ash and shale after wind tunnel test versus maximum penetration force.

The scanning electron micrograph of fly ash and fly ash treated with 1% of GG, XG and CMC solution are shown in Figure 6.27, 6.28, 6.29, respectively. Similarly, the scanning electron micrograph of shale and shale treated with 1% of GG, XG and CMC solution are shown in Figure 6.30, 6.31 and 6.32, respectively. It can be observed that the biotreated materials got agglomerated state by application of gum due to bonding between the fly ash or shale particles with the biopolymer and lead to a compact structure. In case of CMC treated sample (Figure 6.32) a surface coating was observed.



**Figure 6.27:** Fly ash treated with 1.0% of guar gum.



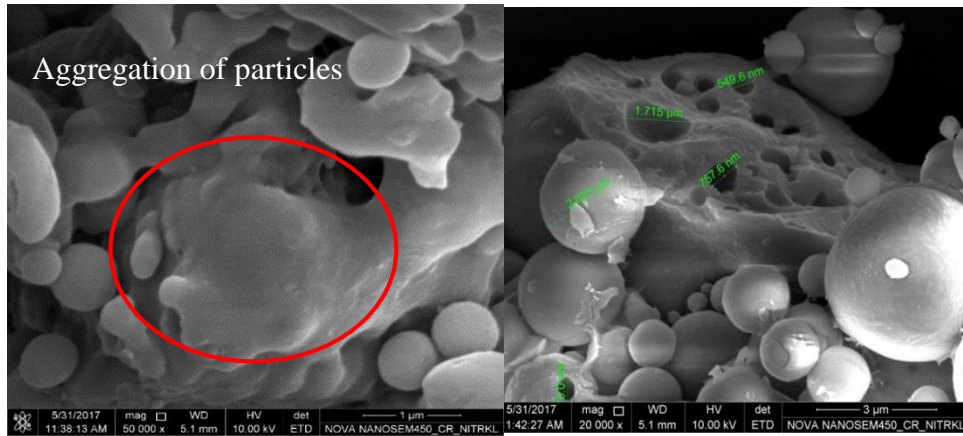


Figure 6.28: Fly ash samples treated with 1.0% of xanthan gum.

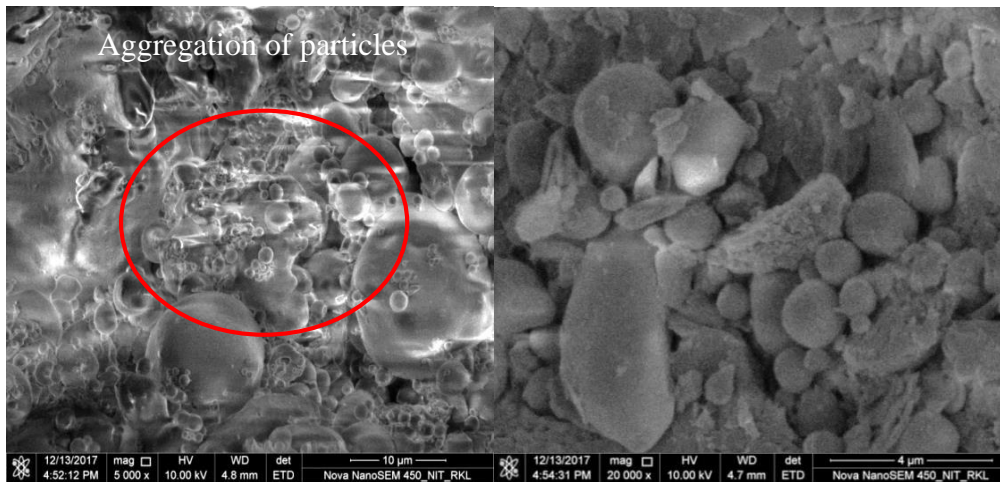


Figure 6.29: Fly ash treated with 1.0% OF CMC.

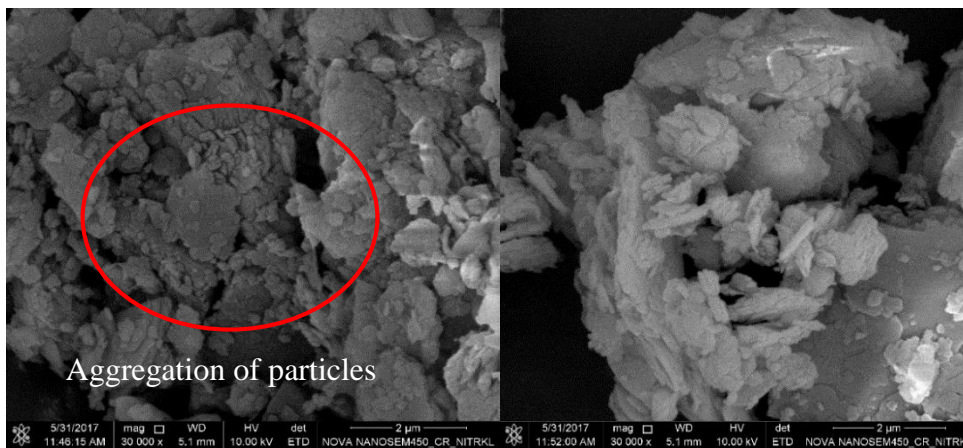


Figure 6.30: Shale treated with 1.0% of XG.

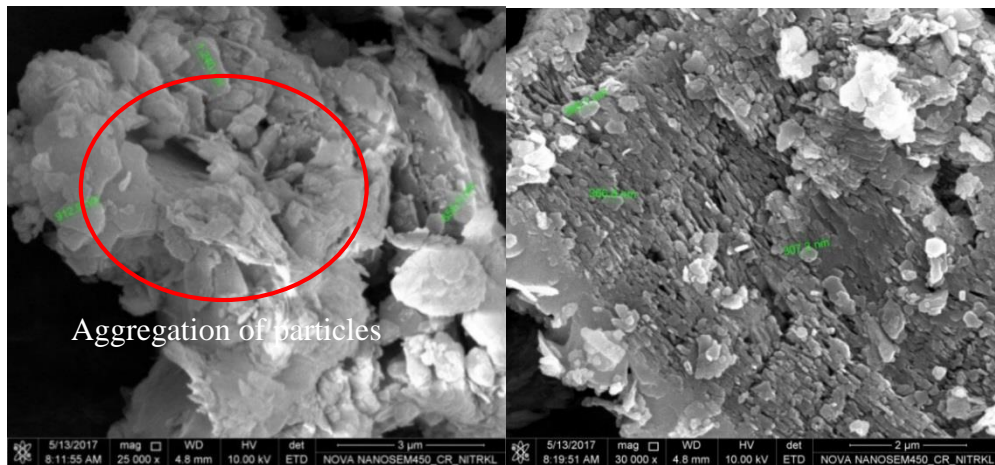


Figure 6.31: Shale sample treated with 1.0% of guar gum.

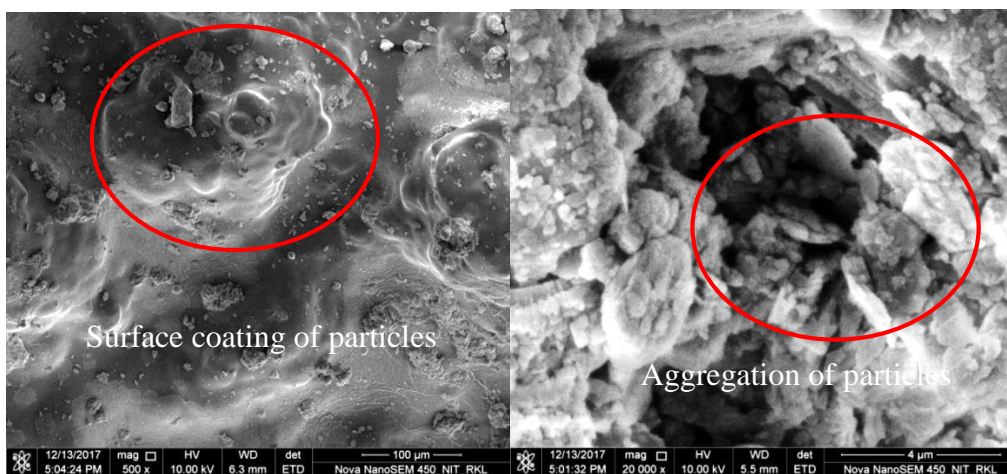


Figure 6.32: Shale sample treated with 1.0% of CMC

### Compaction and Unconfined Compressive Strength Characteristic

The compaction curve fly ash and biopolymer treated fly ash using mini-compactor (Panda et al. 2017) are shown in Figure 6.33. The MDD of biopolymer treated fly ash gradually decreases with increase in the percentage of biopolymer and the OMC increases and the compaction curve becomes flatter on wet of optimum. The MDD of fly ash is  $12.09 \text{ kN/m}^3$  at OMC of 28.95%. The MDD of biopolymer treated fly ash is varying from  $11.45 \text{ kN/m}^3$  to  $12.09 \text{ kNm}^3$ . Similarly, the compaction curve for shale and biopolymer treated shale using mini compactor is shown in Figure 6.34. The OMC increases and MDD decreases with the addition of biopolymer and compaction can be done in wider range of water content. The CMC treated fly ash has a wider compaction curve than the XG treated fly ash. This indirectly also indicated the cohesive nature of the CMC treated fly ash. The consistency of the biopolymer treated fly ash is also studied using flow table test (ASTM 1611M-14) and presented in Figure 6.35. The flowability of CMC treated fly ash is more than that of GG and XG treated fly ash. As it depends upon the viscosity of the

mix and CMC is more viscous than GG and XG. Hence, the flowability is also another factor to use the biopolymer treated geomaterials.

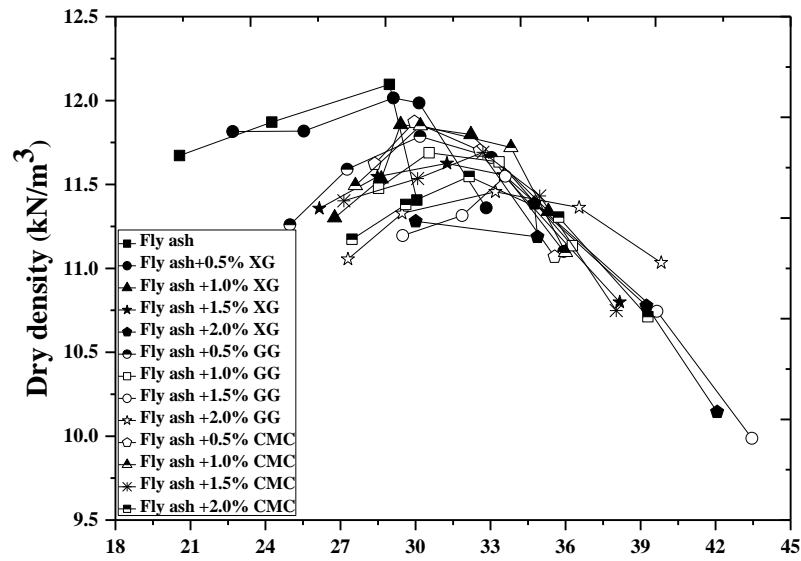


Figure 6.33: Compaction curve of fly ash and biopolymer treated fly ash.

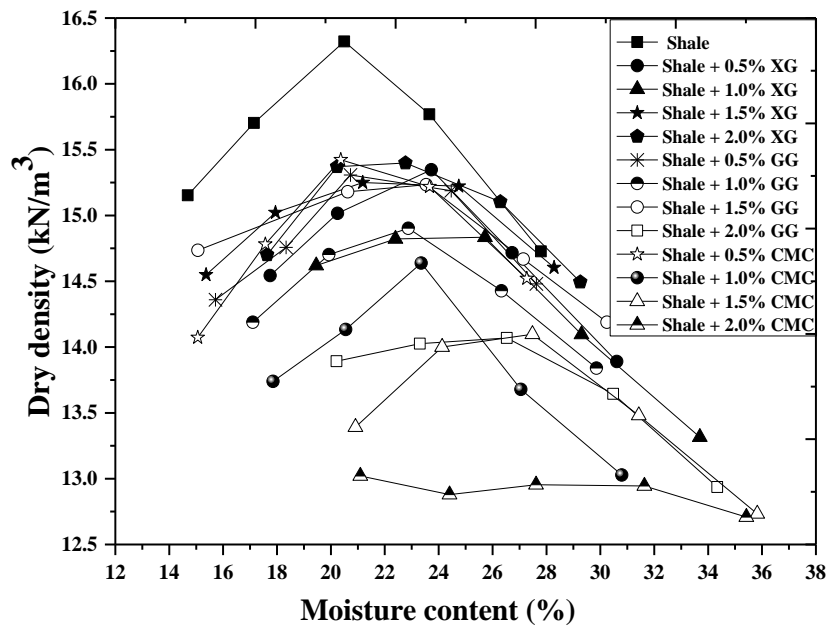


Figure 6.34: Compaction curve of shale and biopolymer treated shale.

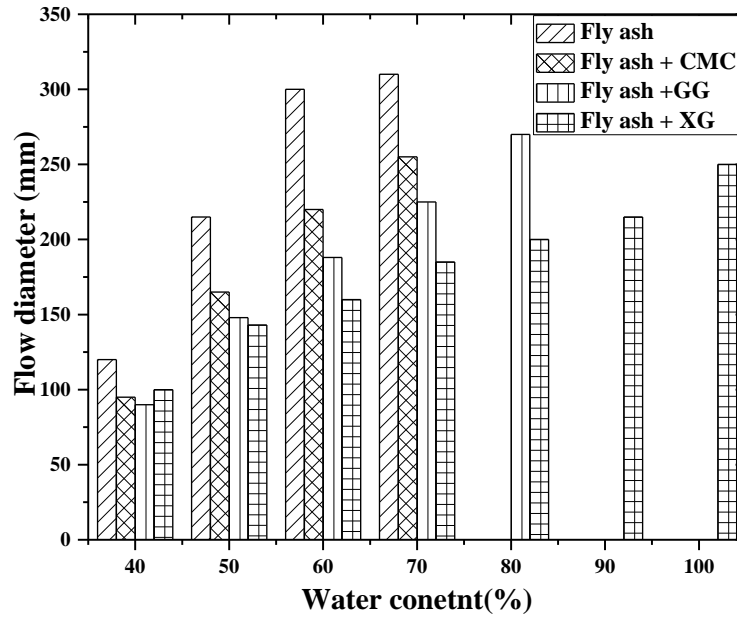


Figure 6.35: Relationship between water content and flow diameter of fly ash and biopolymer treated fly ash samples.

Figure 6.36 shows the relationship between MDD and OMC of fly ash, shale with and without biopolymer treatment. It was observed that CMC treated FA and shale has low MDD and high OMC compared to XG and GG treated geomaterials.

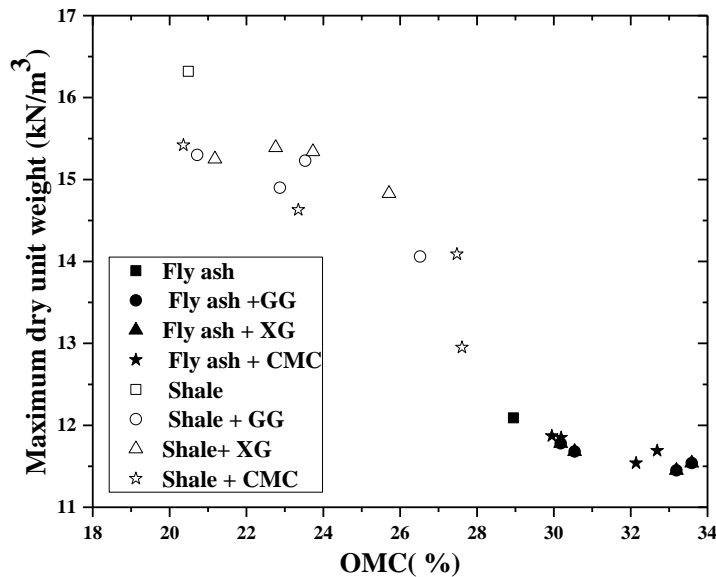


Figure 6.36: Relationship between maximum dry density (MDD) and optimum moisture content (OMC) different biopolymer treated fly ash and shale samples.

To measure the unconfined compressive strength of fly ash and biopolymer treated fly ash and shale cylindrical sample of size (37mm diameter, 75mm height) are cast and tested after 7 days of curing in ambient condition. The unconfined compressive strength of fly ash and

fly ash treated with guar gum, xanthan gum and CMC are shown in Figure 6.37, Figure 6.38 and Figure 6.39 respectively. It can be seen that the maximum stress values are comparable for all cases; strain at peak stress is very less in case of CMC treated fly ash and higher for GG treated fly ash. It may be mentioned here that CMC is more viscous than XG and GG, hence these results need further investigations.

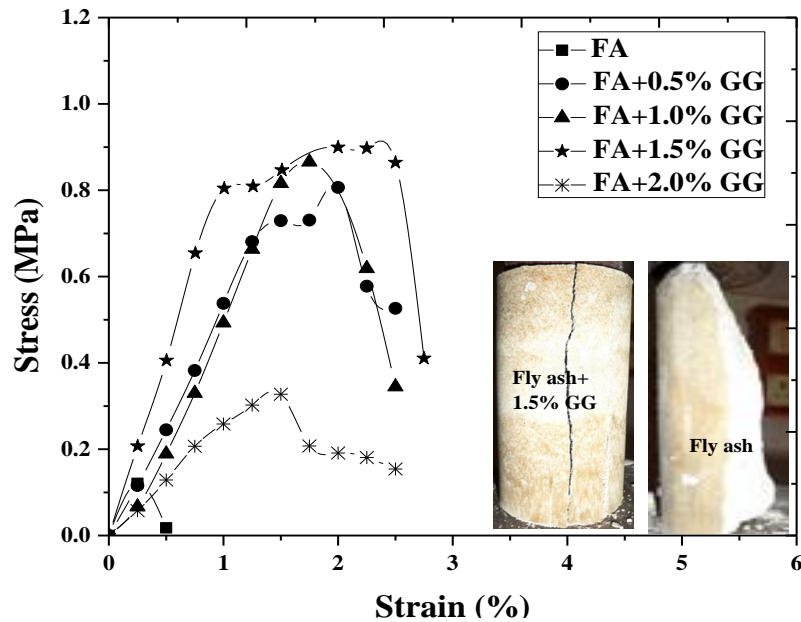


Figure 6.37: UCS curve of fly ash and fly ash treated with different concentration of GG.

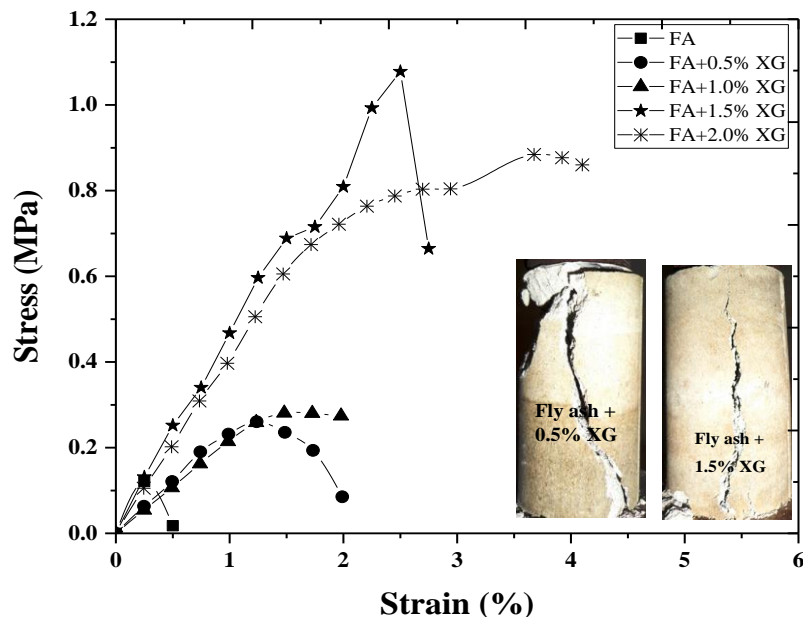
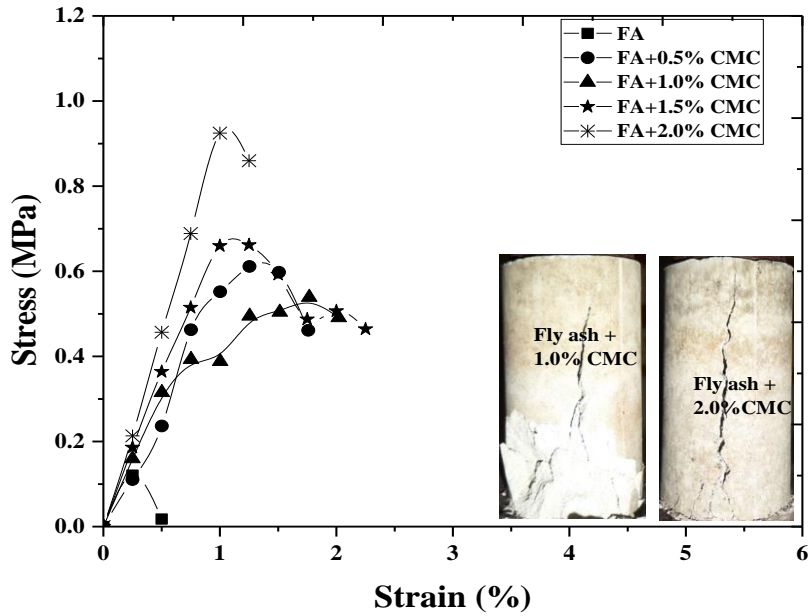


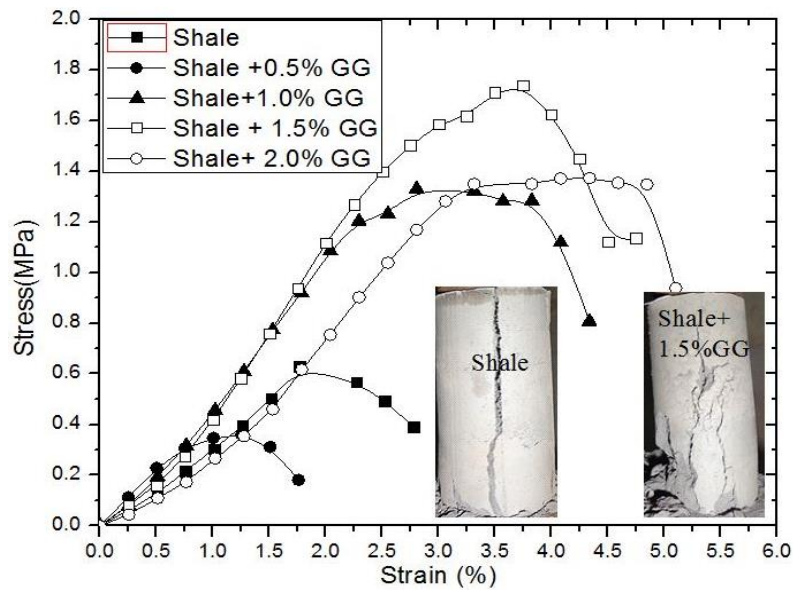
Figure 6.38: UCS curve of fly ash and fly ash treated with different concentration of XG.



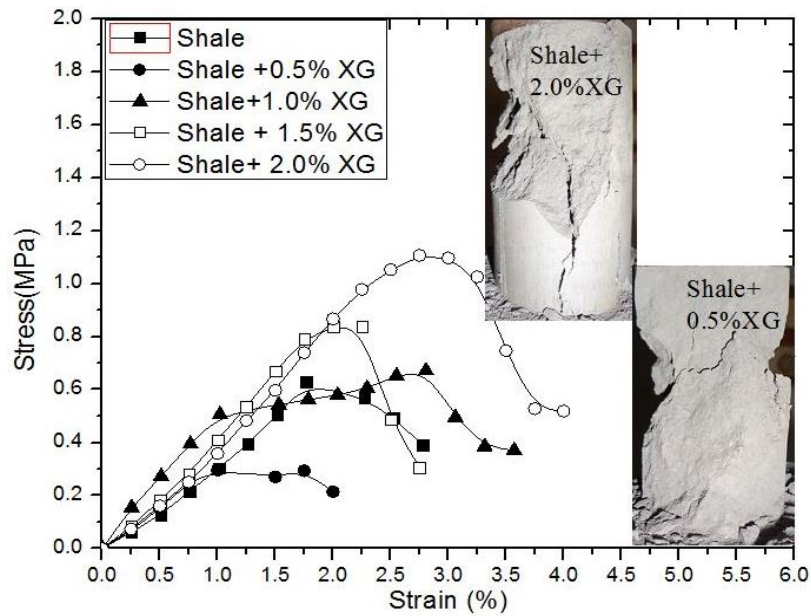


**Figure 6.39:** UCS curve of fly ash and fly ash treated with different concentration of CMC.

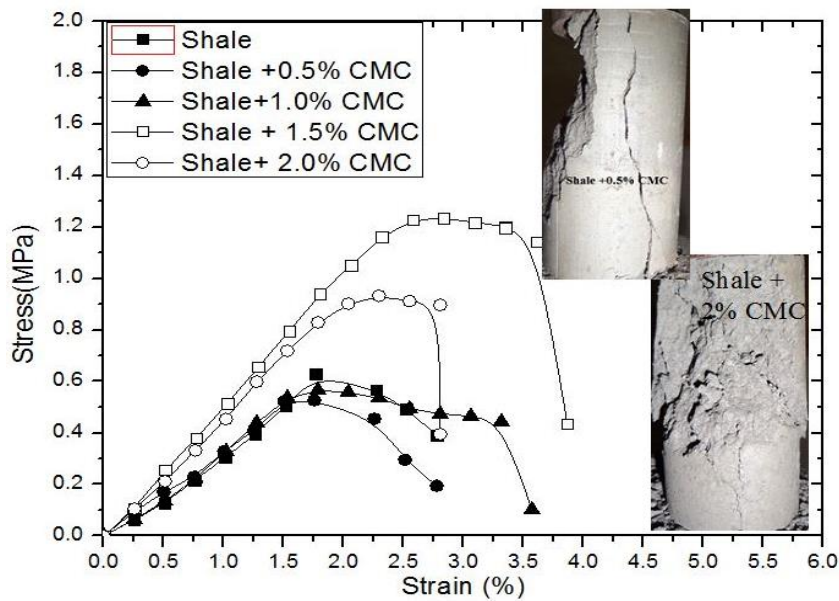
The unconfined compressive strength of shale and shale treated with guar gum, xanthan gum and CMC along with failure patterns of the sample are shown in Figure 6.40, Figure 6.41 and Figure 6.42 respectively. It was found that the GG treated shale shows higher strength and higher strain at peak stress compared to XG and CMC treated shale. The failure pattern for CMC and XG treated shale shows that of a well-compacted material. However, when the sample is immersed in water, it is dispersed within 15 minutes.



**Figure 6.40:** UCS curve of shale and shale treated with different concentration of GG.



**Figure 6.41:** UCS curve of shale and Shale treated with different concentration of XG.



**Figure 6.42:** UCS curve of shale and shale treated with different concentration of CMC.

### Leachate Analysis of Biopolymer Treated FA and Shale

The leachate analysis of fly ash and biopolymer treated fly ash were done using AAS test to know its sustainability and shown in Table 6.1. Similarly, the leachate analysis of shale and biopolymer treated shale was done, shows in Table 6.2. It can be observed that the hazardous material leaching is within the limit as per the permissible.

**Table 6.1:** Leachate analysis of fly ash and biotreated fly ash.

<b>Materials</b>	<b>Zn (ppm)</b>	<b>Pb (ppm)</b>	<b>Cr (ppm)</b>	<b>Ni (ppm)</b>	<b>Cu (ppm)</b>	<b>As (ppb)</b>	<b>Hg (ppb)</b>
JSPL FA	0.049	0	0	0.042	0	2.211	0
FA+2%GG	0.066	0	0	0.080	0.005	5.19	0.098
FA+2%XG	0.103	0	0	0.053	0.018	18.24	0
FA+2%CMC	0.075	0	0	0.069	0	23.3	0.074
Permissible Limit	15.0	0.10	0.05	-	0.10	20.0	10.0

**Table 6.2:** Leachate analysis of shale and biotreated shale.

<b>Materials</b>	<b>Zn (ppm)</b>	<b>Pb (ppm)</b>	<b>Cr (ppm)</b>	<b>Ni (ppm)</b>	<b>Cu (ppm)</b>	<b>As (ppb)</b>	<b>Hg (ppb)</b>
Shale	4.134	0	0	8.413	0.027	4.463	0
Shale+2%GG	2.181	0	0	3.776	0.020	0	0
Shale+2%XG	1.955	0	0	3.173	0.077	0.634	0
Shale 2% CMC	1.808	0.186	0.050	2.125	0.247	6.161	0.94
Permissible Limit	15.0	0.10	0.05		0.10	20.0	10.0

## 6.5 Summary

The fly ash shale is dispersive in nature and makes wind and water erosion in the vicinity of mining areas. In the present study three biopolymers, geomaterial is made using guar gum xanthan gum and carboxymethyl cellulose sodium salt to cover the fly ash and shale against wind and water erosion. The dispersion control is discussed in terms of pinhole test, cylindrical dispersion test for water erosion and wind tunnel test, surface resistance test and water retention test for wind erosion. Based on the experimental investigations and discussions following conclusions can be drawn.

1. Fly ash and shale are highly dispersive in nature and are susceptible to wind and water erosion. It was observed that the biopolymer treated fly ash and shale sample are not dispersive as per cylinder dispersion test. It was observed that guar gum is more effective in preventing dispersiveness compared to xanthan gum.



2. The water retention capacity of fly ash and shale increased after treatment with the biopolymer. Biopolymer treated fly ash and shale sample shows greater resistance to wind erosion, and it increased with increase in biopolymer concentration.
3. Biopolymer treated fly ash and shale sample shows higher surface strength than the sample saturated with only water. Based on penetration test it was found that xanthan gum treated samples shows better surface strength than guar gum treated sample. The surface strength of cohesive material shale is more than that of non-cohesive material fly ash.
4. The microstructure of treated samples shows that biotreated material shows denser surface structure than normal materials due bonding of particles.
5. The present study indicates that biopolymer stabilization can increase the surface strength, enhances the moisture retention capacity and reduces dispersiveness, thereby decreasing the dust erosion and water erosion of the fly ash and shale (mine overburden).
6. It can be observed that the biotreated materials got agglomerated state by application of gum due to bonding between the fly ash or shale particles with the biopolymer and leads to a compact structure. In case of CMC treated sample, a surface coating was observed, which makes it more effective in controlling dispersion.
7. It was observed that CMC treated FA and shale has low MDD and high OMC compared to XG and GG treated geomaterials.
8. The UCS values GG treated shale shows higher strength and higher strain at peak stress compared to XG and CMC treated shale. The failure pattern for CMC and XG treated shale shows that of a well-compacted material, but the sample is dispersed when immersed in water.
9. The leachate analysis of fly ash and biopolymer treated fly ash and shale using AAS showed that the hazardous material leaching is within limit as permissible.

Based on water retention, surface resistance, pinhole test and cylindrical dispersion tests it was found that the biopolymers, XG, GG and CMC are effective in controlling the dispersiveness of OB and fly ash, thereby controlling the wind and water erosion. However, the effect of the biopolymer is restricted to 1-2 weeks. Hence, though, the

biopolymer modified material is sustainable, but its durability is an issue. Hence, in the next chapter a more durable material, alkali activated material is discussed, with emphasis on the durability of the developed material.

## **CHAPTER 7**

# **ALKALI ACTIVATED MATERIAL USING MINING WASTES**

### **7.1 Introduction**

In the previous chapters, two different types of sustainable materials, CLSM and biopolymer treated geomaterial are discussed. The alkali activated material is sustainable and attempts for the development of it using basic materials from mining wastes is very limited. The motivation for the present chapter is to utilize the developed AAM at suitable locations including sulphate leaching conditions. The development of cementless CLSM and stabilization of natural slopes using AAM is also another aspect of this chapter. The development of AAM depends upon the combination of the source material, activators, temperature and curing conditions etc. As discussed in Chapter 2, the durability study of AAM is very limited and durability under short-term weathering agencies, through slake durability test is not reported. Though basic principles of AAM is explained through alkali activation of fly ash (AAFA) as presented in Chapter 3, the alkali activation for low strength material is not reported. Hence, in the 1<sup>st</sup> step, AAM is developed using mine overburden/tailing, then low strength alkali activated fly ash material is discussed. Development of cementless CLSM of FS and coal mine overburden through alkali activator is another novelty of this chapter.

### **7.2 Materials and Methods**

#### **Source Materials**

The mining wastes include the coal mine overburden, termed here as black shale and iron ore mine overburden, termed here as white shale and red shale is used as the basic material for the development of AAM. The ground granulated blast furnace slag is used as the calcium-rich binder material and added to the shale in different proportions of shale to slag as 30: 70 and 50: 50. The fly ash is also used as a partial replacement of GGBS. The mortar strength of the developed AAM is checked with Indian standard sands

(Combination of Grade I, II and III). Fly ashes from three different sources, JSPL fly ash, NALCO fly ash and Paradeep (HCFA) are used for alkali activation using different types of activators,  $\text{Na}_2\text{SiO}_3$ , KOH and NaOH. The activators are added in different molar concentration to know their effect. The basic material properties of above materials have been presented in Chapter 3.

### **Specimen Preparation**

Görhan and Kürklü (2014) observed that strength of water glass in powder form is comparatively lower than water glass in liquid form (Görhan and Kürklü, 2014). Aliabdo et al. (2016) discussed the effect of sample resting time on the compressive strength of alkali activated fly ash concrete and observed higher compressive strength with activator (NaOH and  $\text{Na}_2\text{SiO}_3$ ) solutions prepared with resting time 30 minute than 24h obtained 28days strength as 47MPa.

In the present study,  $\text{Na}_2\text{SiO}_3$  prepared 12-14 h before its casting which is secondary state of solution. NaOH and KOH solution are prepared freshly before casting of sample or 4h before casting which is in primary state of solution. Prepared samples are kept in the mould for a minimum of 14 h.

The alkali-activated materials commonly consist of two phases of curing. Each sample after demoulding are wrapped by cling film to avoid loss of moisture during thermal curing in the oven maintained at 40°C for 24 hours. Cling wrappers are removed after cooling of each specimen at normal room temperature. The second phase of curing of the alkali-activated shale-slag paste, shale-slag mortar and alkali activated fly ash paste is done at (a) ambient, (b) alkali (c) sulphate and (d) water conditions up to testing ages of . 7 and 28 days, which are explained as follows.

### **Ambient Curing Condition**

In this condition, the prepared samples are cured under the normal climatic condition without regulating temperature. The samples are kept at normal room temperatures ( $27 \pm 8$  °C) and humidity up to testing ages.

### **Alkali Curing Condition**

As discussed earlier, Görhan and Kürklü (2014) observed that the activation of fly ash increases with NaOH in the presence of water glass ( $\text{Na}_2\text{SiO}_3$ ) in polymerization process which increases the Si content in the reaction products and developed high mechanical strength. Hence, in the present study, the samples were placed in an alkali solution of 1M

NaOH prepared inside a closed glass container up to testing period at room temperature. After the testing ages, the samples were removed from the container and allowed to come to surface dry condition before testing.

### **Sulphate Curing Condition**

Durability under sulphate solution is the most desirable property as it helps to withstand the aggressive environment of sewers, mines mineral processing units and other industries (Bakharev, 2005; Temuujinet *al.* 2011). In the present study, samples were placed inside sulphate solution within a closed container at room temperature up to testing ages. Sulphate solution is prepared by using distilled water and 5% of sulphate salt (2.5% of sodium sulphate salt +2.5% of magnesium sulphate salt).

## **7.3 Results and Discussion**

### **7.3.1 Development of AAM using Shale - GGBS**

#### *Compressive strength*

Based on literature and previous research in the laboratory on AAM (Garanayak 2017), the shale paste samples with shale: GGBS ratio of 30:70 and 50:50 were prepared. The activator  $\text{Na}_2\text{SiO}_3$  solution of 0.5 mole and 3 moles were used and the samples are cured at ambient, alkali and sulphate conditions. The results as shown in Figure 7.1 indicates that under ambient condition red shale sample has the maximum compressive strength of 55.85MPa after 7 days, which gets marginally increased to 59.0 MPa after 28 days and it is well known that AAM gets early compressive strength (Provis and van Deventer, 2014). But, it can be seen that the compressive strength of white shale paste decreased from 55.75 MPa under the ambient condition to 44.95 MPa under alkali and 31.97 MPa under sulphate solution curing condition. It was observed that the 28 days compressive strength of red shale varies marginally with the curing conditions with values as 59.0 Mpa, 49.54MPa and 50.89MPa, under ambient, alkali and sulphate solution curing. Garanayak (2017) observed an increase in compressive strength of alkali activated FS: slag paste. The compressive strength of black shale paste is in between that of red shale and white shale paste. It may be mentioned here that the red shale is rich in iron content, whereas the white shale is rich in Al. Hence, the basic material plays a role in the compressive strength of AAM under different curing condition and alkali condition of curing is beneficial to the alkali activated shale material. Under similar condition, Garanayak (2017) found the 28

days compressive strength of the GGBS paste, red mud: GGBS (30:70) paste and ferrochrome slag: GGBS (30:70) paste as 67.57MPa, 78.65MPa and 66.85 MPa, respectively with 6 M of Na<sub>2</sub>SiO<sub>3</sub> solution. In terms of cost, the present AAM paste using red shale may be economical.

The reduction of GGBS content (from 70 to 50%) in the paste shows a reduction in the strength under ambient and alkali solution for red shale, but no reduction in strength for red shale under sulphate curing condition (50.44) (Figure 7.2). But for black and white shale, there is a substantial reduction in strength with a reduction in GGBS content. For ferrochrome slag: GGBS (50:50) paste with 6 moles of Na<sub>2</sub>SiO<sub>3</sub> Garanayak (2017) observed a compressive strength of 50MPa after 28days under ambient curing condition.

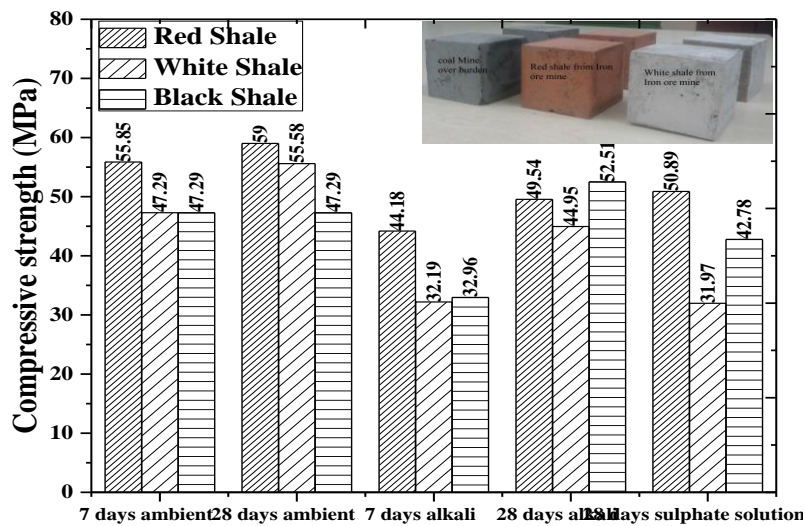


Figure 7.1: Alkali activated shale: GGBS- 30:70 (paste) with 3 mole of Na<sub>2</sub>SiO<sub>3</sub>.

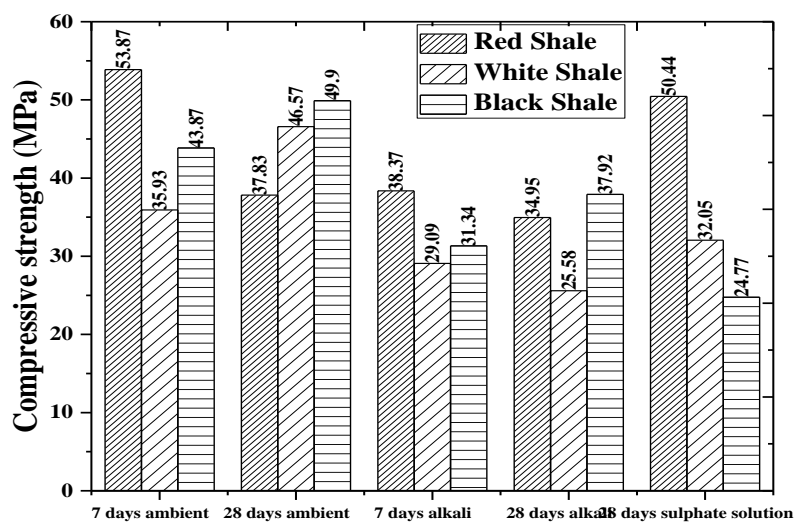
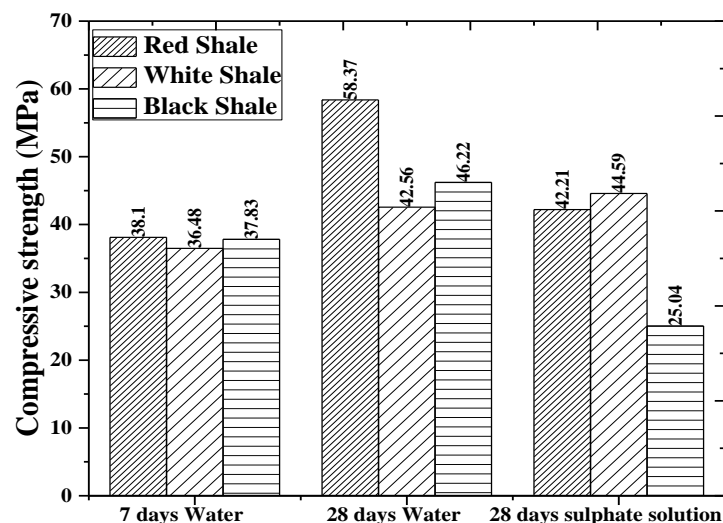


Figure 7.2: Alkali-activated shale: GGBS- 50:50 (paste) with 3 mole of Na<sub>2</sub>SiO<sub>3</sub>

The red shale is rich in iron content and act like a filler in the AAM, hence, the strength reduces with reduction in GGBS content for ambient and alkali condition. However, in sulphate curing condition with solution of the sulphate environment may be increasing the development of N-A-S-H gel, thereby increasing the strength. But, microstructural analysis is required for confirmation of the mechanism.

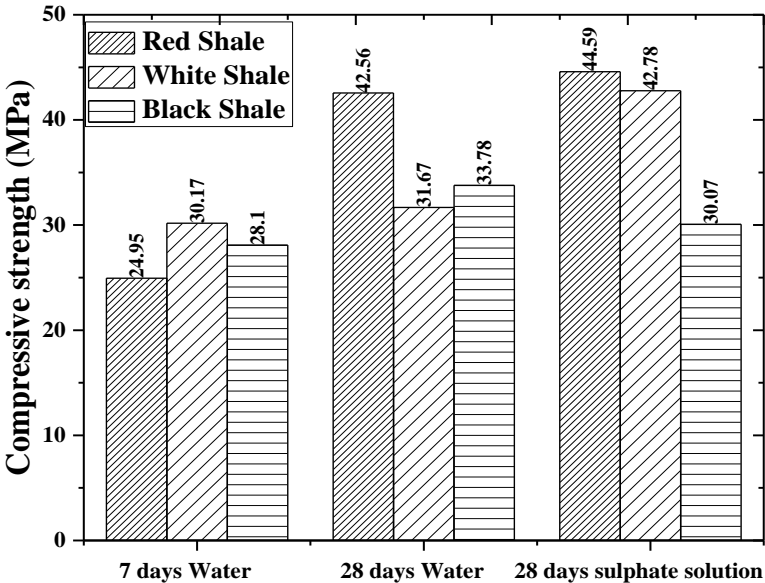
An effort has been made to reduce the use of GGBS in the shale paste, to know the effect of fly ash on sulphate resistance of developed paste. The shale pastes are made of red shale, white and black shale with two different proportion (Shale: FA: GGBS-30:20:50 and Shale: FA: GGBS-50:10:40). The effect of water curing and sulphate solution curing are compared to know the addition of fly ash on the sulphate resistance of developed paste. It was found that for red shale, the compressive strength of water cured sample decreased from 58.37 MPa to 42.21 Mpa (Figure 7.3). Marginal reduction in strength was observed for white shale, but a substantial reduction in case of black shale paste. But, it was interesting to find that under sulphate curing condition, for black shale, there was no reduction in strength with the replacement of slag with fly ash.

Hence, for red shale paste, the replacement of GGBS with fly ash does not vary the compressive strength under water/ambient condition but plays an important role in durability under sulphate curing condition. However, for the black shale replacement of GGBS with fly ash was found to be beneficial. It may be mentioned here that the sulphate solution is expected in coal mines overburden (black shale).



**Figure 7.3:** Alkali-activated shale paste (Shale: FA: GGBS-30:20:50) with 3 moles of  $\text{Na}_2\text{SiO}_3$ .

Figure 7.4 shows shale fly ash-GGBS paste(Shale: FA: GGBS-50:10:40), and it can be observed that the sulphate cured fly ash shale paste shows maximum compressive strength as compared to water cured condition. Comparing with Figure 7.3, It can be concluded that under sulphate curing condition the black shale paste with higher fly ash content has better strength compared to higher GGBS content ( 30.07 MPa vs 25.04 MPa), but for red and white shale paste, the marginal difference was observed for replacement of fly ash with GGBS. However, under water curing, condition higher percentage of GGBS gives higher compressive strength. Hence, it is important to choose a particular type of AAM keeping in mind the environment condition around.

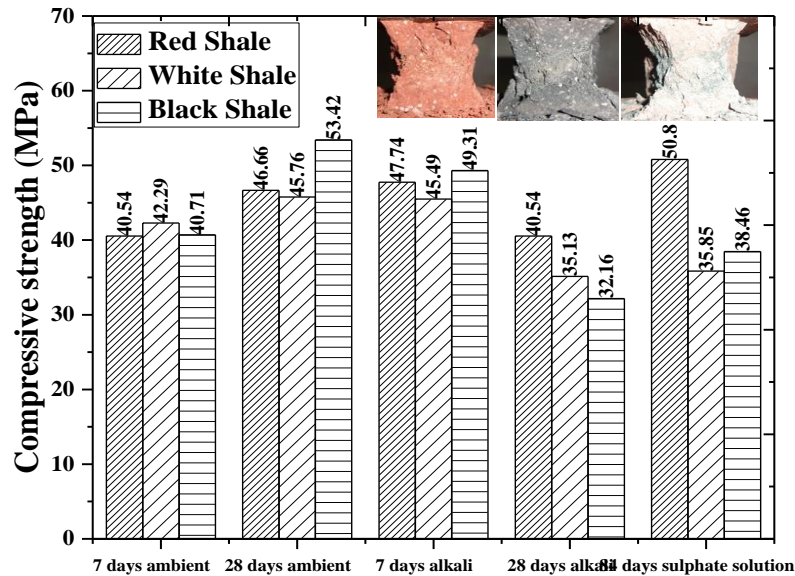


**Figure 7.4:** Alkali activated shale paste (Shale: FA: GGBS-50:10:40) with 3 moles of  $\text{Na}_2\text{SiO}_3$ .

In order to use the developed shale – GGBS paste as mortar material, samples were made for shale mortar with shale: sand: GGBS proportion as 30:30:40, using Indian standard sand of three grades, i.e. grade I (2mm passing 1mm retained), grade II (1mm passing 0.5mm retain) and grade III (0.5mm passing 90micron retained) and cured under ambient condition, alkali condition and sulfate condition. The compressive strength of shale-GGBS mortar is under different curing conditions are shown in Figure 7.5. It can be seen that similar to shale- GGBS paste, the shale- GGBS mortar also get early strength (7 days) under ambient condition. For the white and black shale, the 28 days compressive strength decreased under alkali and sulphate curing condition. But for red shale mortar maximum compressive strength (50.8 MPa) was observed under sulphate solution curing condition.



Under the ambient condition, the mortar strength for black shale was maximum (53.42 MPa), which reduced to 38.46 MPa under sulphate solution curing condition.



**Figure 7.5:** Alkali-activated shale mortar (shale: sand: GGBS-30:30:40) with 3 moles of  $\text{Na}_2\text{SiO}_3$ .

The alkali activation of different shales is also prepared with  $\text{Na}_2\text{SiO}_3$  solution with a lower concentration, i.e. 0.5 moles to find out the effect of activator concentration of alkali activated shale-GGBS paste. The compressive strength of different alkali activated shale paste (shale: GGBS-30:70) with 0.5 mole  $\text{Na}_2\text{SiO}_3$  under ambient and alkali condition is shown in Figure 7.6. It can be observed that the compressive strength increased in alkali condition compared to an ambient condition and comparable 28 days compressive strengths are obtained for black shale (29.58MPa), white shale (27.02 MPa) and red shale (31.75MPa). It may be mentioned here that with the same shale- GGBS proportion (30:70), with 3 M  $\text{Na}_2\text{SiO}_3$ , the compressive strength under ambient conditions (Figure 7.1) is higher than that with 0.5M  $\text{Na}_2\text{SiO}_3$ . But, under alkali curing condition, the compressive strength increased compared to ambient curing with low molar (0.5M) concentration but decreased with high molar (3.0M) concentration of  $\text{Na}_2\text{SiO}_3$ . Similarly, for shale: GGBS-30:70 with 0.5 moles  $\text{Na}_2\text{SiO}_3$  the compressive strength for red shale are comparable for ambient (16.57 and 27.56 MPa) and alkali solution (17.69 and 24.99 MPa) at 7 and 28 days of curing (Figure 7.7). But for black shale, the compressive strength under alkali solution (29.72 MPa) is higher than that under ambient condition (15.31 MPa). In case of higher GGBS content (Shale: GGBS of 30:70), with lower activator (0.5M) solution, the alkali solution help in activation of the GGBS. Hence, the

compressive strength under alkali condition with high GGBS content and low concentration activator is more than that of ambient condition. However, at higher concentration (3M) of activator with higher GGBS proportion does not require the alkali solution for the reaction. Rather, the alkali solution environment retards the geopolymerization, hence the strength reduces. But, microstructural analysis is required for confirmation of the mechanism.

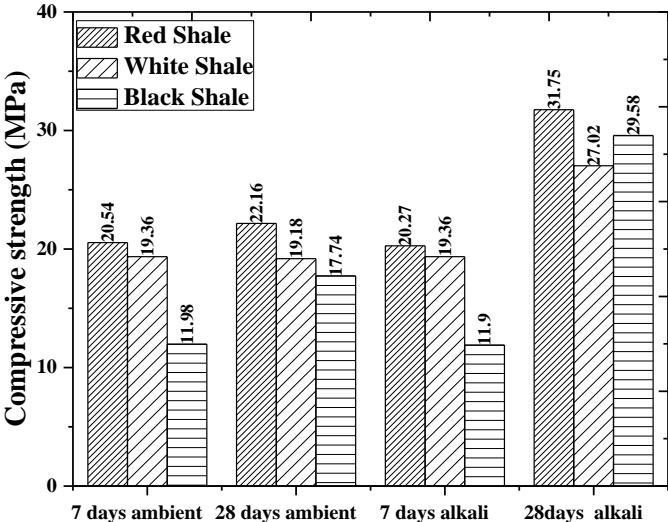


Figure 7.6: Alkali activated shale: GGBS- 30:70 (paste) with 0.5 mole of Na<sub>2</sub>SiO<sub>3</sub>.

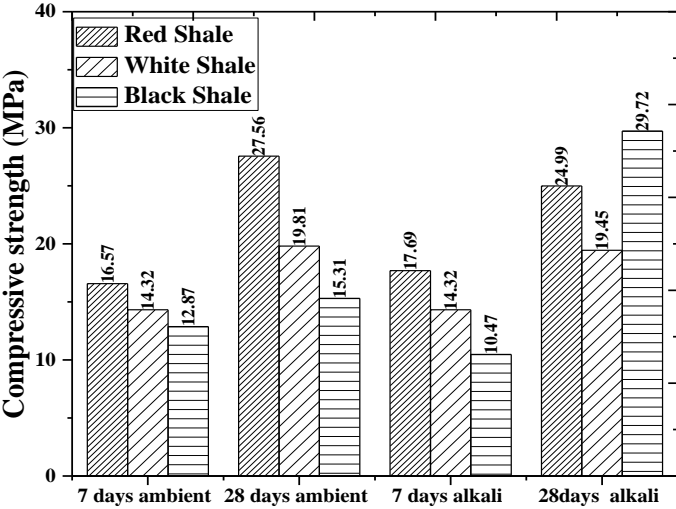
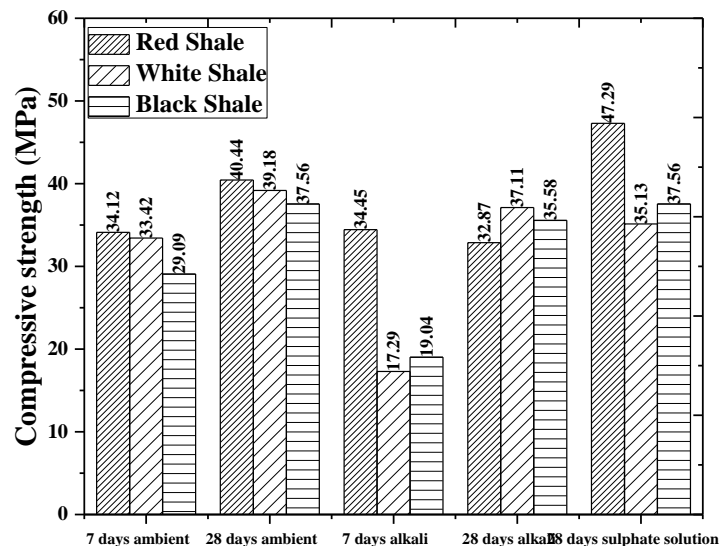


Figure 7.7: Alkali activated shale: GGBS- 50:50 (paste) with 0.5 mole of Na<sub>2</sub>SiO<sub>3</sub>.

An attempt is also made to know the effect of activator type (KOH) on the compressive strength of alkali activated shale- GGBS paste, of shale: GGBS proportion of 30:70 and shale: GGBS- 50:50, under ambient curing, alkali curing and sulphate curing conditions. Figure 7.8 shows the compressive strength of shale samples activated by 6 moles of KOH solution. It can be observed that red shale sample shows the higher strength of 47.29MPa

at sulphate condition at 28 days of curing but white and black shale cube shows the relatively low compressive strength of 35.13MPa and 37.56MPa. At 28 days of ambient curing red shale, white shale and black shale shows the compressive strength of 40.44MPa, 39.18MPa and 37.56MPa respectively. Red shale, white shale and black shale paste cube cured under alkali condition at 28 days of curing shows the compressive strength of 32.87MPa, 37.11MPa and 35.58MPa respectively. The compressive strength values are less than that with 3 M  $\text{Na}_2\text{SiO}_3$ , it may be mentioned here that the cost of 3 M  $\text{Na}_2\text{SiO}_3$  is higher than that of 6 M KOH.

Figure 7.9 shows the compressive strength of shale samples activated by 6 moles of KOH solution. It can be observed that red shale sample shows the higher strength of 47.29MPa (seems very high) at ambient condition after 28 days of curing but white and black shale paste shows relatively low compressive strength values of 22.25MPa and 26.57MPa after curing for 28 days. At 28 days of sulphate curing red shale, white shale and black shale shows the compressive strength of 32.43MPa, 17.26 MPa and 19.18MPa respectively. Red shale, white shale and black shale paste cube cured under alkali condition at 28 days of curing shows the compressive strength of 31.75MPa, 22.34MPa and 23.33MPa respectively. In general, it can be concluded that for the same KOH concentration lower strength was observed for lower GGBS content.



**Figure 7.8:** Alkali-activated shale paste (shale: GGBS- 30:70) with 6 moles of KOH.

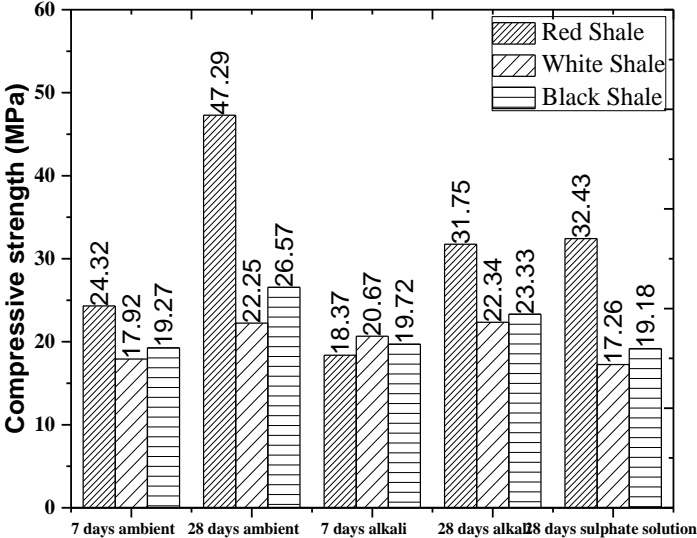


Figure 7.9: Alkali-activated shale paste (shale: GGBS- 50:50) with 6 moles of KOH.

**Slake durability test**

The slake durability tests are conducted as described in Chapter 5 for the above-developed AAM and the results are presented as follows. The slake durability tests for shale: GGBS-30:70 with 3M Na<sub>2</sub>SiO<sub>3</sub> under ambient, alkali and sulphate curing condition in Figures 7.10, 7.11 and 7.12, respectively. It can be seen that high slake durability index (SDI) value (after 2 cycles) are observed for samples under an ambient condition with red and black shale paste as “very high durable” and white shale paste as “high durable” material (Figure 7.10). However, under alkali curing condition the black shale paste is “very high durable” and other two pastes are “medium high durable” (Figure 7.11). A similar trend for durability is observed for the pastes under sulphate solution condition, but with higher SDI values (Figure 7.12). It was also observed that the compressive strength and SDI values (after two cycles) are correlated and will be discussed later.

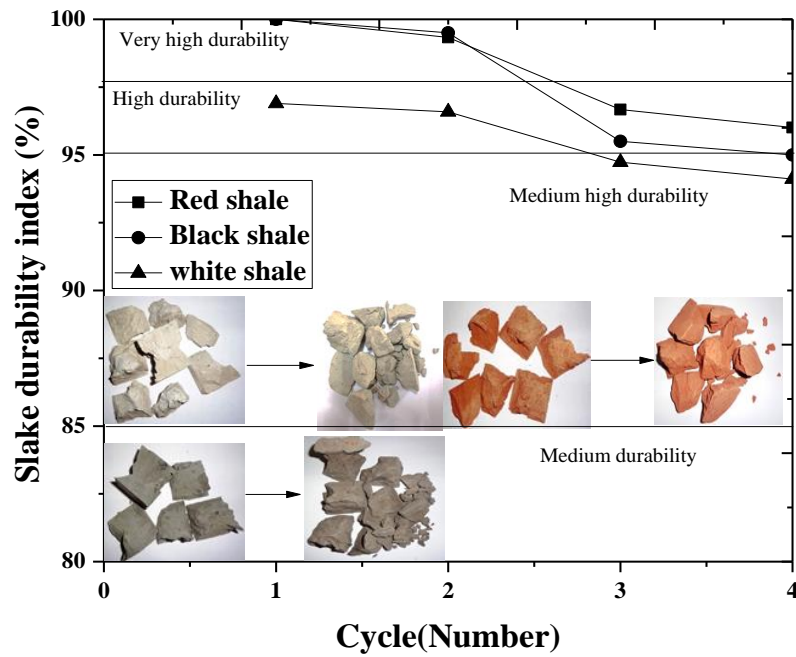


Figure 7.10: Slake durability test for AAM (shale: GGBS-30:70) with 3 moles of  $\text{Na}_2\text{SiO}_3$  under ambient curing after 28 days.

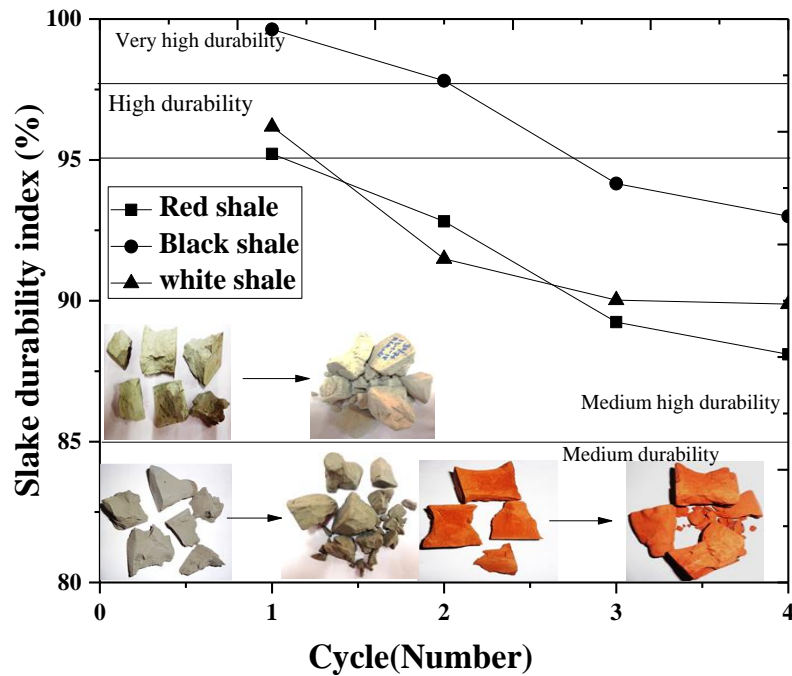


Figure 7.11: Slake durability test for AAM (shale: GGBS-30:70) with 3 moles of  $\text{Na}_2\text{SiO}_3$  under alkali cured after 28 days.

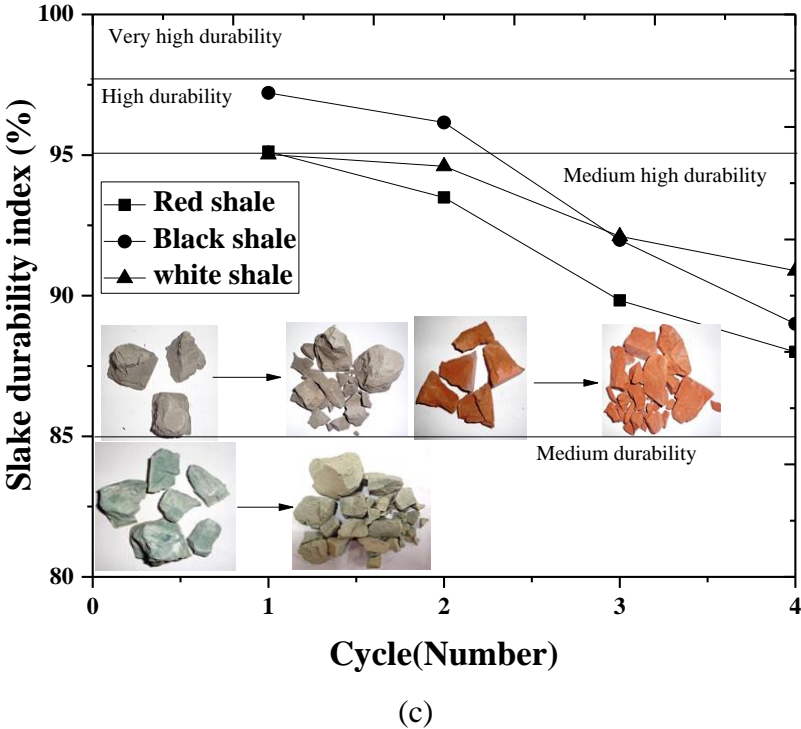


Figure 7.12: Slake durability test for AAM (shale: GGBS-30:70) with 3 moles of Na<sub>2</sub>SiO<sub>3</sub> under sulphate solution curing for 28 days.

The slake durability tests for shale: GGBS-30:70 with 0.5M Na<sub>2</sub>SiO<sub>3</sub> under ambient and alkali conditions in Figures 7.13 and 7.14, respectively. Highly durable materials are observed with a lower concentration of Na<sub>2</sub>SiO<sub>3</sub> under alkali condition (Figure 7.14) and the SDI values are comparable for all the three shales. It may be mentioned here that for the present study, the sample for the slake durability tests were taken from the broken sample of compression tests. The durability was also found to increase with blending of fly ash in the AAM shale – GGBS paste as shown in Figures 7.15 and 7.16, respectively for shale: FA: GGBS-30:20:50 and shale: FA: GGBS-50:10:40, respectively. For shale: FA: GGBS-50:10:40, all the three types of shale paste are found to fall into “very high durable” category. The durability of alkali -activated shale mortar showed a similar type of trend for all the three types of shales with “medium high durable” material (Figure 7.17) for the ambient cured sample and “high durable” for alkali cured samples (Figure 7.18). But for the sample with sulphate solution curing it was observed that red shale and black shale pastes are “high durable” material and white shale paste is “medium high durable” (Figure 7.19). Hence, from durability consideration, alkali curing is better than the sulphate curing condition.

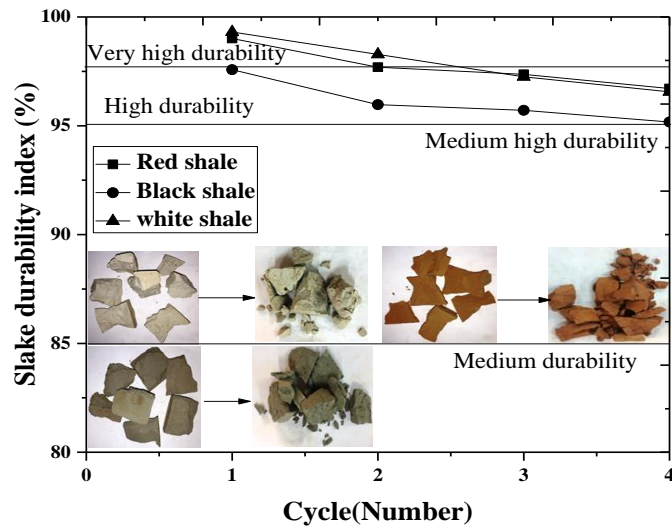


Figure 7.13: Slake durability test for AAM (shale: GGBS-30:70) with 0.5 moles of  $\text{Na}_2\text{SiO}_3$  under ambient curing condition

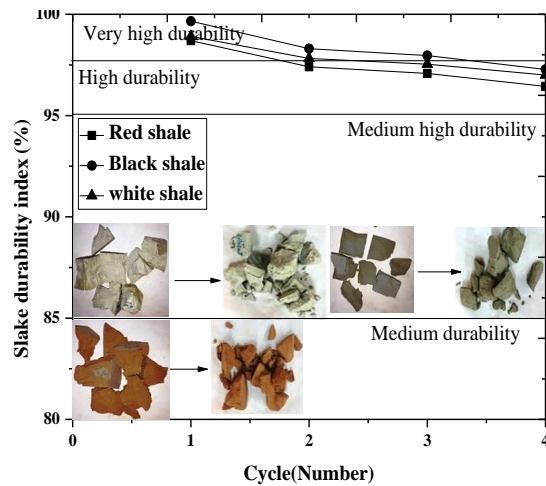


Figure 7.14: Slake durability test for AAM (shale: GGBS-30:70) with 0.5 moles of  $\text{Na}_2\text{SiO}_3$  under alkali curing condition.

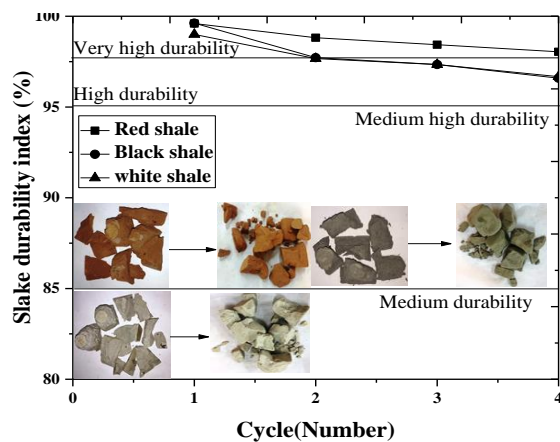


Figure 7.15: Slake durability test for AAM, shale: FA: GGBS-30:20:50 with 3 moles of  $\text{Na}_2\text{SiO}_3$ .

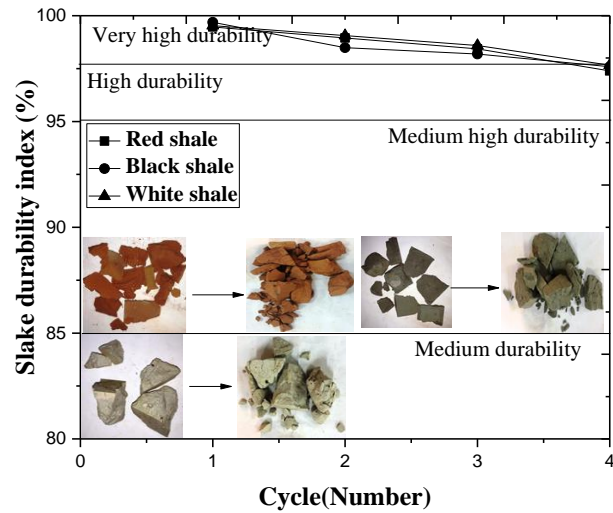


Figure 7.16: Slake durability test for AAM, shale: FA: GGBS-50:10:40 with 3 moles of  $\text{Na}_2\text{SiO}_3$ .

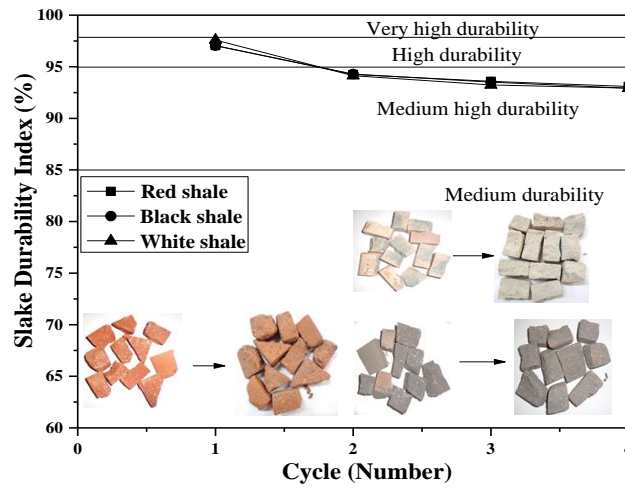


Figure 7.17: Slake durability index test for alkali-activated shale mortar (shale: sand: GGBS-30:30:40) with 3 moles of  $\text{Na}_2\text{SiO}_3$  under ambient curing

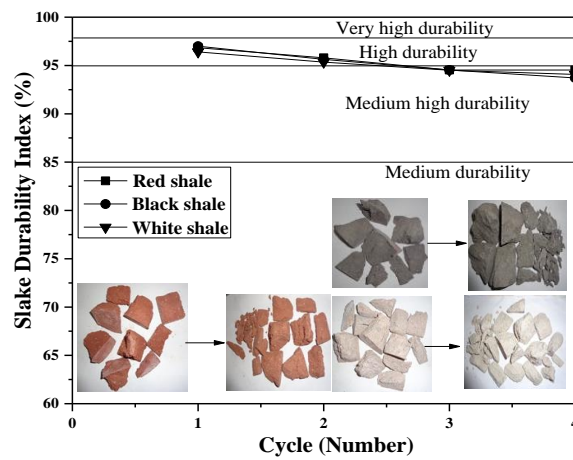
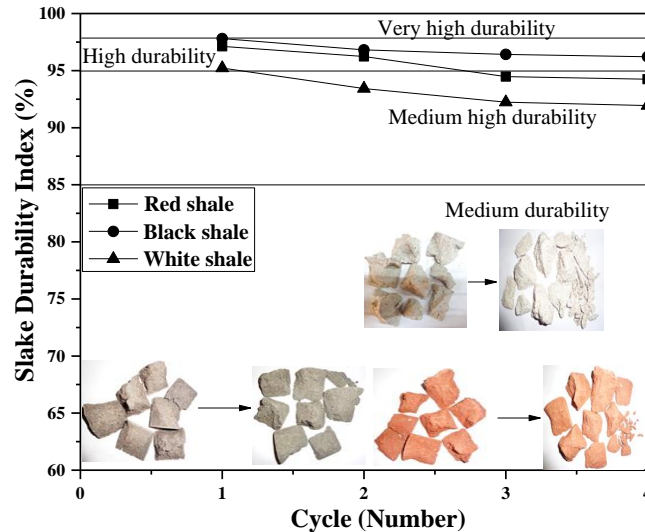


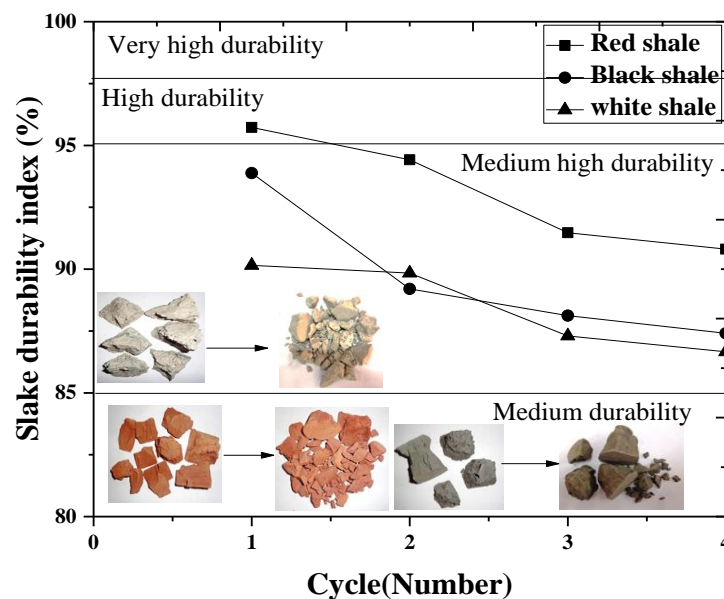
Figure 7.18: Slake durability index test for alkali-activated shale mortar (shale: sand: GGBS-30:30:40) with 3 moles of  $\text{Na}_2\text{SiO}_3$  under alkali curing condition.





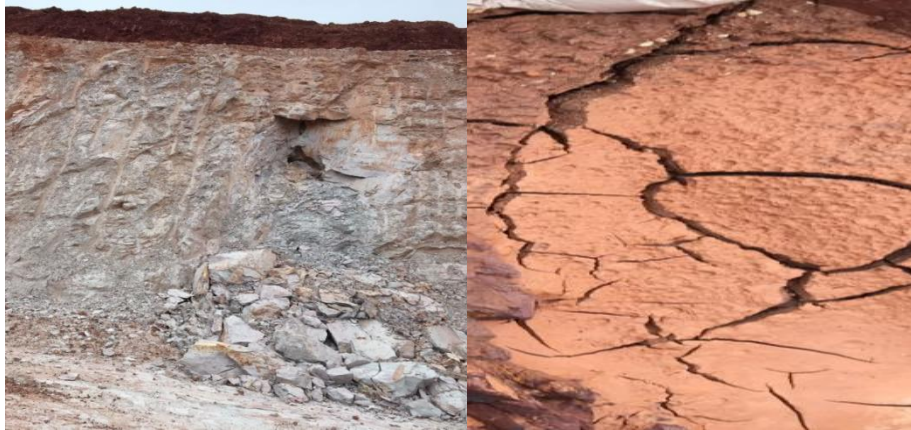
**Figure 7.19:** Slake durability index test for alkali -activated shale mortar (shale: sand: GGBS-30:30:40) with 3 moles of  $\text{Na}_2\text{SiO}_3$  under sulphate solution curing.

It is interesting to note that though, the compressive strength values of 0.5M  $\text{Na}_2\text{SiO}_3$  and 6M KOH is comparable, but the shale paste with 0.5M  $\text{Na}_2\text{SiO}_3$  is having higher SDI values (Figure 7.13) than that of 6M KOH (Figure 7.20).



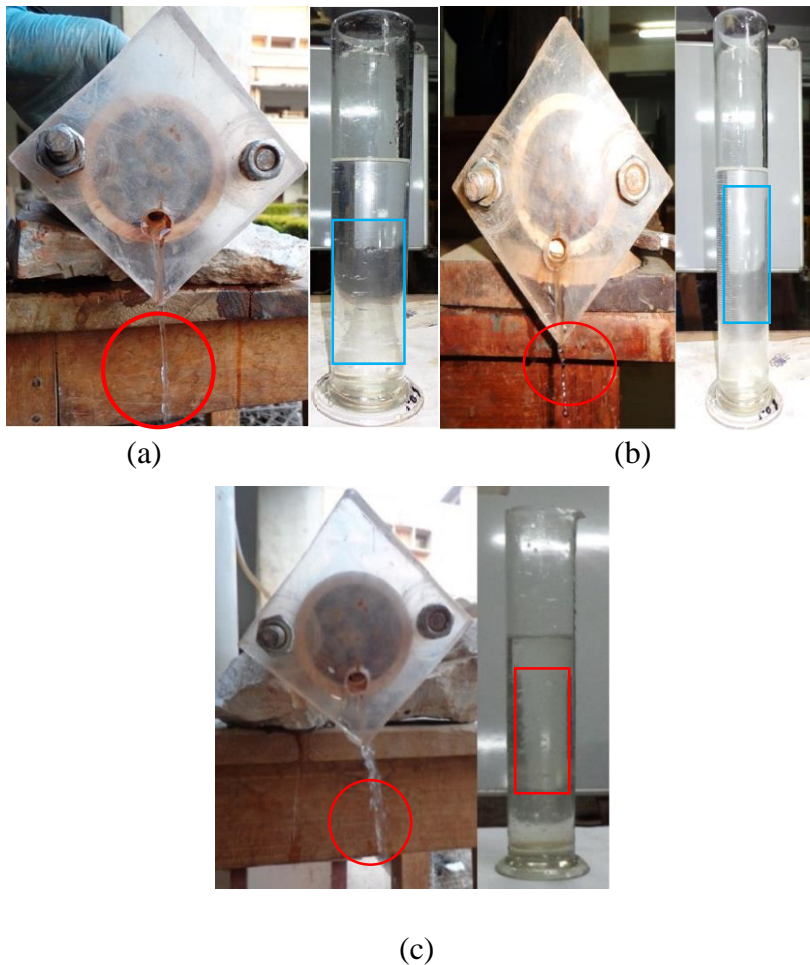
**Figure 7.20:** Slake durability index test for AAM (shale: GGBS-30:70) with 6 moles of KOH under ambient curing

Figure 7.21(a) shows the failure slope of overburden dump of white shale due to erosion, which is very common in iron ore mines. Figure 7.21(b) shows cracks in the red soil,

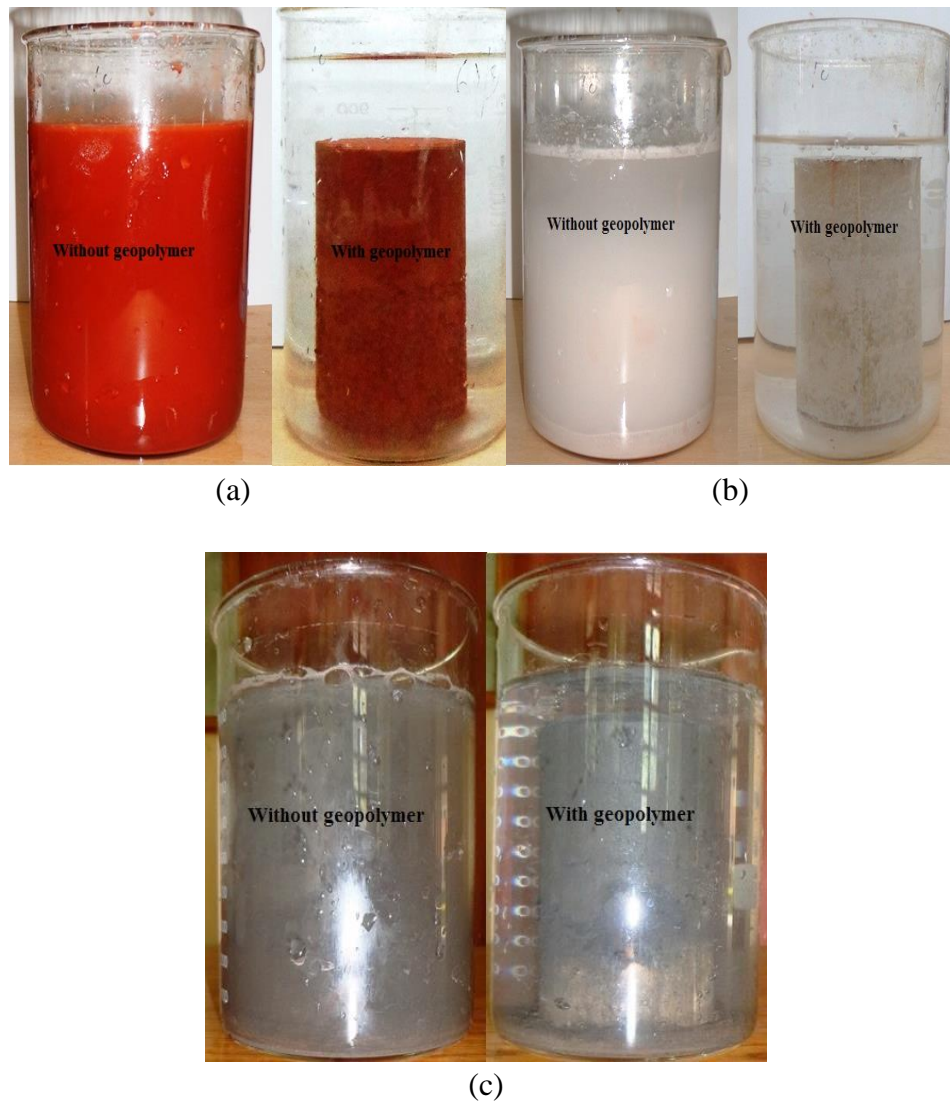


(a) (b)  
**Figure 7.21:** Water erosion of (a) white shale (b) red shale.

showing its susceptibility to erosion. In the present study, 20% GGBS activated with 0.5M  $\text{Na}_2\text{SiO}_3$  showed its effective based on pinhole test (Figure 7.22) and cylindrical dispersion test (Figure 7.23), hence can control the slope failure.



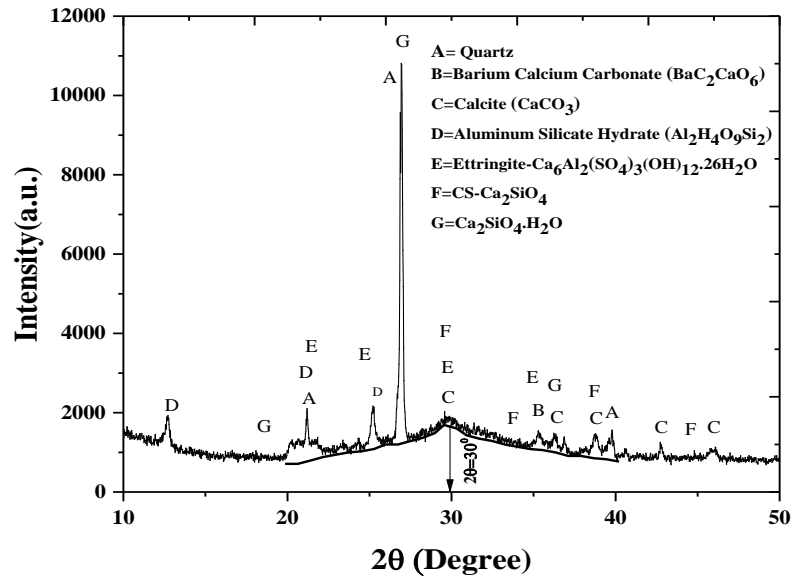
(a) (b) (c)  
**Figure 7.22:** (a) Pin hole test of (a) red shale (b) white shale and (c) black shale treated with 30% GGBS and 0.5% of sodium silicate solution.



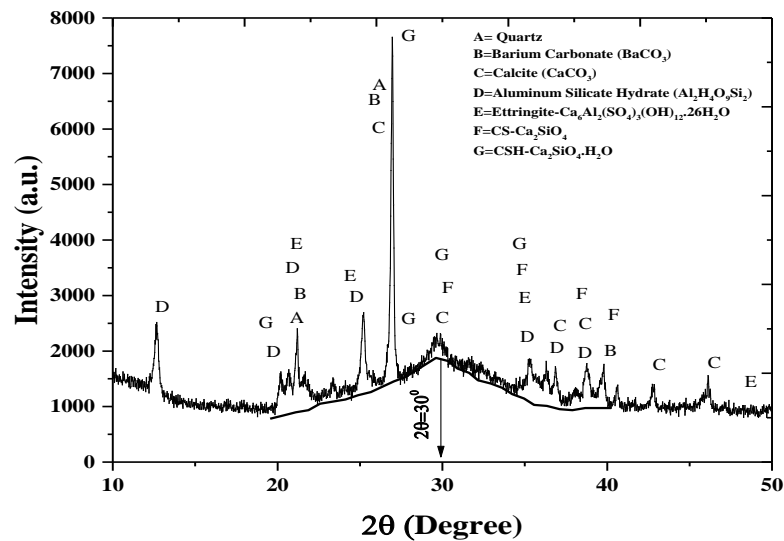
**Figure 7.23:** Cylinder dispersion test on alkali activated (a) red shale (b) white shale (c) black shale treated with 30% GGBS and 0.5% of sodium silicate solution.

#### ***XRD analysis of alkali activated shale-GGBS paste***

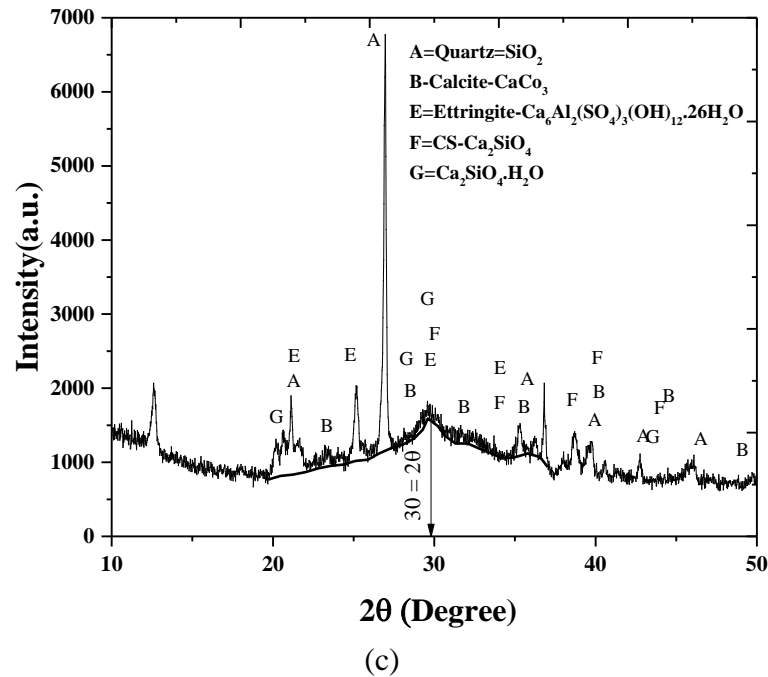
The XRD analysis of black shale activated with 3M of  $\text{Na}_2\text{SiO}_3$  under ambient, alkali and sulphate solution curing condition after 28 days shown in Figure 7.24, 7.25 and 7.26, respectively. It can be seen that minerals like ettringite, calcium silicate and calcite are formed, which are responsible for the development of strength. Similar observations are made for red shale and white shale paste. However, the quantitative analysis of XRD could not be made to find the reason for variations in strength.



**Figure 7.24:** XRD analysis of Alkali activated black shale paste (shale: GGBS- 30:70) with 3 moles of  $\text{Na}_2\text{SiO}_3$  under ambient after 28 days



**Figure 7.25:** XRD analysis of Alkali activated black shale paste (shale: GGBS- 30:70) with 3 moles of  $\text{Na}_2\text{SiO}_3$  under alkali curing condition after 28 days



**Figure 7.26:** XRD analysis of Alkali activated black shale paste (shale: GGBS- 30:70) with 3 moles of  $\text{Na}_2\text{SiO}_3$  under sulphate solution curing condition after 28 days.

### 7.3.2 Alkali Activated Fly Ash as a CLSM

In the present study alkali activation of fly using, sodium hydroxide (NaOH) activator was also investigated. For this purpose, fly ash from three different sources namely JSPL of Chattisgarh, HCFA of Paradeep and NALCO of Odisha, were collected. The detailed chemical, mineralogy and morphological properties are presented in Chapter 3.

The different fly ash cubes were cast, using NaOH as activators in different concentration as NaOH is considered as a better activator for fly ash (Pacheoco-Torgal et al. 2008b). The NaOH is used in different molar concentration (1M, 2M and 4M) and KOH is used in 6 moles. The Alkali activated fly ash samples are cured for 7 days and 28 days under ambient condition. Figure 7.24 shows the compressive strength of alkali activated NALCO fly ash, which is a low calcium Class F fly ash and the maximum compressive strength of 0.57 MPa was obtained with 4M NaOH. It may be mentioned here that the minimum compressive strength is 0.3MPa for CLSM. Another experiment was also made to use another industrial waste red mud, which is alkaline because of high pH value (Panda et al. 2017). The water collected from red mud pond from NALCO, Odisha India was collected. The compressive strength of alkali activated NALCO FA is found to be 0.19MPa, which is close to that of 1M NaOH activated FA. Similarly, the compressive strength of NaOH activated JSPL fly ash at 7 and 28 days is shown in Figure 7.25. The

JSPL with 2M of NaOH can be used as a CLSM material (0.38 MPa) and similar to NALCO fly ash the JSPL fly ash activated with liquid from red mud pond correspond to strength less than that corresponding to 1M NaOH. The sample failure pattern shows that sample is compact with no local failure.

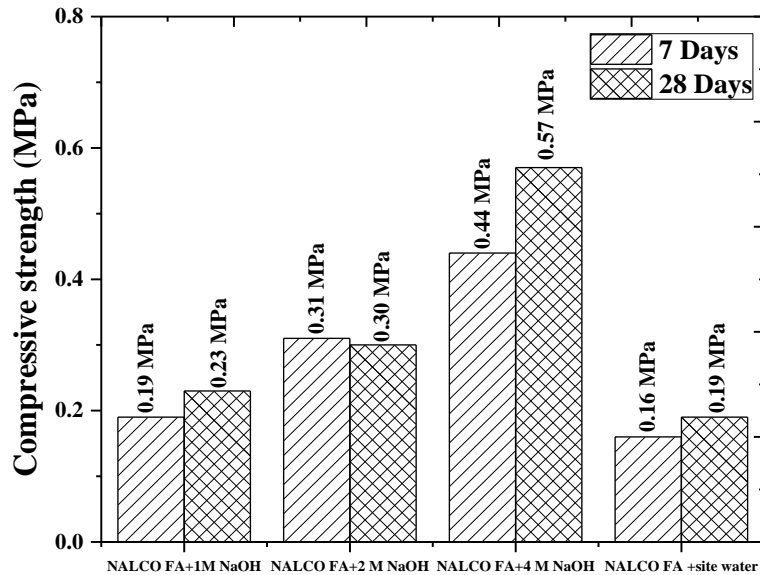


Figure 7.27: Compressive strength of Alkali activated Nalco fly ash.

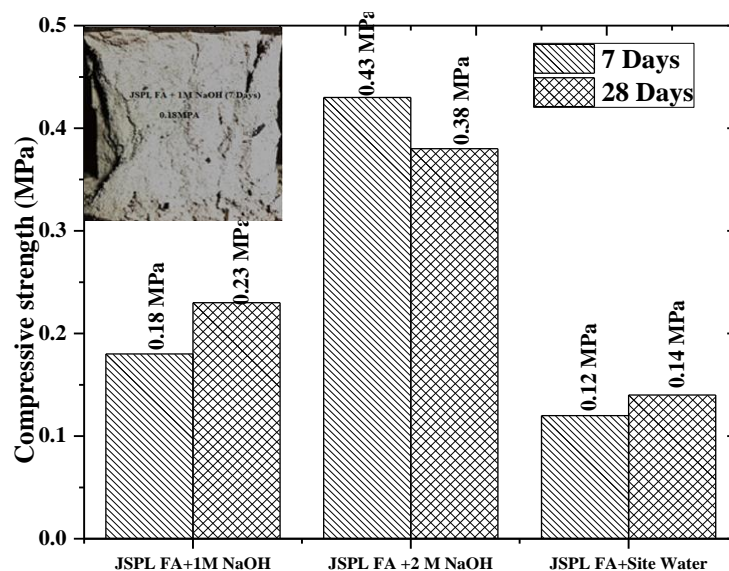


Figure 7.28: Compressive strength of Alkali activated JSPL fly ash.

The results of Paradeep fly ash whose lime (CaO) content is 14.2% as shown in Chapter 3, activated with NaOH is shown in Figure 7.29. The compressive strength HCFA treated with 1M, 2M and 4M of NaOH show 0.8MPa, 1.07MPa and 1.53MPa strengths respectively at 7days of ambient curing. Maximum compressive strength up to 4.01 MPa



was observed for FA activated with 4M NaOH. The FA paste made with red mud pond liquid shows a compressive strength of 0.22MPa and 0.42MPa in 7days and 28 days, respectively. The failure pattern of the paste sample shows the compactness of the sample. The slake durability test on the activated Paradeep fly ash is shown in Figure 7.31. The variation of SDI found to in close proximity for 2M and 4M NaOH sample and all the sample belongs to “medium durability group”. The shape of the sample with 1M NaOH after 4 cycles shows polished surface, whereas 4M NaOH sample shows angular surfaces. The SEM micrograph of compressive strength sample with 4M NaOH is shown in Figure 7.31a, shows the compact surface of it and 7.31b shows the bonding of fly ash particles due to bonding. The alkali activated HCFA fly ash also found to be environmentally sustainable as the leachate analysis using AAS shows heavy metals are within permissible limit. However, another test like flow, bleeding and density tests have not been conducted to find its suitability as a CLSM.

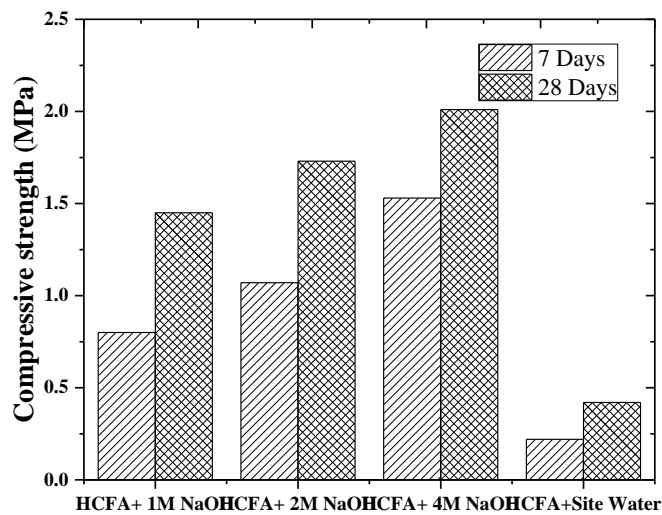


Figure 7.29: Alkali activated Paradeep (HCFA) fly ash.



Figure 7.30: Failure pattern of alkali activated Paradeep fly ash.

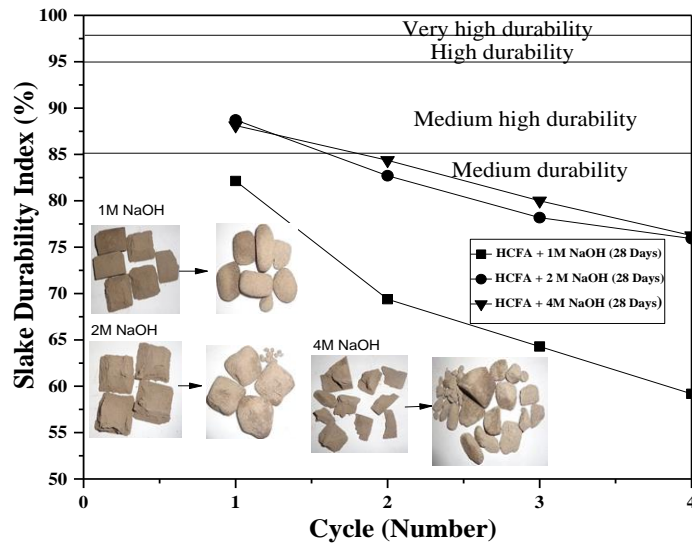
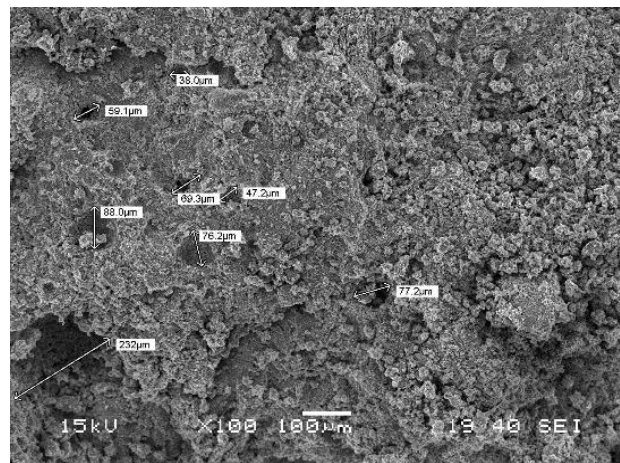
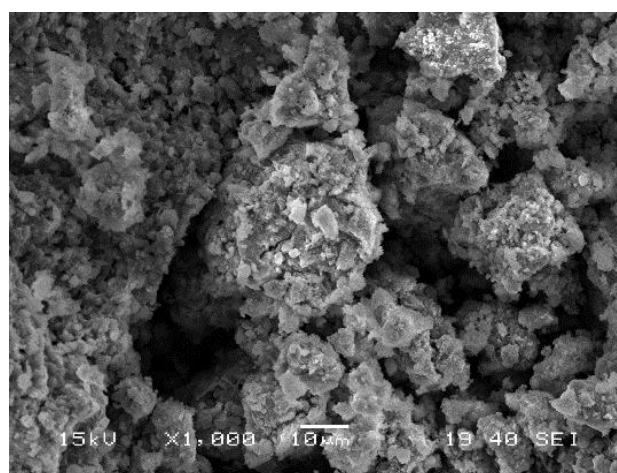


Figure 7.31: slake durability index test for alkali-activated Paradeep fly ash after 28 days of ambient curing.



(a)



(b)

Figure 7.32: SEM analysis of alkali activated HCFA+4 moles of NaOH.



**Table 7.1:** Leachate analysis of HCFA and alkali activated HCFA.

Element/ unit	Zn (ppm)	Pb (ppm)	Cr (ppm)	Ni (ppm)	Cu (ppm)	As (ppb)	Hg (ppb)
HCFA	0.018	0	0	0.077	0.006	0	0.119
HCFA+4mole NaOH	0.067	0.088	0	0.193	0.032	15.72	0.82
Permissible Limit	15.0	0.10	0.05	-	0.10	20.0	10.0

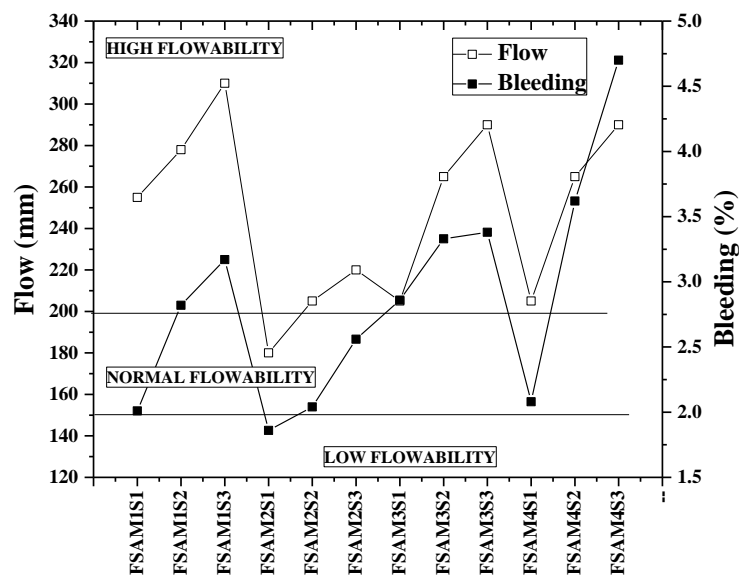
### 7.3.3 Cement Less Alkali Activated CLSM using Ferrochrome Slag

The cementless alkali activated CLSM has been designed using ferrochrome, JSPL fly ash, GGBS in different proportion activated with freshly prepared KOH solution of different concentration with water to binder ratio 0.375 to 0.475 as shown Table 7.2. Based on trials with NaOH and KOH, KOH was chosen due to higher compressive strength. Sample preparation and testing are done as discussed in Chapter 4 and 5.

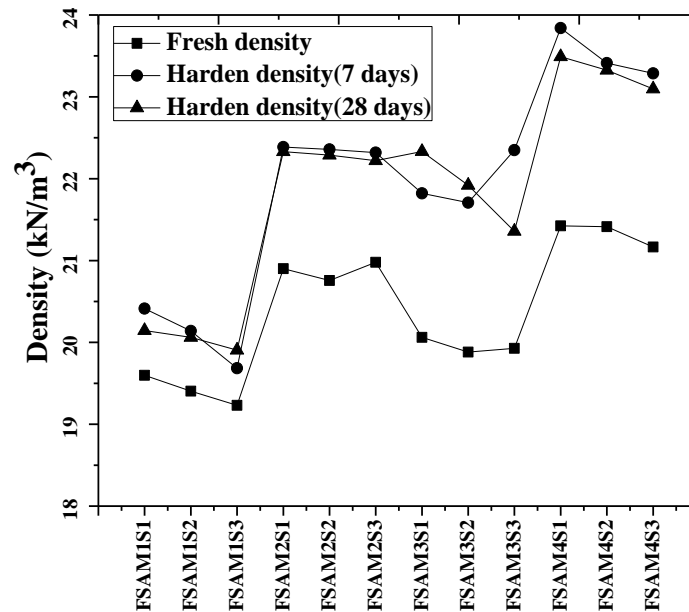
**Table 7.2:** Design mix of alkali activated cement less CLSM using FS

SL N O	W/B Ratio	Sample Name	Solution (%)	Fly ash (gm)	GGBS (gm)	FS (gm)	KOH solution (gm)	KOH (M)
1	0.400	FSAM1S1	24	408	612	680	408	0.75 M
	0.425	FSAM1S2	25.5	408	612	680	433	0.75 M
	0.450	FSAM1S3	27	408	612	680	459	0.75 M
2	0.425	FSAM2S1	17	272	408	1020	289	0.75 M
	0.400	FSAM2S2	18	272	408	1020	306	0.75 M
	0.475	FSAM2S3	19	272	408	1020	323	0.75 M
3	0.375	FSAM3S1	22.5	408	612	680	383	1 M
	0.450	FSAM3S2	24	408	612	680	408	1 M
	0.50	FSAM3S3	25.5	408	612	680	434	1 M
4	0.425	FSAM4S1	17	272	408	1020	289	1 M
	0.450	FSAM4S2	18	272	408	1020	306	1 M
	0.475	FSAM4S3	19	272	408	1020	323	1 M
Note: W-Water, B-Binder								

Figure 7.32 shows the flow and bleeding of CLSM, and it can be seen that the maximum flow diameter value of 310mm was found for FSM1S3 and the minimum flow diameter of 180mm was observed for FSM2S1, an increase of flow diameter with an increase in water content. In case of cement based FS CLSM, the flow values were 85mm to 390 mm as discussed in Chapter 4. A flow diameter within 150mm is considered as low flowable. The CLSM sample having the flow diameter within 150mm to 200mm is normal flowable and the CLSM mixture having a diameter more than that of 200mm is highly flowable. The bleeding of the CLSM material is within 1.86% to 4.7%. The maximum bleeding was observed for FSM4S3 and minimum bleeding was found in FSM2S1. The bleeding value less than 3.5% shows its suitability as a fill material. A mixture having bleeding value less than five percentages is considered as a stable mixture. In the present case the all mixture samples are stable. Similarly, the flow values of low, normal and high flowability show the applicability of the material in different uses. Segregation of the CLSM samples are measured by visual observation and no mixture are found to be segregated.

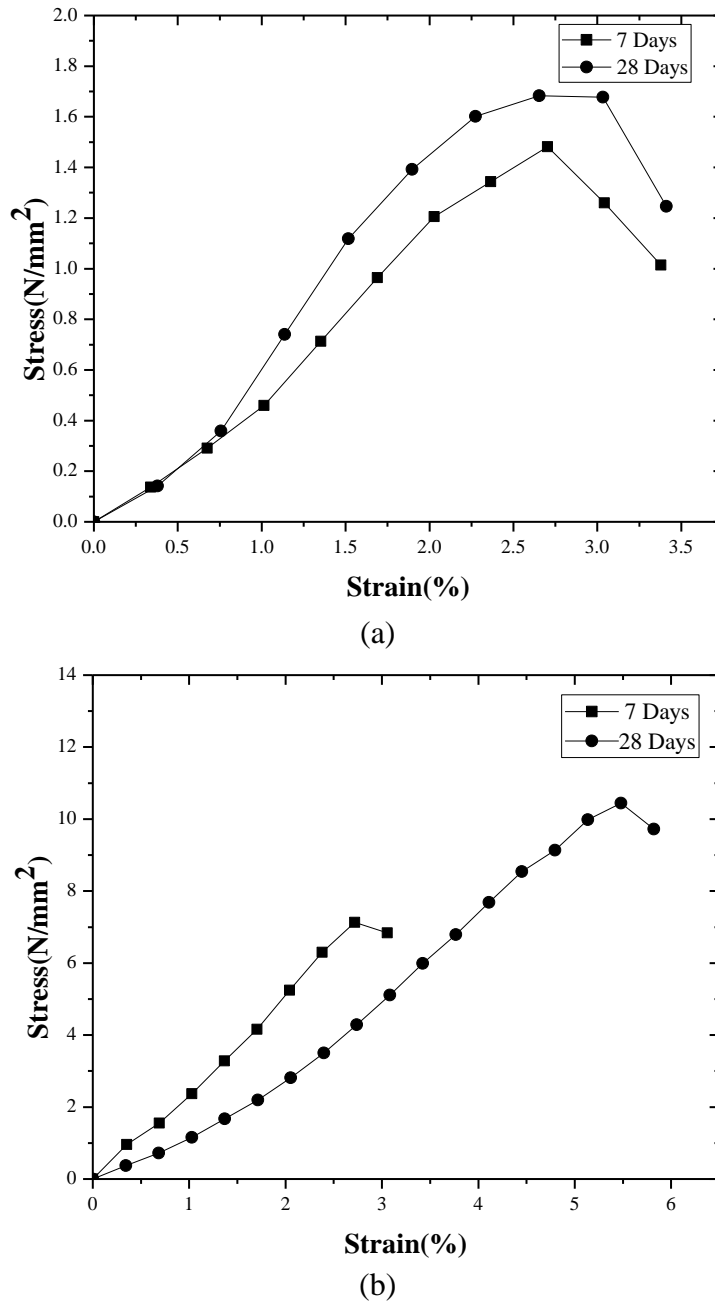


**Figure 7.33:** Flow and bleeding of the FS based cement less alkali activated CLSM material



**Figure 7.34:** Fresh and hardened density of alkali activated CLSM.

The fresh density of alkali activated FS based CLSM (Figure 7.33) is close to the value of cement based CLSM as discussed in Chapter 4. The maximum fresh density is found to be  $21.42 \text{ kN/m}^3$  for FSAM4S1 and the minimum density of  $19.23 \text{ kN/m}^3$  was found for FSAM1S3. The maximum hardened density of  $23.84 \text{ kN/m}^3$  of the CLSM at 7 days of curing was observed for FSAM4S1 and a minimum value of  $19.68 \text{ kN/m}^3$  is found for FSAM1S3. The maximum hardened density of  $23.49 \text{ kN/m}^3$  at 28 days of curing is found for FSAM4S1, and minimum hardened density of  $19.90 \text{ kN/m}^3$  is found for SAM1S3. The hardened density found to be higher for the sample with a higher concentration of KOH and low W/B ratio. The stress-strain curve for typical cementless FS CLSM is shown in Figure 7.34a for FSAM1S2 and Figure 7.34b for FSAM3S1. The sample with lower KOH shows failure at lower strain (Figure 7.34a) and sample with higher KOH (1M) concentration shows failure at higher strain (5%) at 28 days.



**Figure 7.35:** Stress-strain curve of CLSM (a) FSAM1S2 (b) FSAM3S1

The Figure 7.35 shows the unconfined compressive strength of CLSM at its 7days and 28 days of ambient curing. The UCS is observed to vary within 1.47MPa to 7.86MPa at 7days of curing. The maximum value of strength is observed in FSAM3S3 while the minimum strength is observed in FSAM1S2. In comparison to cement based FS CLSM, the UCS varies from 0.67 to 6.73 MPa. The maximum and minimum UCS at 28 days of curing are found in FSAM3S1 and FSAM1S2 are 10.44MPa and 1.72MPa respectively, with 2.54 to 14.48 MPa for cement based FS CLSM. There is a gain in strength for cement based CLSM with curing days, but the change in strength with cementless alkali activated

FS CLSM is marginal. The California bearing ratio (CBR) test is also conducted on different mixture samples at the soaked condition of 11 days (7days of normal curing +4days of water curing) and all the CBR values are found to be more than 200%.

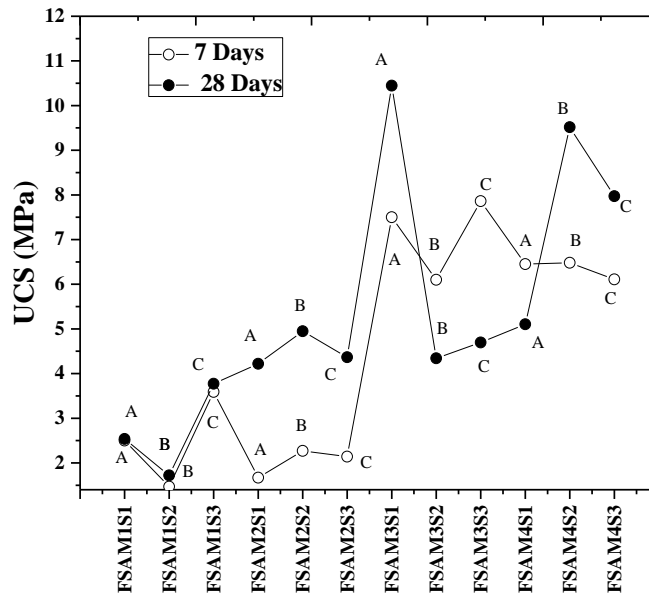


Figure 7.36: UCS of alkali activated FS based CLSM.

The SDI test is conducted on alkali activated FS CLSM samples for four cycles and SDI of some selected CLSM mixture having the comparatively higher strength (UCS value) is shown in Figure 7.36. The values vary from medium durability to medium high durability, corresponding photographs of sample after the slake durability index test is shown in Table.7.3.

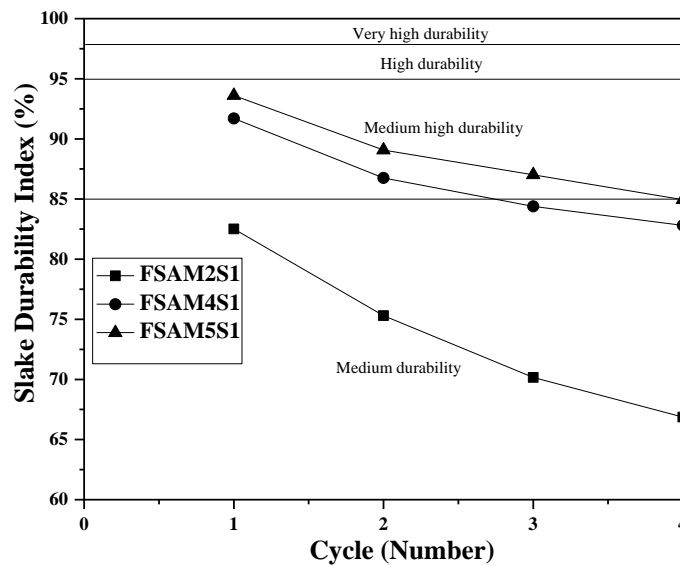

















Figure 7.37: Slake durability index of alkali activated CLSM corresponding to a different cycle.

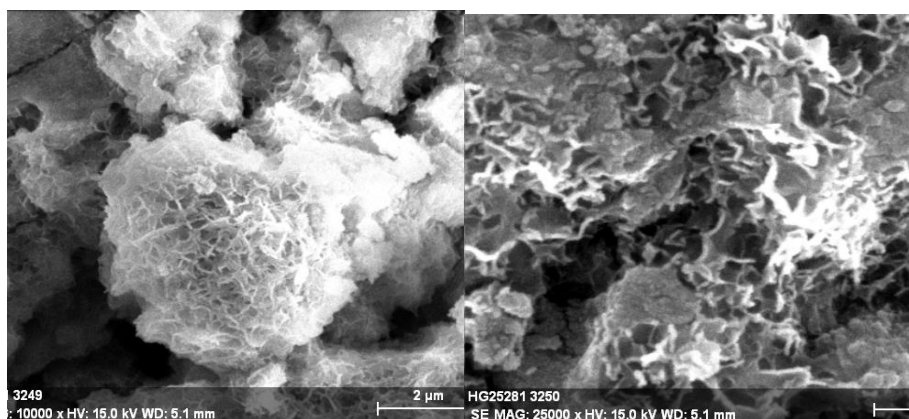
Settlement test is conducted on CLSM samples at different curing age of 3days, 7days and 28 days. Table 7.4 shows settlement analysis of presently prepared CLSM samples. The settlement of the samples varies from 0 to 4mm. The maximum settlement is achieved in FSAM3S3 and sample FSAM2S3 shows no settlement. Figure 7.37 shows the SEM analysis of alkali activated cement less FS based CLSM, and CSH gel structures are observed, which is responsible for gain in strength of alkali activated FS. The leachate analysis of the base material and the CLSM mixture is shown in Table 7.5. The increase in CLSM may be due to leaching from FS under alkali condition, but the values are within permissible limit.

Table 7.3: Slake durability index of CLSM

Sample	Sample before test	Sample after 1 <sup>st</sup> cycle	Sample after 2 <sup>nd</sup> cycle	Sample after 3 <sup>rd</sup> cycle	Sample after the 4 <sup>th</sup> cycle
FSAM2S1					
FSAM3S1					
FSAM4S1					

**Table 7.4:** Settlement of FS CLSM

Sample	3 days (mm)	7 days (mm)	28 days (mm)
FSAM1S3	3	3	3
FSAM2S3	0	0	0
FSAM3S3	4	4	4
FSAM4S3	2	2	2

**Figure 7.38:** SEM image of alkali activated FS CLSM samples**Table 7.5:** Leachate analysis of FS CLSM.

Material/Limits	Zn ( ppm)	Pb ( ppm)	Cr ( ppm)	Ni ( ppm)	Cu ( ppm)	As ( ppb)	Hg ( ppb)
<b>FS</b>	0.085	0	0	0.050	0	10.00	0
<b>JSPL FA</b>	0.004	0	0	0.042	0	2.211	0
<b>GGBS</b>	0.031	0	0.036	0	0	0	0
<b>CLSM</b>	0.029	0	0	0.042	0.003	16.58	0
<b>Permissible Limit</b>	15.0	0.10	0.05	-	0.10	20.0	10.0



### 7.3.4 Alkali Activated Material for the CLSM using Mine Overburden

Similarly, cementless alkali activated CLSM has been designed by using coal mine overburdens (shale), JSPL fly ash and GGBS. The activator used in CLSM mixture is Sodium hydroxide solution. Limited samples are made with 2M NaOH solution, based on trials. Table 7.6 shows design mix of CLSM using alkali activators. The water to binder ratio is maintained within 0.65 to 0.75 as per requirement. The mixing procedure is same as that of described in Chapter 5.

**Table 7.6:** Proportion and properties of Shale, GGBS, Fly ash and NaOH solution- CLSM

SL NO	W/B Ratio	Sample Name	Water (%)	Conc. of solution	FA (gm)	Water	Shale (gm)	GGBS (gm)
1	0.65	SaM1S1	38	2 M	375	950	1500	625
	0.70	SaM1S2	40	2 M	375	1000	1500	625
	0.75	SaM1S3	42	2 M	375	1050	1500	625
2	0.65	SaM2S1	38	2 M	500	950	1500	500
	0.70	SaM2S2	40	2 M	500	1000	1500	500
	0.75	SaM2S3	42	2 M	500	1050	1500	500
3	0.65	SaM3S1	40	2 M	625	1000	1500	375
	0.70	SaM3S2	42	2 M	625	1050	1500	375
	0.75	SaM3S3	44	2 M	625	1100	1500	375

The CLSM Samples are categorized as low flowability, medium flowability and high flowability as per their flow diameter as shown in Figure 7.38. The maximum flow diameter found at SaM3S3 is 295mm and minimum diameter found at SaM1S1 is 175mm.

The bleeding values of the prepared samples are varied within 0.00% to 1.25% and are within limit. Segregation of the CLSM samples are measured by visual observation and samples SaM1S3, SaM2S3 and SaM3S3 showed a little segregation.

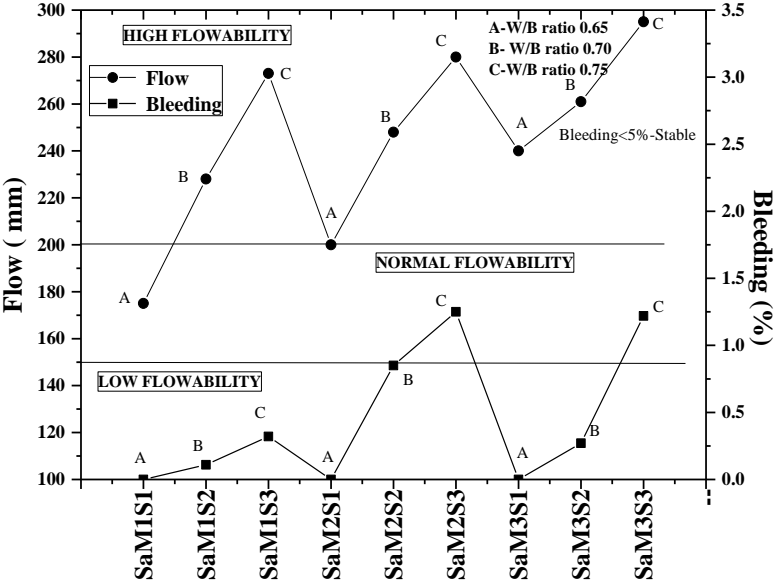


Figure 7.39: Flow and bleeding of alkali activated CLSM.

Figure 7.39 shows the fresh density and harden density of the different CLSM samples. The fresh density of the samples varies from 16.92kN/m<sup>3</sup> to 17.56kN/m<sup>3</sup> in comparison to 17.18 to 18.92 kN/m<sup>3</sup> for cement based OB CLSM as discussed in Chapter 5. The harden density of the samples cured at 7 days of curing is varied 14.71kN/m<sup>3</sup> to 15.16kN/m<sup>3</sup>, in comparison to cement based CLSM variation as 14.96 to 16.70kN/m<sup>3</sup>. The harden density of 28days of curing varies from 14.32 kN/m<sup>3</sup> to 15.23kN/m<sup>3</sup> is comparable to cement based OB CLSM of 15.17 to 16.50kN/m<sup>3</sup>.

Figure 7.40 shows the water absorption of the CLSM samples and their corresponding ultrasonic pulse velocity. The water absorption of the CLSM samples are varied within 0.2% to 1.45% and ultrasonic pulse velocity (UPV) varies from 1952m/s to 2526m/s depending, the voids present the samples at 7days of curing. After 28 days of curing the water absorption of the CLSM samples varies within 0.43% to 1.92% and ultrasonic pulse velocity varies from 1736m/s to 2481m/s (Figure 7.41). The variations in the water absorption, UPV may be due to evaporation of excess moisture from CLSM.

A linear relationship between the ultrasonic pulse velocity and water absorption of CLSM samples are observed at 7days (Figure 7.42) and 28 days (Figure 7.43) under ambient curing condition.

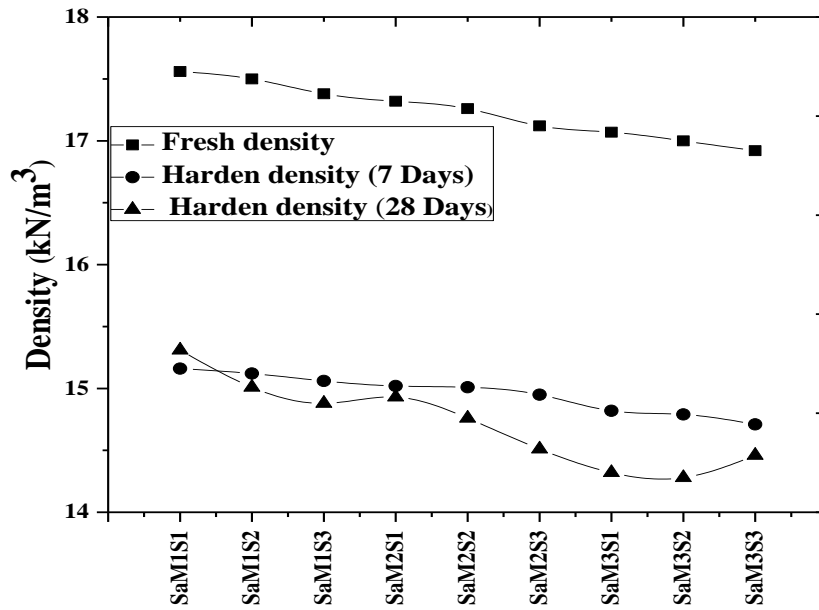


Figure 7.40: Fresh and harden density of CLSM.

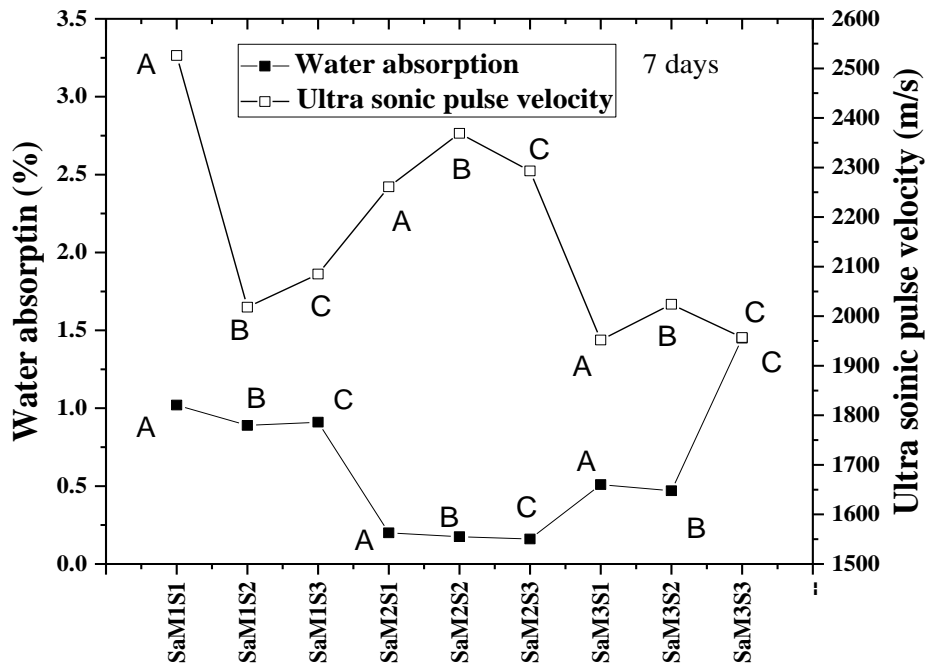


Figure 7.41: Ultrasonic pulse velocity and water absorption of CLSM at 7 days curing.

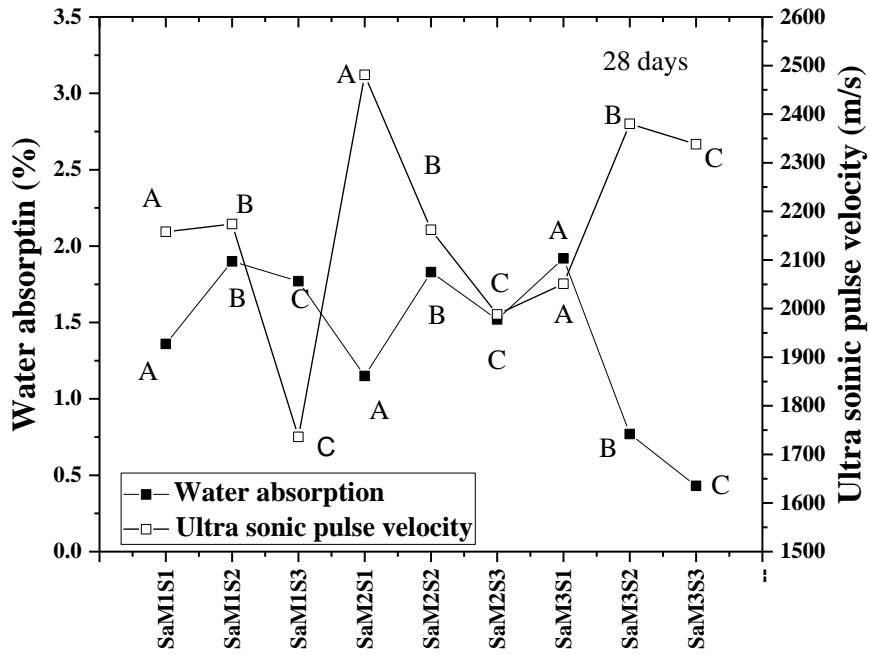


Figure 7.42: Ultrasonic pulse velocity and water absorption of CLSM at 28 days curing.

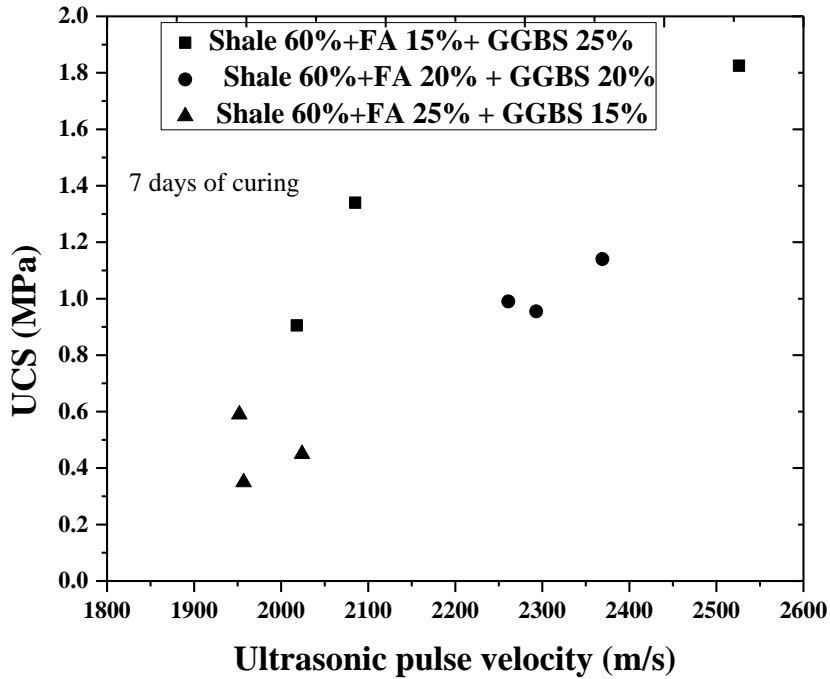
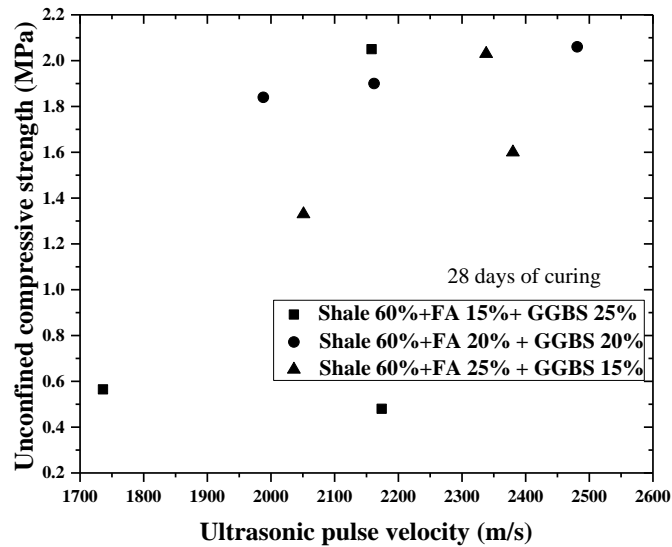
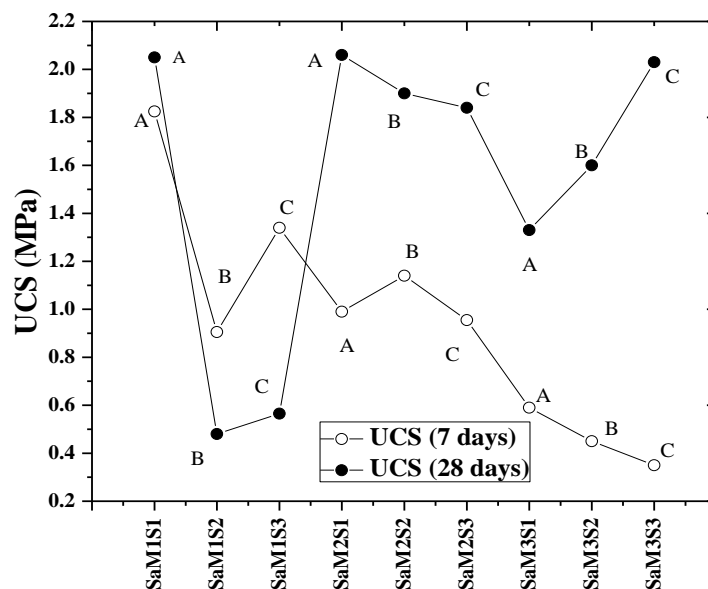


Figure 7.43: Relationship between ultra-sonic pulse velocity and UCS of alkali activated CLSM at 7 days of curing.



**Figure 7.44:** Relationship between ultra-sonic pulse velocity and UCS of alkali activated CLSM at 28 days of curing.

Figure 7.44 shows the unconfined compressive strength of CLSM samples at 7 days and 28 days of curing at ambient condition. The UCS at 7 days of curing is found to within 0.35MPa to 2.06MPa. The maximum and minimum UCS value find at SaM2S1 and SaM1S respectively at 28 days of curing.



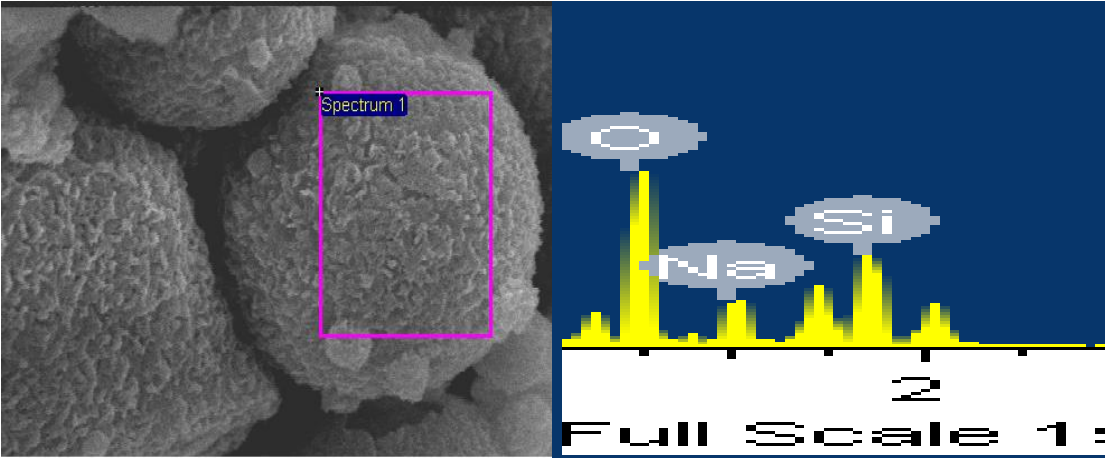
**Figure 7.45:** UCS of alkali activated shale based CLSM at 7 days and 28 days.

The settlement test is conducted on the CLSM samples at its different curing age of 3 days, 7 days and 28 days. Table 7.7 shows settlement analysis of presently prepared CLSM samples. The settlement of the developed samples varies from 0 to 1mm. It can be seen that very negligible settlement was found at their early age of curing of 3 days and there is no settlement at later age.

**Table 7.7:** Settlement test of CLSM (Cylinder size 10cm dia, 20cm height) (in mm from top)

Sample	3days settlement	7days settlement	28days settlement
SaM1S3	1mm	1mm	1mm
SaM1S3	1mm	1mm	1mm
SaM1S3	1mm	1mm	1mm

The SEM image of fly ash particle (Figure 7.46a) of the alkali activated OB CLSM and the corresponding EDX (Figure 7.46b) shows the presence of sodium aluminate silicate.



(a) (b)  
**Figure 7.46:** shows the SEM and EDX analysis of CLSM.

After unconfined compressive strength test of the cylindrical specimen after cured for 28days, broken samples are subjected to the slake durability index (SDI) test. Figure 7.47 shows the SDI of some selected CLSM mixtures and the samples are “medium durability” to “medium high durability”. Finally based on various slake durability tests on AAM, cement based and cementless alkali activated CLSM a variation of SDI with UCS is shown in Figure 7.48 along with results of natural rocks (Sharma and Singh 2008). It was observed that CLSM samples followed a trend, but the SDI of alkali activated material varied in a wide range for the same UCS values. This is an important aspect to study, particularly, when using the CLSM in a water erodible environment.

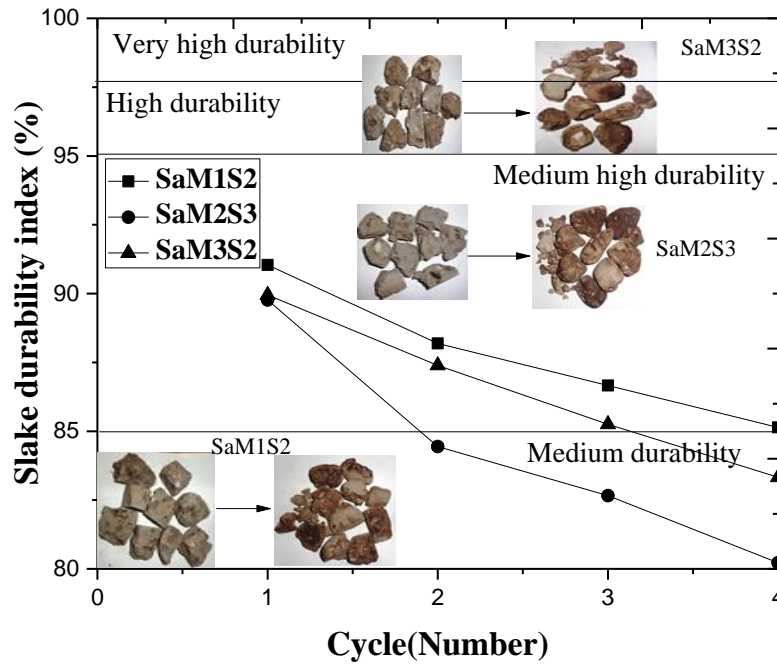


Figure 7.47: slake durability index test for alkali-activated CLSM at its 28 days of ambient curing.

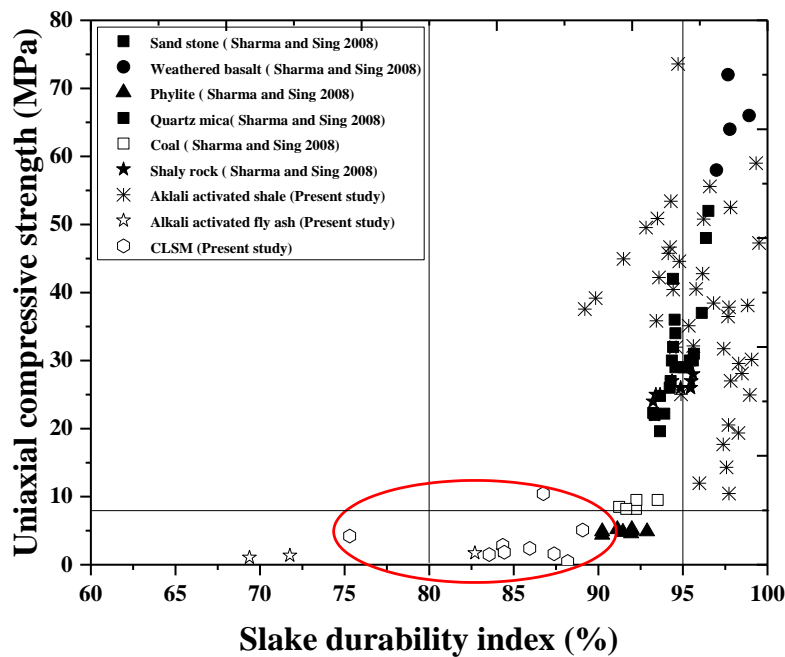


Figure 7.48: Variation of unconfined compressive strength and slake durability index of AAM and CLSM developed in the present study and its comparison with natural rocks.

Leachate analysis of the basic materials is conducted by AAS (Atomic absorption spectroscopy) test through base leaching procedure. In the present study leachate analysis has been conducted for the hazardous element like zinc, lead, chromium, copper, arsenic and mercury. The Table 7.8 shows the details of leachate analysis of base material and all the values of leachate of heavy metals are within the permissible limit, hence the CLSM

material may be considered as sustainable, though leachate analysis of the CLSM could not be done..

**Table 7.8:** Leachate analysis of shale CLSM.

<b>Material/Limits</b>	<b>Zn ( ppm)</b>	<b>Pb ( ppm)</b>	<b>Cr ( ppm)</b>	<b>Ni ( ppm)</b>	<b>Cu ( ppm)</b>	<b>As ( ppb)</b>	<b>Hg ( ppb)</b>
<b>Shale (B)</b>	4.134	0	0	8.413	0.027	0.00446	0
<b>JSPL FA</b>	0.004	0	0	0.042	0	2.211	0
<b>GGBS</b>	0.031	0	0.036	0	0	0	0
<b>Permissible Limit</b>	15.0	0.10	0.05	-	0.10	20.0	10.0

## 7.4 Summary

This chapter discussed about another sustainable material, alkali activated material using basic materials from mining and industrial wastes. An attempt is also made to develop low strength AAM using fly ashes from different sources of both Class F and Class C. Development of cementless CLSM of FS and coal mine overburden through alkali activator is another novelty of this chapter. Based on the experimental investigations and discussion thereof following conclusions can be made.

1. Red shale sample has very high compressive strength at early stages (7 days) 55.85MPa, which gets marginally increased to 59.0 MPa. But, the compressive strength of white shale paste decreased from 55.75 MPa under the ambient condition to 44.95 MPa under alkali and 31.97 MPa under sulphate solution curing condition. But, the compressive strength of red shales is 59.0 MPa, 49.54MPa and 50.89MPa, under ambient, alkali and sulphate solution curing, respectively.
2. The reduction of GGBS content (from 70 to 50%) in the paste shows a reduction in the strength under ambient and alkali solution for red shale, but no reduction in strength for red shale under sulphate curing condition (50.44) (Figure 7.2). But for black and white shale, there is a substantial reduction in strength with a reduction in GGBS content.



3. Hence, for red shale paste, the replacement of GGBS with fly ash does not vary the compressive strength under water/ambient condition but plays an important role in durability under sulphate curing condition. However, for the black shale replacement of GGBS with fly ash found to be beneficial. It may be mentioned here that the sulphate solution is expected in coal mines overburden (black shale).
4. Under sulphate curing condition the black shale paste with higher fly ash content has got better strength compared to higher GGBS content ( 30.07 MPa vs 25.04 MPa), but for red and white shale paste, the marginal difference was observed for replacement of fly ash with GGBS. However, under water curing, condition higher percentage of GGBS gives higher compressive strength. Hence, it is important to choose a particular type of AAM keeping in mind the environment condition around.
5. But for red shale mortar maximum compressive strength (50.8 MPa) was observed under sulphate solution curing condition. Under the ambient condition, the mortar strength for black shale was maximum (53.42 MPa), which reduced to 38.46 MPa under sulphate solution curing condition.
6. It may be mentioned here that with the same shale- GGBS proportion (30:70), with 3 M  $\text{Na}_2\text{SiO}_3$ , the compressive strength under ambient conditions is higher than that with 0.5M  $\text{Na}_2\text{SiO}_3$ . But, under alkali curing condition, the compressive strength increased compared to ambient curing with low molar (0.5M) concentration but decreased with high molar (3.0M) concentration of  $\text{Na}_2\text{SiO}_3$ . Similarly, for shale: GGBS-30:70 with 0.5 moles  $\text{Na}_2\text{SiO}_3$  the compressive strength for red shale are comparable for ambient (16.57 and 27.56 MPa) and alkali solution (17.69 and 24.99 MPa) at 7 and 28 days of curing. But for black shale, the compressive strength under alkali solution (29.72 MPa) is higher than that under ambient condition (15.31 MPa).
7. It was observed that red shale sample with 6M KOH shows the higher strength of 47.29MPa at sulphate condition at 28 days of curing but white and black shale cube shows the relatively low compressive strength of 35.13MPa and 37.56MPa. At 28 days of ambient curing red shale, white shale and black shale shows the compressive strength of 40.44MPa, 39.18MPa and 37.56MPa respectively. Red shale, white shale and black shale paste cube cured under alkali condition at 28days of curing show the compressive strength of 32.87MPa, 37.11MPa and 35.58MPa respectively. The compressive strength values are less

than that with 3 M  $\text{Na}_2\text{SiO}_3$ , it may be mentioned here that the cost of 3 M  $\text{Na}_2\text{SiO}_3$  is higher than that of 6 M KOH.

8. The slake durability tests for shale: GGBS-30:70 with 3M  $\text{Na}_2\text{SiO}_3$  under ambient condition with red and black shale paste as “very high durable” and white shale paste as “high durable” material ambient, however, under alkali curing condition the black shale paste is “very high durable” and other two pastes are “medium high durable”. A similar trend for durability is observed for the pastes under sulphate solution condition, but with higher SDI values. It was also observed that the compressive strength and SDI values (after two cycles) are correlated and will be discussed later.
9. It is interesting to note that though, the compressive strength values of 0.5M  $\text{Na}_2\text{SiO}_3$  and 6M KOH are comparable, but the shale paste with 0.5M  $\text{Na}_2\text{SiO}_3$  is having higher SDI values than that of 6M KOH.
10. The minerals like ettringite, calcium silicate and calcite are formed for the alkali activated shale- GGBS paste, which is responsible for the development of strength.
11. The JSPL and NALCO fly ash with 2M of NaOH can be used as a CLSM material (0.38 MPa). The sample failure pattern shows that sample is compact with no local failure.
12. The variation of SDI found to in close proximity for Paradeep fly ash (HCFA) with 2M and 4M NaOH sample and all the sample belongs to “medium durability group”.
13. The alkali activated HCFA fly ash also found to be environmentally sustainable as the leachate analysis using AAS shows heavy metals are within permissible limit. However, other tests like flow, bleeding and density tests have not been conducted to find its suitability as a CLSM.
14. The flow and bleeding of AA FS CLSM shows maximum flow diameter value of 310mm and minimum flow diameter of 180mm. In case of cement based FS CLSM, the flow values were 85mm to 390 mm.
15. The fresh density of alkali activated FS based CLSM is close to the value of cement based CLSM.
16. There is a gain in strength for cement based CLSM with curing days, but the change in strength with cementless alkali activated FS CLSM is marginal.
17. The bleeding values of the alkali activated coal mine overburden samples varies within 0.00% to 1.25%.

18. A linear relationship between the ultrasonic pulse velocity and water absorption of CLSM samples are observed at 7days and 28 days under ambient curing condition. The UCS at 7 days of curing is found to within 0.35MPa to 2.06MPa.
19. Finally based on various slake durability tests on AAM, cement based and cementless alkali activated CLSM a variation of SDI with UCS is shown in Figure 7.48 along with results of natural rocks. It was observed that CLSM samples followed a trend, but the SDI of alkali activated material varied in a wide range for the same UCS values. This is an important aspect to study, particularly, when using the CLSM in a water erodible environment.
20. Leachate analysis of the basic materials are conducted by AAS (Atomic absorption spectroscopy) test through base leaching procedure.
21. The alkali activated material also can be used for erosion control of dispersive soil.



## **CHAPTER 8**

# **GENERAL OBSERVATIONS, CONCLUSIONS AND SCOPE OF FUTURE STUDIES**

### **8.1 Summary**

The rapid increase in industrialization causes accumulation of the enormous amount of industrial waste and by-products day by day, which affects the ecosystem in terms of water, air and soil pollution. The sustainable development is required in terms of conservation of natural resources and utilization of industrial wastes. Though efforts have been made to develop geopolymers from industrial wastes, the same using mine wastes are limited. With 80% of a coal mine in India as open cast mines, huge space is required for storage of such material as dump slope. The steel and thermal industries are the major industries in India, contributing to the economy and at the same time generating a huge amount of industrial wastes in terms of slag and fly ash, respectively. Hence, there is also a need to develop CLSM using these wastes with mine wastes to compensate the engineering material required for the development of infrastructures.

Another challenge in the coal mine sector with power plants in the vicinity is the air pollution due to dispersive nature of coal mine overburden and fly ash. Keeping in mind the geoenvironment condition, biopolymer cement may be an effective alternative method to chemical stabilization. The primary focus of this research was to explore the development of sustainable geomaterial based on industrial and mining wastes for their utilization and management.

## 8.2 General Observation and Concluding Remarks for Material Characterization.

1. NALCO fly ash and JSPL fly ash belongs to Class F ( $\text{SiO}_2 + \text{Al}_2\text{O}_3 + \text{Fe}_2\text{O}_3 > 70\%$ ) with low calcium content (0.70%). Paradeep fly ash belongs to Class C, with  $\text{SiO}_2 + \text{Al}_2\text{O}_3 + \text{Fe}_2\text{O}_3 < 70\%$  and CaO content less than 15% (14.20%). The NALCO and JSPL fly ashes belong to Sialic group of highly acidic, with low calcium content and Paradeep fly ash belong to Calsialic group.
2. The RSP slag contains 34.75% of CaO followed by 32.44% of  $\text{SiO}_2$  and 17.06% of  $\text{Al}_2\text{O}_3$ . The present slag has a good hydration property with hydration modulus HM (1.94) greater than 1.4. The CaO/ $\text{SiO}_2$  ratio as  $1.07 > 1.0$  and the  $\text{Al}_2\text{O}_3/\text{SiO}_2$  ratio of 0.52, indicate the suitability of present slag as a pozzolanic and cementitious material.
3. The ferrochrome slag contains about 43% of aluminosilicate compound, 24.99 % of MgO and 19.53% of chromium oxide ( $\text{Cr}_2\text{O}_3$ ) as the major components. The utilization of the present ferrochrome slag is limited due to high MgO and  $\text{Cr}_2\text{O}_3$  content. However, as the CaO/ $\text{SiO}_2$  ratio is  $0.19 < 2.0$ , Cr exist as magnesiochromite spinel phase, which is stable against oxidation and is resistant to dissolution in aqueous media.
4. NALCO fly ash contains quartz ( $\text{SiO}_2$ ), mullite ( $\text{Al}_6\text{Si}_2\text{O}_{13}$ ), and hematite ( $\text{Fe}_2\text{O}_3$ ) as the major compounds. A broad hump in between  $15^\circ$  and  $30^\circ$  with hump position at  $22.5^\circ$  ( $2\theta$ ) indicates the presence of an alumino-silicate type of glassy phase. Though the Paradeep fly ash shows quartz ( $\text{SiO}_2$ ), mullite ( $\text{Al}_6\text{Si}_2\text{O}_{13}$ ), and hematite ( $\text{Fe}_2\text{O}_3$ ) as the major mineral phases, the broad amorphous hump in between  $25^\circ$  to  $35^\circ$  with a peak of the hump  $27^\circ$  shows the presence of both alumino-silicate and calcium- aluminate type of glassy phase.
5. GGBS contains minerals, akermanite ( $\text{Ca}_2\text{Mg} [\text{Si}_2\text{O}_7]$ ), gehlenite ( $\text{Ca}_2\text{Al} [\text{AlSiO}_7]$ ), wagnerite ( $\text{MgFe})_2 \text{PO}_4\text{F}$ , and melilite ( $\text{Ca, Na})_2(\text{Al, Mg, Fe}^{2+}) [( \text{Al, Si) SiO}_7]$ . Wide humps are observed in between  $20^\circ$  and  $40^\circ$ , centred at  $30^\circ$  which confirm the significant amount of amorphous phases.
6. The FS consist of quartz ( $\text{SiO}_2$ ), gismondine ( $\text{CaAl}_2\text{Si}_2\text{O}_8 \cdot 4\text{H}_2\text{O}$ ), gypsum ( $\text{CaSO}_4 \cdot 2\text{H}_2\text{O}$ ), spinel ( $\text{MgAl}_2\text{O}_4$ ), enstatite-ferroan ( $\text{Mg, Fe) SiO}_3$ , fayalite

( $\text{Fe}_2\text{SiO}_4$ ), and Cochromite- syn ( $\text{CoCr}_2\text{O}_4$ ). It shows a wide hump that lies in between  $20^\circ$  and  $35^\circ$  with peak angle  $2\theta$  at  $27^\circ$ . The magnetic part consists of different types of minerals of different shape, colour and transparency with surface chemistry showing the presence of Mg, Si, Al and Ca. The FTIR analysis of the above industrial wastes shows the bonds of the materials as per chemical compound and confirms the presence of the glassy and amorphous phase as observed in XRD analysis.

7. The XRD analysis of coal mine overburden shows, the major minerals present are quartz, kaolinite and calcite and it is denoted as black shale.
8. The NALCO fly ash particles are mostly spherical with a smooth surface known as cenospheres, with particle size varying from 1- 100 $\mu\text{m}$ . The RSP slag shows an angular shape with sharp edges and exhibits an irregular pattern, and ferrochrome slag shows the irregular plate-like structure of different sizes.
9. Based on EDX analysis and optical microscope photograph of magnetically separated FS, bright and glossy surface represent the position of light alkali metals like Mg, Al and Si on the surface of FS particles, which is a good sign of pozzolanic reactivity of FS.
10. The black shale is highly acidic, whereas white and red shale are basic. The variations of EC, TDS and pH is very sensitive to liquid/solid (L/S) ratio for black shale, but the variations for white and red shale is negligible. For the same L/S value, HCFA shows the higher value of EC and TDS than GGBS, JSPL and NALCO fly ash.

### **8.3 General Observations and Concluding Remarks for Characterization of Ferrochrome Slag as a Controlled Low Strength Material**

1. The specific gravity of FS is high (2.90) due to iron and chromium-bearing minerals. Though, FS contains a high amount of MgO (24.99%), based on sodium sulfate soundness test, the percentage loss value comes as 11.89%, which is within the permissible limit (12%).

2. The FS contains 66.25% of oblate, 7.5% equant, 6.25% of prolate and 20% of bladed shaped particles, as obtained using image analyzer, and a linear relationship was obtained between sphericity and void ratio.
3. Based on the comparison of properties of FS with that of Indian standard sand, the FS can be used as an alternate fine aggregate.
4. In CLSM for every mixture, flow is a linear function of water content, and bleeding takes place beyond a limiting water content value. The bleeding value of presently used CLSM varied from 1.55% to 11.75%. The fly ash helps in giving a stable mix and the bleeding decreases with increase in fly ash quantity.
5. The 7 days' strain corresponding to peak stress is varying from 2.78% to 4.91%. The 28 days' strain corresponding to peak stress is varying from 2.18% to 3.37% and the corresponding value after 56 days varies from 3.03% to 3.36%.
6. The UCS of 7 days of curing varies from 0.67 N/mm<sup>2</sup> to 7.53 N/mm<sup>2</sup> and after 56 days of curing the UCS value increased up to 18.32 N/mm<sup>2</sup> with minimum UCS value of 3.79 N/mm<sup>2</sup>. Hence, the developed CLSM can be used in structural and non-excavation applications. The CBR values after 56 days are found to vary from 57.8% to 184.3%, hence can be used for subbase and base course of the pavement. The settlements of the CLSM mixes are 1mm after 56 days.
7. The C-S-H gel is responsible for gain in strength of CLSM mixes as per SEM micrograph.
8. The leachate analysis of CLSM confirmed that the heavy metals are within the limit as per environmental norms. Based on the present investigation on FS, it can be used as an alternate fine aggregate.
9. Development and characterization of CLSM using FS suggests that FS can be used in large quantities in structural fill for infrastructure development. This will conserving the natural resources, reduce the burden on ferrochrome industry by utilizing the wastes and helping in sustainable development, which was one of the objectives of the present study.



## 8.4 General Observations and Concluding Remarks for Characterization of Coal Mine Overburden as a Controlled Low Strength Material

- 1 The water absorption of shale aggregate is higher (8.87%) than permissible limit of 2% and the percentage void of is 37.86%. The impact value, crushing value, abrasion value, flakiness index, elongation index and angularity number of the shale aggregate are found to be 37.13%,36%,56.43%,23.01%,25.63% and 1.71% respectively. Hence, it is not suitable for roads and pavements and is being dumped near the mine.
- 2 The crushing of shale rock resulted in giving both fine and coarse aggregate at the same time, which is termed as all-in-aggregate as per Indian standard. For the CLSM using above aggregate, the spread diameter increases with increase in water content and flow diameter vary from 128mm to 320mm. Hence, it satisfies self-flowing and self-levelling consistency as needed for CLSM. Increase in the finer content of shale and decrease of fly ash content decreased the flowability of CLSM. The bleeding value of the CLSM varied from 0.01% to 3.28% depending upon the cement content and fine content of shale, but all are stable mix (< 5%).
- 3 The fresh density of CLSM is found to be minimum for ScM3S4 is (17.18 kN/m<sup>3</sup>) and maximum for ScM6S1 is (18.92 kN/m<sup>3</sup>). The harden density of the CLSM at 7days and 28 days of ambient curing was found to vary within 14.96kN/m<sup>3</sup> to 16.70kN/m<sup>3</sup> and 15.17kN/m<sup>3</sup> to 14.47kN/m<sup>3</sup> respectively. The low density is due to higher percentage of fly ash and density increased with a decrease in fly ash content.
- 4 The strain corresponding to peak stress (1.02 MPa) is 2.14% and sustained upto 2.67% at 28 days, corresponding to soft to medium clay. Similarly, ScM1S1, at 28 days strain at peak stress (1.71 MPa) is 1.85% and sustained upto 2.36%. Hence, decrease in fly ash content, decreases the ductility, due to spherical shape of the fly ash but the strength increased due to pozzolanic reaction of fly ash.
- 5 The unconfined compressive strength (UCS) of CLSM samples varies from 0.17MPa to 2.44MPa at 7days of curing and 0.58MPa to 2.85MPa after 28 days of curing. The CBR test was conducted on CLSM sample with soaked condition

(7days +4days soaking=11days) vary from 32% to 176%. Hence, the material can be used as structural fill.

- 6 As per SDI value the durability of the developed shale CLSM varies from “medium durability” to “medium high durability”. Leachate analysis shows that leaching of heavy metals of developed shale are within permissible limit. Hence, the developed CLSM is environmentally sustainable.
- 7 Based on the strength, durability and leachate analysis of the developed CLSM using coal mine overburden suggest that, the sustainable material satisfies the strength and durability criteria required for the structural fill and pavement material. This will help in bulk utilization of the mine OB in different infrastructure project, thereby helping in conservation of natural resources and rehabilitation of dumped OB areas.

## **8.5 General Observations and Concluding Remarks for Dispersive Soil and its Stabilization using Biopolymer for Environmental Control**

1. Fly ash and shale are highly dispersive in nature and are susceptible to wind and water erosion. It was observed that the biopolymer treated fly ash and shale sample are not dispersive as per cylinder dispersion test. It was observed that guar gum is more effective in preventing dispersiveness compared to xanthan gum.
2. The water retention capacity of fly ash and shale increased after treatment with the biopolymer. Biopolymer treated fly ash and shale sample shows greater resistance to wind erosion, and it increased with increase in biopolymer concentration.
3. Biopolymer treated fly ash and shale sample shows higher surface strength than the sample saturated with only water. Based on penetration test it was found that xanthan gum treated samples shows better surface strength than guar gum treated sample. The surface strength of cohesive material shale is more than that of non-cohesive material fly ash.
4. The microstructure of treated samples shows that biotreated material shows denser surface structure than normal material due bonding of particles.

5. The present study indicates that biopolymer stabilization can increase the surface strength, enhances the moisture retention capacity and reduces dispersiveness, thereby decreasing the dust erosion and water erosion of the fly ash and shale (mine overburden).
6. It can be observed that the biotreated materials got agglomerated state by application of gum due to bonding between the fly ash or shale particles with the biopolymer and leads to a compact structure. In case of CMC treated sample, a surface coating was observed, which makes it more effective in controlling dispersion.
7. It was observed that CMC treated FA and shale has low MDD and high OMC compared to XG and GG treated geomaterials.
8. The UCS values GG treated shale shows higher strength and higher strain at peak stress compared to XG and CMC treated shale. The failure pattern for CMC and XG treated shale shows that of a well-compacted material, but the sample is dispersed when immersed in water.
9. The leachate analysis of fly ash and biopolymer treated fly ash and shale using AAS showed that the hazardous material leaching is within the limit as permissible. Hence, the developed biopolymer based sustainable material using XG, GG and CMC are effective in controlling water and air erosion of the dispersive geomaterials; fine fraction of coal mine overburden and fly ash.

## **8.6 General Observations and Concluding Remarks for Alkali Activated Material (Geopolymer)**

1. Red shale sample has very high compressive strength at early stages (7 days) 55.85MPa, which gets marginally increased to 59.0 MPa. But, the compressive strength of white shale paste decreased from 55.75 MPa under the ambient condition to 44.95 MPa under alkali and 31.97 MPa under sulphate solution curing condition. But, the compressive strength of red shales is 59.0 Mpa, 49.54MPa and 50.89MPa, under ambient, alkali and sulphate solution curing, respectively.

2. The reduction of GGBS content (from 70 to 50%) in the paste shows a reduction in the strength under ambient and alkali solution for red shale, but no reduction in strength for red shale under sulphate curing condition (50.44) (Figure 7.2). But for black and white shale, there is a substantial reduction in strength with a reduction in GGBS content.
3. Hence, for red shale paste, the replacement of GGBS with fly ash does not vary the compressive strength under water/ambient condition but plays an important role in durability under sulphate curing condition. However, for the black shale replacement of GGBS with fly ash found to be beneficial. It may be mentioned here that the sulphate solution is expected in coal mines overburden (black shale).
4. Under sulphate curing condition the black shale paste with higher fly ash content has got better strength compared to higher GGBS content ( 30.07 MPa vs 25.04 MPa), but for red and white shale paste, marginal difference was observed for replacement of fly ash with GGBS. However, under water curing, condition higher percentage of GGBS gives higher compressive strength. Hence, it is important to choose a particular type of AAM keeping in mind the environment condition around.
5. But for red shale mortar maximum compressive strength (50.8 MPa) was observed under sulphate solution curing condition. Under the ambient condition, the mortar strength for black shale was maximum (53.42 MPa), which reduced to 38.46 MPa under sulphate solution curing condition.
6. It may be mentioned here that with the same shale- GGBS proportion (30:70), with 3 M  $\text{Na}_2\text{SiO}_3$ , the compressive strength under ambient conditions is higher than that with 0.5M  $\text{Na}_2\text{SiO}_3$ . But, under alkali curing condition, the compressive strength increased compared to ambient curing with low molar (0.5M) concentration but decreased with high molar (3.0M) concentration of  $\text{Na}_2\text{SiO}_3$ . Similarly, for shale: GGBS-30:70 with 0.5 moles  $\text{Na}_2\text{SiO}_3$  the compressive strength for red shale are comparable for ambient (16.57 and 27.56 MPa) and alkali solution (17.69 and 24.99 MPa) at 7 and 28 days of curing. But for black shale, the compressive strength under alkali solution (29.72 MPa) is higher than that under ambient condition (15.31 MPa).

7. It was observed that red shale sample with 6M KOH shows the higher strength of 47.29MPa at sulphate condition at 28 days of curing but white and black shale cube shows the relatively low compressive strength of 35.13MPa and 37.56MPa. At 28 days of ambient curing red shale, white shale and black shale shows the compressive strength of 40.44MPa, 39.18MPa and 37.56MPa respectively. Red shale, white shale and black shale paste cube cured under alkali condition at 28 days of curing show the compressive strength of 32.87MPa, 37.11MPa and 35.58MPa respectively. The compressive strength values are less than that with 3 M  $\text{Na}_2\text{SiO}_3$ , it may be mentioned here that the cost of 3 M  $\text{Na}_2\text{SiO}_3$  is higher than that of 6 M KOH.
8. The slake durability tests for shale: GGBS-(30:70) with 3M  $\text{Na}_2\text{SiO}_3$  under ambient condition should red and black shale paste as “very high durable” and white shale paste as “high durable” material. However, under alkali curing condition the black shale paste is “very high durable” and other two pastes are “medium high durable”. A similar trend for durability is observed for the pastes under sulphate solution condition, but with higher SDI values. It was also observed that the compressive strength and SDI values (after two cycles) are correlated and will be discussed later.
9. It is interesting to note that though, the compressive strength values of 0.5M  $\text{Na}_2\text{SiO}_3$  and 6M KOH are comparable, but the shale paste with 0.5M  $\text{Na}_2\text{SiO}_3$  is having higher SDI values than that of 6M KOH.
10. The minerals like ettringite, calcium silicate and calcite are formed for the alkali activated shale- GGBS paste, which is responsible for the development of strength.
11. The JSPL and NALCO fly ash with 2M of NaOH can be used as a CLSM material (0.38 MPa). The sample failure pattern shows that sample is compact with no local failure.
12. The variation of SDI found to in close proximity for Paradeep fly ash (HCFA) with 2M and 4M NaOH sample and all the sample belongs to “medium durability group”.
13. The alkali activated HCFA fly ash also found to be environmentally sustainable as the leachate analysis using AAS shows heavy metals are within permissible

limit. However, other tests like flow, bleeding and density tests have not been conducted to find its suitability as a CLSM.

14. The flow and bleeding of AA FS CLSM shows maximum flow diameter value of 310mm and minimum flow diameter of 180mm. In case of cement based FS CLSM, the flow values were 85mm to 390 mm.
15. The fresh density of alkali activated FS based CLSM is close to the value of cement based CLSM.
16. There is a gain in strength for cement based CLSM with curing days, but the change in strength with cementless alkali activated FS CLSM is marginal.
17. The bleeding values of the alkali activated coal mine overburden samples varies within 0.00% to 1.25%.
18. A linear relationship between the ultrasonic pulse velocity and water absorption of CLSM samples are observed at 7days and 28 days under ambient curing condition. The UCS at 7 days of curing is found to within 0.35MPa to 2.06MPa.
19. Finally based on various slake durability tests on AAM, cement based and cementless alkali activated CLSM a variation of SDI with UCS is shown in Figure 7.48 along with results of natural rocks. It was observed that CLSM samples followed a trend, but the SDI of alkali activated material varied in a wide range for the same UCS values. This is an important aspect to study, particularly, when using the CLSM in a water erodible environment.
20. Leachate analysis of the basic materials is conducted by AAS (Atomic absorption spectroscopy) test through base leaching procedure.
21. Hence, cementless AAM with GGBS and  $\text{Na}_2\text{SiO}_3$  was found to be effective in developing a sustainable geomaterial, which is durable and also can also be used for erosion control of dispersive soil.

## 8.6 Scope of Future Studies

1. The alkali activated cementitious material is not cost effective due to higher cost of activators/chemicals.
2. Hence, the challenge lies in identifying a cost-effective activator, suitability with an industrial waste.

3. The CLSM using locally available material requires suitable machinery for its implementation in the field. The future challenge also lies in identifying suitable admixtures in terms of industrial wastes in improving other properties of the CLSM
4. The use of biopolymer cement for wind and water erosion control needs a pilot study.

The present thesis is an effort in development of sustainable material to conserve the natural resources and ease the burden of industrial wastes. The chief deliverables of the present work include use of coal mine overburden as a CLSM, dust control in mine areas using biopolymer and alkali activated material using mine overburden and mine tailings and are environmentally sustainable. Development of cementless CLSM using alkali activated material, use of coal mine overburden as CLSM and biopolymer cementitious materials for erosion control in mine areas are some of the innovative approach in the chapter. The future challenge lies in identifying suitable industrial wastes as admixtures of CLSM, cost-effective alkali activator activators, and another challenge is development of suitable plants and equipment for implementation of the present work at site.





# REFERENCES

- Abbasi, N., and Nazifi, M. H. (2013). Assessment and modification of sherard chemical method for evaluation of dispersion potential of soils. *Geotechnical and Geological Engineering*, 31(1), 337-346.
- Abedinzadeh, R. (1991). Quantification of particle shape and angularity using the image analyzer. *Geotechnical Testing Journal*, 14(3), 296-308.
- Abelleira, A., Berke, N. S., and Pickering, D. G. (1998). Corrosion activity of steel in cementitious controlled low-strength materials vs. that in soil, in: A.K. Howard, A. K., and Hitch, J. L. (1998, October). The design and application of controlled low-strength materials (flowable fill). STM STP 1331, *American Society for Testing and Materials*.
- ACI 229R-13: (2013). Test methods for controlled low-strength material (CLSM): past, present, and future, in: A.K. Howard, J.L. Hitch (Eds.), The Design and Application of Controlled Low-Strength Materials (Flowable Fill), ASTM STP 1331, *American Society for Testing and Materials*, 1998, 3-10.
- Adam, A. A. (2009). Strength and Durability Properties of Alkali Activated Slag and Fly Ash-Based Geopolymer Concrete. A thesis for the degree of Doctor of Philosophy. School of Civil, Environmental and Chemical Engineering RMIT University Melbourne, Australia.
- Adaska, W. S., and Luhr, D. R. (2004, May). Control of reflective cracking in cement stabilized pavements. *In Proceedings of 5th International RILEM Conference on Cracking in Pavements*, 309-316.
- Alam, S., Das, S. K., and Rao, B. H. (2017). Characterization of coarse fraction of red mud as a civil engineering construction material. *Journal of Cleaner Production*, 168, 679-691.
- Albusoda, B. S., and Salem, L. A. (2012). Stabilization of dune sand by using cement kiln dust (CKD). *Journal of Earth Sciences and Geotechnical Engineering*, 2(1), 131-143.
- Ali, M. B., Saidur, R., and Hossain, M. S. (2011). A review on emission analysis in cement industries. *Renewable and Sustainable Energy Reviews*, 15(5), 2252-2261.
- Aliabdo, A. A., Elmoaty, A. E. M. A., and Salem, H. A. (2016). Effect of cement addition, solution resting time and curing characteristics on fly ash based geopolymer concrete performance. *Construction and building materials*, 123, 581-593.

- 
- Alomayri, T., and Low, I. M. (2013). Synthesis and characterization of mechanical properties in cotton fiber-reinforced geopolymer composites. *Journal of Asian Ceramic Societies*, 1(1), 30-34.
- Antoni, W. D., Vianthi, A., Putra, P., Kartadinata, G., and Hardjito, D. (2015). Effect of particle size on properties of sidoarjo mud-based geopolymer. *In Materials Science Forum Trans Tech Publications*, 803, 44-48.
- ASTM C597 (2016). Standard test method for pulse velocity through concrete. West Conshohocken, PA.
- ASTM C618 – 15 (2015). Standard specification for coal fly ash and raw or calcined natural pozzolan for use in concrete. *American Society for Testing material*, /.
- ASTM C642 (2016). Standard test method for density, absorption, and voids in hardened concrete. West Conshohocken, PA.
- ASTM C88-13 (2013). Standard Test Method for Soundness of Aggregates by Use of Sodium Sulfate or Magnesium Sulfate, *ASTM International*, West Conshohocken, PA.
- ASTM D 422- 63 (2007). Standard Test Method for Particle-Size Analysis of Soils. *ASTM International*, West Conshohocken, PA.
- ASTM D1557-12e1. (2012). Standard Test Methods for Laboratory Compaction Characteristics of Soil Using Modified Effort (56,000 ft-lbf/ft<sup>3</sup> (2,700 kN-m/m<sup>3</sup>)). *ASTM International*, West Conshohocken, PA.
- ASTM D2487-11. (2011). Standard Practice for Classification of Soils for Engineering Purposes (Unified Soil Classification System). *ASTM International*, West Conshohocken, PA.
- ASTM D4318-10e1. (2010). Standard Test Methods for Liquid Limit, Plastic Limit, and Plasticity Index of Soils. *ASTM International*, West Conshohocken, PA.
- ASTM D4647.(2013). Standard Test Methods for Identification and Classification of Dispersive Clay Soils by the Pinhole Test. *ASTM International*, West Conshohocken, PA.
- ASTM D854-14. (2014). Standard Test Methods for Specific Gravity of Soil Solids by Water Pycnometer. *ASTM International*, West Conshohocken, PA.
- Atkinson, J. H., Charles, J. A., and Mhach, H. K. (1990). Examination of erosion resistance of clays in embankment dams. *Quarterly Journal of Engineering Geology and Hydrogeology*, 23(2), 103-108.
- Badanoiu, A. I., Al Saadi, T. H. A., Stoleriu, S., and Voicu, G. (2015). Preparation and characterization of foamed geopolymers from waste glass and red mud. *Construction and Building Materials*, 84, 284-293.

- Bakharev, T. (2005). Durability of geopolymer materials in sodium and magnesium sulfate solutions. *Cement and Concrete Research*, 35(6), 1233-1246.
- Barbosa, V. F., MacKenzie, K. J., and Thaumaturgo, C. (2000). Synthesis and characterisation of materials based on inorganic polymers of alumina and silica: sodium polysialate polymers. *International Journal of Inorganic Materials*, 2(4), 309-317.
- Bell, F. G. (2007). *Engineering Geology*. Butterworth-Heinemann, UK.
- Bernal, S. A., Rodríguez, E. D., de Gutiérrez, R. M., Provis, J. L., and Delvasto, S. (2012). Activation of metakaolin/slag blends using alkaline solutions based on chemically modified silica fume and rice husk ash. *Waste and Biomass Valorization*, 3(1), 99-108.
- Bernal, S., De Gutierrez, R., Delvasto, S., and Rodriguez, E. (2010). Performance of an alkali-activated slag concrete reinforced with steel fibers. *Construction and Building Materials*, 24(2), 208-214.
- Bhuvaneshwari, S., Soundra, B., Robinson, R. G., and Gandhi, S. R. (2007). Stabilization and microstructural modification of dispersive clayey soils. In *Proceedings of the First International Conference on Soil and Rock Engineering*, Srilankan Geotechnical Society, Colombo, Sri Lanka (pp. 1-7).
- Bigozzi, M. C., Manzi, S., Natali, M. E., Rickard, W. D., and Van Riessen, A. (2014). Room temperature alkali activation of fly ash: The effect of Na<sub>2</sub>O/SiO<sub>2</sub> ratio. *Construction and Building Materials*, 69, 262-270.
- Bouzalakos, S., Dudeney, A. W. L., and Chan, B. K. C. (2013). Formulating and optimising the compressive strength of controlled low-strength materials containing mine tailings by mixture design and response surface methods. *Minerals Engineering*, 53, 48-56.
- Brinkley, D., and Mueller, P. E. (1998). Ten-year performance record of non-shrink slurry backfill. In *The Design and Application of Controlled Low-Strength Materials (Flowable Fill)*. ASTM International.
- BSI (1990). BS 1377: 1990-Methods of Test for Soils for Civil Engineering Purposes. British Standards Institute, Milton Keynes.
- Butalia, T. S., Wolfe, W. E., Zand, B., and Lee, J. W. (2004). Flowable fill using flue gas desulfurization material, in: J.L Hitch, A.K. Howard, W.P. Bass, (Eds.), *Innovations in Controlled Low-strength Material (Flowable fill)*, ASTM STP 1459, American Society for Testing and Materials, 3-14.
- Cabrera-Real, H., Romero-Serrano, A., Zeifert, B., Hernandez-Ramirez, A., Hallen-Lopez, M., and Cruz-Ramirez, A. (2012). Effect of MgO and CaO/SiO<sub>2</sub> on the immobilization of

- chromium in synthetic slags. *Journal of Material Cycles and Waste Management*, 14(4), 317-324.
- Cerato, A.B., Lutenegeger, A.J., (2002). Determination of surface area of fine-grained soils by the ethylene glycol monoethyl ether (EGME) method. *Geotech. Test. J.*, 25(3), 315-321.
- Chen, H., and Wang, Q. (2006). The behaviour of organic matter in the process of soft soil stabilization using cement. *Bulletin of Engineering Geology and the Environment*, 65(4), 445-448.
- Chen, R., Zhang, L., and Budhu, M. (2013). Biopolymer stabilization of mine tailings. *Journal of geotechnical and geoenvironmental engineering*, 139(10), 1802-1807.
- Chen, R., Lee, I., and Zhang, L. (2015). Biopolymer stabilization of mine tailings for dust control. *Journal of Geotechnical and Geoenvironmental Engineering*, 141(2), 04014100.
- Cheng, T. W., and Chiu, J. P. (2003). Fire-resistant geopolymer produced by granulated blast furnace slag. *Minerals engineering*, 16(3), 205-210.
- Chi, M. (2012). Effects of dosage of alkali-activated solution and curing conditions on the properties and durability of alkali-activated slag concrete. *Construction and Building Materials*, 35, 240-245.
- Chi, M., and Huang, R. (2013). Binding mechanism and properties of alkali-activated fly ash/slag mortars. *Construction and Building Materials*, 40, 291-298.
- Coates, J. (2000). Interpretation of infrared spectra, a practical approach. *Encyclopedia of analytical chemistry*, 12, 10815-10837.
- Collins, F. G., and Sanjayan, J. G. (1999). Workability and mechanical properties of alkali activated slag concrete. *Cement and Concrete Research*, 29, 455-458.
- Cortes, D. D., Kim, H. K., Palomino, A. M., and Santamarina, J. C. (2008). Rheological and mechanical properties of mortars prepared with natural and manufactured sands. *Cement and Concrete Research*, 38(10), 1142-1147.
- Criado, M., A. F. Jiménez, I. Sobrados, A. Palomo and J. Sanz (2012). Effect of relative humidity on the reaction products of alkali activated fly ash. *Journal of the European Ceramic Society* 32, 2799-2807.
- Criado, M., Bastidas, D. M., Fajardo, S., Fernández-Jiménez, A. and Bastidas, J. M. (2011). *Cement and Concrete Composites*, 33, 644-652.

- Criado, M., Fernández-jiménez, A. and Palomo, A. (2007). Alkali activation of fly ash: Effect of SiO<sub>2</sub>/Na<sub>2</sub>O ratio: Part I, FTIR study. *Microporous and Mesoporous Materials*, 106, 180-191.
- Criado, M., Fernández-Jiménez, A., and Palomo, A. (2010). Alkali activation of fly ash. Part III: Effect of curing conditions on reaction and its graphical description. *Fuel*, 89, 3185-3192.
- Criado, M., Fernández-Jiménez, A., Palomo, A., Sobrados, I., and Sanz, J. (2008). Effect of the SiO<sub>2</sub>/Na<sub>2</sub>O ratio on the alkali activation of fly ash. Part II: <sup>29</sup>Si MAS-NMR Survey. *Microporous and Mesoporous Materials*, 109, 525-534.
- Criado, M., Palomo, A., and Fernández-jiménez, A. (2005). Alkali activation of fly ashes. Part 1: Effect of curing conditions on the carbonation of the reaction products. *Fuel*, 84, 2048–2054.
- Crouch, L. K., Dotson, V. J., Badoe, D. A., Maxwell, R. A., Dunn, T. R., and Sparkman, A. (2004). Long term study of 23 excavatable Tennessee flowable fill mixtures. *Journal of ASTM International*, 1(6), 1-11.
- Das S.K., and Yudhbir. (2006). A simplified model for prediction of pozzolanic characteristics of fly ash, based on chemical composition. *Cement and Concrete Research*, 36(10), 1827-1832.
- Das, S. K., and Yudhbir. (2005). Geotechnical characterization of some Indian fly ashes. *Journal of materials in civil engineering*, 17(5), 544-552.
- Das, S. K., Mahamaya, M., Panda, I., and Swain, K. (2015). Stabilization of pond ash using biopolymer. *Procedia Earth and Planetary Science*, 11, 254-259.
- Davidovits, J. (2005). Geopolymer, Green Chemistry and Sustainable Development Solution, Geopolymer Institute Géopolymère, 16 rue Galilée, F-02100 Saint-Quentin, France.
- DeJong, J. T., Fritzges, M. B., and Nüsslein, K. (2006). Microbially Induced Cementation to Control Sand Response to Undrained Shear. *Journal of Geotechnical and Geoenvironmental Engineering*, 132(11), 1381–1392.
- DeJong, J. T., Mortensen, B. M., Martinez, B. C., and Nelson, D. C. (2010). Bio-mediated soil improvement. *Ecological Engineering*, 36(2), 197-210.
- Derrick, MR, Stulik D, Landry JM (1995). Scientific tools for conservation. *Infrared spectroscopy in conservation science*. The United States of America.
- Diamond, S. (1982). The Characterization of Fly Ashes, in Proc. Symposium N, Effects of Fly Ash Incorporation in Cement and Concrete, Boston, Ed., S. Diamond, 12-23; Mater.

- Res. Soc., University Park, PA (1982). *The Utilization of Fly Ash, Cem. Concr. Res.*, 14(4), 455-462 (1984).
- Dingrando, J. S., Edil, T. B., and Benson, C. H. (2004). Beneficial reuse of foundry sands in controlled low strength material, in: J.L Hitch, A.K. Howard, W.P. Bass, (Eds.), *Innovations in controlled low-strength material (Flowable fill)*, ASTM STP 1459, *American Society for Testing and Materials*, 15-30.
- Dockter, B. A. (1998). Comparison of dry scrubber and class c fly ash in controlled lowstrength materials (CLSM) applications, in: A.K. Howard, J.L. Hitch (Eds.), *The Design and Application of Controlled Low-Strength Materials (Flowable Fill)*, ASTM STP 1331, *American Society for Testing and Materials*, 13-26.
- Duxson, P., and Provis J. L. (2008). Designing Precursors for Geopolymer Cements. *Journal of the American Ceramic Society*, 91(12), 3864-3869.
- Duxson, P., Fernández-Jiménez, A., Provis, J. L., Lukey, G. C., Palomo, A. and Deventer, J. S. J. van. (2007b). Geopolymer technology: the current state of the art. *Journal of Material Science*, 42, 2917-2933.
- Duxson, P., Lukey, G. C., Separovic, F., and Van Deventer, J. S. J. (2005). Effect of alkali cations on aluminum incorporation in geopolymeric gels. *Industrial and Engineering Chemistry Research*, 44(4), 832-839.
- Duxson, P., Provis, J. L., Lukey, G. C., Deventer, J. S. J. van. (2007a). The role of inorganic polymer technology in the development of ‘green concrete’. *Cement and Concrete Research*, 37, 1590-1597.
- Elibol, C. and Sengul, O. (2016). Effects of Activator Properties and Ferrochrome Slag Aggregates on the Properties of alkali-activated Blast Furnace Slag Mortars. *Arabian Journal for Science and Engineering*, 41, 1561-1571.
- Fay, L., Cooper, P., and de Morais, H. F. (2014). Innovative interlocked soil–cement block for the construction of masonry to eliminate the settling mortar. *Construction and Building Materials*, 52, 391-395.
- Fernández-Jiménez, A. and Palomo, A. (2003). Characterisation of fly ashes. Potential reactivity as alkaline cements. *Fuel*, 82, 2259-2265.
- Fernandez-Jimenez, A., and Palomo, A. (2005). Composition and microstructure of alkali activated fly ash binder: Effect of the activator. *Cement and Concrete Research*, 35, 1984 - 1992.

- Fernández-Jiménez, A., Palomo, A., and Criado, M. (2005). Microstructure development of alkali-activated fly ash cement: a descriptive model. *Cement and Concrete Research*, 35, 1204–1209.
- Fernández-jiménez, A., Palomo, J. G., Puertas, F. (1999). Alkali-activated slag mortars Mechanical strength behavior. *Cement and Concrete Research*, 29, 1313–1321.
- Folliard, K. J., Du, L., Trejo, D., Halmen, C., Sabol, S., and Leshchinsky, D. (2008). Development of a recommended practice for use of controlled low-strength material in highway construction. *NCHRP Report 597*. Transportation Research Board, Washington, D.C.
- Franklin, J. A. (1981). A shale rating system and tentative applications to shale performance. *Transportation Research Record*, 790(3), 2-12.
- Gabr, M. A., and Bowders, J. J. (2000). Controlled low-strength material using fly ash and AMD sludge. *Journal of Hazardous Materials*, 76(2-3), 251-263.
- Gao, X., Yu, Q. L. and Brouwers, H. J. H. (2015b). Properties of alkali activated slag–fly ash blends with limestone addition. *Cement and Concrete Composites*, 59, 119–128.
- Gao, X., Yu, Q. L., and Brouwers, H. J. H. (2015a). Reaction kinetics, gel character and strength of ambient temperature cured alkali activated slag–fly ash blends. *Construction and Building Materials*, 80, 105-115.
- Garnayak, L. (2017). Development and characterization of alkali- activated red mud- slag cementitious material. *Ph.D Thesis submitted to National Institute of Technology, Rourkela, India*.
- Ghataora, G. S., and Alobaidi, I. M. (2000). Assessment of the performance of trial trenches backfilled with cementitious materials. *International Journal of Pavement Engineering*, 1(4), 297-316.
- Goncalves, J. P., Tavares, L. M., Filho, R. D. T., Fairbairn, E. M. R., Cunha, E. R. (2007). Comparison of natural and manufactured fine aggregates in cement mortars. *Cem. Concr. Res.* 37, 924-932.
- Gong, C., and Yang, N. (2000). Effect of phosphate on the hydration of alkali-activated red mud–slag cementitious material. *Cement and Concrete Research*, 30(7), 1013-1016.
- Goodarzi, A. R., and Salimi, M. (2015). Stabilization treatment of a dispersive clayey soil using granulated blast furnace slag and basic oxygen furnace slag. *Applied Clay Science*, 108, 61-69.

- Görhan, G., and Kürklü, G. (2014). The influence of the NaOH solution on the properties of the fly ash-based geopolymer mortar cured at different temperatures. *Composites: Part B*, 58, 371-377.
- Guerrieri, M., Sanjayan, J., and Collins, F. (2010). Residual strength properties of sodium silicate alkali activated slag paste exposed to elevated temperatures. *Materials and Structures*, 43, 765-773.
- Hafid, K. El, Hajjaji, M., and Hafid, H. El. (2017). Influence of NaOH concentration on microstructure and properties of cured alkali-activated calcined clay. *Journal of Building Engineering*, 11, 158–165.
- Halmen, C., Trejo, D., Folliard, K. J., and Du, L. (2005). Corrosion of metallic pipe in controlled low-strength materials—Parts 3, *ACI Mater. J.*, 102 (6), 429-437.
- Halmen, C., Trejo, D., Folliard, K. J., and Du, L. (2006). Corrosion of metallic pipe in controlled low-strength materials—Parts 4, *ACI Mater. J.*, 103 (1), 53-59.
- He, J., Chu, J., and Ivanov, V. (2013). Mitigation of liquefaction of saturated sand using biogas. *Géotechnique*, 63(4), 267-275.
- He, J., Zhang, J., Yu, Y. and Zhang, G. (2012). The strength and microstructure of two geopolymers derived from metakaolin and red mud-fly ash admixture: A comparative study. *Construction and Building Materials*, 30, 80-91.
- Inyang, H. I., Bae, S., Mbamalu, G. and Park, S. (2007). Aqueous Polymer Effects on Volumetric Swelling of Na-Montmorillonite. *J. Mater. Civ. Eng.*, 19(1), 84-90.
- Ivanov, V., and Chu, J. (2008). Applications of microorganisms to geotechnical engineering for biocloguar guming and biocementation of soil in situ. *Rev Environ Sci Biotechnol*, 7, 139.
- Jaarsveld, J. G. S. van, Deventer, J. S. J. van, Lukey, G. C. (2003). The characterization of source materials in fly ash-based geopolymers. *Materials Letters*, 57, 1272-1280.
- Jayanthi, P. N. V. and Singh, D.N. (2016). Utilization of Sustainable Materials for Soil Stabilization: State-of-the-art. *Advances in Civil Engineering Materials, ASTM*, 5(1), 46-79.
- Joshi, S. V. and Kadu, M. S. (2012). Role of Alkaline Activator in Development of Eco-friendly Fly Ash Based Geo Polymer Concrete. *International Journal of Environmental Science and Development*, 3(5), 417-421.
- Kalkan, E. (2009). Influence of silica fume on the desiccation cracks of compacted clayey soils. *Applied clay science*, 43(3-4), 296-302.



- Kaneshiro, J., Navin, S., Wendel, L., and Snowden, H. (2001). Controlled low strength material for pipeline backfill—Specifications, case histories and lessons learned. In *Pipelines 2001: Advances in Pipelines Engineering and Construction*, 1-13.
- Karakoç, M. B., Türkmen, İ., Maraş, M. M., Kantarci, F., and Demirboğa, R. (2016). Sulfate resistance of ferrochrome slag based geopolymer concrete. *Ceramics International*, 42(1), 1254-1260.
- Karakoç, M. B., Türkmen, İ., Maraş, M. M., Kantarci, F., Demirboğa, R., Toprak, M. U. (2014). Mechanical properties and setting time of ferrochrome slag based geopolymer paste and mortar. *Construction and Building Materials*, 72, 283-292.
- Karakurt, C. and Topçu, İ. B. (2012). Effect of blended cement with natural zeolite and industrial by-products on rebar corrosion and high-temperature resistance of concrete. *Construction and Building Materials*, 35, 906–911.
- Karimi, S. (1998). A study of geotechnical applications of biopolymer treated soils with an emphasis on silt. *Ph.D. dissertation*, Univ. of Southern California, Los Angeles.
- Kavazanjian, E. Jr, Iglesias, E. and Karatas, I. (2009). Biopolymer soil stabilization for wind erosion control. Proc. 17th Int. Conf. Soil Mech. *Geotech. Engng, Alexandria*, 2, 881-884.
- Kazemian, A., Gholizadeh V. A., and Rajabipour, F. (2015). Quantitative assessment of parameters that affect strength development in alkali activated fly ash binders. *Construction and Building Materials*, 93, 869-876.
- Ken, P. W., Ramli, M., and Ban, C. C. (2015). An overview on the influence of various factors on the properties of geopolymer concrete derived from industrial by-products. *Construction and Building Materials*, 77, 370-395.
- Khale, D., and Chaudhary, R. (2007). Mechanism of geopolymerization and factors influencing its development: a review. *Journal of Materials Sciences*, 42, 729-746.
- Khatami, H. R., and O’Kelly, B. C. (2013). Improving mechanical properties of sand using biopolymers. *J. Geotech. Geoenviron. Eng.*, 1402-1406.
- Kilau, H. W., and Shah, I. D. (1984, January). Chromium-bearing waste slag: evaluation of leachability when exposed to simulated acid precipitation. In *Hazardous and Industrial Waste Management and Testing: Third Symposium*. ASTM International.
- Kolay, P. K., and Singh D. N. (2001). Physical, chemical, mineralogical, and thermal properties of cenospheres from an ash lagoon. *Cement and Concrete Research*, 31, 539-542.

- 
- Komnitsas, K., and Zaharaki, D. (2007). Geopolymerisation: A review and prospects for the minerals Industry. *Journal of Minerals Engineering*, 20, 1261-1277.
- Koshy, N. and Singh, D.N. (2016). Textural alterations in coal fly ash due to alkali activation. *Journal of Materials in Civil Engineering*, 28 (11), 04016126.
- Kosmulski, M., Gustafsson, J., and Rosenholm, J. B. (1999). Correlation between the zeta potential and rheological properties of anatase dispersions. *Journal of colloid and interface science*, 209(1), 200-206.
- Kovalchuk, G., Fernández-Jiménez, A., and Palomo, A. (2007). Alkali-activated fly ash: Effect of thermal curing conditions on mechanical and microstructural development – Part II. *Fuel*, 86, 315-322.
- Kuhn, Behmenburg., Capodilupo, and Romera, Q., (2000). Report on Decreasing the scorification of chrome. ECSC steel publications, Brussels.
- Kumar, G., Cecchin, I., Thomé, A., and Reddy, K.R. (2016). Failure of coal ash containment facilities: Causes, impacts, remediation, and lessons earned. *Proceedings of 5th International Conference on Forensic Geotechnical Engineering, Indian Institute of Science, Bangalore, India, December 8-10*, 145-156.
- Kumar, R., Kumar, S., Badjena, S., and Mehrotra, S. P. (2005). Hydration of mechanically activated granulated blast furnace slag. *Metallurgical and Materials Transactions B*, 36(6), 873-883.
- Kuo, W. T., Wang, H. Y., Shu, C. Y., and Su, D. S. (2013). Engineering properties of controlled low-strength materials containing waste oyster shells. *Construction and Building Materials*, 46, 128-133.
- Lachemi, M., Hossain, K. M. A., Shehata, M., and Thaha, W. (2008). Controlled low strength materials incorporating cement kiln dust from various sources. *Cement and Concrete Composites*, 30(5), 381-392.
- Landa, V. R., and Santamarina, J. C. (2012). Mechanical Effects of Biogenic Nitrogen Gas Bubbles in Soils. *Journal of Geotechnical and Geoenvironmental Engineering*, 138(2), 128-137.
- Lemougna, P. N., Melo. U. F. C., Delplancke, M. P., Rahier, H. (2014). Influence of the chemical and mineralogical composition on the reactivity of volcanic ashes during alkali activation. *Ceramics International*, 40(1), 811-820.
- Lovell, C. W. (1983). Standard laboratory testing for compacted shales. *Proc., ISRM International Congress on Rock Mechanics*, 1, 197-202.

- Lovley, D. R. (1995). Bioremediation of organic and metal contaminants with dissimilatory metal reduction. *Journal of Industrial Microbiology*, 14(2), 85–93.
- Mahamaya, M., and Das, S. K. (2017). Characterization of mine overburden and fly ash as a stabilized pavement material. *Particulate Science and Technology*, 35(6), 660-666.
- Marrero, J., Polla, G., Rebagliati, R. J., Plá, R., Gómez, D., and Smichowski, P. (2007). Characterization and determination of 28 elements in fly ashes collected in a thermal power plant in Argentina using different instrumental techniques. *Spectrochimica Acta Part B*, 62, 101-108.
- Martin, G. R., Yen, T. F., and Karimi, S. (1996). Application of biopolymer technology in silty soil matrices to form impervious barriers. Proc., 7<sup>th</sup> *Australia-New Zealand Geomechanics Conf.*, Institution of Engineers, Barton, Australia, 814-819.
- Morales, L., Romero, E., Jommi, C., Garzón, E., and Giménez, A. (2014). Feasibility of a soft biological improvement of natural soils used in compacted linear earth construction. *Acta Geotechnica*, 10(1), 157–171.
- Mužek, M. N., Zelić, J. and Jozić, D. (2012). Microstructural Characteristics of Geopolymers Based on Alkali-Activated Fly Ash. *Chem. Biochemical Engineering*. 26 (2), 89-95
- Naganathan, S., Razak, H. A., and Hamid, S. N. A. (2010). Effect of kaolin addition on the performance of controlled low-strength material using industrial waste incineration bottom ash. *Waste Management and Research*, 28(9), 848-860.
- Naganathan, S., Razak, H. A., and Hamid, S. N. A. (2013). Corrosivity and leaching behavior of controlled low-strength material (CLSM) made using bottom ash and quarry dust. *Journal of environmental management*, 128, 637-641.
- Nägele, E., and Schneider, U. (1989). The zeta-potential of blast furnace slag and fly ash. *Cement and Concrete Research*, 19(5), 811-820.
- Nägele, E., and Schneider, U. (1989). The zeta-potential of blast furnace slag and fly ash. *Cement and Concrete Research*, 19(5), 811-820.
- Naik, T. R., and Singh, S. S. (1997). Flowable slurry containing foundry sands. *Journal of Materials in Civil Engineering*, 9(2), 93-102.
- Naik, T. R., Kraus, R. N., and Siddique, R. (2003). Controlled low-strength materials containing mixtures of coal ash and new pozzolanic material. *Materials Journal*, 100(3), 208-215.

- Naik, T. R., Kraus, R. N., Ramme, B. W., Chun, Y. M., and Kumar, R. (2006). High-carbon fly ash in manufacturing conductive CLSM and concrete. *Journal of materials in civil engineering*, 18(6), 743-746.
- Naik, T. R., Kraus, R. N., Siddique, R., and Chun, Y. M. (2004). Properties of controlled lowstrength materials made with wood fly ash, in: J.L Hitch, A.K. Howard, W.P. Bass, (Eds.), *Innovations in controlled low-strength material (Flowable fill)*, ASTM STP 1459, American Society for Testing and Materials, 31–40.
- Naik, T. R., Singh, S. S., and Ramme, B. W. (2001). Performance and leaching assessment of flowable slurry. *Journal of Environmental Engineering*, 127(4), 359-368.
- Natarajan, K. A. (2008). Microbial aspects of acid mine drainage and its bioremediation. *Transactions of Nonferrous Metals Society of China*, 18(6), 1352-1360.
- Nataraja, M. C., and Nalanda, Y. (2009). Performance of industrial by-products in controlled low-strength materials (CLSM). *Waste management*, 28(7), 1168-1181.
- Nath, S. K., Maitra, S., Mukherjee, S., and Kumar, S. (2016). Microstructural and morphological evolution of fly ash based geopolymers. *Construction and Building Materials*, 111, 758-765.
- Niemelä, P., and Kauppi, M. (2007). Production, characteristics and use of ferrochromium slags. *In Proceedings of the 11th International Ferro Alloys Conference*, 171-179.
- Oh, J. E., Monteiro, P. J., Jun, S. S., Choi, S., and Clark, S. M. (2010). The evolution of strength and crystalline phases for alkali-activated ground blast furnace slag and fly ash-based geopolymers. *Cement and Concrete Research*, 40(2), 189-196.
- Özbay, E., Erdemir, M., and Durmuş, H. İ. (2016). Utilization and efficiency of ground granulated blast furnace slag on concrete properties - A review. *Construction and Building Materials*, 105, 423–434.
- Pacheco-Torgal, F., Abdollahnejad, Z., Camões, A. F., Jamshidi, M., Ding, Y. (2012). Durability of alkali-activated binders: A clear advantage over Portland cement or an unproven issue. *Construction and Building Materials*, 30, 400-405.
- Pacheco-Torgal, F., Castro-Gomes, J., and Jalali, S. (2008a). Alkali-activated binders: A review Part 1. Historical background, terminology, reaction mechanisms and hydration products. *Construction and Building Materials*, 22 (7), 1305-1314.
- Pacheco-Torgal, F., Castro-Gomes, J. and Jalali, S. (2008b). Alkali-activated binders: A review. Part 2. About materials and binders manufacture. *Construction and Building Materials*, 22, 1315-1322.

- Padmakumar, G. P., Srinivas, K., Uday, K. V., Iyer, K. R., Pathak, P., Keshava, S. M., and Singh, D. N. (2012). Characterization of aeolian sands from Indian desert. *Engineering geology*, 139, 38-49.
- Palomo, A., Grutzeck, M. W. and Blanco, M. T. (1999). Alkali-activated fly ashes A cement for the future. *Cement and Concrete Research*, 29, 1323-1329.
- Panda, C. R., Mishra, K. K., Panda, K. C., Nayak, B. D., and Nayak, B. B. (2013). Environmental and technical assessment of ferrochrome slag as concrete aggregate material. *Construction and Building Materials*, 49, 262-271.
- Panda, I., Jain, S., Das, S. K., and Jayabalan, R. (2017). Characterization of red mud as a structural fill and embankment material using bioremediation. *International Biodeterioration and Biodegradation*, 119, 368-376.
- Papadakis, V. G. (2000). Effect of fly ash on Portland cement systems, Part II: High calcium fly ash. *Cement and Concrete Research*, 30, 1647-1654.
- Parmar, D., and Steinmanis, J. (2003). Underground cables need a proper burial. *TandD World Magazine*, Geotherm Inc. Apr. 1, 2003, <http://tdworld.com/underground-tamp/underground-cables-need-proper-burial> accessed on 23 May, 2017.
- Phair, J. W. and Van Deventer, J. S. J. (2001). Effect of silicate activator pH on the leaching and material characteristics of waste-based inorganic polymers. *Journal of Mineral Engineering*. 14(3), 289-304.
- Phoon, K. K., Kulhawy, F. H., and Grigori, M. D. (1995). Reliability based design of foundations for transmission line structures. Rep. TR-105000, *Electric Power Research Institute*, Palo Alto, Calif.
- Phoo-Ngernkham, T., Maegawa, A., Mishima, N., Hatanaka, S., and Chindaprasirt, P. (2015). Effects of sodium hydroxide and sodium silicate solutions on compressive and shear bond strengths of FA-GBFS geopolymer. *Construction and Building Materials*, 91, 1-8.
- Pierce, C. E., and Blackwell, M. C. (2003). Potential of scrap tire rubber as lightweight aggregate in flowable fill. *Waste Management*, 23(3), 197-208.
- Provis, J. L. and Deventer, J. S. J. van. (2014). Alkali activated materials. *RILEM State-of-the-Art Reports. RILEM TC 224-AAM*, 13, 1-388.
- Provis, J. L., and Deventer, J. S. J. van. (2009). Geopolymers. Structure, processing, properties and industrial applications. *Woodhead publishing limited*. Oxford Cambridge New Delhi, 1- 441.

- Puertas, F., Martínez-Ramírez, S., Alonso, S., and Vázquez, T. (2000). Alkali-activated fly ash/ slag cement Strength behavior and hydration products. *Cement and Concrete Research*, 30, 1625-1632.
- Raghavendra, T., and Udayashankar, B. C. (2014). Flow and strength characteristics of CLSM using ground granulated blast furnace slag. *Journal of Materials in Civil Engineering*, 26(9), 04014050.
- Rahier, H., Denayer, J. F., van Mele, B. (2003). Low-temperature synthesized aluminosilicate glasses. Part IV. Modulated DSC study on the effect of particle size of metakaolinite on the production of inorganic polymer glasses. *Journal of Materials Science*, 38, 3131–3136.
- Rai A.K., Paul B. and Singh G. (2011). A study on physico chemical properties of overburden dump materials from selected coal mining areas of Jharia coalfields, Jharkhand, India. *Int. Journal of Environmental Sc.*, 1, 1350-1360.
- Rajasekaran, G. (2005). Sulphate attack and ettringite formation in the lime and cement stabilized marine clays. *Ocean Engineering*, 32(8-9), 1133-1159.
- Rajasekaran, G. (2005). Sulphate attack and ettringite formation in the lime and cement stabilized marine clays. *Ocean Engineering*, 32(8-9), 1133-1159.
- Rashad, A. M. (2014). A comprehensive overview about the influence of different admixtures and additives on the properties of alkali-activated fly ash. *Materials and Design*, 53, 1005-1025.
- Razak, H. A., Naganathan, S., and Hamid, S. N. A. (2009). Performance appraisal of industrial waste incineration bottom ash as controlled low-strength material. *Journal of Hazardous Materials*, 172(2-3), 862-867.
- Rees, C. A., Provis, J. L., Lukey, G. C., and Deventer, J. S. J. van. (2007). In Situ ATR-FTIR Study of the Early Stages of Fly Ash Geopolymer Gel Formation. *Langmuir*, 23, 9076-9082.
- Rice, M. A., Willetts, B. B., and McEwan, I. K. (1996). Wind erosion of crusted soil sediments. *Earth Surf. Processes Landforms*, 21(3), 279– 293.
- Sahu, N., Biswas, A., and Kapure, G. U. (2016). A Short Review on Utilization of Ferrochromium Slag. *Mineral Processing and Extractive Metallurgy Review*, 37(4), 211-219.
- Saraswathy, V., Muralidharan, S., Thangavel, K., and Srinivasan, S. (2003). Influence of activated fly ash on corrosion-resistance and strength of concrete. *Cement and Concrete Composites*, 25(7), 673–680.

- Saraswathy, V., Muralidharan, S., Thangavel, K., and Srinivasan, S. (2003). Influence of activated fly ash on corrosion-resistance and strength of concrete. *Cement and Concrete Composites*, 25(7), 673–680.
- Sathwik, S. R., Sanjith, J., and Sudhakar, G. N. (2016). Development of high-strength concrete using ferrochrome slag aggregate as replacement to coarse aggregate. *American Journal of Engineering Research (AJER)*, 5, 83-87.
- Schneider, M., Romer, M., Tschudin, M., and Bolio, H. (2011). Sustainable cement production-present and future. *Cement and Concrete Research*, 41, 642–650.
- Schwerdtfeger, W. J., and Romanoff, M. (1972). National Bureau of Standards Papers on Underground Corrosion of Steel Piping 1962-1971. *US Department of Commerce, National Bureau of Standards Monograph*, 127.
- Scola, A. A., and Alto, P. (2009). Method of manufacture and installation flowable thermal backfills. United States Patent, Patent No.: US 7,581,903 B1. Date of Patent: 1 September 2009.
- Sheen, Y. N., Huang, L. J., Wang, H. Y., and Le, D. H. (2014). Experimental study and strength formulation of soil-based controlled low-strength material containing stainless steel reducing slag. *Construction and Building Materials*, 54, 1-9.
- Siddique, R. (2009). Utilization of waste materials and by-products in producing controlled low-strength materials. *Resources, conservation and recycling*, 54(1), 1-8.
- Singh, B., Ishwarya, G., Gupta, M., and Bhattacharyya, S. K. (2015). Geopolymer concrete: A review of some recent developments. *Construction and Building Materials*, 85, 78-90.
- Song, H. W., and Saraswathy, V. (2006). Studies on the corrosion resistance of reinforced steel in concrete with ground granulated blast-furnace slag-an overview. *Journal of Hazardous Materials B*, 138, 226–233.
- Sridharan, A., and Prakash, K. M. (2007). *Geotechnical engineering characterisation of coal ashes*. CBS Publishers and Distributors.
- Sunku, J. (2006, November). Advantages of using fly ash as supplementary cementing material (SCM) in fibre cement sheets. In Proceedings of 10th International Inorganic-bonded Fiber Composites Conference (pp. 25-32).
- T.-C. Ling et al. (2018). *Construction and Building Materials* 158, 535–548 547.
- Talling, B., and Brandstetr, J. (1989). Present state and future of alkali-activated slag concretes. *Special Publication*, 114, 1519-1546.

- Tchakoute, H. K., Elimbi, A., Yanne, E., and Djangang, C. N. (2013). Utilization of volcanic ashes for the production of geopolymers cured at ambient temperature. *Cement and Concrete Composites*, 38, 75-81.
- Temuujin, J., Minjigmaa, A., Lee, M., Chen-Tan, N., and van Riessen, A. (2011). Characterisation of class F fly ash geopolymer pastes immersed in acid and alkaline solutions. *Cement and Concrete Composites*, 33, 1086-1091.
- Temuujin, J., Williams, R. P., and Riessen, A. van. (2009). Effect of mechanical activation of fly ash on the properties of geopolymer cured at ambient temperature. *Journal of Materials Processing Technology*, 209, 5276-5280.
- Trejo, D., Folliard, K. J., and Du, L. (2004). Sustainable development using controlled low-strength material. In *Proceedings of International Workshop on Sustainable Development and Concrete Technology*, 231-250.
- Turanli, L., Uzal, B., and Bektas, F. (2004). Effect of material characteristics on the properties of blended cements containing high volumes of natural pozzolans. *Cement and Concrete Research*, 34(12), 2277-2282.
- Turkoz, M., Savas, H., Acaz, A., and Tosun, H. (2014). The effect of magnesium chloride solution on the engineering properties of clay soil with expansive and dispersive characteristics. *Applied Clay Science*, 101, 1-9.
- Turner, L. K., and Collins, F. G. (2013). Carbon dioxide equivalent (CO<sub>2</sub>-e) emissions: A comparison between geopolymer and OPC cement concrete. *Construction and Building Materials*, 43, 125-130.
- Ulusay R., Arkan F., Yoleri M.F. and Caglan D. (1995). Engineering geological characterization of coal mine waste material and an evaluation in the context of back-analysis of spoil pile instabilities in a strip mine, SW Turkey, *Journal of Engineering Geology*, 40, 77-101.
- Umesha, T. S., Dinesh, S. V., and Sivapullaiah, P. V. (2009). Control of dispersivity of soil using lime and cement. *International journal of geology*, 3(1), 8-16.
- Vakili, A. H., Selamat, M. R., and Moayedi, H. (2013). Effects of using pozzolan and portland cement in the treatment of dispersive clay. *The Scientific World Journal*, 2013.
- Van Jaarsveld J. G. S., Van Deventer J. S J., and Lorenzen L. (1997). The potential use of geopolymeric materials to immobilise toxic metals: Part I. Theory and applications. *Minerals Engineering*, 10(7), 659-669.



- Vassilev S. V., and Vassileva, C. G. (2007). A new approach for the classification of coal fly ashes based on their origin, composition, properties and behaviour. *Fuel*, 86, 1490-1512.
- Wang, S. D., Scrivener, K. L., and Pratt, P. L. (1994). Factors affecting the strength of alkali-activated slag. *Cement and Concrete Research*, 24(6), 1033-1043.
- Xu, H. and van Deventer, J. S. J. (2003). Effect of Source Materials on Geopolymerization. *Industrial and Engineering Chemistry Research*, 42(40), 1698-1706.
- Xu, H., and van Deventer, J. S. J. (2000). The geopolymerisation of aluminosilicate minerals. *International Journal of Mineral Processing*, 59, 247-266.
- Xu, H., Gong, W., Syltebo, L., Izzo, K., Lutze, W., and Pegg, I. L. (2014). Effect of blast furnace slag grades on fly ash based geopolymer waste forms. *Fuel*, 133, 332-340.
- Yahya, Z., Abdullah, M. M. A. B., Hussin, K., Ismail, K. N., Razak, R. A., and Sandu, A. V. (2015). Effect of solids-to-liquids,  $\text{Na}_2\text{SiO}_3$ -to- $\text{NaOH}$  and curing temperature on the palm oil boiler ash (Si + Ca) geopolymerisation System. *Materials*, 8, 2227-2242.
- Yan, D. Y., Tang, I. Y., and Lo, I. M. (2014). Development of controlled low-strength material derived from beneficial reuse of bottom ash and sediment for green construction. *Construction and Building Materials*, 64, 201-207.
- Ye, N., Yang, J., Liang, S., Hu, Y., Hu, J., Xiao, B., and Huang, Q. (2016). Synthesis and strength optimization of one-part geopolymer based on red mud. *Construction and Building Materials*, 111, 317-325.
- Yılmaz, A., and Karaşahin, M. (2010). Mechanical properties of ferrochromium slag in granular layers of flexible pavements. *Materials and structures*, 43(3), 309-317.
- Yudhbir, and Rahim, A. (1991). Quantification of particle shape and angularity using the image analyser. *Geotechnical Testing Journal*, 14(3), 296-308.
- Yukselen, Y., and Kaya, A. (2003). Zeta potential of kaolinite in the presence of alkali, alkaline earth and hydrolyzable metal ions. *Water, Air, and Soil Pollution*, 145(1-4), 155-168.
- Yunsheng, Z., Wei, S., Wei, S., and Guowei, S. (2009). Synthesis and heavy metal immobilization behaviors of fly ash based geopolymer. *Journal of Wuhan University Technology Mater. Sic. Ed*, 24(5), 819-825.
- Zhang, M., El-Korchi, T., Zhang, G., Liang, J., and Tao, M. (2014). Synthesis factors affecting mechanical properties, microstructure, and chemical composition of red mud-fly ash based geopolymers. *Fuel*, 134, 315-325.

Zhang, Z., Provis, J. L., Reid, A., and Wang, H. (2014a). Fly ash-based geopolymers: The relationship between composition, pore structure and efflorescence. *Cement and Concrete Research*, 64, 30-41.

Zhang, Z., Wang, H., Zhu, Y., Reid, A., Provis, J. L. and Bullen, F. (2014b). Using fly ash to partially substitute metakaolin in geopolymer synthesis. *Applied Clay Science*, 88-89, 194-201.

Zhen, G., Lu, X., Zhao, Y., Niu, J., Chai, X., Su, L., and Hu, Y. (2013). Characterization of controlled low-strength material obtained from dewatered sludge and refuse incineration bottom ash: Mechanical and microstructural perspectives. *Journal of environmental management*, 129, 183-189.

# Dissemination

## A. Patent: Published

A corrosion resistant cementitious material from industrial waste, Inventors: Sarat Kumar Das, Lasyamayee Garanayak, **Mahasakti Mahamaya**, Patent Appl No. 201731017301/Kol Dt 17.05.2017.

[http://www.ipindia.nic.in/writereaddata/Portal/IPOJournal/1\\_2575\\_1/Part-1.pdf](http://www.ipindia.nic.in/writereaddata/Portal/IPOJournal/1_2575_1/Part-1.pdf).

## B. Book Chapter

**Mahamaya, M.** and Das, S. K. (2017). “Biopolymer Stabilization of Fly ash and Coal Mine Overburden for Erosion Resistance.,” **Chapter 11, *Biopolymers: Structure, Performance and Applications.*, Nova Publisher, USA. (Scopus)**

## C. Journal Publications

1. **Mahamaya, M.**, and Das, S. K. (2018). “Characterization of ferrochrome slag as a controlled low-strength structural fill material.” *International Journal of Geotechnical Engineering*, 1-10 (**ESCI**).
2. **Mahamaya, M.** and Das, S. K. (2017). “Characterization of Mine Overburden and Fly Ash as a Stabilized Pavement Material.,” *Particulate Science and Technology*, 35(6), 660-666. (**SCI**).
3. Suman, S., **Mahamaya, M.** and Das, S. K. (2016). “Prediction of Maximum Dry Density and Unconfined Compressive Strength of Cement Stabilised Soil Using Artificial Intelligence Techniques.,” *Int. J. of Geosynth. and Ground Eng.* 2, 11. (**ESCI**)
4. Das, S. K., Priyadarshini, S. and **Mahamaya, M.** (2016) “Characterization and design of coal-reject as a Highway Pavement Material.,” *Indian Highways*. 44(4), pp 17-21.

## D. Publications in Proceedings with DOI Nos.

1. **Mahamaya, M.**, Das, S. K. and Bhuyan, P.K. (2018). “Characterization of ferrochrome slag as a controlled low strength material.” Compendium of Annual meeting **Transportation research board**, Washington, USA

2. **Mahamaya, M.**, Suman, S., Anand, A. and Das, S. K. (2015). Prediction of UCS and CBR Values of Cement Stabilized Mine Overburden and Fly Ash Mixture. *Procedia Earth and Planetary Science*. **Elsevier**, 11, 294-302.
3. **Mahamaya, M.**, Mishra, P. N., Suman. S. and Das, S. K. (2015). Estimation of Thermal Migration Around Buried Coolant Ducts with Engineered Backfill Material.,”*Procedia Earth and Planetary Science*, **Elsevier**, 11, 410-417.
4. Das, S. K., **Mahamaya, M.**, Panda, I. and Swain, K. (2015). Stabilization of Pond Ash Using Biopolymer. *Procedia Earth and Planetary Science*.,**Elsevier**,11,254-259.
5. Swain, K., **Mahamaya, M.**, Alam, S., and Das, S. K. (2017). Stabilization of Dispersive Soil Using Biopolymer. *Sustainable Civil Infrastructures book series*, **Springer**, pp 132- 147, [https://doi.org/10.1007/978-3-319-61612-4\\_11](https://doi.org/10.1007/978-3-319-61612-4_11).
6. Parhi, P.S., Garanayak.L., **Mahamaya, M.** and Das, S. K.(2017). “Stabilization Of An Expansive Soil Using Alkali Activated Fly Ash Base Geopolymer., *Sustainable Civil Infrastructures* book series, **Springer**., DOI 10.1007/978-3-319-61931-6\_4.

## **E. Other Publications with recognitions**

1. **Institution award for Best Paper**, “Characterization of Controlled Low Stregth Material using Fly ash and mine overburden”. Institution of Engineers (India), Odisha Chapter. 2017 Civil Engineering.
2. **Muralidhar Satapathy Award for best paper**, “Dispersive soil and its stabilization using Biopolymer for Environmental Control” Institution of Engineers (India), Odisha Chapter, 2018.